TECHNICAL UNIVERSITY OF SOFIA

FACULTY AUTOMATION

DEPARTMENT THEORETICAL ELECTRICAL ENGINEERING

SUMMER SCHOOL

ADVANCED ASPECTS OF THEORETICAL ELECTRICAL ENGINEERING - SOZOPOL'09

Sozopol'09

in the framework of

THE DAYS OF SCIENCE OF THE TECHNICAL UNIVERSITY OF SOFIA, SOZOPOL, BULGARIA, SEPT. 2009

Part II: Regular Papers

Edited by Valeri Mladenov

The main sponsor of the Summer School is:
RESEARCH AND DEVELOPMENT SECTOR,
TECHNICAL UNIVERSITY – SOFIA

Dedicated to prof. Mincho Zlatev's
100 years birthday anniversary

ISSN: 1313-9487

Organizing Committee

Honorary Chairmen:

V. Georgiev – Bulgaria
S. Farchy – Bulgaria
L. Kolev – Bulgaria
S. Papasow – Bulgaria
V. Savov – Bulgaria

Chair:
V. Mladenov, TU-Sofia, Bulgaria

Co Chairs:
S. Guninski, TU-Sofia, Bulgaria
J. Georgiev, TU-Sofia, Bulgaria
I. Iachev, TU-Sofia, Bulgaria

Members:

K. Brandisky, TU-Sofia, Bulgaria
A. Chervenkov, TU-Sofia, Bulgaria
K. Ivanov, TU-Sofia, Bulgaria
N. Petkova, TU-Sofia, Bulgaria
S. Petrakieva, TU-Sofia, Bulgaria
N. Radev, TU-Sofia, Bulgaria
K. Stanchev, TU-Sofia, Bulgaria
R. Stancheva, TU-Sofia, Bulgaria
I. Tabahnev, TU-Sofia, Bulgaria
S. Terzieva, TU-Sofia, Bulgaria
K. Todorova, TU-Sofia, Bulgaria
G. Toshev, TU-Sofia, Bulgaria
S. Vladov, TU-Sofia, Bulgaria
I. Trushev, TU-Sofia, Bulgaria
G. Tsenov, TU-Sofia, Bulgaria
I. Yacheva, TU-Sofia, Bulgaria

International Programme Committee

D. Baldomir, Spain
A. Bossavit, France
A. Brykalski, Poland
H. Butterweck, Netherlands
T. Chady, Poland
K. Demirtchyan, Russia
S. Gratkowski, Poland
K. Hameyer, Germany
W. John, Germany
L. Klinkenbusch, Germany
L. Kolev, Bulgaria
A. Kost, Germany
Z. Leonowicz, Poland
N. Mastorakis, Greece
W. Mathis, Germany
V. Mladenov, Bulgaria
M. Ogorzałek, Poland
S. Osowski, Poland
L. Pichon, France
B. Reljin, Serbia
R. Sikora, Poland (Honorary Chairman)
L. Sumichrast, Slovakia
J. Sykulski, UK
M. Tadeusiewicz, Poland
H. Toepfer, Germany
H. Uhlmann, Germany
R. Weigel, Germany

PREFACE

These Proceedings are organized in two parts and contain the plenary lectures and the regular papers presented at the 7th Summer School *Sozopol‘09*, which took place in Sozopol, Bulgaria, between 20 and 23 Sept. 2009 in the framework of the Days of the Science of the Technical University of Sofia. The Summer School covers the advanced aspects of Theoretical Electrical Engineering and it is a platform for postgraduate training of Ph.D. students and young scientists. During the Summer School well-known experts presented some advanced aspects of circuits and systems theory, electromagnetic field theory and their applications. Apart from the educational part of the Summer School a presentation of original authors’ papers took place.

The main topics of the Summer School *Sozopol’09* include Circuits and Systems Theory, Signal Processing and Identification Aspects, Electromagnetic Fields, Theoretical Concepts, Applications and Innovative Educational Aspects.

The Summer School *Sozopol’09* has been organized by the Department of Theoretical Electrical Engineering of the Technical University of Sofia with the sponsorship of the Research and Development Sector of the Technical University of Sofia. This has been the seventh edition of the event, after the Summer Schools in 1986, 1988, 2001, 2002, 2005 and 2007. This Summer School is especially dedicated to prof. Mincho Zlatev's 100 years birthday anniversary.

There were 52 participants from 5 different countries at the Summer School this year. There were 14 plenary lectures and 29 regular papers that are published in these Proceedings. Providing the recent advances in Theoretical Electrical Engineering the Proceedings will be of interest to all researchers, educators and Ph.D. students in the area of Electrical Engineering.

Special thanks are due to the Research and Development Sector, Faculty of Automation and the Section of Social Services of the Technical University of Sofia about the overall support of the event. We also want to thank to the World Scientific and Engineering Academy and Society (WSEAS) and company Antipodes Ltd. which partially sponsored the event. We hope to meet again in the following edition of the Summer School to continue the good tradition and collaboration in the field of Theoretical Electrical Engineering.

Organizing Committee
Sofia, Oct. 2009

CONTENTS

SECTION 2 – THEORETICAL CONCEPTS, SIGNAL PROCESSING AND IDENTIFICATION ASPECTS

SECTION 3 – ELECTROMAGNETIC FIELDS

SYSTEMATIC FORMULATION OF STATE VARIABLE EQUATIONS FOR CIRCUITS WITH EXCESS ELEMENTS

Paul Dan Cristea and Rodica Tuduce

Biomedical Engineering Center, University "Politehnica" of Bucharest,
Spl. Independentei 313, 060042 Bucharest, Romania,
phone: +40 21 316 9569, e-mail: {pcristea, trodica}@dsp.pub.ro

Abstract: *The paper presents a systematic method to derive the state variable equations of electrical circuits, for both cases of circuits with and without excess elements. A circuit is said to have excess elements when it contains capacitor loops, i.e., loops consisting only of ideal capacitors and (possibly) of ideal independent voltage sources, or of inductor cut-sets, i.e., closed surfaces cutting only ideal inductors and (possibly) ideal independent current sources. For circuits with excess elements it is not possible to use all capacitor voltages and all inductor currents as state variables, as they are not mutually independent. In such cases, a sub-set of essential capacitor voltages and inductor currents must be used as state variables, while the remaining ones are treated as dependent variables.*

Keywords: State variable equations, Systematic equation formulation, Excess circuit elements, Essential circuit elements

1. INTRODUCTION

The state variables method is a valuable tool for the description and analysis of systems, in particular electrical circuits [1], [2]. Among its many strong points, it can be used directly in the time domain with a simple computer implementation and it can be easily extended from linear to nonlinear systems. Moreover, in the case of constant (DC) or harmonic (AC) excitations, the state variable approach can readily be combined with specific DC or AC methods to efficiently determine the steady state component determined by the excitations (the forced component), so that the state variable method is used only to find the component determined by the system initial conditions (the free component).

For a linear and time invariant systems, the state equations are

$$\dot{x}\rfloor = \lfloor A \rfloor x \rfloor + \lfloor B \rfloor y \rfloor \tag{1}$$

where $x\rfloor \in R^{n\times 1}$ is the (column) state variables vector, $y\rfloor \in R^{m\times 1}$ is the (column) excitation vector (sources and inputs), $\lfloor A \rfloor \in R^{n\times n}$ is the system coefficient matrix and $\lfloor B \rfloor \in R^{n\times m}$ – the input coefficient matrix[1].

[1] Notice the notation with double square brackets for square or rectangular matrices and with a single square bracket placed on the right for column matrices (vectors).

The corresponding solution is given by

$$x(t)] = e^{[A](t-t_0)}\, x(t_0)] + \int_{t_0}^{t} e^{[A](t-\tau)}\, [B]\; y(\tau)]\, d\tau \tag{2}$$

where $x(t)]$ is the state variable vector at the moment t, whereas $x(t_0)]$ is its initial value at the moment t_0, ($t_0 \leq t < \infty$).

For electric circuits, one common choice of the state variables is:

$$x] = \begin{matrix} u_C] \\ i_L] \end{matrix}], \tag{3}$$

where $u_C]$ is the vector of capacitor voltages and $i_L]$ - the vector of inductor currents. Correspondingly, the state co-variables vector contains the complementary variables:

$$X] = \begin{matrix} I_C] \\ U_L] \end{matrix}], \tag{4}$$

where $I_C]$ is the vector of capacitor currents and $U_L]$ - the vector of inductor voltages.

The total energy stored in the reactive elements of the circuit, *i.e.*, in the capacitors and the inductors, can readily be computed in terms of the state variables:

$$w = w_e + w_m = \sum_{k=1}^{n_C} \frac{C_k\, u_{C_k}}{2} + \sum_{k=1}^{n_L} \frac{L_k i_{L_k}}{2} + \frac{1}{2}\sum_{j=1}^{n_L} \sum_{k=1}^{n_L} L_{jk}\, i_{L_j}\, i_{L_k} \;. \tag{5}$$

By introducing the matrices of capacitances, inductances and reactive parameters:

$$[C] = \mathrm{diag}\left(C_1, C_2, \cdots, C_{n_C}\right),\; [L] = \begin{bmatrix} L_1 & L_{12} & \cdots & L_{1n_L} \\ L_{21} & L_2 & \cdots & L_{2n_L} \\ \vdots & \vdots & \ddots & \vdots \\ L_{n_L 1} & L_{n_L 2} & \cdots & L_{n_L} \end{bmatrix} \text{ and } [P] = \begin{bmatrix} [C] & \\ & [L] \end{bmatrix}, \tag{6}$$

the equation (5) takes the more compact matrix form:

$$w = w_e + w_m = \frac{1}{2} u_C]^{\mathrm{T}}\, [C]\, u_C] + \frac{1}{2} i_L]^{\mathrm{T}}\, [L]\, i_L] = \frac{1}{2} x]^{\mathrm{T}}\, [P]\, x] \tag{7}$$

In the following, we show how the state variable equations (1), for circuits without or with excess elements, can be established systematically by reducing the problem to the computing of transfer functions in a resistive multiport [3].

2. STATE VARIABLE EQUATIONS OF CIRCUITS WITHOUT EXCESS ELEMENTS

If the circuit has neither *capacitor loops* (loops consisting only of ideal capacitors and, possibly, of ideal independent voltage source), nor *inductor cut-sets* (closed surfaces cutting only ideal inductors and, possibly, ideal independent current sources). all variables are mutually independent from the interconnection point of view and it is possible to chose the state variables and co-variables as shown in equations (3) and (4). In this case, all capacitors and inductors are called *essential circuit elements*, and there are no *excess circuit elements*.

To systematically establish the state variable equations of such a circuit without excess elements, let us consider a circuit as represented in Fig. 1, in which the capacitors, inductors, ideal voltage sources and ideal current sources are shown as connected to the terminals of a resistive passive multiport that might contain any type of controlled sources.

It is a simple resistive circuit problem to compute I_C and U_L from the equations of the multiport, in terms of the state variables u_C and i_L, and of the sources e and j. All these variables can be considered as the parameters of ideal voltage and ideal current sources, connected at multiport terminals, as shown in Fig. 2.

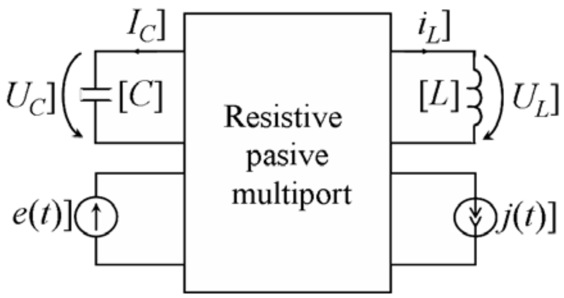

Fig. 1. Electric circuit represented as a resistive passive multiport, possibly containing controlled sources, at which terminals are connected all the capacitors, inductors and independent sources in the circuit.

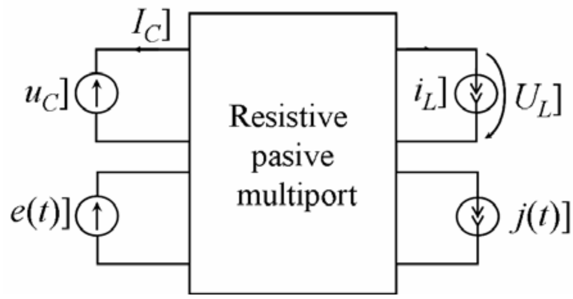

Fig. 2. The electric circuit in Fig.1, in which the focus is on computing the currents of all capacitors and the voltages of all inductors, when knowing the excitations at multiport terminals.

The state co-variables are computed as the output variables at multiport terminals:

$$\begin{bmatrix} I_C] \\ U_L] \end{bmatrix} = \begin{bmatrix} G_{CC} & B_{Cj} \\ A_{Le} & R_{Lj} \end{bmatrix} \begin{bmatrix} u_C] \\ i_L] \end{bmatrix} + \begin{bmatrix} G_{Ce} & B_{Cj} \\ A_{Le} & R_{Lj} \end{bmatrix} \begin{bmatrix} e] \\ j] \end{bmatrix}, \tag{8}$$

or, more compactly:

$$X] = [a]\,x] + [b]\,y], \tag{9}$$

where the hybrid transfer function matrices $[a]$ and [b] contain the transfer conductances G, transfer resistances R, voltage gains A and current gains B, explicitly shown in (8).

The capacitors and inductors are described by the constitutive equations:

$$I_C] = \dot{q}_C] = [C]\,\dot{u}_C] \text{ and } U_L] = \dot{\varphi}_L] = [L]\,\dot{i}_L], \tag{10}$$

which allows to express the state co-variables vector $X]$ in function of the time derivative of the state variables vector $\dot{x}]$, and the reverse:

$$X] = [P]\,\dot{x}] \text{ and } \dot{x}] = [P]^{-1}[X]. \tag{11}$$

Combining (11) with (9), one finally gets the state variable equations (1):

$$\dot{x}] = [P]^{-1}[X] = [P]^{-1}\left([a]\,x] + [b]\,y]\right) = [A]\,x] + [B]\,y], \tag{12}$$

in which the system coefficient matrix [A] and the input coefficient matrix [B] have been computed as:

$$A] = [P]^{-1}[a] \text{ and } B] = [P]^{-1}[b] \tag{13}$$

3. STATE VARIABLE EQUATIONS OF CIRCUITS WITH EXCESS ELEMENTS

Consider now a circuit in which there are *capacitor loops* and/or *inductor cut-sets*. In this case, there is a link between the capacitor voltages, on one hand, and between the inductor currents, on the other, links imposed by the circuit topology (from the circuit interconnection point of view). One capacitor voltage can be expressed in terms of the other in the same *capacitor loop*. Such a voltage must be eliminated from the vector $u_C]$ with the independent capacitor voltages and can be introduced in a vector $U_{C'}]$ comprising dependent capacitor voltages. Similarly, one inductor current can be expressed in terms of the other in the same *inductor cut-set.* This current must be eliminated from the vector $i_L]$ of independent inductor currents and can be introduced in a vector $I_{L'}]$ comprising the dependent inductor currents.

The state variables vector $x]$ has the same structure as in (3), but comprises only independent capacitor voltages and independent inductor currents, which belong to the *essential circuit elements*. The dependent variables $U_{C'}]$ and $I_{L'}]$ are parts of an *excess circuit element* co-variables vector $X']$.

The variables and co-variables for the essential and excess elements are:

$$x] = \begin{matrix} u_C] \\ i_L] \end{matrix}\Bigg],\quad X] = \begin{matrix} I_C] \\ U_L] \end{matrix}\Bigg];\quad x'] = \begin{matrix} i_{C'}] \\ u_{L'}] \end{matrix}\Bigg],\quad X'] = \begin{matrix} U_{C'}] \\ I_{L'}] \end{matrix}\Bigg] \tag{14}$$

Consider the circuit represented in Fig. 3, in which the capacitors, inductors, ideal voltage sources and ideal current sources are shown connected to the terminals of a resistive passive multiport, which can contain any type of controlled sources. In this case, there are two types of capacitors and inductors, represented distinctly. To reduce the problem to solving a resistive multiport, the reactive elements will be

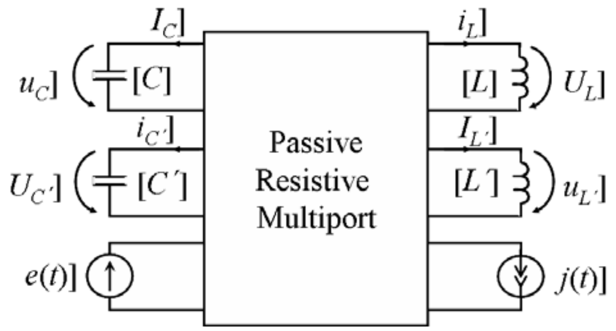

Fig. 3. Electric circuit with excess elements represented as a resistive passive multiport, possibly containing controlled sources, at which terminals are connected all the essential and excess capacitors and inductors, as well as all the independent sources in the circuit.

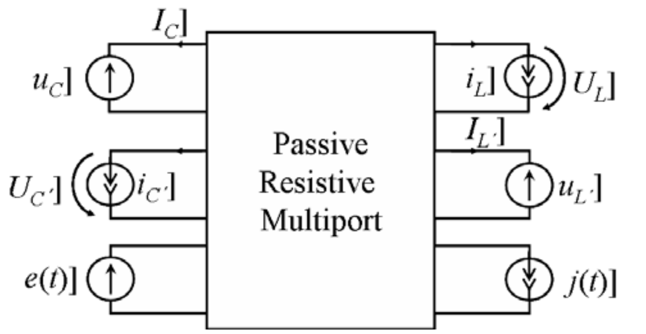

Fig. 4. The electric circuit in Fig.3, in which the capacitors and inductors have been replaced by ideal sources as explained in the text. The problem has been reduced to the solving of a resistive multiport.

replaced by ideal voltage or current sources, giving the same inputs to the resistive multiport, as shown in Fig. 4. The essential capacitors have independent voltages $u_C]$ that can be chosen arbitrarily, so that these elements will be replaced by ideal voltage sources giving the same voltage at the terminals. This is not possible for the excess capacitors, for which the voltages $U_{C'}]$ depend on the voltages $u_C]$**.** But the currents of these elements have no interconnection restrictions, so that the excess capacitors are replaced by ideal current sources giving the same currents $i_{C'}]$. Similarly, the essential inductors are replaced with ideal current sources giving $i_L]$, whereas the excess inductors are replaced with ideal voltage sources giving $u_{L'}]$.

The dependent variables at the terminals of the resistive multiport result:

$$\left.\begin{bmatrix} I_C] \\ U_L] \end{bmatrix}\right] = \begin{bmatrix} G_{CC} & B_{Cj} \\ A_{Le} & R_{Lj} \end{bmatrix} \left.\begin{matrix} u_C \\ i_L \end{matrix}\right] + \begin{bmatrix} G_{Ce} & B_{Cj} \\ A_{Le} & R_{Lj} \end{bmatrix} \left.\begin{matrix} e \\ j \end{matrix}\right] + \begin{bmatrix} B_{CC'} & B_{CL'} \\ R_{LC'} & A_{LL'} \end{bmatrix} \left.\begin{matrix} i_{C'} \\ u_{L'} \end{matrix}\right] \tag{15}$$

$$\left.\begin{bmatrix} U_{C'}] \\ I_{L'}] \end{bmatrix}\right] = \begin{bmatrix} A_{C'C} & 0 \\ 0 & B_{L'C} \end{bmatrix} \left.\begin{matrix} u_C \\ i_L \end{matrix}\right] + \begin{bmatrix} A_{C'e} & 0 \\ 0 & B_{L'j} \end{bmatrix} \left.\begin{matrix} e \\ j \end{matrix}\right] \tag{16}$$

Or, written more compactly:

$$X] = [a]\,x] + [b]\,y] + [c]\,x'] \tag{17}$$

$$X'] = [d]\, x] + [f]\, y] \tag{18}$$

Matrices [*d*] and [*f*] can have elements only with the values +1, -1 and 0.
By introducing the parameter matrices for the essential and the excess elements:

$$[P] = \begin{bmatrix} [C] & \\ & [L] \end{bmatrix} \text{ and } [P'] = \begin{bmatrix} [C'] & \\ & [L'] \end{bmatrix}, \tag{19}$$

the reactive elements' constitutive equations can be written:

$$X\ ] = [P]\, \dot{x}] \text{ and } x'\ ] = [P']\, \dot{X}'] \tag{20}$$

Reversing the first equation above and taking the derivative of (18), one gets:

$$\dot{x}] = [P]^{-1} X\ ] \text{ and } \dot{X}'] = [d]\, \dot{x}] + [f]\, \dot{y}] \tag{21}$$

From the equations (17), (18), (20), and (21) it results successively:

$$\begin{aligned} \dot{x}] &= [P]^{-1} X\ ] \\ &= [P]^{-1} \{[a]\, x] + [b]\, y] + [c][x']\} \\ &= [P]^{-1} \{[a]\, x] + [b]\, y] + [c][P']([d]\, \dot{x}] + [f]\, \dot{y}])\} \end{aligned} \tag{22}$$

from where the terms containing $\dot{x}]$ can be separated:

$$([P] - [c][P'][d])\, \dot{x}] = ([a]\, x] + [b]\, y] + [c][P'][f]\, \dot{y}]) \ . \tag{23}$$

Defining

$$[\Pi] = [P] - [c][P'][d],. \tag{24}$$

the state variable equations for the circuit with excess elements is obtained:

$$\dot{x}] = [\Pi]^{-1}([a]\, x] + [b]\, y] + [c][P'][f]\, \dot{y}]) \ . \tag{25}$$

This equation can be put in the standard form (1), with:

$$[A] = [\Pi]^{-1}[a], \qquad [B] = [\Pi]^{-1}[\,[b] \quad [c][P'][f]\,] \tag{26}$$

and replacing $y(t)]$ with a new vector of excitation:

$$Y(t)] = \begin{bmatrix} y(t)] \\ \dot{y}(t)] \end{bmatrix}, \tag{27}$$

which comprises both the vector of the sources and its time derivative.

4. EXAMPLE

In this section we illustrate the method of systematically establishing the state variable equations of a circuit with excess elements presented in Section 3, by considering the circuit in Fig. 5.

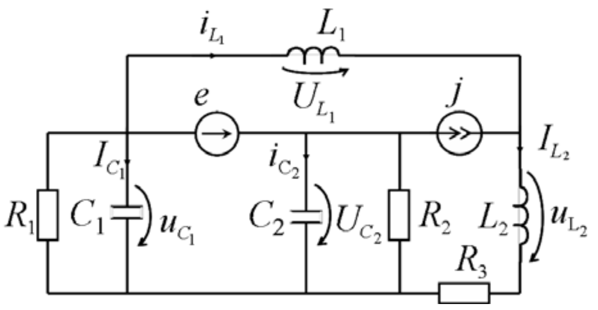

Fig. 5. Example of electric circuit with excess elements.

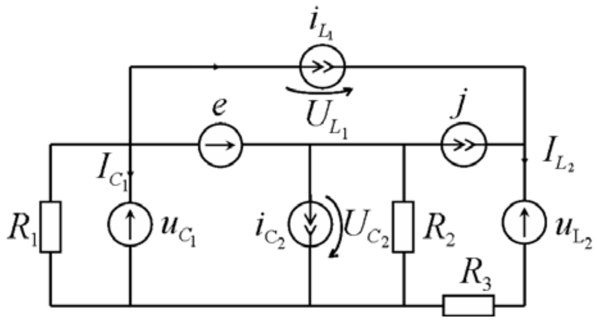

Fig. 6. Resistive multiport of the circuit in Fig. 5, after replacing the capacitors and inductors with sources as explained in the text.

The circuit comprises the capacitor loop (C_1 - e – C_2) and the inductor cut-set (L_1 – L_2 – j) . We select C_1, L_1 as essential elements, and C_2, L_2 as excess elements. Accordingly, in the resistive circuit of Fig.6, the capacitor C_1 is replaced an ideal voltage source u_{C_1}, the inductor L_1 with an ideal current source i_{L_1}, the capacitor C_2 with an ideal current source i_{C_2}, and the inductor L_2 with an ideal voltage source u_{L_2}.

A superposition approach is used to compute successively the transfer functions in equations (15) and (16) for the resistive multiport in Fig.6. Each source in the circuit is kept active alone, in sequence, while all the other sources are passivated.

To passivate an ideal voltage source, its *emf* must be made zero, *i.e.*, the source must be replaced with a short circuit (s.c.). Similarly, an ideal current source is passivated by making zero its current, *i.e.*, by replacing it with an open circuit (o.c.). The method is illustrated for two instances: În Fig. 7 only the source giving u_{C_1} is maintained active, whereas in Fig. 8 only the source giving i_{L_1} is active. In each case the remaining sources are passive. The outputs I_{C_1}, U_{L_1}, U_{C_2} and I_{L_2}, are calculated, which gives the corresponding transfer functions by a simple (symbolic) division.

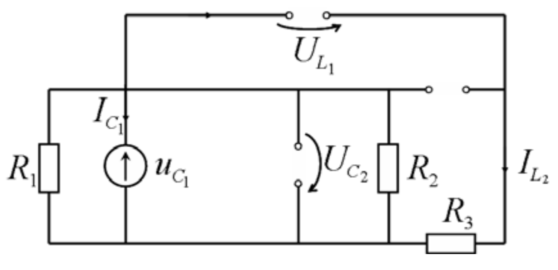

Fig. 7. Example of computing the resistive multiport transfer functions for the source u_{C1}, the other sources being passivated. .

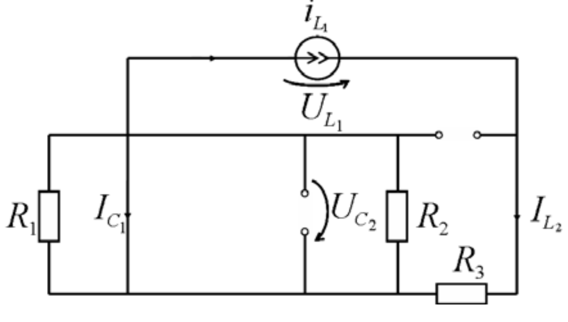

Fig. 8. Example of computing the resistive multiport transfer functions for the source i_{L1}, the other sources being passivated. .

The equations (15) and (16) which give the dependent variables at the terminals of the resistive multiport in Fig. 6 result:

$$\begin{bmatrix} I_{C_1} \\ U_{L1} \end{bmatrix} = \begin{bmatrix} -\dfrac{R_1+R_2}{R_1R_2} & -1 \\ 1 & -R_3 \end{bmatrix} \begin{bmatrix} u_{C_1} \\ i_{L_1} \end{bmatrix} + \begin{bmatrix} -\dfrac{1}{R_2} & -1 \\ 0 & -R_3 \end{bmatrix} \cdot \begin{bmatrix} e \\ j \end{bmatrix} + \begin{bmatrix} -1 & 0 \\ 0 & -1 \end{bmatrix} \cdot \begin{bmatrix} i_{C_2} \\ u_{L_2} \end{bmatrix} \tag{28}$$

$$\begin{bmatrix} U_{C2} \\ I_{L2} \end{bmatrix} = \begin{bmatrix} 1 & 0 \\ 0 & 1 \end{bmatrix} \begin{bmatrix} u_{C_1} \\ i_{L_1} \end{bmatrix} + \begin{bmatrix} 1 & 0 \\ 0 & 1 \end{bmatrix} \begin{bmatrix} e \\ j \end{bmatrix}. \tag{29}$$

The parameters of the essential and excess circuit elements are, respectively:

$$[P] = \begin{bmatrix} C_1 & 0 \\ 0 & L_1 \end{bmatrix} \text{ and } [P'] = \begin{bmatrix} C_2 & 0 \\ 0 & L_2 \end{bmatrix}. \tag{30}$$

The matrix $[\Pi]$ given by equation (24) for this circuit is a diagonal matrix:

$$[\Pi] = [P] - [c][P'][d] = \begin{bmatrix} C_1 & 0 \\ 0 & L_1 \end{bmatrix} - \begin{bmatrix} -1 & 0 \\ 0 & -1 \end{bmatrix} \begin{bmatrix} C_2 & 0 \\ 0 & L_2 \end{bmatrix} \begin{bmatrix} 1 & 0 \\ 0 & 1 \end{bmatrix} = \begin{bmatrix} C_1+C_2 & 0 \\ 0 & L_1+L_2 \end{bmatrix} \tag{31}$$

so that its inverse is simply:

$$[\Pi]^{-1} = \begin{bmatrix} \dfrac{1}{C_1+C_2} & 0 \\ 0 & \dfrac{1}{L_1+L_2} \end{bmatrix} \tag{32}$$

and the matrices in the state variable equation result:

$$[A] = [\Pi]^{-1}[a] = \begin{bmatrix} -\dfrac{R_1+R_2}{R_1R_2(C_1+C_2)} & -\dfrac{1}{C_1+C_2} \\ \dfrac{1}{L_1+L_2} & -\dfrac{R_3}{L_1+L_2} \end{bmatrix},$$

$$[B] = [\Pi]^{-1}[\,[b] \quad [c][P'][f]\,] = \begin{bmatrix} -\dfrac{1}{R_2(C_1+C_2)} & -\dfrac{1}{C_1+C_2} & -\dfrac{C_2}{C_1+C_2} & 0 \\ 0 & -\dfrac{R_3}{L_1+L_2} & 0 & -\dfrac{L_2}{L_1+L_2} \end{bmatrix}, \tag{33}$$

$$Y(t)] = \begin{bmatrix} e(t) & j(t) & \dfrac{\mathrm{d}e(t)}{\mathrm{d}t} & \dfrac{\mathrm{d}j(t)}{\mathrm{d}t} \end{bmatrix}$$

5. CONCLUSIONS

State variable equations can be established systematically by separating the resistive part, which can contain controlled sources, from the capacitor, inductor and source components. As shown in the paper, this allows finding the state variable equations by solving a simple purely resistive problem a number of times equal to the number of capacitors, resistors and independent voltage and current sources.

State variable equations are a powerful tool for studying switching in circuits with inconsistent initial conditions [4], [5], [6], [7].

REFERENCES

[1] Paul M. DeRusso, Rob J. Roy, Charles M. Close, Alan A. Desrochers, State Variables for Engineers, 2nd Edition, Wiley Knowledge for Generations, 1998.

[2] M. Preda, P. D. Cristea, F. Spinei *et al.*, Circuit Analysis – State Variables (in Romanian), University “Politehnica” Publishing House, Bucharest, 1973.

[3] M. Preda, P. D. Cristea et al, Fundamentals of Electrotechnics (in Romanian), Didactic and Pedagogic Publishing House, Bucharest, vol. 2, 920 pages, 1980

[4] J. Vlach, J.M. Wojciechowski and A. Opal, Analysis on nonlinear networks with inconsistent initial conditions, IEEE Transactions on Circuits and Systems, vol. 42, no. 4, April 1995, pp. 195-200.

[5] D. Biolek, "Initial conditions of linear switched networks", ECCTD'95 European Conference on Circuit Theory Design, pp. 115-118, 1995, I.T.Ü.

[6] P. D. Cristea and Rodica Tuduce, State variable analysis of linear switched networks with excess elements and inconsistent initial conditions, Rev. Roum. Sci. Techn. - Électrotechn. et Énerg., vol. 42, no.2, Bucharest, 1997, pp.209-218.

[7] P. D. Cristea, Rodica Tuduce, Switching Processes in Idealized Networks with excess Elements and Inconsistent Initial Conditions", 5th Electronic Devices and Systems International Conference, Brno, Czech Republic, June 11-12, 1998, http://www.dsp.pub.ro/articles/switchingproces/brno98.htm

DIAGNOSABILITY INVESTIGATION OF LINEAR ANALOG CIRCUITS USING PARAMETERIZED SENSITIVITY SPICE MACROMODELS

Ekaterina Nikolova Dimitrova[1], Elissaveta Dimitrova Gadjeva[2], Dimitar Yordanov Shikalanov[3], Vencislav Cekov Valchev[4]

[1]Department of Electronics, Technical University of Varna, 1 Studentska Str., 9010 Varna, Bulgaria, phone: +359 52 383 624, e-mail: edimitrowa@yahoo.com

[2]Department of Electronics and Electronics Technologies, Technical University of Sofia, 8 Kliment Ohridski Blvd., 1000 Sofia, Bulgaria, phone +395 2 3725, e-mail: egadjeva@tu-sofia.bg

[3]Department of Informatics, New Bulgarian University, 21 Montevideo Str., 1635 Sofia, Bulgaria, phone: +359 2 481 7049, e-mail: dys@nbu.bg

[4]Department of Electronics, Technical University of Varna, 1 Studentska Str., 9010 Varna, Bulgaria, phone: +359 52 383 266, e-mail: vencivalchev@hotmail.com

Abstract: *In the present paper, a computer-aided approach is developed to diagnosability investigation of linear analog circuits. The method is based on sensitivity investigation of the test characteristics. The sensitivity model approach is realized using the PSpice simulator and parameterized sensitivity PSpice macromodels are built in order to calculate the sensitivity characteristics in the frequency domain. The determination of the needed sensitivities is reduced to a parametric analysis of the constructed sensitivity model. The test frequencies are selected maximizing the sensitivity of the magnitude and phase of the test characteristics. Applying post-processing of the simulation results using macro-definitions in the graphical analyzer Probe, a fault diagnosability investigation of the circuit is performed. Sensitivity measures are defined in Probe for diagnosability investigation of multiple faults using pre-defined macrodefinitions. The fault masking, fault dominance and fault equivalence are also investigated. The frequency ranges, corresponding to maximal sensitivity measures, are automatically obtained for the multiple fault isolation. An example is given illustrating the possibilities and the applicability of the proposed approach.*

Keywords: Analog circuit diagnosis, Sensitivity, Diagnosability, SPICE simulation

1. INTRODUCTION

The development of wireless communication leads to an increasing demand for reliable and high performance RF products. In order to achieve high performance, efficient test and diagnosis procedures are needed. Due to the complexity of testing at higher frequencies, the testing of RF analog circuits requires the performing a quick and efficient test with a limited number of test vectors. In [1] a method is developed for improving fault detection in high frequency circuits based on sensitivity analysis and *S*-parameter measurements. The test frequencies are selected maximizing the sensitivity of the magnitude and phase of the *S*-parameters. The influence of the faults on the output characteristics is investigated in [2]. The concepts fault masking, fault dominance, fault equivalence and fault isolation are defined. Based on sensitivity analysis, test nodes and test frequencies selection is performed for every category of faults (single, double, multiple). An approach is proposed in [3] to automated diagnosis of parametric faults in analog electronic circuits using *PSpice*-like circuit simulators. Based on circuit responses that well characterize the faults, the set of typical faulty variants of the circuit is simulated. The fault generation is reduced to a parametric analysis of the diagnosis model of the circuit.

In the present paper, a computer-aided approach is developed to diagnosability investigation of linear analog circuits. The method is based on sensitivity investigation of the test characteristics. The sensitivity model approach is realized using the *PSpice* simulator and parameterized sensitivity *PSpice* macromodels are built in order to calculate the sensitivity characteristics in the frequency domain. The determination of the needed sensitivities is reduced to a parametric analysis of the constructed sensitivity model. The test frequencies are selected maximizing the sensitivity of the magnitude and phase of the test characteristics. Applying post-processing of the simulation results using macro-definitions in the graphical analyzer *Probe*, a fault diagnosability investigation of the circuit is performed. Sensitivity measures are defined in *Probe* for diagnosability investigation of multiple faults using pre-defined macrodefinitions. The fault masking, fault dominance and fault equivalence are also investigated. The frequency ranges, corresponding to maximal sensitivity measures, are automatically obtained for the multiple fault isolation. An example is given illustrating the possibilities and the applicability of the proposed approach.

2. SENSITIVITY MODEL

The sensitivity model approach is used to calculate the sensitivity coefficients of the output characteristics in the frequency domain. According to this method, in order to obtain the derivative of the output voltage V_{out} in respect to the admittance Y_i in the circuit, an analysis of the original circuit N is performed and the resulting voltage V_{Yi} is used as a control voltage for the sensitivity model N_d. A voltage controlled current source is connected in parallel with the element Y_{id} with controlling coefficient of Y_c = 1S. The output voltage $V_{out,d}$ of the circuit N_d is equal to the derivative $\partial V_{out} / \partial Y_i$: $V_{out,d} = \partial V_{out} / \partial Y_i$.

In order to obtain the sensitivity

$$S_{Y_i}^{V_{out}} = \frac{\partial V_{out}}{\partial Y_i} \cdot \frac{Y_i}{V_{out}} \tag{1}$$

automatically in the computer *PSpice* model, the controlling coefficient of Y_c is multiplied by Y_i in the model and the result $V_{out,d}$ is divided by V_{out} in the graphical analyzer *Probe*.

The sensitivity model of the resistor is represented in Fig. 1. It is built using a block definition. In order to analyze simultaneously the circuits N and N_d, the equivalent circuit contains the element R_1 from the original circuit N and the element R_{1sen}

from the sensitivity model N_d. The VCCS G_{gen} is added in parallel with R_{1sen} in the sensitivity model. The circuit connections are represented using busses. The node 1 has a bus name 1[1..2] and represents node 11 of the circuit N and node 12 in the circuit N_d (Fig. 1c). The attributes of the block are shown in Fig. 1b. The *ID* number is assigned to the element. In order to obtain the sensitivities for a group of elements simultaneously in the graphical analyzer *Probe*, a parametrtic sweep is used. A parameter *par* is defined with a linear variation from 1 to *n* with increment 1. When the current value of *par* is equal to the *ID* number of a given element, the controlling coefficient G_{gen} of its *VCCS* is equal to the nominal element value *val* and the sensitivity with respect to this element is calculated, otherwise G_{gen}=0. This is accomplished by the **IF-THEN-ELSE** statement, included in the expression for G_{gen} (Fig. 1c). The sensitivity model of the capacitor is represented in Fig. 2. It is built similarly to the resistor model. The block representation is shown in Fig. 2c and the attributes are given in Fig. 2b.

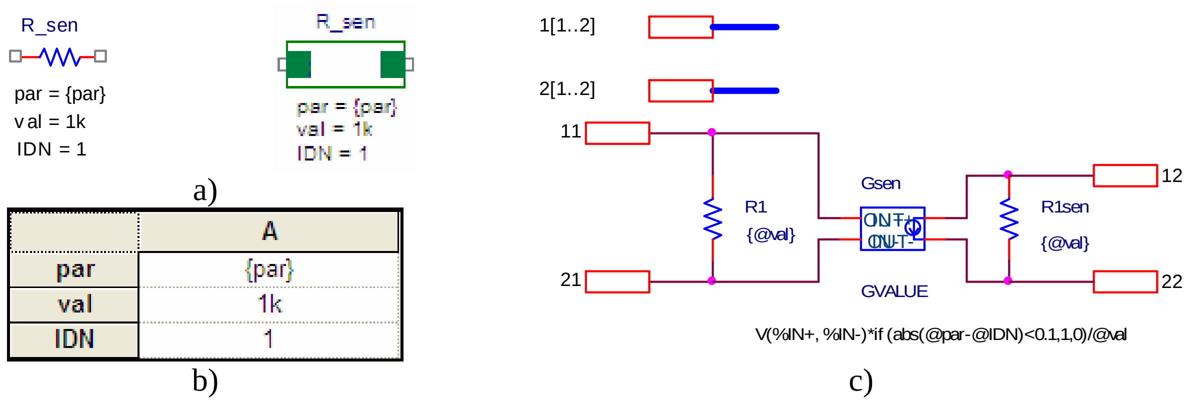

Fig. 1. Sensitivity model of the resistor

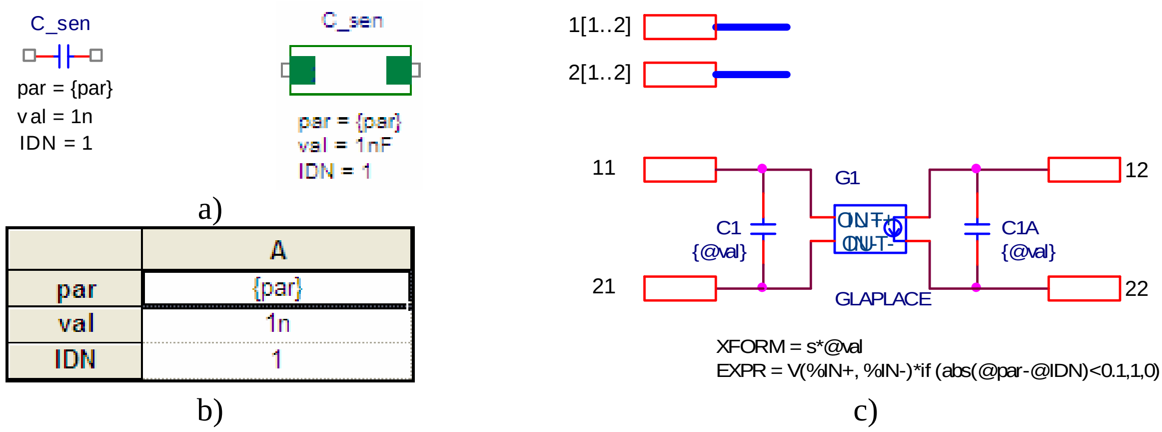

Fig. 2. Sensitivity model of the capacitor

The sensitivity model of the OpAmp is represented in Fig. 3. It consists of two identical OpAmps – one in the circuit N and one in the circuit N_d. The ground node is modeled by a block, consisting of two short circuit branches connected to the ground - one for circuit N and one for circuit N_d. They are modeled by independent voltage source of value 0 as shown in Fig. 4. The independent voltage source in the sensitivity model is shown in Fig. 5. The value of the signal is defined for the source V_1 in the circuit N and the value of V_2 is equal to zero. The example circuit for the sensitivity determination is shown in Fig. 6a and the frequency characteristic is represented in Fig. 6b.

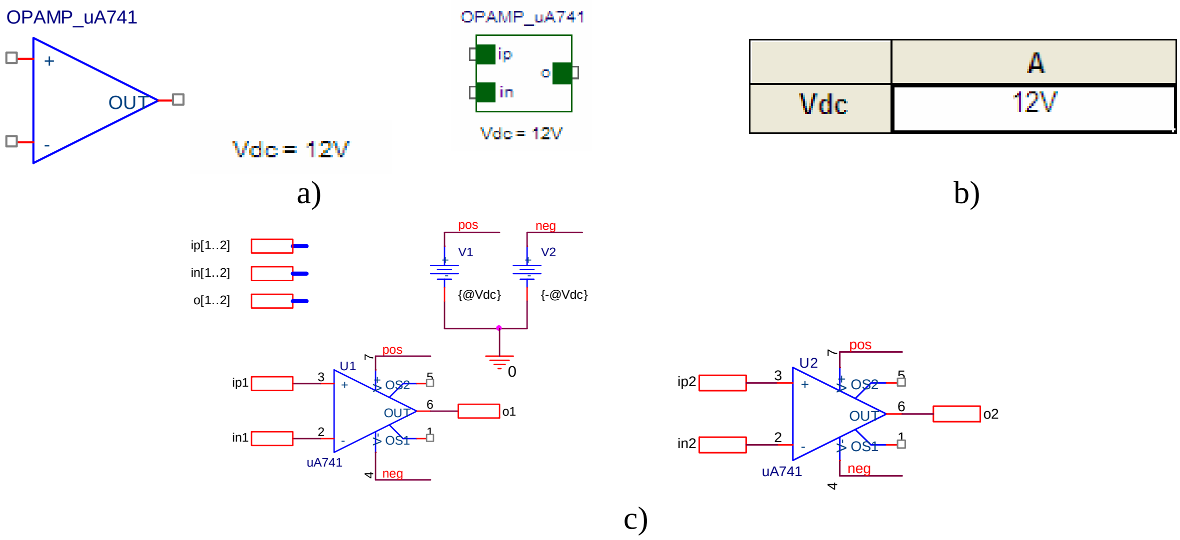

Fig. 3. Sensitivity model of the OpAmp

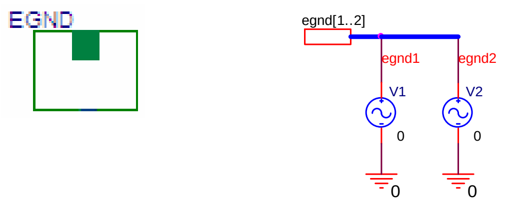

Fig. 4. Modeling the ground in the sensitivity model

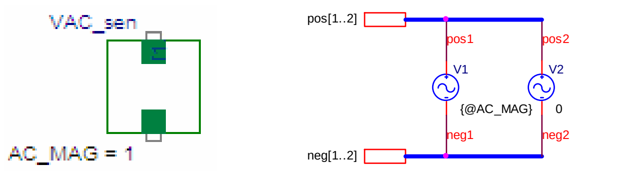

Fig. 5. Modeling the independent voltage source in the sensitivity model

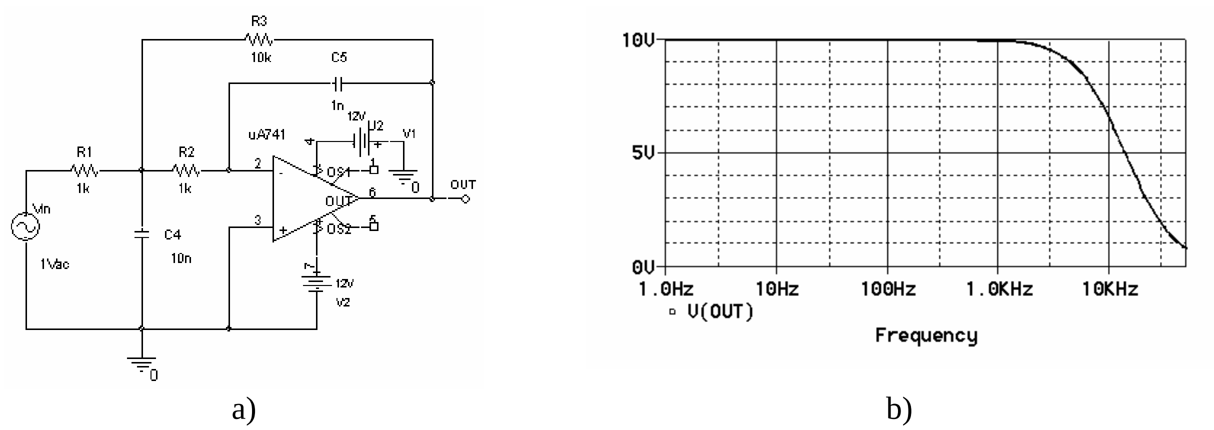

Fig. 6. Example circuit

3. OBTAINING THE SENSITIVITIES IN PROBE

The sensitivities are obtained using the following macrodefinitions in *Probe*:

SEN(p) = M(V(OUT2)@p/V(OUT1)@p)

where p is the *ID* number of the circuit element. The sensitivities SEN(1), SEN(2), SEN(3), SEN(4) and SEN(5) for the circuit in Fig. 6 are presented in Fig. 7. The measure SEN2(p1,p2) is defined giving the sum of the modules of the sensitivities S_{p1} and S_{p2}. The frequency ranges, corresponding to high values of SEN2(p1,p2), can be used to detect a double fault of elements p_1 and p_2. In the case when the sensitivity $|S_{p1}| >> |S_{p2}|$, the fault of the element p_2 can be masked. In this case another measure IND2(p1,p2) for the diagnosability investigation can be applies in the form:

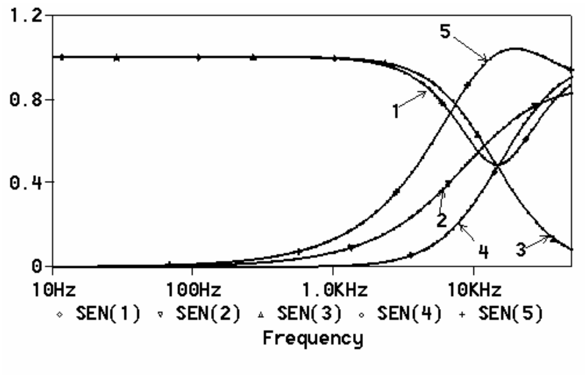

Fig. 7. First order sensitivities

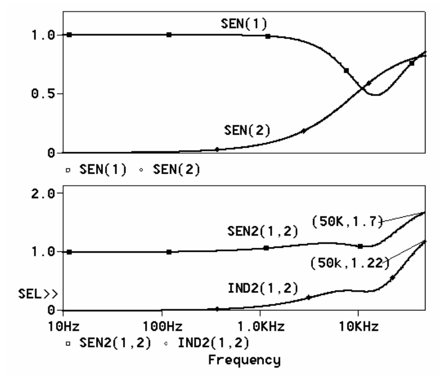

Fig. 8. Diagnosability of double faults

IND2(p1,p2) = (M(SEN(p1))+M(SEN(p2)))*M(SEN(p1))*M(SEN(p2))

The measures SEN2(1,2), INSD(1,2) are presented in Fig. 8.

The macroses for diagnosability investigation of triple faults SEN3(p1, p2, p3) and IND3(p1, p2, p3) are obtained as follows:

SEN3(p1, p2, p3) = M(SEN(p1))+M(SEN(p2))+M(SEN(p3))
IND3(p1, p2, p3) =
(M(SEN(p1))+M(SEN(p2))+M(SEN(p3)))*M(SEN(p1))*M(SEN(p2))*M(SEN(p3))

The measures SEN3(2,3,4) and IND3(2,3,4) are presented in Fig. 9. The measures SEN4(1,2,3,4) and IND4(1,2,3,4) are presented in Fig. 10.

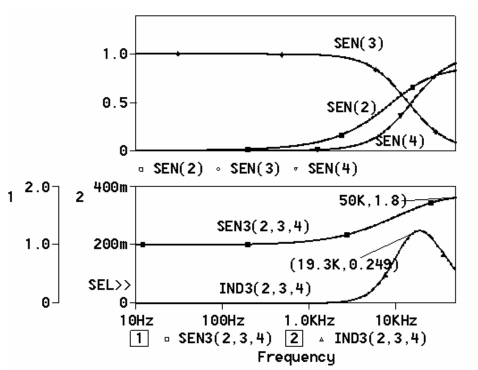

Fig. 9. Determination of the measures SEN3 and IND3

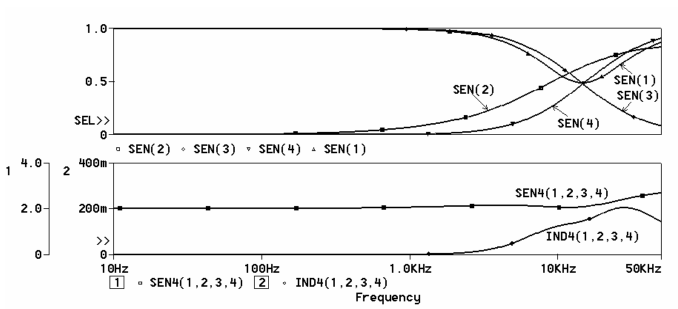

Fig. 10. Determination of the measures SEN4 and IND4

For a five-fold fault:

```
SEN5(p1,p2,p3,p4,p5)=
M(SEN(p1))+M(SEN(p2))+M(SEN(p3))+M(SEN(p4))+M(SEN(p5))
IND5(p1,p2,p3,p4,p5)=(M(SEN(p1))+M(SEN(p2))+M(SEN(p3))+M(SEN(p4))+
M(SEN(p5)))*M(SEN(p1))*M(SEN(p2))*M(SEN(p3))*M(SEN(p4))*M(SEN(p5))
```

The diagnosability can be precisely investigated using the measure *DSEN*. It is defined as the measure *SEN* for the frequency intervals, where the ratio between each of the sensitivities and the measure *SEN* is greater than a given number *eps*. The macroses for double and triple faults are in the form:

```
ena2(p1,p2)=0.5*(sgn(M(SEN(p1)/SEN2(p1,p2))-
eps)+1)*0.5*(sgn(M(SEN(p2)/SEN2(p1,p2))-eps)+1)
DSEN2(p1,p2)=SEN2(p1,p2)*ENA2(p1,p2)
ena3(p1,p2,p3)=0.5*(sgn(M(SEN(p1)/SEN3(p1,p2,p3))-
eps)+1)*0.5*(sgn(M(SEN(p2)/SEN3(p1,p2,p3))-
eps)+1)*0.5*(sgn(M(SEN(p3)/SEN3(p1,p2,p3))-eps)+1)
DSEN3(p1,p2,p3)=SEN3(p1,p2,p3)*ENA3(p1,p2,p3)
ena4(p1,p2,p3,p4)=0.5*(sgn(M(SEN(p1)/SEN4(p1,p2,p3,p4))-
eps)+1)*0.5*(sgn(M(SEN(p2)/SEN4(p1,p2,p3,p4))-
eps)+1)*0.5*(sgn(M(SEN(p3)/SEN4(p1,p2,p3,p4))-
eps)+1)*0.5*(sgn(M(SEN(p4)/SEN4(p1,p2,p3,p4))-eps)+1)
```

The measures *SEN*3, *ENA*3 and *DSEN*3 for parameters p_1, p_3 and p_5 are presented in Fig. 11. Similarly, the measures *SEN*5, *DSEN*5 and *IND*5 for parameters p_1, p_2, p_3, p_4 and p_5 are obtained as shown in Fig. 12.

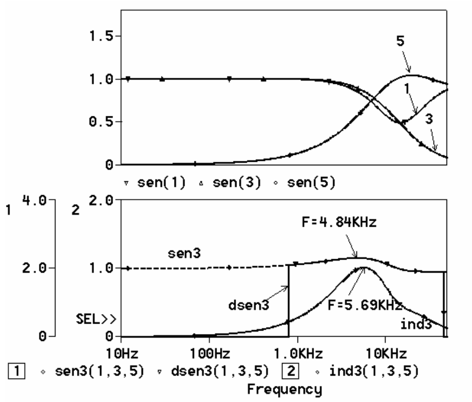

Fig. 11. Comparison of the diagnosability results using the measures SEN3, DSEN3 and IND3

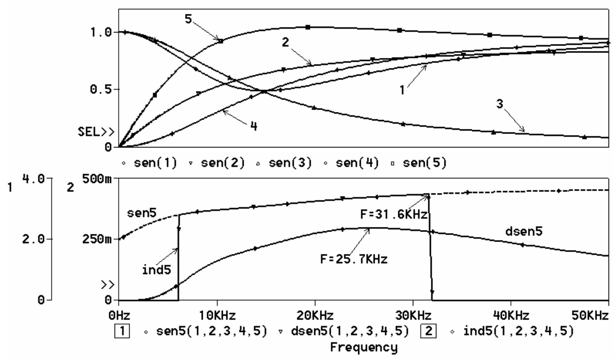

Fig. 12. Diagnosability results using the measures SEN5, DSEN5 and IND5

4. CONCLUSIONS

A computer-aided approach has been proposed to diagnosability investigation of linear analog circuits based on sensitivity investigation of the test characteristics. Using parameterized sensitivity *PSpice* macromodels, the sensitivity is obtained in the frequency domain and sensitivity measures are defined in *Probe* for diagnosability investigation of multiple faults using pre-defined macrodefinitions. The frequency ranges, corresponding to maximal sensitivity measures, are automatically obtained for the multiple fault isolation.

5. ACKNOWLEDGEMENT

The investigations are supported by the project 091ni041-03/2009 with the R&D sector of the Technical University of Sofia.

REFERENCES

[1] I. Sylla and M. Slamani, "Improving Design and Fault Detection in Linear and Nonlinear High Frequency Circuits by Performing a Sensitivity Based Analysis", Analog Integrated Circuits and Signal Processing, Kluwer Academic Publishers , v. 27, pp. 249–260, 2001

[2] M. Slamani and B. Kaminska, "Fault observability analysis of analog integrated circuits in frequency domain." IEEE Transactions on Circuits and Systems, pp. 134–139, February 1996.

[3] E. Dimitrova, E. Gadjeva, A. Van den Bossche and V. Valchev, "A Model-Based Approach to Automatic Diagnosis Using General Purpose Circuit Simulators, 2006 IEEE International Symposium on Industrial Electronics,9-13 July 2006, Vol. 4, pp 2972-2977, Montreal, Que., Canada.

INVESTIGATION OF RESIDUAL CURRENT DEVICES (RCD) IN HIGH FREQUENCIES

Jordan Shopov*, Simona Petrakieva**

* Department of Electrical Apparatus, Technical University of Sofia,
1156 Sofia, Bulgaria, E-mail: shopov@tu-sofia.bg

** Department of "Theoretical Electrical Engineering", Technical University of Sofia,
1156 Sofia, Bulgaria, E-mail: petrakievas-te@tu-sofia.bg

Abstract: *In the paper, the results from the investigation and analysis of the working process of the breakers for residual currents in the frequencies different than 50 Hz, are presented. The main aim of the investigation is to estimate the applicability of the breakers considered in the systems consist of modern converting devices and its protective measures from the electric current breaking in the frequencies over than 50 Hz.*

Keywords: electrical safety, residual current devices

1. INTRODUCTION

The applicability of the electrical devices and systems, which transform some electrical quantities to the others (with respect to their values or parameters), increases as in the industry as in the home appliances. These devices are such as rectifiers, invertors, UPS systems, power control systems with semiconductors' elements, modern home electronic devices and etc. Nowadays the complex control systems, where the voltage, the frequency and etc. transforms repeatedly, are used. The most popular are electrical devices, working with frequencies over than 50 Hz (resp. 60 Hz).

The equipments, working with frequency 50 Hz (resp. 60 Hz), the reliability safety systems (Residual Current Devices - RCD) are made. The requirement rules about these devices are defined in the regulation N 3 "Structure and exploitation of the electrical equipments and electro-conductive lines" – from 15.01.2005. The regulation specifies the fact that the installations of the RCD is binding in the new or reconstruct residential, administration buildings and public works.

The serious problems, guaranteed the electro-safety[1], arise in the equipments, included to the converters, working with the frequencies, which are different than 50 Hz (resp. 60 Hz). This fact specifies the aim of the investigation in this paper – to check if it is possible and how much the RCD can to ensure the safety of the users when the devices works with frequencies different than 50 Hz (resp. 60 Hz).

---

[1] For industrial applications, where the working frequencies are previously known, the leaders' manufactures of the residual current devices (ABB, Schneider Electric, Moeller, Siemens) are developed the special safety apparatuses, ensuring the electrical safety in emergency situations.

As it is well known the RCD consist of summing transformer, polarization turning off relay with a high sensitivity, switching off mechanism with contact system and control circuit (fig. 1). All conductors pass through the orifice of the summing transformer (L1, L2, L3 and N for the 3-phase circuits or L and N for the mono-phase circuits). In normal mode the sum of the respective currents' vectors, passed through the summing transformer, is equal to 0 or it is so slightly small the polarization relay cannot switch over.

When arises trouble (leak to the Earth or touch to the current-carrying parts of the device and etc.), if the current flow through to the Earth or to the safety conductor PE, the sum of the currents vectors becomes different by 0. In this case the electromotive voltage induces in the sensor coil. This voltage supplies the polarization relay and as a result the switching off mechanism activates. This opens the contact system of the RCD and the supplying voltage to the defect part of the circuit interrupts.

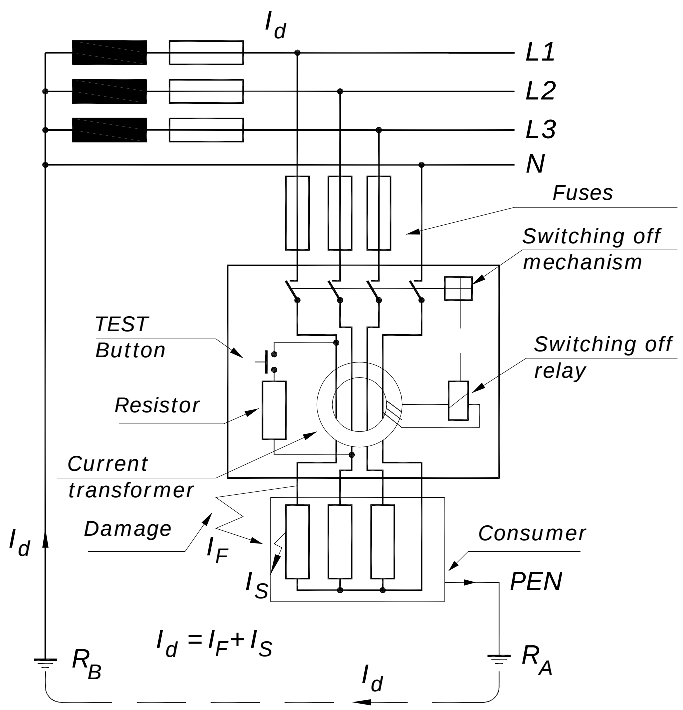

Fig. 1

2. SUBJECT AND PROBLEMS OF THE INVESTIGATION

The subject of the investigation is the behavior of the residual current device (RCD) in frequencies which are different than 50 Hz (resp. 60 Hz). For collecting the necessary data and for their analysis the following problems are solved:

1. Creating the experimental base.
2. Examination the RCD in frequencies, which are different than 50 Hz (resp.60 Hz).
3. Presentation of the results in tables and the respective graphs.
4. Analysis of the results and making the conclusions.

3. EXPERIMENTAL INVESTIGATIONS

The investigations are implemented using the following apparatus:

- residual current device type FH204 (I=25 A, I_n=0,03 A, U_{max}=440 V⊔);
- residual current device type NL1-63 (I=63 A, I_n=0,03 A, U_{max}=660 V⊔);
- residual current device type LS 25A 2P (I=25 A, I_n=0,03 A, U_{max}=440 V);
- residual current device type SE 63A 2P (I=63 A, I_n=0,03 A, U_{max}=660 V);
- signal generator type 83-33 - [20, 20000] Hz;
- digital multimeter type WENS 700;
- digital multimeter type DT830D;
- regulated resistance.

4. SCHEME OF THE EXPERIMENTAL BASE

The experimental base is designed for investigation of the mono- and three-phase residual current devices. The scheme allows investigation of its working process as in different from 50 Hz frequencies as in pulse disturbances with different form or these disturbances which has DC component. The experimental base is shown on the fig. 2.

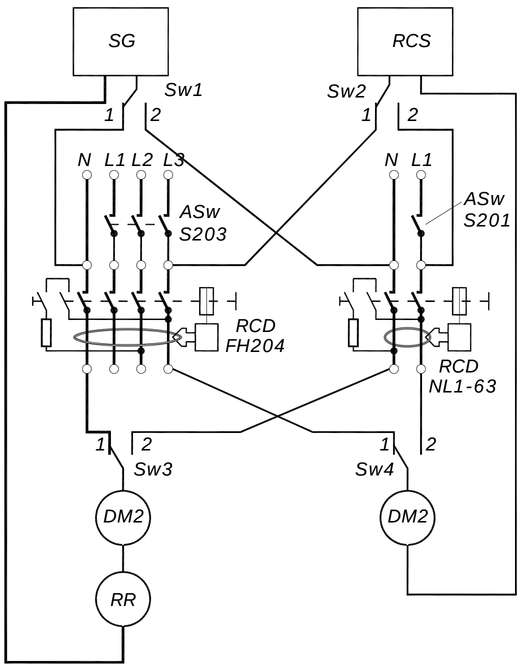

Fig. 2. Scheme of the experimental base

- *SG* – signal generator for the sinusoidal, rectangular and triangular type voltage - type 83-33, range [20-20000] Hz;
- *RCS* – stabilized regulated current supplier generating DC component U=0-12 V DC, I=0-1 A/DC (not used in this case);
- *Sw 1÷4* – two-positions electrical switchers;
- *ASw* – automatic switchers - 6A;

– *DM 1,2* – digital multimeters;
– *RR* – regulated resistance.

It makes 5 measurements for each frequency considered and then it calculates the respective average value of the switching over current I_d.

$$I_d = \frac{I_{d1} + I_{d2} + ... + I_{dp}}{p},$$

where p is the number of the measurements in the same frequency.

Next, the associated graph $I_d = I_d(f)$ draws.

The data from the measurements are given in tabl. 1 and they are visualized on fig. 3. In the table, each of the average value for the respective fifth measurements I_d and the nominal value of the current necessary for switching over of the RCD, are presented.

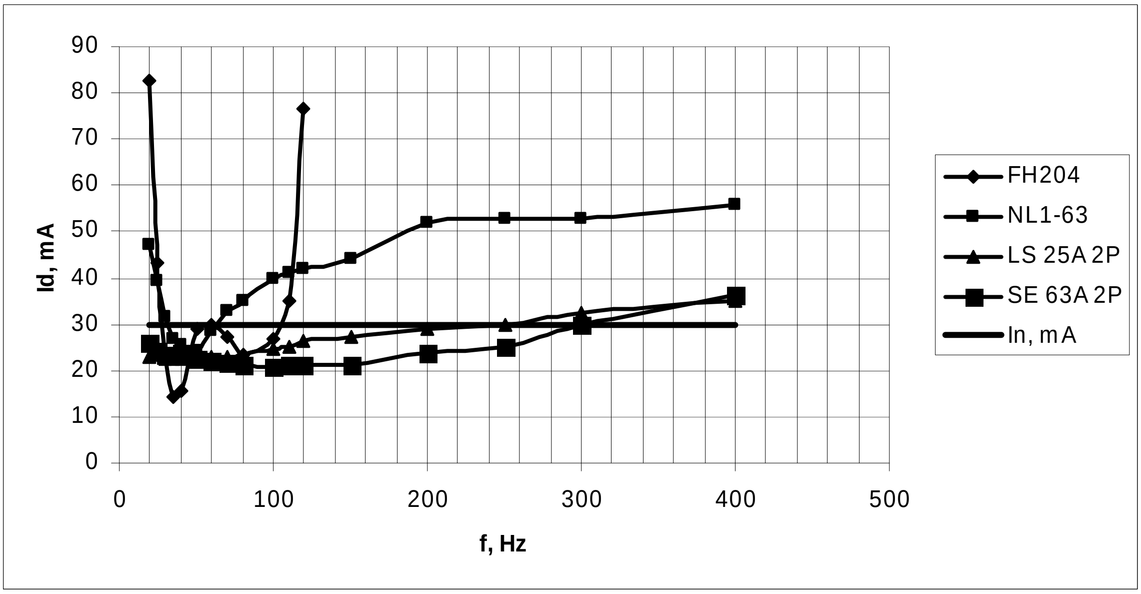

Fig. 3. Switching over current of the RCD in different frequencies

Table 1 and the respective graph from fig. 3 show the work of fourth studied types RCDs when it considers the switching over current in the different frequencies in the range [20, 400] Hz.

Table 1. Switching over current of the RCD in different frequencies

Measurment	FH204	NL1-63	LS 25A 2P	SE 63A 2P	Dimension
20Hz (AC)	82,80	47,10	23,06	26,04	mA
25Hz (AC)	43,10	39,30	23,2	24,11	mA
30Hz (AC)	23,10	31,70	22,6	23,36	mA
35Hz (AC)	14,20	27,00	22,6	23,5	mA
40Hz (AC)	15,70	25,60	22,64	24,0	mA
50Hz (AC)	29,10	24,10	22,42	22,64	mA
60Hz (AC)	29,70	28,60	22,8	22,2	mA

70Hz (AC)	27,20	33,00	23,12	21,8	mA
80Hz (AC)	23,40	35,00	23,5	21,35	mA
100Hz (AC)	27,00	39,60	24,5	20,9	mA
110Hz (AC)	35,00	41,00	25,1	21	mA
120Hz (AC)	76,80	42,00	26,3	21,12	mA
150Hz (AC)	*over*	44,00	27,1	21,12	mA
200Hz (AC	*over*	52,10	28,94	23,7	mA
250Hz (AC)	*over*	52,60	29,96	25,3	mA
300Hz (AC)	*over*	52,60	32,3	29,9	mA
400Hz (AC)	*over*	56,00	35,14	36,4	mA

5. CONCLUSIONS

- The implemented detailed investigation of the behavior of the residual current devices show, that they work reliable when the supplying currents, voltages and frequencies are the same as they are designed.
- When the frequency is 50 and 60 Hz and the DC components is missing, the RSDs switch off when the current reaches the "safety" value 30 mA.
- When the frequencies are upper than mentioned above, the mechanical characteristics and the parameters of the polarized relay, control the switching off process, essentially influent on their electrical characteristics.
- The RSDs considered show the different behavior when they work in the frequencies different than 50 Hz.
- The models FH204 and NL1-63 cannot ensure the reliable safety in these frequencies.
- The other ones (LS 25A and SE 63A) have the stability characteristics till the frequencies of 250 Hz and they can be applied only in some specifically cases. They can ensure the reliable safety in case of fire, because the restriction is 300 mA. They work excellent in the range 30 – 70 Hz. In frequencies down than 30 Hz and up than 70 Hz these types RDS are not recommended.
- In frequencies till 1 kHz and above are recommended the models, which are designed just for this mode.

REFERENCES

[1] ABB - „Technical catalogue – System pro M compact and other modular devices for low voltage installation", Edition 2007-2008

[2] ABB - „Ръководство и технически каталог System Pro M", Edition 2007 г.

[3] „Ръководство по електрически инсталации", АББ, България ЕООД.

[4] „Устройства защитного отключения управляемые дифференциальным током" – Moeller, 2004 г.

ANALYSIS OF PARTIAL DISCHARGES

Nikolina Petkova

Department of Theoretical Electrical Engineering, Technical University of Sofia, 8 Kliment Ohridski blvd., 1000 Sofia, Bulgaria, phone: +3599652498, e-mail: npetkova@tu-sofia.bg,

Abstract: One of the most important criteria for the power transformer's state is the presence of partial discharges. Electric discharges that do not completely bridge the electrodes are called "partial discharges". Although the magnitude of such discharges is usually small, they cause progressive deterioration and may lead to ultimate failure. It is therefore essential to detect their presence in a nondestructive control test. The methods for discovering and evaluating the partial discharges are based on the power exchange, which comes simultaneously with the discharge. This exchange can be found at AC or DC voltage.

1. DISCHARGES AT AC VOLTAGE

The behavior of *internal discharges* at AC voltage can be described using the *a-b-c* circuit (Fig. 1a). The capacity of the cavity is represented by a capacitance *c,* which is shunted by a breakdown path. The capacity of the dielectric in series with the cavity is represented by a capacitance *b.* The sound part of the dielectric is represented by capacitance *a.*

In Fig. 1a, the faulty part of the dielectric corresponds to I, the sound part to II.

The same representation can be given for *surface discharges* as may follow from Fig.1b. The surface that is covered by the discharge has a capacity *c* to the electrode and a capacity *b* through the insulation. The rest of the dielectric is again represented by capacity *a.* [3]

If such circuits are energized with AC voltage, a recurrent discharge occurs: *c* is capacitive charged, reaches the breakdown voltage of the cavity, is charged again, breaks down, etc.

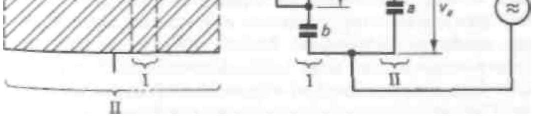

Fig.1a. Dielectric circuit

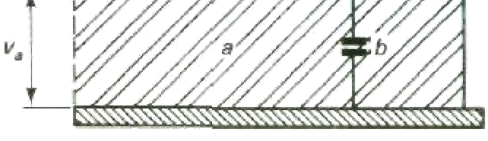

Fig. 1b. Dielectric circuits with internal discharge surface discharges

1.1. Recurrence of discharges

This is shown in more detail in Fig. 2. The high voltage across the dielectric is v_a, the voltage across the cavity, v_c. When voltage v_c reaches the breakdown voltage U^+, a discharge occurs in the cavity. The voltage then drops to V^+ (usually less than 100

V) where the discharge extinguishes. This voltage drop takes place in less than 10^{-7}s - an extremely short period compared with the duration of a 50 c/s sine wave - so the voltage drop may be regarded as a step function. After the discharge has been extinguished, the voltage over the cavity increases again.

This voltage is given by the superposition of the main electric field and the field of the surface charges at the cavity walls left after the last discharge. The fields counteract one another. When the voltage over the void reaches U^+, a new discharge occurs. This happens several times, after which the high voltage v_a over the sample decreases and the voltage v_c drops to U^- before a new discharge occurs. In this way, groups of regularly recurrent discharges will be found.

The discharges in the cavity cause current impulses in the leads of the sample. Note that these impulses are concentrated in regions where the voltage applied to the sample increases or decreases most, i.e. at the zero points. Austen and Whitehead have shown that if the voltage-drops in both half cycles are equal (i.e. $\Delta V^+ = \Delta V^-$) the impulses will give a stationary picture on a 50 c/s time base on the oscilloscope screen of a discharge detector. If $\Delta V^+ \neq \Delta V^-$, the impulses move around the time base. Austen and Whitehead actually built the analogue circuit of Fig. 1a with capacitors. They obtained discharge patterns which were similar to those in Fig. 2. [1]

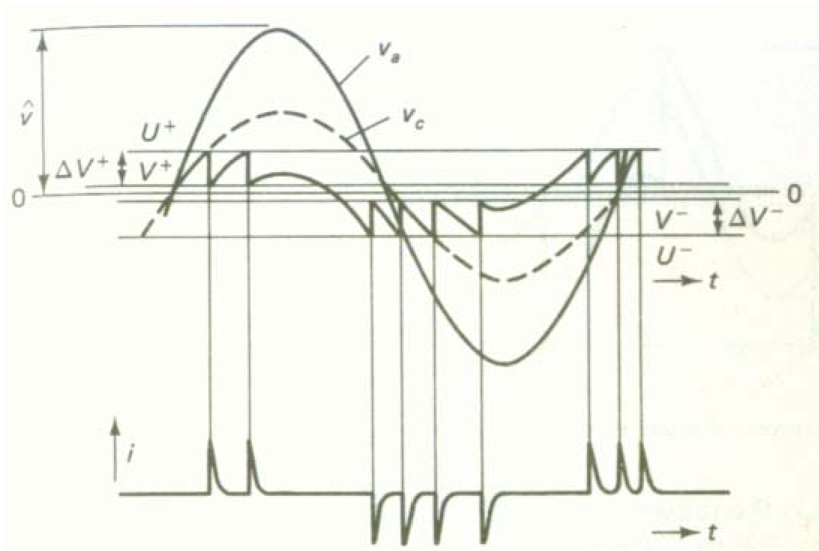

Fig. 2 Recurrence of discharges

The AC voltage across the sample at which discharges start to occur when the voltage is increased is called the inception voltage and the corresponding stress in the surrounding dielectric, the inception stress. If the voltage is decreased after discharges have been started, the voltage at which the discharges extinguish is usually lower than the inception voltage.

This voltage is called the extinction voltage and the corresponding stress the extinction stress. The breakdown strength of the cavity U^+ or U^-, is sometimes called the ignition voltage of the cavity.

1.2. Discharges occurring below the inception voltage

Once a discharge has started, it can persist at a voltage lower than the inception voltage (theoretically as low as half the inception voltage). This is shown in Fig. 3, where it is assumed that the first discharge starts due to a short overvoltage at A. The voltage v_c over the cavity - originally smaller than the ignition voltage U^+ or U^- reaches the ignition voltage at the other half cycle owing to the surface charges which are left after the preceding discharge. Now the voltage v_c and the residual charge in the cavity co-operate and the discharge can persist at almost half the inception voltage. The extinction voltage is often found in practice to be lower than the inception voltage, although not as much as half. This is the reason for samples being prestressed in many test procedures at 1.5 to 2 times nominal voltage before being turned down to a test voltage at about nominal voltage. [3]

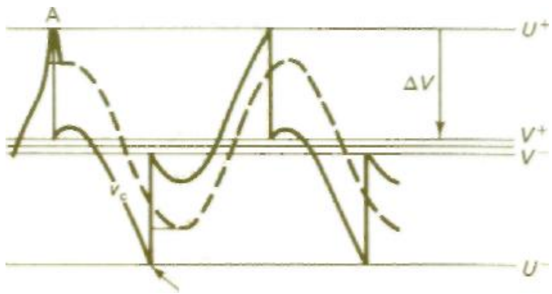

Fig. 3. Occurrence of discharges below the inception voltage

2. DISCHARGES AT DC VOLTAGE

2.1. Analogue circuit

When DC voltage is applied, discharges occur during the rise of the voltage. After the voltage has become constant, discharges occur only infrequently. The dielectric can be represented by the circuit shown in Fig.4.

The capacity of the void *c* is continually charged by the conductivity *g* of the dielectric in series with *c; c* discharges when the voltage has reached the ignition voltage of the cavity.

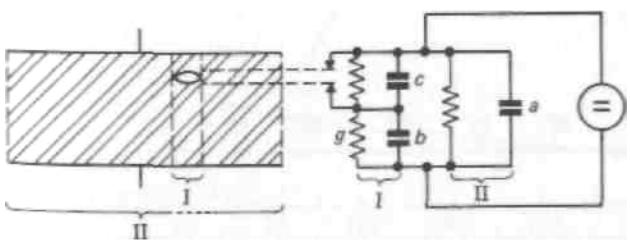

Fig. 4. Cavity in a dielectric stressed at DC voltage

2.2. Recurrence

The repetition rate under DC voltage is several orders of magnitude less than at AC voltage. As a result, partial discharges at DC are considered far less dangerous than at AC and comparatively few studies have been made of DC discharges. [2]

The repetition rate of DC discharges increases with the stress *E* in the dielectric and the specific conductivity *δ*. In the case of a laminar cavity (with zero conductivity of the cavity walls) the repetition frequency can be calculated as:

$$f = 1{,}13.10^{11}\delta\left(\frac{E}{E_i}\right), \sec^{-1} \tag{1}$$

where E_i, is the ignition stress of the flat cavity.

In practice, the repetition rate is found to be greater than predicted here. This is caused by the presence of more than one discharge site per cavity.

2.3. Variables

The repetition rate usually follows Equation (1) when changing the variables.

If the DC operating stress in the material is raised, the frequency will increase considerably, as *δ* usually increases with the applied stress.

If the temperature is increased, the repetition rate also will be increased considerably as δ increases. The repetition rate will also vary with time, as follows from the decrease in volume conductivity. [2]

The volume restivity is usually so high that at stresses where a sample shows discharges at AC voltage, discharges at DC occur at intervals which range from a few hours to several weeks. Only at very high stresses (up to 100 kV/mm DC) and high operating temperatures (90°C or so) can the repetition rate approach an order of magnitude that is customary for AC tests.

2.4. Inception voltage

The inception voltage under DC conditions is difficult to ascertain because the interval between discharges may be of the order of weeks at the theoretical inception voltage. Moreover, this low repetition rate is overshadowed by the impulses caused by the rising voltage during increase of the DC voltage. In the American Society of Testing and Materials Standard D 1868-1973 the inception voltage is reached if the repetition rate exceeds one discharge per minute. [3]

An extinction voltage cannot be defined, as discharges continue to occur for a considerable time after the applied DC voltage has been switched off.

3. CONCLUSION

Although the repetition rate of impulses at DC is lower than at AC by 10^4 to 10^5 times, the impulses themselves are the same as at AC. Duration, magnitude, wave, shape, etc. are equal to those of AC discharges. Consequently, the same detection techniques, calibration methods, observation systems etc. can be used as for AC. For this reason no special emphasis is given here to discharge detection at DC voltage.

REFERENCES

[1] A. E. Austen, S. Whitehead, "Discharges in insulation under alternating-current stresses", Proc. Inst. Elect. Eng., Pt. II, 1988

[2] S. Shihab, "Partial Discharges in Voids using HVDC" Thesis, Braunschweig, Germany, 1972

[3] F. H. Kreuger, „Partial Discharge Detection in High – Voltage equipment", Butterwords, England, 1989

CONTROL METHODS FOR SWITCHED DC/DC CONVERTERS

Ivan Mitkov Trushev, Tanya Ilieva Stoyadinova

Department of Theoretical Electrical Engineering, Faculty of Automatics,
Technical University of Sofia, 8 Kliment Ohridski St, Sofia-1000
BULGARIA, phone: +35929653319, e-mail: ivant@tu-sofia.bg

Abstract: This paper describes some of the most commonly used linear and nonlinear methods to control the switched DC/DC converters: Pulse-width modulation (PWM), Pulse-frequency modulation (PFM), Current programmed control, which are linear methods and Sliding mode control (SMC), which is nonlinear method. Conclusions are made about the advantages and disadvantages of each method.

Keywords: switched DC/DC converter, Pulse-width modulation, Sliding mode control

1. INTRODUCTION

Battery operated portable systems such as notebooks, mobile phones etc. require signals processing functions at minimum power consumption with a strong variation in speed requirements. In digital signal processing a clear trade-off can be made between the speed and supply voltage, and supply voltages as low as 0.5V can be expected. From other side the supply voltage requirements for analog circuitry are often dictated by external signal sources and loads. The difference at the requiring levels of the supply voltage for the digital and analog circuitry imposes utilization of switched DC/DC converters. They are essential for efficient conversion of the battery voltage to various supply voltages, needed to perform every function with minimum power drain. An important goal for the converters is achieving of high efficiency.

Switched DC/DC converters are time-varying systems because of their specific switching action. They are nonlinear systems with unstable parameters and unavoidable significant interference during the operation. Therefore, to stabilize their parameters and to reduce the negative effects of switching the chosen method of control is essential.

Control methods for switched DC/DC converters require not only to ensure the stability of the system, but also to achieve good dynamic characteristics. There are basically two ways to control DC/DC converters – linear and nonlinear control. Nonlinear control often produces better results but sometimes increases the complexity of the practical implementation of the scheme.

This paper describes some of the most commonly used linear and nonlinear methods to control the switched DC/DC converters: Pulse-width modulation (PWM), Pulse-frequency modulation (PFM), Current programmed control, which are linear methods and Sliding mode control (SMC), which is nonlinear method. Conclusions are made about the advantages and disadvantages of each method.

2. PULSE-WIDTH MODULATION (PWM) CONTROL

The PWM control technique employs switching at constant frequency, i.e., *Ts=ton+toff* where *Ts* is constant time switching period and *ton* and *toff* represent the time the switch is on and off, respectively (Figure 1). By adjusting the *ton/toff* ratio the average output voltage can be controlled. This operation can be represented by the following equation

$$D = \frac{t_{on}}{T_s} = \frac{V_0}{V_i}, \qquad (1)$$

where D is duty cycle, and V_0 и V_i. are respectively the output and input voltage.

A popular solution for generation of switch control signal is to compare $v_{control}$ with a repetitive waveform. $v_{control}$ is obtained by amplifying the difference between the actual output voltage from the converter and its desired value (Fig. 1). The frequency of the repetitive waveform, represented by the sawtooth voltage in Figure 2, establishes the switching frequency [1], [2]. This frequency is kept constant in a PWM control. When the amplified error signal, which varies slowly with time relative to the switching frequency, is greater then the sawtooth waveform, the switch control signal becomes high, causing the switch to turn on. Otherwise, the switch is off.

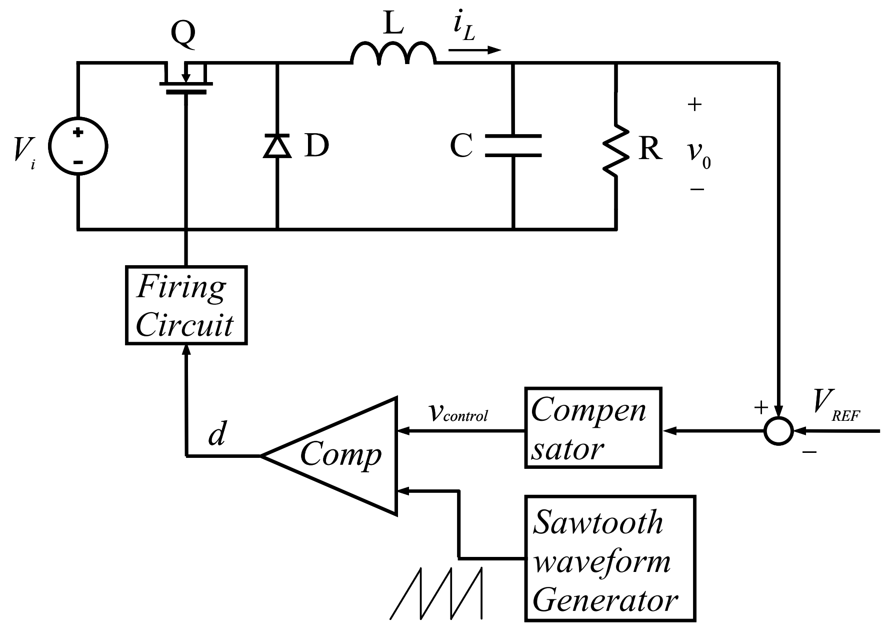

Fig. 1. PWM control scheme for buck DC/DC converter

Lower power efficiency for small load is the main drawback of this control scheme [3]. The main advantage is the use of single switching frequency, which makes the level of output ripple highly controllable.

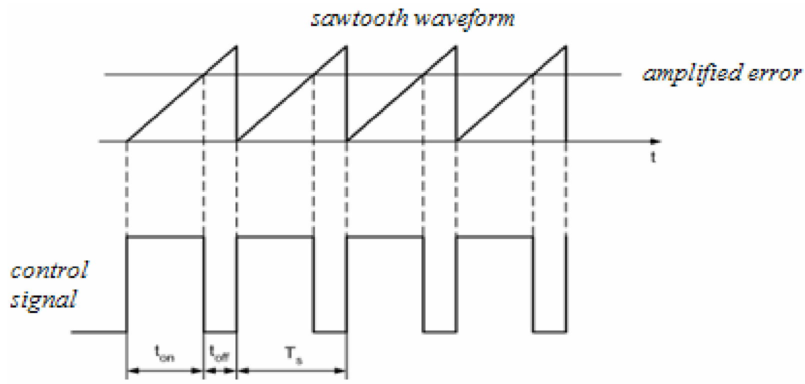

Fig. 2. Signals in control of PWM

3. PULSE-FREQUENCY MODULATION (PFM) CONTROL

One control scheme which obtains high power efficiency over a wide range of loads is pulse-frequency modulation (PFM). In this scheme, the converter is operated only in short bursts at small load as is conceptually illustrated in Figure3 and Figure4.

Between bursts, both switches in Figure 3 are turned off, and the circuit is idle with zero inductor current. During this period, the filtering capacitor at the output sources the load current. When the output is discharged to a certain threshold V_0-, the converter is activated for another burst, charging capacitor C. Thus, the load-independent losses in the circuit are reduced [3]. Further, for smaller load current the idle time increases and thereby decreases power consumption. Output is regulated when the charge delivered through the inductor is equal to the charge consumed by the load. This implies that the inductor must be designed to be able to deliver the maximum charge consumed by the load during system operation.

The major drawback of PFM control is that the switching period (the time between charge bursts) is a function of the load. Thus, the converter appears almost chaotic and the switching noise is unpredictable. This is not well suited for wireless communications applications.

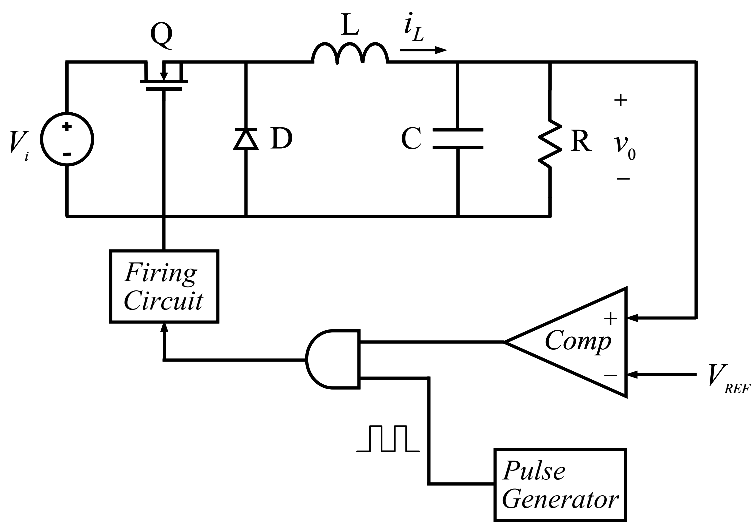

Fig. 3. PFM control scheme for buck DC/DC converter

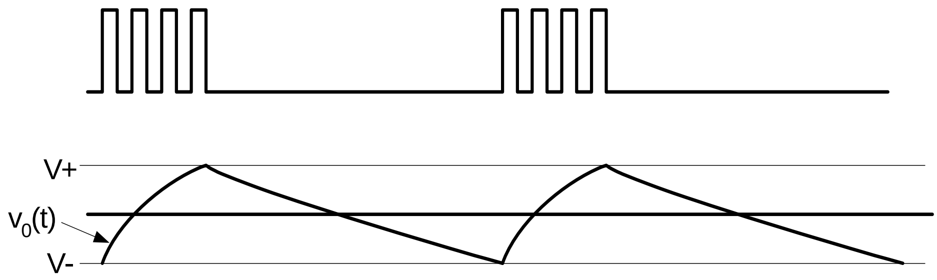

Fig. 4. Signals in control of PWM

4. CURRENT PROGRAMMED CONTROL

In current programmed control (Fig. 5), the output of the converter is controlled by a suitable choice of the peak current of the transistor switch Q [4]. Control signal in this case is $i_c(t)$, and control circuit switches the transistor so that the peak current through the transistor follows current $i_c(t)$ (Fig. 6).

Cycle pulse on the input "SET" of the RS-trigger opens the switching period in determining the outcome of the trigger in a high level, and transistor is switching on. While the transistor conducts, its current $i_s(t)$ is equals the current through the coil $i_L(t)$, which grows in a positive direction with a slope depending on the value of coil (L) and voltage of the converter. At a point where $i_s(t)$ becomes equal to $i_c(t)$ the control scheme produces a signal to switch off the transistor and current through the coil decreases during the remainder of the period of switching. In practice, voltages proportional to the currents $i_s(t)$ and $i_c(t)$, with constant of proportionality R_f are compared. The comparator resets triggers when $i_s(t)>i_c(t)$.

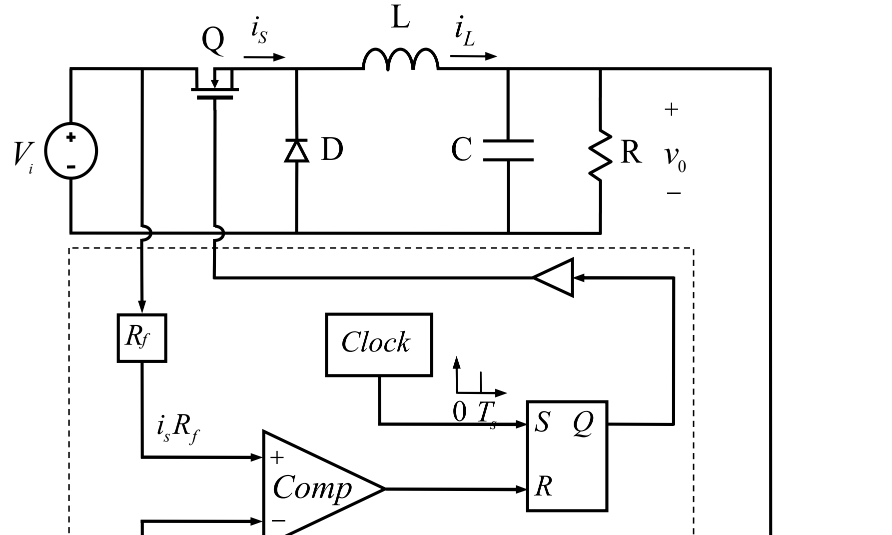

Fig. 5. Current programmed control scheme for buck DC/DC converter

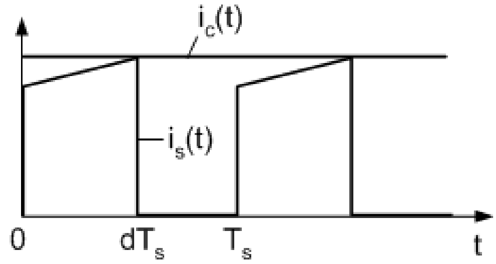

Fig. 6. Signals in control of current programmed control

Feedback can be constructed to regulate the output voltage *v(t)*. It is compared with voltage $v_{ref}(t)$ and generates an error signal which is fed to the entrance of the compensation scheme, the output of which receives control signals $i_c(t)R_f$.

The main advantage of this type of control is simplified dynamics of the scheme, because of one pole less. Indeed the pole is moved to high frequencies near the switching frequency of the converter.

One disadvantage of this control method is sensitivity of the currents $i_s(t)$ and $i_c(t)$ to noise. Moreover, control scheme with programmed current is unstable when the duty cycle is greater than 0.5(D> 0.5), regardless of its topology. Therefore, for stable operation of the current programmed control scheme the duty cycle not exceed 0.5. Stabilization can be achieved by artificially added signal with a specified slope [4].

5. SLIDING MODE CONTROL (SMC)

In sliding mode control the controller [5], [6], [7], employs a sliding surface or line to decide its control input states *u*, which corresponds the turning on and off the power converter's switch, to the system:

$$S = \alpha x_1 + x_2 \tag{2}$$

where *α* is a positive quantity in some literature called a convergence factor and is taken to be

$$\alpha = \frac{1}{R_L C} \tag{3}$$

Graphically the sliding line is a straight line on the state plane with gradient *α* that determines the dynamic response of the system in sliding mode with a first order time constant $\tau = 1/\alpha$.

To ensure that a system follows its sliding surface, a control law must be imposed:

$$u = \begin{cases} 1 = 'ON' & when\ S > 0 \\ 0 = 'OFF' & when\ S < 0 \end{cases} \tag{8}$$

The existing condition for sliding mode [2], [6] is:

$$\dot{S} = \begin{cases} \dot{S} < 0 & for\ S > 0 \\ \dot{S} > 0 & for\ S < 0 \end{cases} \tag{9}$$

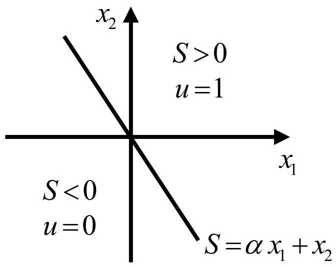

Fig. 7. A diagram of sliding mode control

Based on this we get the following expression for $\dot{s}$:

$$\dot{S} = \alpha\dot{x}_1 + \dot{x}_2 = \alpha x_2 + \dot{x}_2 = \alpha x_2 - \frac{\beta}{LC}(uV_i) - \frac{1}{LC}x_1 - \frac{1}{R_L C}x_2 + \frac{V_{ref}}{LC} \tag{10}$$

Depending on S and u the state space is divided into two regions:
region 1: $S > 0$ and $u = 1$

$$\dot{S}_1 = \left(\alpha - \frac{1}{R_L C}\right)x_2 - \frac{\beta}{LC}(uV_i) - \frac{1}{LC}x_1 + \frac{V_{ref}}{LC} < 0 \tag{11}$$

region 2: $S < 0$ and $u = 0$

$$\dot{S}_2 = \left(\alpha - \frac{1}{R_L C}\right)x_2 - \frac{1}{LC}x_1 + \frac{V_{ref}}{LC} > 0 \tag{12}$$

Sliding mode will only exist on the portion of the sliding line that covers both of the region 1 ($\dot{S}_1 < 0$) and region 2 ($\dot{S}_2 > 0$) [8].

From one side the speed of the system increases with increasing of α (sliding line become steeper), but from other side the existing region of the sliding mode decreases that can cause an overshoot in the voltage response ($\alpha >> 1/R_L C$) [8].

The basic operation of the sliding control is shown in Figure 8 where the output voltage, V_0, is the regulated output. The comparator switches the input to the buck converter based on the polarity of the compensator output. Unlike in PWM regulators, the switching frequency of the buck converter with sliding control is not fixed by an external source and is a function of V_{ref}. The feedback is highly nonlinear due to the comparator. However, this kind of system can be intuitively understood by its phase portrait, as shown in Figure 9.

The buck converter contains two poles, so the feedback loop is a second-order system. The phase portrait in Figure 9 describes the transient operation of the circuit by the time trajectories of the state variable, (V, dV/dt), with the time variable being implicit. The comparator introduces a boundary line that divides the state space into two regions. In the upper region, the input signal to the buck converter is low and the state follows the light trajectory curves. In the lower region, the input signal to the buck converter is high and the state follows the dark curves. When certain, so called sliding condition on τ is met, the trajectories from both regions point towards the boundary line, and thus the state is constrained on the line. Therefore, the system operates approximately as a first-order system with the time constant τ. This ideal sliding control law forces the switching frequency to be infinitely high. Use of comparator with hysteresis like schmittrigger solves this problem. The comparator drives the buck converter low when the compensator output is greater than +Δ, and high when it is less than -Δ. The larger the hysteresis, the lower the switching frequency and the larger the voltage ripple. Sliding control offers high power efficiency over a wide range of loads. However, as in the case of PFM, switching frequency is not constant making noise control difficult.

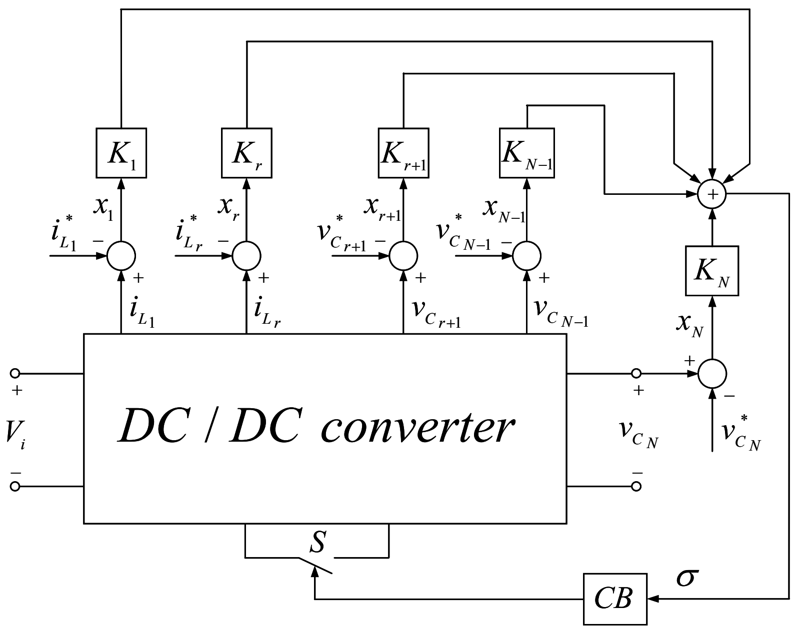

Fig. 8. Sliding mode control scheme for DC/DC converter

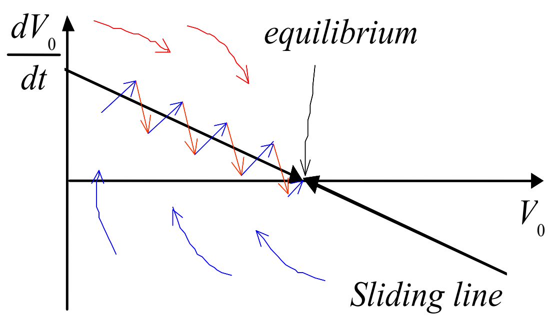

Fig. 9. Sliding mode control – phase portrait

The buck converter contains two poles, so the feedback loop is a second-order system. The phase portrait in Figure 9 describes the transient operation of the circuit by the time trajectories of the state variable, (V, dV/dt), with the time variable being implicit. The comparator introduces a boundary line that divides the state space into two regions. In the upper region, the input signal to the buck converter is low and the state follows the light trajectory curves. In the lower region, the input signal to the buck converter is high and the state follows the dark curves. When certain, so called sliding condition on τ is met, the trajectories from both regions point towards the boundary line, and thus the state is constrained on the line. Therefore, the system operates approximately as a first-order system with the time constant τ. This ideal sliding control law forces the switching frequency to be infinitely high. Use of comparator with hysteresis like schmittrigger solves this problem. The comparator drives the buck converter low when the compensator output is greater than $+\Delta$, and high when it is less than $-\Delta$. The larger the hysteresis, the lower the switching frequency and the larger the voltage ripple. Sliding control offers high power efficiency over a wide range of loads. However, as in the case of PFM, switching frequency is not constant making noise control difficult.

6. CONCLUSION

The article describes some of the basic control methods for DC/DC converters. In conclusion we can say that, in most cases nonlinear control methods give better results than linear, because of nonlinear nature of the converters. Sometimes nonlinear control methods for DC/DC converters increase the complexity of practical implementation of the control scheme. However, in comparison of advantages and disadvantages of linear and nonlinear methods we conclude that although the nonlinear control as an unfamiliar and rarely used control method it gives more perspective.

REFERENCES

[1] R. W. Erickson, *Fundamentals of Power Electronics*, 1st ed. NewYork: Chapman and Hall, 1997.
[2] A. P. Dancy, A. P. Chandrakasan, *Ultra low power control circuits for PWM converters*, IEEE PESC 1999.
[3] Anthony John Stratakos, *High-Efficiency Low-Voltage DC-DC Conversion for Portable Applications*, 1998
[4] R. W. Erickson, *Fundamentals of Power Electronics*, 1st ed. NewYork: Chapman and Hall, 1997.
[5] E. Fossas and D. Biel, *A sliding mode approach to robust generation on DC-to-DC nonlinear converters*, in Proceedings,IEEE International Workshop on Variable Structure Systems, pp. 67–71, Dec 1996.
[6] C. Morel, J.-C Guignard, and M. Guillet, *Sliding mode control of DC-to-DC power converters*, in Proceedings, 9th International Conference on Electronics, Circuits and Systems, vol. 3, pp. 971–974, Sep. 2002.
[7] G. Spiazzi and P. Mattavelli, *Sliding-mode control of switched mode power supplies*, Ch. 8, The Power Electronics Handbook, Boca Raton FL: CRC Press LLC, 2002.
[8] V.I. Utkin, *Sliding Modes in Control and Optimization*, Springer-Verlag, 1992.

MODELING AND VERIFICATION APPROACH BASED ON IEC 61499 FUNCTION BLOCKS

Desislava Ivanova*, Idilia Batchkova, Georg Frey*****

*Computer Systems Department, Technical University of Sofia, Bul. "Kl. Ohridski"8, 1000 Sofia, Bulgaria, e-mail: d_ivanova@tu-sofia.bg

**Industrial Informatics Department, University of Chemical Technology and Metallurgy, Bul."Kl. Ohridski"8, 1000 Sofia, Bulgaria, e-mail: idilia@uctm.edu

***Automation Department, Saarland University, D-66123 Saarbrücken, Germany, e-mail: georg.frey@aut.uni-saarland.de

Abstract: *Component based automation is a very promising technique in achieving reconfigurable control systems. To support the development of such systems new rapid, high-quality and cost-effective approaches for their design and maintenance are needed. On the base of an analysis of the latest trend in industrial automation such as the IEC 61499 standard and in the software engineering such as formal techniques, a new approach for their integration is proposed. A formal modelling approach based on Signal Interpreted Petri Nets and formal methods for verification using NuSMV tool are combined in order to model and verify the IEC 61499 based basic function blocks.*

Keywords: formal modeling, verification, IEC 61499 function blocks

1. INTRODUCTION

The global market competition is changing the manufacturing from mass production to mass customization that requires the concept of agile manufacturing. The development of agile manufacturing systems is supported by the rapid development of ICT and allows the manufacturing of the right products and their distributions at the right places in the right time and to the right people. To achieve an agile manufacturing, reconfigurable control systems are needed and should be developed and used. The Component Based Automation (CBA) seems a very promising technique in achieving these goals.

There are different approaches supporting the development of component based control systems. The most appropriate and most used are UML and JAVA based applications but until now they are more suitable for design of soft real time applications. Many hybrid approaches are known too. As the Component Based Software Engineering (CBSE) has become a relevant approach for building software systems, people already pay more attention on how to develop a component-based system in a rapid, high-quality and cost-effective way. Of utmost importance towards these trends is to enforce the standardization processes in automation domain. In this connection the new standard for development of distributed process measurement and control systems IEC 61499 may play a crucial role in achieving the goal of CBA. The methodology suggested in the standard allows the development of modular, reusable, open and vendor independent distributed control applications, characterized through the three main features: interoperability, portability and configurability.

One of the main disadvantages of IEC 61499 is the absence of formal semantic for describing control applications. This makes the validation and verification processes of designed control systems difficult. One way to overcome this shortcoming is to involve formal modeling and verification approaches in the development processes. These approaches are hardly studied in the field of software engineering and can be adapted in the control domain.

The main purpose of the presented work is to investigate the compatibility of Signal Interpreted Petri Nets (SIPN) as a formal modeling language and NuSMV as a formal verification tool to model and verify IEC 61499 based basic function blocks.

The paper is organized as follows: In the next Section IEC 61499 specification and Execution Control Chart (ECC) are shortly introduced. The third Section describes the proposed research framework, and is followed by a short overview of SIPN and their transformation to IEC 61499 based function blocks. In the next Section the SMV code generated from the Execution Control Chart (ECC) of the function block and NuSMV tool are used in order to verify the designed control. All the tasks are solved using the benchmarking example of an air compressor system [1]. Finally some conclusions with respects to the future work are made.

2. IEC 61499 AND STATE OF THE ART RESEARCH ACTIVITIES

2.1. Basics on IEC 61499

IEC 61499 standard defines the basic concept and methodology for design of reusable and component based control systems.

The component model proposed in this standard is based on the basic function block concept (Fig.1). The basic function block is presented by an input and an output interface composed of input and output events and data. The internal view of a basic function block includes an Execution Control Chart (ECC), internal data and internal algorithms. The ECC is a state machine used to control the execution of algorithms associated to the function block. A function block is characterized by its type name and instance name, which are used to identify a function block, the event and data inputs and outputs are required for the interconnection of different function blocks to function block systems, while the ECC, internal data and internal algorithm describe the internal behaviour of the function block.

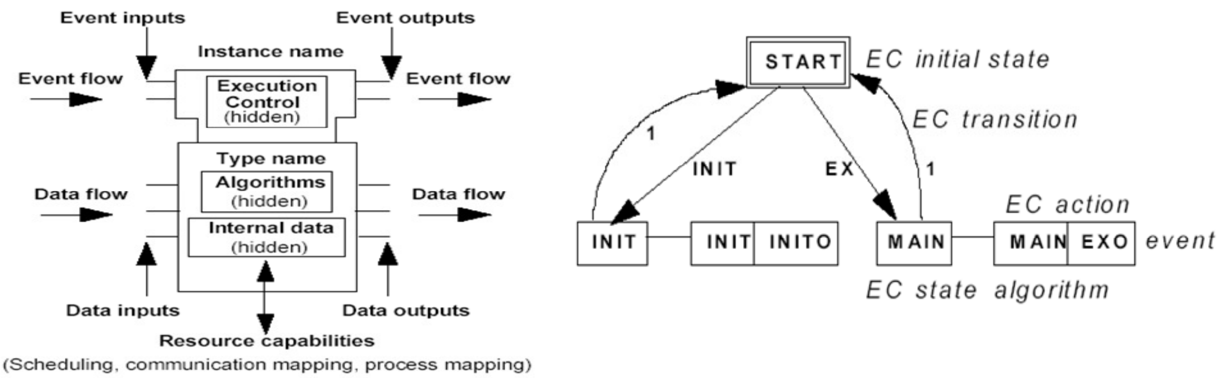

Fig. 1. Structure of a basic function block and associating Execution Control Chart state machine

The kernel of the function block is its Execution Control Chart, which consists of states, transitions and actions and invokes the algorithm execution in response to event inputs (Fig.1). Algorithms are associated to the ECC states. One of the states is the initial state, which has not execution control action. Every one of the other execution control states may have one or more execution control actions associated. Each execution control action may include one algorithm or one output event associated. The evolution of the ECC state machine from an execution control state to another is realized by the execution control transitions, described by conditions, referring to an input event arrival or to an input or an internal data value change.

2.2. State of the art

There are several research groups worldwide working in the direction of formal modeling and verification of IEC61499 compliant applications. Different formal modeling and verification techniques are used to model and check different aspects of IEC61499 based functionality and networks. Hanisch and Vyatkin [4, 5] are using the modular formalism of Net Condition/Event systems (NCES), which helps to obtain models with modular structure very similar to that of the original source. The verification task is solved via model checking based on VEDA (Verification Environment for Distributed Application) and SESA (Signal/Event System Analyser) tools. They check the reachability of dangerous states, search for never executable codes and validation of input/output specifications. The research of Wurmus is also based on an extension of Petri nets namely C-Net. The aim of his verification is oriented to the synchronization of the blocks and the absence of deadlocks. Lastra propose modeling formalism using Time Net Condition/Event Systems (TNCES). Their approach translates the LD instruction set in TNCES and the verification of plant model is realized by model checking combining iMATCH and SESA. Another approach suggested by Faureis based on the synchronous data flow language SIGNAL where the formal models are presented in terms of polynomial dynamical equation systems, and the verification provided via SynDEx tool is done using the theory of algebraic geometry representing all the concepts of the IEC 61499 Specifications as signals. Finally Marius Stanica investigates the application of timed automata for formal modeling the dynamical behavior of a controller represented as an IEC61499 basic function block.

Models for processing and clearing of input events, algorithm scheduling and ECC invocation are presented. The formal verification is supported through the tool UPPAAL that allows model checking regarding execution time and coherence of output/input actions.

3. RESEARCH FRAMEWORK

The main aim of the proposed research is to investigate the compatibility of SIPN as a formal modeling approach for describing the functionality and architecture specified in IEC 61499 and to prove the integration suitability of NuSMV tool for Formal Verification purposes in an IEC 61499 based application.

The tasks, which are solved, are shown in Fig.2. The first task is to use the SIPN editor for describing the behaviour of a control application in the algorithm level recording IEC 61499. The next task includes the transformation of SIPN model to IEC 61499 compliant XML. The third task is to build the SMV code from ECC of the IEC 61499 function block, which is specified with Function Block Development Kit (FBDK). The last task is connected with the investigation of verification capability by using NuSMV tool.

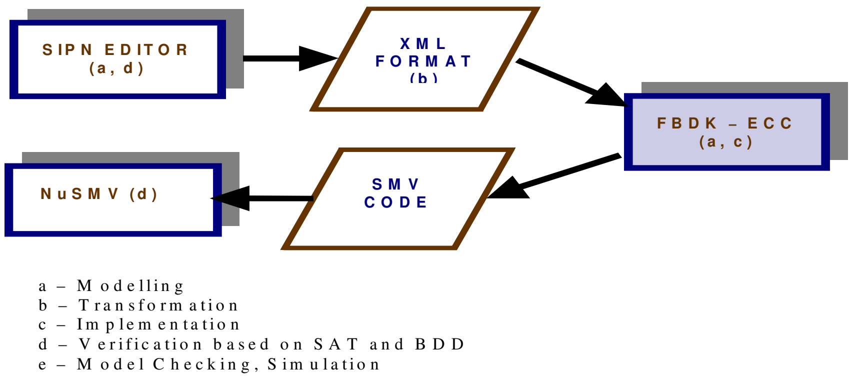

Fig. 2. Research framework

4. FORMAL MODELING OF IEC 61499 BASIC FUNCTION BLOCKS USING SIPN

4.1. Short overview of SIPN

SIPNs are an extension of ordinary place/transition net with input and output elements. Graphically, they have two basic types of nodes, i.e. places and transitions, connected through directed arcs. The places are associated with the output signals, and the transitions are labelled by Boolean expressions of input signals, which serve as firing conditions. An SIPN is described by a 10-tuple expression (1), [1].

$$SIPN = (P, T, F, m_0, I, O, \varphi, \omega, \Omega, \nu)$$

- » (P, T, F, m0) is an ordinary Petri net with places P, transitions T, arcs F, and binary initial marking m0, with $|P|, |T|, |F| > 0$;
- » I is a set of input signals with $|I| > 0$;
- » O is a set of output signals with $I \cap O = \emptyset$, $|O| > 0$;
- » φ is a mapping associating every transition $ti \in T$ with a firing condition $\varphi(ti)$ =Boolean function in I;
- » ω is a mapping associating every place $pi \in P$ with an output $\omega(pi)$. The output is assigned as an interval over the corresponding domain of the output signal (2). This interval definition includes as special cases an unspecified output (don't care) and the specification of a single value.
- » $\omega(pi)$: $O \rightarrow ([v1,l, v1,h],\dots, [v|O|,l ,v|O|,h])$
- » $vi,l \leq vi,h$ and $vi \in$ domain (Oi).
- » Ω is an output function which combines the output ω of all marked places.
- » ν is a variable definition, which assigns a numeric data type according to IEC61131 (e.g. BOOL, INT, REAL) to every signal $s \in I \cup O$.

The dynamic behaviour of an SIPN is given by the flow of tokens through the net i.e. the change of its marking. This flow is enabled by the transitions firing. The firing of a transition ti removes a token from each of its pre-places and puts a token on each of its post-places.

In this early research stage a formal modelling technique based on SIPN is used in order to investigate its compatibility for describing the behaviour of a control application at the algorithm level according IEC 61499 standard specifications. As a control application the benchmarking example of air compressor control system is selected [15].

4.2. Air Compressor Control System

An air compressor is applied to supply the compressed air for the consumers. The consumers can draw off the compressed air via a valve from the air chamber. Two binary sensors ps1 and ps2 are used to monitor the pressure in the chamber. Via two compressor motors Ma and Mb, air can be fed into the chamber. Another two binary sensors Dist_Ma and Dist_Mb are used to detect the disturbance of the motors. The system is depicted in Fig.3.

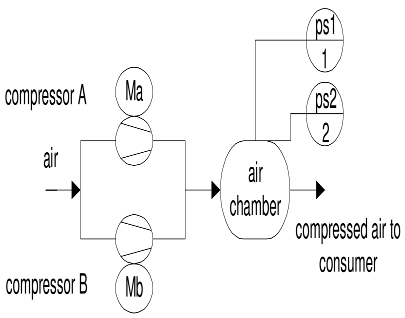

No	Sensors	Description	Actuator	Description
1	PS1	Air pressure is under 6.1 bars	Ma	Motor A turns on
2	PS2	Air pressure is under 5.9 bars	Mb	Motor B turns on
3	Dist_Ma	Motor A is disturbed		
4	Dist_Mb	Motor B is disturbed		

Fig. 3. Schema of an air compressor and input/output signals

The developed logic controller should meet the following requirements:

1. If the pressure is less than 6.1 bars (ps1 switches on), one compressor should run;
2. If one motor is disturbed (Dist_Ma or Dist_Mb switches on), the other one should substitute it;
3. If the pressure is less than 5.9 bars (ps2 switches on), both motors should run;
4. If the pressure is greater than 6.1 bars no compressors should run.

The sensor and actuator signals are listed in Table 1. The formal model of a controller, which satisfies the above-described requirements is developed using SIPN and is shown in Fig. 5. Further the model is presented in XML format, which differs from the same used in FBDK tool. The transformation to IEC 61499 compliant XML model is done manually. This transformation should be automated later through appropriate mapping rules. This way the FBDK tool from Holobloc Incorporation may be used to implement the application on the lower level.

In our framework the SIPN example of air compressor is realized in algorithm REQ by using Structured Text (ST).

The next section presents and discuses an approach for formal verification of the modelled example.

5. FORMAL VERIFICATION OF IEC 61499 BASIC FUNCTION BLOCKS USING NUSMV TOOL

The formal verification techniques, such as model checking, provide means to verify whether the designed system satisfies the formalized specification. For formal verification of the basic function block presented in previous section, the symbolic model checker NuSMV2 is used. The main novelty in NuSMV2 is the integration of model checking techniques based on Binary Description Diagram (BDD) and propositional satisfiability (SAT). In our case the SMV description contains a module called MAIN, which code is presented in Fig.4. It forms the root of the model hierarchy and the starting point for building the finite state model in a given description. The other modules REQ and INIT1 describing the behaviour in corresponding algorithms of the IEC 61499 function block are linked to the module MAIN by “assign” declaration.

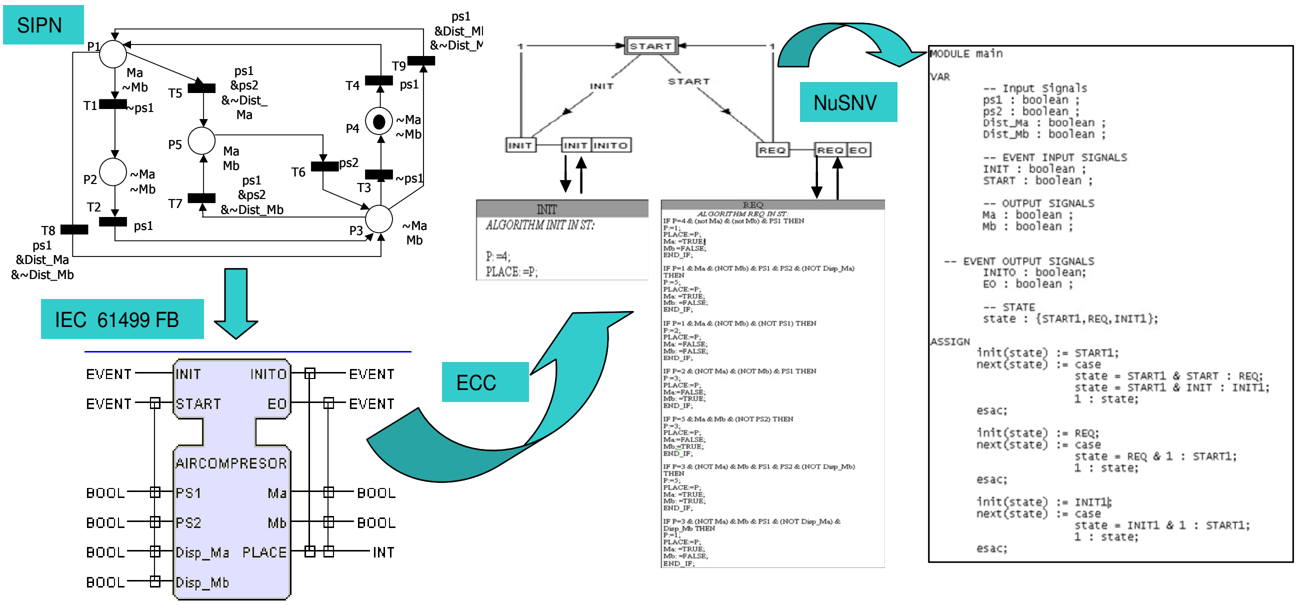

Fig. 4. Realization of the proposed approach for air compressor example

6. CONCLUSIONS

The main aim of this paper is to investigate the combined application of SIPN and NuSMV for formal modeling and verification of IEC61499 based function block specification. The integration of such approaches in the CBA development phases provides means to perform early analysis and verification of the applications, which enable early error detection and increasing of the control systems quality, dramatically decreasing of the application development time and building cost effective systems.

The future work will include in more details definition of the Component-Based Automation concept and further development of the corresponding development methodologies and tools.

REFERENCES

[1] Frey, G., Design and formal Analysis of Petri Net based Logic Control Algorithms Dissertation, University of Kaiserslautern, Shaker Verlag, Aachen, April 2002.

[2] Lewis R., Modelling control systems using IEC 61499, The Institution of Electrical Engineers, London, United Kingdom, 2001.

[3] http://www.holobloc.com/

[4] Vyatkin V., H. M. Hanisch, Modelling of IEC 61499 Function Blocks: A clue to their verification, 11th Workshop on Supervising and Diagnostics of Machining Systems, Karpacz, Poland, March 2000, Proceedings, pp. 59 – 68.

[5] Vyatkin V., H. M. Hanisch, Modular typed formalism for systematic modelling of automation systems, 1st IEEE Conf. on Industrial Informatics, (INDIN'03), Proceedings, Banff, Canada, 2003.

REDUCING FALSE ALARM RATIO IN OUTDOOR PASSIVE INFRARED DETECTORS

Desislava Ivanova, George Popov

Computer Systems Department, Technical University of Sofia, Bul."Kl. Ohridski"8, 1000 Sofia, Bulgaria,
e-mail: popovg@tu-sofia.bg, d_ivanova@tu-sofia.bg

Absract. *This paper concerns outdoor PIR detection. Suggested solution aims to reduce the false alarms caused by sun light. Complementary photo sensor is added to catch any harmful sun radiation that makes false alarms.*

Keywords: PIR, motion detector, security systems, alarm, outdoor PIR

1. INTRODUCTION

The modern trends in security system are outdoor protection. For this purpose are used perimeter and volumetric detectors.

The perimeter detectors used barrier type. It is composed by couple transmitter and receiver. It is many principles to realize - infrared, microwave, field (trough perforated cables), seismic cables and etc. The main advantage of this detector is great range (up to 500m for IR and MW barriers). They have also relatively low False Alarm Ratio (FAR).

The disadvantage of barrier detectors is possibility of finding pass over route. After analysis of type and model, the intruder can eliminate security system by jump over, step, rope, crawling etc.

Generally, the ***volumetric outdoor detectors*** are constructed as double dual passive infrared detectors (PIR). The detector has two sensor, as every sensor have own optical system, “watched” alternated and not overlaid sectors of protected area. The signals of both sensors are compared by software trough a microcontroller. When the human bogy (relatively big object with infrared emission) moves in the protected volume, the radiation is captured by both pyroelements and generates voltage in to both channels. When the animals (cat, dog, bird etc.) move in the protected area, because of their little size voltage is generated in one of the sensors. By analogy at rain, snow, wind and another meteorological conditions is received the signals, differently of these of real intrusion situation.

The main source of false alarms at PIS is sunlight, because in the rays is consist high quantity infrared energy with wavelength 8-14μm. This energy penetrated trough optical system filters. At most situations - at broken clouds the sun is alternate hidden/shown, at movement of the shades during a day, at movement by tree branch, curtains etc. is received the signals like these of an intrusion.

The security producers is tried to solve the problem by adding microwave element combined with PIR's track by logical AND. Practically, this reduced FAR, but problem is not solved, because air movements, wind and movement of tree branches makes Doppler shift (effect).

2. FORMULATION OF RESEARCH TASK - INVESTIGATION OF OUTDOOR PIR DETECTORS

At balcony with south position, at 12 floor of building with flats is realized experimental situation. At both corners of balcony is mounted two types outdoor PIR detectors D&D (by Crow -Israel) and Digigard 85 (by Paradox - Canada). At near every couple detectors is situated PIR (Paradox Light) witch pyrosensor is replaced with photo-transistor. This unit senses change of daylight.

All detectors are connected with control panel (Digiplex NE 96) with event memory, time and date stamped. During one mount (from 15 Mart to 15 April) system is armed and all events is stored in to memory. The table with events is shown in Table 1.

Table 1. Events time and date referenced

DATE	EASTERN CORNER			WESTERN CORNER			POSSIBILITY CAUSE
	DG85	D&D	LIGHT	DG85	D&D	LIGHT	
19.03			6:55	6:55	6:55	6:55	SUNRISE
19.03				7:01	7:01	7:01	SUNRISE
23.03	16:55	16:56	16:56		16:56		SUNSHINE
23.03		17:11	17:11				SUNSET
23.03	17:34	17:34	17:34		17:34		SUNSET
24.03	7:10	7:10	7:10				SUNRISE
28.03		14:47					WIND
28.03	15:15	15:15	15:15				SUN+CLOUDS
2.04		11:08		11:08	11:08		SUN+CLOUDS
2.04		12:05		12:05	12:05	12:05	SUN+CLOUDS
11.04	3:41	3:41			3:44		STORM
11.04	19:10	19:10	19:10				SUNSET
14.04				7:10	7:10	7:10	SUNRISE

The results means, so mostly of false alarms are generated by direct sun radiation. A part of alarms are caused by early morning and evening when sun rays going directly in to optical system of detector. Another part of false alarms are triggered by change of sun shining as result to broken clouds.

Most of false alarms are coincided with triggering of photo-detector Paradox Light.

3. REALIZATION OF SUN RAYS RESISTANT PIR

The idea is to add one photo sensor into PIR's housing. If there is a signal alternation from the this sensor, it is doubt, so pyro's signal is from real motion.

One solution is photo-sensor triggers MOS switch and increase operation amplifier's feedback in the analog PIR's. For example, it is possible to make a shunt of R14 (fig. 1).

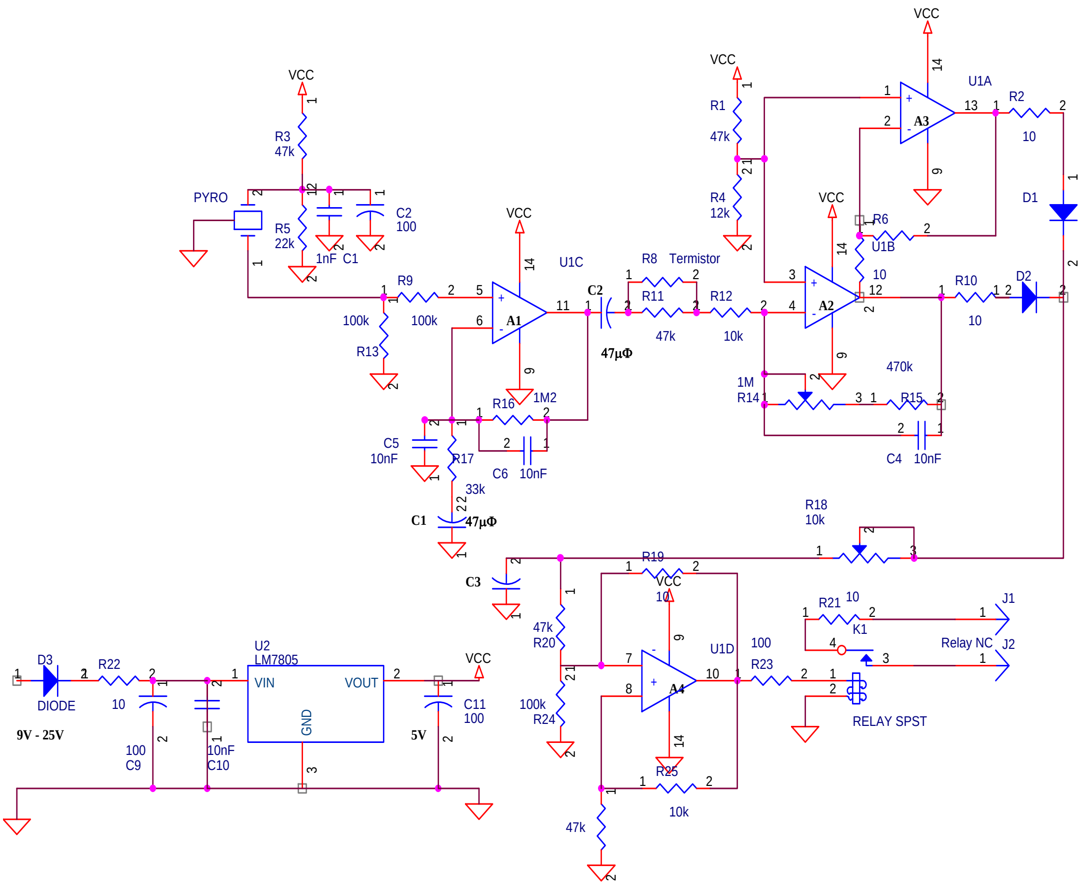

Fig. 1. The analogue PIR detector scheme.

4. CONCLUSION

Microcontoller based solution is more advantageous. The signals from both pyroelements and signals from photo-sensor input in to a microcontroller. If there is a photo-sensor signal, it is possible to initiate a special algorithm for false alarm analysis.

However, this approach is useful to make PIR detector stable against RFI interference. A small antenna with detector may be useful symptom of these phenomena

The suggested method is very good known in the automatics theory. With the purpose of system steadily, it is introduce disturbance signal with opposite sign or as negative feedback.

REFERENCES

[1] Hristov H., Popov G., Adequacy of Identification of Controlled Phenomena in the Security Systems, International Scientific Conference Communication, Electronic and Computer Systems 2000, Sofia, May 2000, Vol. 1, p 188-193.

[2] Capel V., Security Systems and Intruder Alarms, Oxford, 1993.

[3] Popov G., Mirchev M., Passive Infrared Detectors. International Conference “Security 99”, Sofia, NDC, Febr., 23-27-nt, 1999

[4] Technical documentation Digigard 55,75 and 85 by Paradox Security Systems - Canada.

МЕТОДИКА ЗА ОПРЕДЕЛЯНЕ ВЛИЯНИЕТО НА ВЪЗНИКНАЛИ КЪСИ СЪЕДИНЕНИЯ В СГРАДНИ ЕЛЕКТРИЧЕСКИ ИНСТАЛАЦИИ ПРИ ПОРАЖДАНЕ НА ПОЖАР

Стоян Христов Божков

Катедра 'Електротехника, Електроника и Автоматика', Технически Университет – София,
Инженерно Педагогически Факултет – Сливен, бул. 'Бургаско шосе' № 59,
Сливен 8800, България, e-mail: s_bozhkov@abv. bg

Резюме: *В доклада е представен проблем свързан с точното определяне на възможните причини възникналите къси съединения в електрическите инсталации на сгради да бъдат причина за възникване на пожар.*

Извършен е анализ на основните изисквания за безопасна работа и експлоатация на сградни инсталации.

Изготвена и представена е методика за определяне причините за възникване на пожар, изхождайки от параметрите, начина на защита и конфигурацията на електрическата инсталация в помещението огнище на пожара.

Направен е числен анализ на електрическа инсталация, чрез използване на програмния пакет за инженерно проектиране ECODIAL.

Представени са изводи относно предимствата и недостатъците на съставената методика и нейната приложимост при изготвяне на съдебно-електротехнически експертизи.

Ключови думи: електрическа инсталация, ток на късо съединение, автоматичен прекъсвач, време на задействане, време за изключване.

1. ВЪВЕДЕНИЕ

Интерес и предизвикателство в инженерната практика представлява точното определяне на причините за възникване на пожар в комунално – битови помещения. Тези причини могат да бъдат разделени на две отделни категории – пожаротехническа и електротехническа.

Към първата категория се причисляват причините за възникване на пожар в следствие на умишлен палеж или неправилно боравене и съхранение на горивни материали, както и забравен включени електроуреди.

При втората категория причините за възникване на инцидент се дължат на неизправност, най често в следствие на претоварване, късо съединение в електротехническата инсталация на помещението или обекта.

Точното определяне на влиянието на всяка една от категориите в много от случаите е изключително трудно поради липсата на преки доказателства и улики от една страна, а от друга липсата на единна методика за установяване причините и предпоставките за възникване на инцидента.

В доклада е представена методика за определяне на причините за възникване на пожар, изхождайки от параметрите, начина на защита и конфигурацията на електрическата инсталация в помещението огнище на пожара.

2. ТЕОРЕТИЧНИ ЗАВИСИМОСТИ

Както е показано в [4], кабелната мрежа и нейната защита на всяко ниво трябва да едновременно да удовлетворяват едновременно по няколко условия за да се осигури безопасна и надеждна работа на уредбата.

Ето защо едновременно с критериите за избор на проводниците при проектиране и експлоатация на електрическите инсталации е необходимо да бъдат съблюдавани и някой принципи за защита от претоварване и къси съединения.

При изолирани проводници и кабели които не са защитени с бързодействащи предпазители, може да протече продължително време ток (няколко милисекунди) т.к.с. , многократно превишаващ допустимият ток по нагряване .

Топлината коя се разсейва от трайния ток на късо съединение, е

$$\frac{I_\infty^2}{s^2}\tau_\phi = A_{\max} - A_{start.} \tag{1}$$

където:

I_∞ - е трайният ток на к.с.; s – сечението на проводника ,а τ_ϕ - фиктивно времетраене на тока на късо съединение

$A_{\max}$ $и$ A_{start} са величини които са функция на температурата , специфичното съпротивление на проводника и специфичният му топлинен капацитет.

Фиктивното време на периодичната компонента се определя чрез отношението на свръхпреходния ток на късо съединение, към трайния ток на късо съединение т.е.:

$$\beta'' = \frac{I''}{I_\infty} \tag{2}$$

Надеждната и безотказна работа на електрическата инсталация и точното задействане на защитната апаратура е пряко свързана с ефективността на зануляването [1]. Основни критерии за определянето, на който е осигуряване на ниско съпротивление на контура фаза-нула. . Необходимо е да бъде изпълнено условието:

$$Z_S = Z_M + \frac{Z_T}{3} \le \frac{U}{kI_n} \tag{3}$$

Импедансът Z_S на контура е необходимо да бъде достатъчно малък , за да може протичащият ток на еднофазно късо съединение да задейства максимално – токовата защита за приетите допустими времена.

3. МЕТОДИКА ЗА РАБОТА ПРИ АНАЛИЗ НА ЕЛЕКТРИЧЕСКА ИНСТАЛАЦИЯ

3.1. Извършва се оглед и се установява мястото на късото съединение.

3.2. Определя се конфигурацията на ел. инсталацията, начина на нейното захранване и типа предпазител защитаващ токовият излаз, в чиято част се намира късото съединение.

3.3. Определя се пълното съпротивление Z_S на контура фаза-нула до мястото на късото съединение **.**

$$Z_S = Z_M + \frac{Z_T}{3} \tag{4}$$

Пълното съпротивление на фазовия и нулев проводник ще бъде $Z_M = \sqrt{R_L^{\,2} + X_L^{\,2}}$, а пълно съпротивление на захранващият трансформатор на страна ниско напрежение ще е $Z_T = \frac{U^2{}_{20}}{S_H} . \frac{U_{SC}}{100}$

Тук U_{20} и U_{SC} – са респ. линейното напрежение на ПХ на вторичната намотка на трансформатора във волтове и неговото напрежение на късо съединение в %

3.4. Пресмята се тока на късо съединение

$$I_{KC} = \frac{U_F}{Z_S}, \quad kA \tag{5}$$

3.5. Изчислява се необходимото допустимо време за изключване на защитата предпазваща кабела t_{IZ}

$$t_{IZ} = \sqrt{\frac{I^2 t_D}{I_{CS}}}, \quad s \tag{6}$$

За съответния тип кабел в зависимост от сечението и вида на изолацията се намира [2] допустимият ток през жилата за времетраене на късото съединение 1s – I_D

3.6. Определя се големината на автоматичния прекъсвач (предпазител), защитаващ повреденият участък и се намира времето му на задействане t_Z

3.7. Сравняват се двете времена t_Z и t_{IZ}

ако $t_Z \rangle\ t_{IZ}$ – възпламеняването на изолацията е неизбежно

ако $t_Z \langle\ t_{IZ}$ – ел. инсталацията не е причина за пожара .

4. ЧИСЛЕН АНАЛИЗ

Стъпка 1 – изходно условие: Приемаме , че точката на късо съединение е в края на клона на извод осветление.

Стъпки от 2÷4 на предложената методика се реализират с помощта на пакета Ecodial.

Чрез програмния продукт Ecodial се съставя еднолинейна схема на електрическата инсталация (фиг. 1), която е предмет на анализа.

Задават се стойностите на захранващият източник, типа на кабелите с вида и параметрите на защипващите ги автоматични прекъсвачи /предпазители/, както и мощностите присъединени към всеки един извод от разпределителното табло.

Чрез функцията пълно автоматично изчисляване се пресмятат и визуализират параметрите на въведената като конфигурация електрическа инсталация.

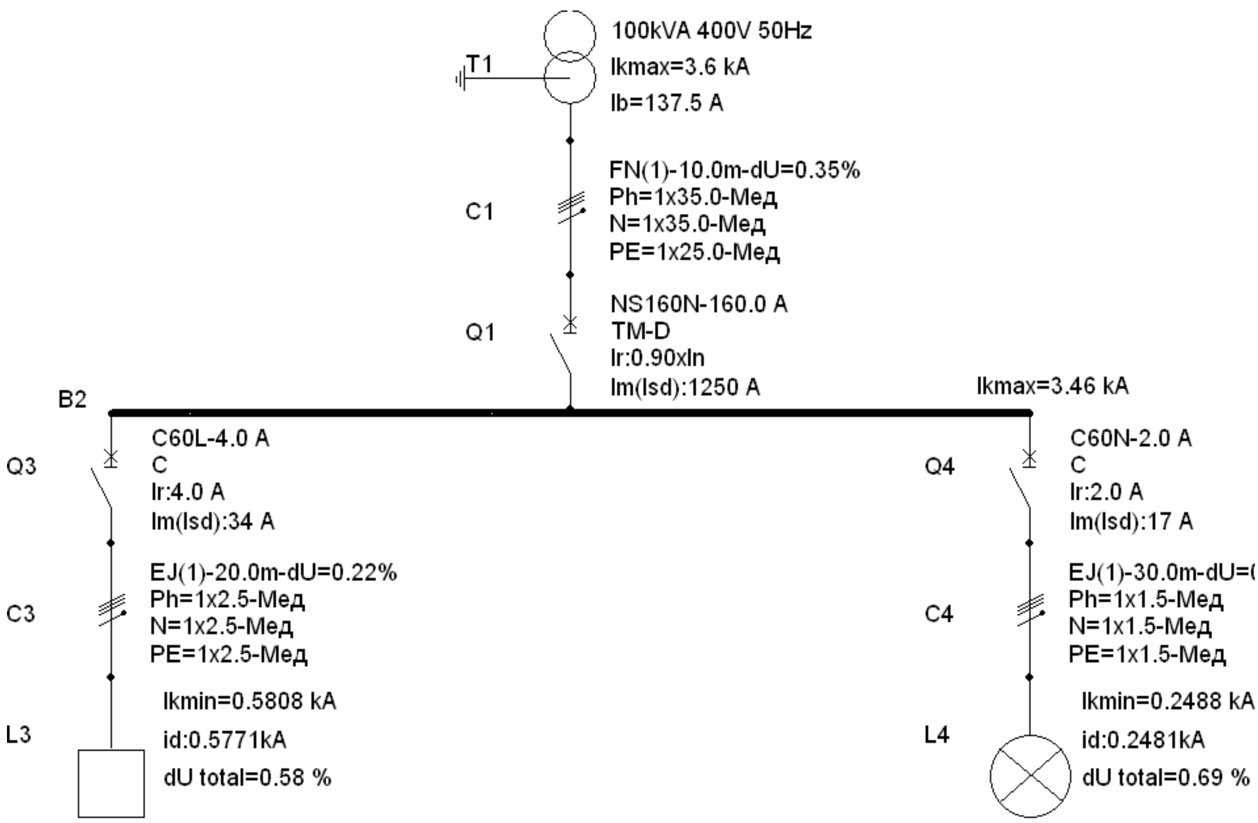

Фиг. 1

Основните резултати от численото моделиране са показани в *таблица (1.).*

Стъпка 5. Отчита се от табл. (1) $I_{CS} = 0.631\ kA$

Стъпка 6. Пресмята се $t_{IZ} =$ 0,27s

Стъпка 7. Определя се $t_Z \leq 0.2$ s

Стъпка 8. $t_Z \leq t_{IZ}$, следователно прекъсвачът ще изключи надеждно възникналото късо съединение.

Електрическата инсталация в конкретният случай не е причина за пораждане на пожар.

Таблица 1

	Тр - 1	Контакти	Осветление
	T1-C1-Q1	Q3-C3-L3	Q4-C4-L4
Захранва табло	Табло НН		
Ib (A)		3.61	1.73
Наименование	NS100N	C60L	C60N
Изключвателна възможност	38.0	25.0	10.0
Ном. ток на защитния блок	60.0	4.0	2.0
Защита / крива на изключване/	M-D	C	C
Изолация на проводника	PVC	PVC	PVC
Дефектнотокова защита	Не	Не	Не
Материал			
Дължина (m)	10.0	20.0	30.0
Начин на полагане	FN(1)	EJ(1)	EJ(1)
Брой проводници на фаза	1	1	1
Сечение на фазов проводник (mmq)	35.0	2.5	1.5
Брой нулеви проводници	1	1	1
Сечение нулев проводник (mmq)	35.0	2.5	1.5
Брой проводници PE	1	1	1
Сечение на PE проводник (mmq)	25.0	2.5	1.5
Ikc в началото на веригата (kA)	3.5934	3.4641	3.4641
Ikc в края на веригата (kA)	3.464	1.349	0.631
I повреда фаза – земя (kA)	2.9337	0.5771	0.2481
Пад dU на веригата (%)	0.35	0.22	0.33
Натрупан пад dU (%)	0.35	0.58	0.69

5. ЗАКЛЮЧЕНИЕ

Предимството на изготвената методика е нейната леснота на използване като същевременно с това се постига бърз и лесен анализ на факторите причинители за възникване на пожар.

От извършеният числен анализ се вижда, че методиката е лесно съвместима за работа със специализиран софтуер за инженерно проектиране. По този начин многократно се съкращава времето за обработка и анализ на резултатите и се повишава точността на работа.

Предложената методика успешно би могла да подпомогне електро-експертите при изготвяне на съдебно-електротехнически експертизи.

ЛИТЕРАТУРА

[1] Ананиев Г., С. Стоянов, Електрически системи I ч., София, АБС Техника, 2004 г.
[2] Стоянов С., В. Господинов, Б.Бойчев, Ръководство за проектиране и избиране по технически данни на силови кабели, проводници за средно и ниско напрежение и неизолирани проводници, София, Авангард Прима, 2005 г.
[3] Schneider Elektric, Ръководство за електрически уредби, 2008 г.
[4] Schneider Elektric, Ръководство за работа с ecodial 3, 2008 г.
[5] Николов Д., Електрически мрежи и системи, София, Техника, 1994 г.

РЕВИЗИЯ НА ОСНОВЕН ФИЗИЧЕН ЗАКОН? НЕ, ОПИТИ ЗА ТЪРСЕНЕ И ДОКАЗВАНЕ НА ИСТИНАТА

Георги Рашков Георгиев

[1]Катедра „Теоретична и измервателна електротехника”,
Русенски университет „Ангел Кънчев”,
България, 7017 Русе, ул. „Студентска” № 8,: (00359 82) 888 412,
e-mail: grashkov@ru.acad.bg,

Резюме: *С нарастването на енергийното потребление и очертаваща се перспектива за енергиен недостиг и особено през последните 4-5 години лавинообразно нараства потокът информация за всевъзможни концепции, изобретения, разработки, патенти и пр., предлагащи решения на енергийните проблеми. Някои от тях звучат невероятно като концепция, други противоречат на основни физични закони, трети съществуват само в главите на авторите си. Логично е да се зададе въпросът: Къде все пак е капката истина в този поток? Как да бъде открита? И (най-важното) безспорно доказана ли е тя? В тази работа, която е по-скоро популяризираща, се прави опит да се съпоставят резултати от реални изпитания с предварителни концепции и почти невероятни твърдения, с единствена цел – търсене и доказване на истината. При това само в едно (от немалкото) направления на “енергийните вълшебства” – синхронни генератори с висок КПД (ще ги наричаме СГВКПД).*

Ключови думи: Електроенергия; Синхронен генератор; Коефициент на полезно действие; Експериментални доказателства.

1. ВЪВЕДЕНИЕ

Във времената на задъхваща се от енергийна недостатъчност свят, борбата за всяка капка енергия става все по-ожесточена. Наред с основното и направление – търсенето на алтернативни източници на енергия (най-вече електрични), е налице и друго – развитие и усъвършенстване на съществуващите такива. Плод на второто е създаването на синхронни генератори с висок к.п.д. (съкратено СГВКПД), обект на тази работа.

В основата на идеята за тях е т.н. от авторите й технология EWM – енергия чрез движение. За създател на EWM-технологията се приема унгарският професор по електротехника Leslie Szabo. Изследванията и развитието на тази уникална технология започват през 1980г. Едновременно в четири лаборатории: - Лондон, Торонто, Хюстън и Будапеща. Енергия чрез движение, твърдят авторите, е възобновяем, чист и евтин енергиен ресурс, който използва електромагнитен поток като източник на "гориво". На този етап, поради липса на пълна и ясна информация, с достатъчна степен на достоверност, може да се предположи, че това би могло да се постигне с използването на много силни магнити (да ги наречем свръхмагнити), на базата на специални феромагнитни смеси (например неодимови). За момента информации сочат, че в тази посока се работи реално в Канада, САЩ [5], Китай, Русия, Испания, Унгария, Германия [3], Австралия

[2]. Това доказва сериозността на тематиката и би било добър ефект, ако с този материал се постави началото на дискусия, защо не и по-силни (реални) действия в тази посока. Все пак в България темата е непозната и това би трябвало да определя по-силен интерес към нея.

2. ИЗЛОЖЕНИЕ

Всъщност казаното все още едва ли е толкова впечатляващо. Не че всеки процент, дори десета от него, по-висок к.п.д. на синхронен генератор (към този тип ел.машина се насочва вниманието тук) не е нещо интересно и важно. Но в сравнение с основните тези твърдения и експериментални резултати (!!!!) на авторите на тази нова технология, това е по-скоро дребна забава. Защото там става въпрос за постигнат к.п.д. на генератора от 1,2 до 1,7!!!! Да, ясно е, че настоящата работа се представя в научни среди, в които разрезът й с основния закон на физиката - за съхранение на енергията, я прави абсурдна. И дори (зависи от опонентите) може да предизвика насмешка. Но, без да се оспорва посоченият закон, не бива да се пренебрегва, че от друга страна стоят все повече информации, резултати от реални изследвания, сертификати (под които са подписите на професори от сериозни организации) в подкрепа на еретично високия к.п.д. И дилемата е дали да се махне (с елемент на догматизъм) с ръка и да се игнорират тези факти, което е по-лесно. Или да се последва философската мъдрост всичко да се подлага на съмнение (без това да звучи ревизиращо основни закони) и да се направи опит, според силите и финансовите възможности (които на този етап не са големи), да се проверят поне някои основни позиции от наличната информация. В тази работа очевидно е избрана втората алтернатива.

На сегашния начален етап на навлизане и запознаване с тематиката, едва ли сериозните теоретични изследвания трябва да стоят на първо място. Още повече СГВКПД вече са създадени, което означава и проектирани, и изследвани. По друг начин биха изглеждали нещата, ако тепърва те трябва да се разработват и изследват.

Стъпвайки на наличното количество предварителна информация (за части от нея ще стане дума в работата, друга част може да се представи като видеоинформация), имайки ориентири от някои центрове в работата по въпроса, се поставя задача да се добие и изследва реален СГВКПД с мощност м поне от порядъка на 5 – 10 киловата. Пряката и непосредствена цел е да бъде изпитан съвсем целенасочено, за да се установи достатъчно категорично големината на неговия к.п.д.

За да не звучи предварителната обосновка голословно, а и смисълът на работата да не изглежда толкова абсурдно, е добре да се обърне внимание на съвсем официалния сертификат от фиг. 1., съставен в Унгария и подписан от 5 титулувани учени, в който става въпрос за доказан к.п.д. на синхронен генератор от порядъка на 1,15 [4].

This is Exhibit „A" attached to the Statutory Declaration, dated August 16th, 2006.

EXHIBIT „A"

We, the undersigned examined, operated and tested Electro Erg Ltd's („EEL") so called BB-Lego, the C4/4 and the E-720 Excess Shaft Power Producing Equipment (the "EBM" Units) in the Testing Station of EEL at Budapest, Hungary, and found the following for the largest E-720 Midget Power Plant:

A: 1. Total Inputted Power: Average of several tests: (Hundred five) 105 kW

2. Total Output Power: Average of several tests: (Hundred twenty) 120 kW

3. Excess Output Power [(2) minus (1)]: **Fifteen (15)** kW

B: From earlier Due Diligent Tests, enumerated in Exhibit "B" in D below. The same Excess Output Power, in descending order for the smaller units are:

1. C 4/4 Unit (The Smaller Unit): 1,200 Watt
2. BB-LEGO Unit (The Smallest Unit): 80 Watt

C: Based on the above findings, the EBM Units in scaled up version can produce increasing quantities of excess power ("sellable power"), as Power Plants, after installations.

D: For a more detailed and exhaustive verification of the underlying tests, we attached hereto log books and Due Diligent tests on which the above A, B, C are based, assembled into a binder, marked Exhibit "B".

Signed, sealed and delivered at Budaörs, Hungary, on August 16, 2006

Prof. Dr. László Szentirmai — Prof. Dr. Ernő Petz

Prof. Dr. Ferenc Mádai — Prof. Dr. Béla Tolvaj

Dr. Tibor Kiss Ph. D.

Както и да се цитират (за по-голяма убедителност) частично описания и експерименти на испански автори по темата [5], а именно:

Като се изключи фотоволтаичната енергия крайното звено в производството на електрическа енергия се явява генераторът на променлив ток. Независимо от приложената система за преобразуване на енергията, общото й к.п.д. обаче не надвишава 50%.

Предмет на настоящото изследване представлява електричен генератор за променлив ток! То може да събуди съмнения, че някои физични закони, смятани досега за фундаментални, може би не са?! Може да породи насмешка, или скептицизъм към създателите на този генератор! И все пак.

Да опишем кратко генератора - предмет на това изследване и някои от неговите характеристики. Принципът му на действие се основава на биполярното трептене на постоянни магнитни полета и не се различава съществено от познатите принципи и схеми. В конкретния случай се цели да се мултиплицира получената енергия, подсилвайки действието на постоянните магнитни полета, чрез двойка фронтални електромагнитни бобини с висока вертикална индуктивност, които от своя страна действат биполярно, позволявайки голямо проникване на биполярното трептене на постоянните магнитни полета.

Предвид голямото трептене на постоянните магнитни полета можем да повлияем върху приемния им фокус с дуалитет, надвишаващ 85%. Така получаваме голяма разлика в реактивната мощност, получавайки като резултат големи напрежения при относително малки обороти. Интензитетът се получава, чрез вертикалното съпоставяне на приемните фокуси в обратна посока, давайки ел. магнитна индуктивност на соленоидите! Двойното действие на постоянните магнитни полета се основава на прилагането на законите на Максуел, Фарадей и собствените изследвания на създателя на генератора.

<u>Провеждане на опита и измерване на основните параметри</u>

Генераторът се задвижва от трифазен електродвигател, чиято скорост на въртене се регулира чрез електронен инвертор, за да се осигури плавно стартиране на генератора.

При измерването на изходящите напрежение и ток се получават следните данни: $U_{изх} = 885\ V$; $I_{изх} = 2{,}2\ A$.

Прилагайки формулата $P_{изх} = I_{изх} . U_{изх} = 1947\ W$.

Приложеният към прототипа товар е чисто активно съпротивление - обикновени електрични крушки. След това измерваме същите данни на входа на инвертора. Предвид прецизността на изчисленията поискахме сертификат от производителя за **К.П.Д.*****-то на електро двигателя. За инверторите се знае, че техният*** **К.П.Д.*****не може да навиши 0,94. Следва измерване на входа на инвертора и се получава:*** $U_{вх} = 400\ V$; $I_{вх} = 4{,}25\ A$, ***или:*** $P_{вх.Генр.} = I_{вх} . U_{вх}$. **К.П.Д.** ***-инвертор .*** **К.П.Д.** ***-Двиг. (%)= 1176,4 W. Сравнявайки мощностите*** $P_{изх} / P_{вх}$, ***получаваме*** **К.П.Д.** ***на генератора от 165,5 %***

Нека това е покана, ако искате да потвърдите казаното тук с ваши средства и технически специалисти.

Горните информационни доказателства са сведени до минимум, с оглед ограничения обем на тази статия, но могат да бъдат разширени значително с видеоматериали.

3. ЕКСПЕРИМЕНТАЛНИ ИЗСЛЕДВАНИЯ

Тръгвайки по следите на наличните информации, бе набавен от производител синхронен генератор от това ново поколение - СГВКПД (произведен в Китай), с номинална мощност 10 kW. и номинална честота на въртене 260 об/мин. След компановката му с трифазен асинхронен двигател (АД) с мощност 7,5 kW, а след това и с 11 kW и обикновена зъбна предавка между тях (за редукция на оборотите на АД), се пристъпи директно към изследване на възловия параметър к.п.д. Натоварването на СГВКПД бе с активен товар (реотанни съпротивления). Пак поради ограничения обем не се представя електричната схема на постановката, но тя е тривиална трифазна схема генератор – консуматор, с включени измервателни уреди за ток, напрежение, честота и мощност. Измервани бяха електричните мощности на входа на АД и на изхода на СГВКПД. За по-голяма точност те бяха измервани с ватметри от два различни типа, а за товара на генератора мощността контролно бе и изчислявана посредством ток и напрежение.

Табл. 1

U_1	I_1	P_1	к.п.д.АД	U_2	I_2	P_2	f_2	к.п.д.общ	к.п.д.'	к.п.д.сг	ДАТА
		1500				1015		0,68			16.12.2008г. АД-7,5 kW 130 об/мин вместо 260 08.01.2009г. АД-7,5kW
		2100				1387		0,66			
		2520				1867		0,75			
		3120				2270		0,73			
220	9,8	2220		380 (666)	1,1	1225	45,5	0,55			
219	10,2	2700		380 (662)	1,5	1710	45,5	0,63			
212	13,8	6720		368	4,7	5189	45,5	0,77			
212	14,2	8400		361 (625)	6	6503	45,5	0,78			
220	16,8	9000	0,87	356 (616)	6,8	7264	45,5	0,81	0,93	0,96	
238	9,0	9300	0,885	624	6,7	7232	45	0,81	0,915	0,95	01.04.2009г. АД-11kW 20.04.2009г. АД-11kW
230	20	11400	0,882	608	8,4	8835	45	0,77	0,873	0,91	
	16,6	9300	0,886	362	7,15	7720		0,83- 0, 87	0,936	0,976	
	15,2	8400	0,885	364	6,25	6825		0,81	0,92	0,96	
	19,4	10200	0,885	359	8	8350		0,825	0,93	0,97	
	16,4	9100	0,885	360	6,77	7380		0,81	0,916	0,955	
	16	9150	0,885	364	6,8	7400		0,81	0,916	0,95	
	18,8	10900	0,882	356	8,55	9100		0,835	0,947	0,986	25.04.2009г. АД-11kW
	20	12200	0,88	344	9,75	10050		0,824	0,936	0,975	

Проведени са много изпитания, като за краткост резултатите от основните от тях са представени в табл.1. При избраната методика, за да се определи к.п.д. само на СГВКПД, са необходими к.п.д. на зъбната предавка и на АД. За зъбната предавка след консултации със специалисти, е приет к.п.д.ЗП = 0,96, а за АД (подобно на испанските автори, цитирани по-горе) изискахме от производителя сертификат с к.п.д на машината при различни мощности. И така в табл.1. са получени: общият к.п.д. на системата ($P_{вх.}$ АД/$P_{изх.}$СГ), к.п.д.' (к.п.д.общ/к.п.д.СГ) и накрая – основната цел на изпитанията - к.п.д.СГ (к.п.д.'/к.п.д.ЗП).

4. ИЗВОДИ

В резултат на проведените доста подробни изследвания, се налагат две много важни заключения:

1. Предричаният, по-голям от 1 коефициент на полезно действие (к.п.д.) на синхронния генератор (СГ), не беше доказан, което на този етап почти отхвърля тезите на горепосочените автори и организации, като все пак недоумението остава.

2. Получава се к.п.д. на СГ доста по-голям от нормалния за машини с мощност от този порядък, за конвенционалните генератори с мощност около 10 kW. Реално той е около 0, 85 – 0,87. Надвишаването с близо 10% е достатъчно сериозно и заслужава да му се обърне подобаващо внимание, както и да се помисли дори за реални стъпки към евентуално производство на подобни синхронни генератори с висок коефициент на полезно действие (СГВКПД). Този висок к.п.д. дава и нов материал за размисли по темата.

ЛИТЕРАТУРА

[1] info@technopatent.com

[2] luteec.com.au

[3] www.akoill.de

[4] www.gammammanager.com

[5] www.innovataivetech.us/genside.htm

СИНТЕЗ И АНАЛИЗ НА НИСКОЧЕСТОТНИ И ВИСОКОЧЕСТОТНИ АКТИВНИ ФИЛТРИ ОТ ВТОРИ РЕД С ЕДИН ИЗТОЧНИК НА НАПРЕЖЕНИЕ, УПРАВЛЯВАН С НАПРЕЖЕНИЕ (ИНУН), МОДЕЛИРАНИ ПО СХЕМИТЕ НА САЛЕН–КИЙ, С ИЗПОЛЗВАНЕТО НА MATLAB И MICROCAP

Таня Методиева Стоянова[1], Адриана Найденова Бороджиева[2]

[1]Катедра „Теоретична и измервателна електротехника", [2]Катедра „Комуникационна техника и технологии",
Русенски университет „Ангел Кънчев",
България, 7017 Русе, ул. „Студентска" № 8,: [1](00359 82) 888 502, [2](00359 82) 888 734,
e-mail: [1]tstoyanova@ru.acad.bg, [2]aborodjieva@ecs.ru.acad.bg

Резюме: *В тази публикация се синтезират и анализират нискочестотни и високочестотни активни филтри от втори ред с един източник на напрежение, управляван с напрежение, моделирани по схемите на Сален-Кий. Това се извършва по зададена нормализирана предавателна функция по напрежение и при известни нормиращо съпротивление и срязваща честота. Синтезът се реализира чрез програмата MATLAB, а анализът на проектираните филтри след избора на стандартни стойности на съпротивленията на резисторите и на капацитетите на кондензаторите в синтезираните вериги, се извършва чрез програмата MicroCAP, предназначена за симулация на аналогови и цифрови вериги. Резултатите ще бъдат използвани в процеса на обучение по дисциплината „Комуникационни вериги", изучавана от студентите от специалност „Комуникационна техника и технологии" от образователно-квалификационната степен „бакалавър".*

Ключови думи: Анализ, синтез, активни филтри, източник на напрежение, управляван с напрежение (ИНУН).

1. ВЪВЕДЕНИЕ

Разглежданите активни филтри от втори ред с източник на напрежение, управляван с напрежение (ИНУН), моделирани по схемите на Сален-Кий [3], са изградени от един операционен усилвател, резистори и кондензатори (фиг. 1).

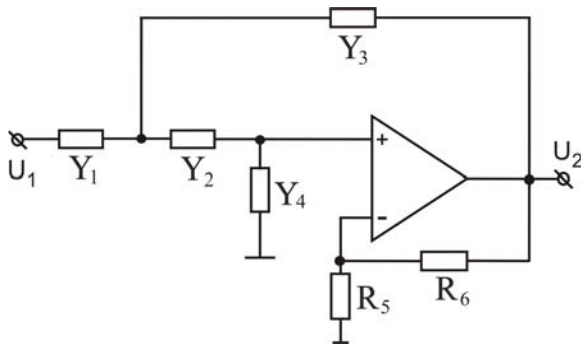

Фиг. 1. Активен филтър от втори ред с източник на напрежение, управляван с напрежение (ИНУН), моделиран по схемата на Сален-Кий

Y_1, Y_2, Y_3 и Y_4 са операторните проводимости (по Лаплас) на двуполюсниците (за резисторите $Y_k = G_k = R_k^{-1}$, а за кондензаторите $Y_k = pC_k$ за $k = 1...4$).

Лапласовият образ на предавателната функция по напрежение [1, 3, 7] на тази верига има вида (1):

$$K_U(p)_{\text{пх}} = \frac{\mu Y_1 Y_2}{(Y_2 + Y_4)(Y_1 + Y_2 + Y_3) - Y_2^2 - \mu Y_2 Y_3}. \tag{1}$$

2. СЪСТОЯНИЕ НА ПРОБЛЕМА – АНАЛИЗ И СИНТЕЗ НА НИСКОЧЕСТОТНИ И ВИСОКОЧЕСТОТНИ АКТИВНИ ФИЛТРИ ОТ ВТОРИ РЕД С ИНУН, МОДЕЛИРАНИ ПО СХЕМИТЕ НА САЛЕН-КИЙ

В Таблица 1 са дадени нормализираните предавателни функции по напрежение на активни нискочестотни (НЧ) и високочестотни (ВЧ) филтри от втори ред, както и техните предавателни функции, записани чрез коефициента на усилване в лентата на пропускане k_0, кръговата срязваща честота ω_c и полюсния качествения фактор Q на съответните филтри [2, 4, 5, 6].

Таблица 1. Предавателни функции по напрежение на НЧФ и ВЧФ от втори ред

Активни филтри от втори ред		
Нискочестотен филтър (НЧФ)	$T(p) = \dfrac{a}{p^2 + b_1 p + b_0}$	$T(p) = \dfrac{k_0 \omega_c^{\,2}}{p^2 + \dfrac{\omega_c}{Q} p + \omega_c^{\,2}}$
Високочестотен филтър (ВЧФ)	$T(p) = \dfrac{a p^2}{p^2 + b_1 p + b_0}$	$T(p) = \dfrac{k_0 p^2}{p^2 + \dfrac{\omega_c}{Q} p + \omega_c^{\,2}}$

Нискочестотните (НЧ) и високочестотните (ВЧ) активни филтри от втори ред с ИНУН, моделирани по схемите на Сален-Кий, имат вида, съответно от фиг. 2 и фиг. 3, т.е.:

– за НЧФ – $Y_1 = G_1$, $Y_2 = G_2$, $Y_3 = pC_3$, $Y_4 = pC_4$;

– за ВЧФ – $Y_1 = pC_1$, $Y_2 = pC_2$, $Y_3 = G_3$, $Y_4 = G_4$.

3. РЕЗУЛТАТИ

Алгоритъмът за синтез и анализ на нискочестотните и високочестотните активни филтри от втори ред с ИНУН, моделирани по схемите на Сален-Кий, съдържа следните стъпки:

1. Въвеждане на коефициентите a, b_0 и b_1 в предавателната функция по напрежение $T(p)$ на синтезираните филтри.

2. Изчисляване на нормираните стойности на елементите на синтезираните филтри. Схемите на синтезираните НЧФ и ВЧФ са показани на фиг. 2 и фиг. 3.

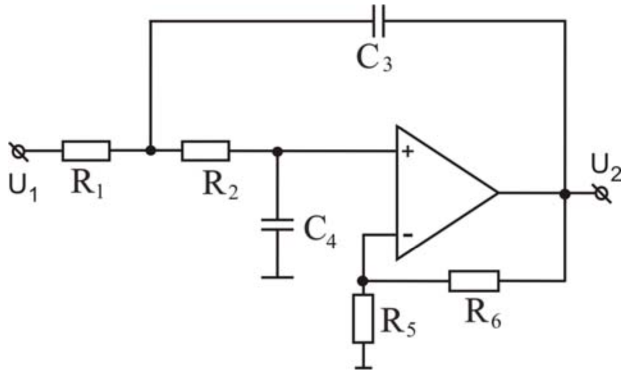

Фиг. 2. Нискочестотен активен филтър от втори ред с ИНУН, моделиран по схемата на Сален-Кий

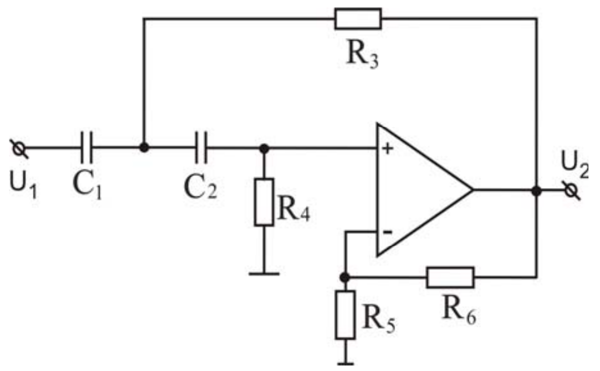

Фиг. 3. Високочестотен активен филтър от втори ред с ИНУН, моделиран по схемата на Сален-Кий

Условие за проектиране – еднакви капацитети в схемата (като нормирани стойности): $C_3 = C_4 = 1$ (за НЧФ) и $C_1 = C_2 = 1$ (за ВЧФ). Параметрите на останалите елементи се получават от решението на следните системи уравнения:

$$\text{– за НЧФ –}\left|\begin{array}{l} \mu = \dfrac{a}{b_0},\ G_2 = \dfrac{b_0}{G_1} \\ G_1 + (2-\mu)\dfrac{b_0}{G_1} = b_1 \end{array}\right.\text{, а за ВЧФ –}\left|\begin{array}{l} \mu = a,\ G_4 = \dfrac{b_0}{G_3} \\ 2\dfrac{b_0}{G_3} + (1-\mu)G_3 = b_1 \end{array}\right..$$

Решенията на системата са:

– за НЧФ:

<u>Случай I:</u>

$$\mu = 2\text{, т.е. } a = 2b_0 \Rightarrow G_1 = b_1;\ G_2 = \frac{b_0}{b_1},\ \mu = 1 + \frac{R_6}{R_5} = 2 \Rightarrow \frac{R_6}{R_5} = 1 \Rightarrow R_6 = R_5.$$

<u>Случай II:</u>

Квадратно уравнение по отношение на G_1 с дискриминанта D:

Необходими условия за проектиране:

1) $D = (-b_1)^2 - 4.1.(2b_0 - a) = b_1^2 - 8b_0 + 4a \geq 0$ – за наличие на реален корен;

2) $G_1 > 0$; $G_1^{\mathrm{I,II}} = \dfrac{b_1 \pm \sqrt{b_1^2 - 8b_0 + 4a}}{2}$, избират се положителните корени (ако има такива); ако няма положителен корен – системата няма решение.

$G_2 = \dfrac{b_0}{G_1}$.

– за ВЧФ:

Случай I:

$a = 1$, т.е. $\mu = 1 \Rightarrow G_3 = \dfrac{2b_0}{b_1}$; $G_4 = \dfrac{b_0}{G_3} = \dfrac{b_1}{2}$; $\mu = 1 + \dfrac{R_6}{R_5} = 1 \Rightarrow \dfrac{R_6}{R_5} = 0 \Rightarrow R_6 = 0$.

Случай II:

Квадратно уравнение по отношение на G_3 с дискриминанта D:

Необходими условия за проектиране:

1) $D = (-b_1)^2 - 4.2b_0.(1-a) = b_1^2 - 8b_0 + 8b_0 a \geq 0$ – за наличието на реален корен;

2) $G_3 > 0$; $G_3^{\mathrm{I,II}} = \dfrac{b_1 \pm \sqrt{b_1^2 - 8b_0 + 8b_0 a}}{2(1-a)}$, избират се положителните корени (ако има такива); ако няма положителен корен – системата няма решение.

$G_4 = \dfrac{b_0}{G_3}$.

3. Въвеждане на стойността на нормиращото съпротивление R_N.

4. Въвеждане на срязващата честота f_c за НЧФ и ВЧФ и изчисляване на нормиращата кръгова честота $\omega_N = 2\pi f_c$.

5. Изчисляване на денормираните стойности на елементите на двуполюсниците:

– за резисторите – получените стойности за съпротивления $R_k = 1/G_k$ за $k = 1...6$ се умножават с нормиращото съпротивление R_N;

– за кондензаторите – получените стойности за капацитети се разделят на произведението $\omega_N.R_N$.

6. Избор на стандартни стойности на елементите на филтъра.

7. Извеждане на предавателните функции по напрежение $T(p)$ на НЧФ и ВЧФ съответно от фиг. 2 и фиг. 3.

– за НЧФ – $T(p) = \dfrac{\mu G_1 G_2}{p^2 C_3 C_4 + p\left[(G_1 + G_2)C_4 + (1-\mu)G_2 C_3\right] + G_1 G_2}$,

където $\mu = 1 + \dfrac{R_6}{R_5}$;

– за ВЧФ – $T(p) = \dfrac{\mu p^2 C_1 C_2}{p^2 C_1 C_2 + p\left[(C_1 + C_2)G_4 + (1-\mu)C_1 G_3\right] + G_3 G_4}$,

където $\mu = 1 + \dfrac{R_6}{R_5}$.

8. Изчисляване на коефициента на усилване k_0 в лентата на пропускане, на полюсния качествен фактор Q и на срязващата честота f_c за НЧФ и ВЧФ след избора на стандартни стойности на елементите.

– за НЧФ:

$$\omega_c = \sqrt{\frac{1}{R_1 R_2 C_3 C_4}}, rad/s, \quad f_c = \frac{1}{2\pi}\sqrt{\frac{1}{R_1 R_2 C_3 C_4}}, Hz; \;\; k_0 = \mu;$$

$$Q = \frac{\sqrt{R_1 R_2 C_3 C_4}}{(R_1 + R_2)C_4 + (1-\mu)R_1 C_3}.$$

– за ВЧФ:

$$\omega_c = \sqrt{\frac{1}{R_3 R_4 C_1 C_2}}, rad/s, \quad f_c = \frac{1}{2\pi}\sqrt{\frac{1}{R_3 R_4 C_1 C_2}}, Hz; \;\; k_0 = \mu;$$

$$Q = \frac{\sqrt{R_3 R_4 C_1 C_2}}{(C_1 + C_2)R_3 + (1-\mu)R_4 C_2}.$$

9. Симулационно изследване на синтезирания филтър с използване на програмния продукт MicroCAP – изчертаване на амплитудно-честотната характеристика, определяне на параметрите k_0, Q и f_c от снетата амплитудно-честотна характеристика и сравнение с получените от изчисляването в точка 8.

Разработени са скриптове на MATLAB [8] за изчисляване на нормализираните и денормализираните стойности на компонентите за НЧФ и ВЧФ при зададена нормирана предавателна функция по напрежение.

Пример: Проектиране на НЧФ и ВЧФ с ИНУН, моделирани по схемата на Сален-Кий, със срязваща честота $f_c = 1\,kHz$ и нормирана предавателна функция по напрежение $T(p) = \dfrac{3p^*}{p^2 + 0{,}25p + 1}$ ($p^* = p^0$ – за НЧФ, $p^* = p^2$ – за ВЧФ). Денормализирането по честота и по съпротивление се извършва с нормиращо съпротивление $R_N = 10\,k\Omega$. Резултатите са показани в таблица 2. След това е извършен избор на стандартни стойности по скалата Е-24, които се използват при симулацията с MicroCAP [9] за изчертаване на амплитудно-честотните характеристики (в dB) на проектираните филтри (таблица 3).

Таблица 2. Резултати от проектирането на НЧФ и ВЧФ с ИНУН с MATLAB

Тип на филтъра	Нормали-зирани стойности	Денормализирани стойности	Стандартни стойности (E-24)	Забележка
НЧФ	$R_1 = 0{,}8828$ $R_2 = 1{,}1328$ $C_3 = 1$ $C_4 = 1$ $\mu = 3$	$R_1 = 8{,}8278\ k\Omega$ $R_2 = 11{,}3278\ k\Omega$ $C_3 = 15{,}9155\ nF$ $C_4 = 15{,}9155\ nF$ $R_5 = 10\ k\Omega$ * $R_6 = 20\ k\Omega$	$R_1 = 9{,}1\ k\Omega$ $R_2 = 11\ k\Omega$ $C_3 = 16\ nF$ $C_4 = 16\ nF$ $R_5 = 10\ k\Omega$ $R_6 = 20\ k\Omega$	По-големият корен на квадратното уравнение
ВЧФ	$C_1 = 1$ $C_2 = 1$ $R_3 = 1{,}0645$ $R_4 = 0{,}9395$ $\mu = 3$	$C_1 = 15{,}9155\ nF$ $C_2 = 15{,}9155\ nF$ $R_3 = 10{,}6445\ k\Omega$ $R_4 = 9{,}3945\ k\Omega$ $R_5 = 10\ k\Omega$ * $R_6 = 20\ k\Omega$	$C_1 = 16\ nF$ $C_2 = 16\ nF$ $R_3 = 11\ k\Omega$ $R_4 = 9{,}1\ k\Omega$ $R_5 = 10\ k\Omega$ $R_6 = 20\ k\Omega$	По-големият корен на квадратното уравнение

Таблица 3. Резултати от изследването на НЧФ и ВЧФ с ИНУН с MicroCAP

НЧФ	ВЧФ
Определяне на качествения фактор и на граничната честота на синтезирания филтър (Analysis→AC→db(v(OUT)), Peak)	
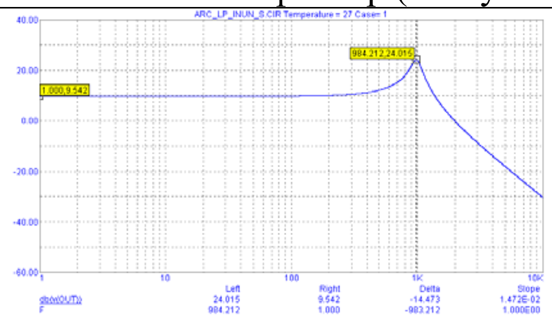	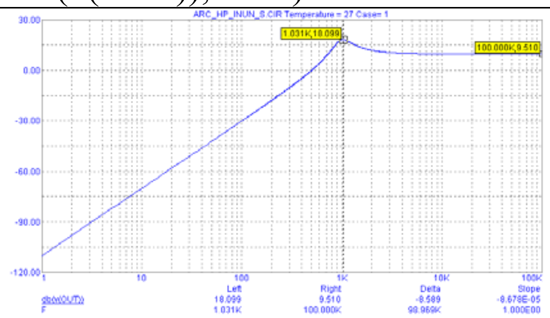
$f_m = 984{,}212\ Hz$ $T_m = 24{,}015\ dB$ $T_k = 9{,}542\ dB$	Координати на левия маркер: $f_m = 1{,}031\ kHz$ $T_m = 18{,}099\ dB$ Координати на десния маркер: $f_k = 100{,}000\ kHz$ $T_k = 9{,}510\ dB$ Качествен фактор на филтъра:
Go to Y → T_k (записва се конкретната стойност в появилото се прозорче, в случая: 9,542) → натиска се Right	

<table>
<tr>
<td>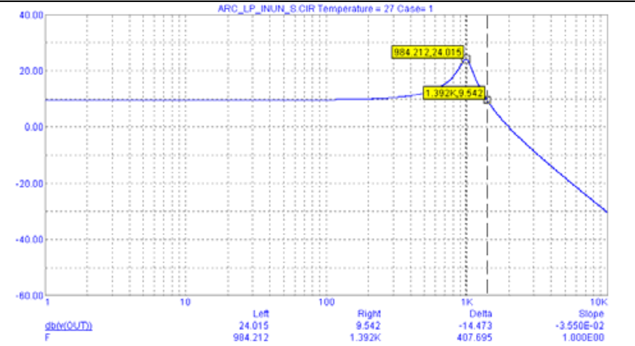
</td>
<td rowspan="2">$T_m - T_k = 20\lg Q$
$Q = 10^{\frac{T_m - T_k}{20}} = 10^{\frac{18{,}099 - 9{,}510}{20}} = 2{,}688$
Гранична честота на филтъра:
$f_c \approx f_m = 1{,}031\, kHz$</td>
</tr>
<tr>
<td>Координати на левия маркер:
$f_m = 984{,}212\, Hz \quad T_m = 24{,}015\, dB$
Координати на десния маркер:
$f_k = 1{,}392\, kHz \qquad T_k = 9{,}542\, dB$
Качествен фактор на филтъра:
$Q = 10^{\frac{T_m - T_k}{20}} = 10^{\frac{24{,}015 - 9{,}542}{20}} = 5{,}292$
Гранична честота на филтъра:
$f_c = \dfrac{f_m}{\sqrt{1 - \dfrac{1}{2Q^2}}} = 993{,}117\, Hz$</td>
</tr>
<tr>
<td colspan="2">Определяне на коефициента на усилване в лентата на пропускане на филтъра</td>
</tr>
<tr>
<td>$k_0 = 10^{\frac{T_{k,dB}}{20}} = 10^{\frac{9{,}542}{20}} = 3{,}000$</td>
<td>$k_0 = 10^{\frac{T_{k,dB}}{20}} = 10^{\frac{9{,}510}{20}} = 2{,}989$</td>
</tr>
</table>

4. ИЗВОДИ

1. В публикацията е описан алгоритъм, заложен в програмен модул, с използване на MATLAB, създаден за синтез и анализ на нискочестотни и високочестотни активни филтри от втори ред с ИНУН, моделирани по схемите на Сален-Кий с един операционен усилвател.

2. Изведени са изрази за предавателните функции по напрежение на синтезираните филтри. Представени са и получените изрази за срязващата честота, за коефициента на усилване в лентата на пропускане и за полюсния качествен фактор на синтезираните филтри.

3. Разработеният програмен модул ще послужи и за автоматизиране на процеса на генериране на варианти на задания за курсови задачи по дисциплината „3110 Комуникационни вериги", включена като задължителна в новия учебен план на специалността „Комуникационна техника и технологии" за образователно-квалификационна степен „Бакалавър".

ЛИТЕРАТУРА

[1] Huelsman, L.P., P.E. Allen. “Introduction to the Theory and Design of Active Filters”, Moscow, 1984 (in Russian).

[2] Manukova, A., A. Borodzhieva. “Communications Circuits – Handbook of Exercises”, Rousse, 2002 (in Bulgarian).

[3] Stoyanov, G. “Fundamentals of Communication Engineering”, Sofia, Techniques, 1993 (in Bulgarian).

[4] Stoyanova, T., A. Borodzhieva. Synthesis and Analysis of Single-Amplifier Single-Loop Negative Feedback Active Filters Using MATLAB and MicroCAP. Summer School, Advanced Aspects of Theoretical Electrical Engineering, Sozopol ’07, 22.09. – 25.09.2007, Sozopol, Bulgaria, Regular papers, Part II, pp. 51 – 57.

[5] Stoyanova, T., A. Borodzhieva. Design and Computer Simulation of Low-Pass and High-Pass Single-Amplifier Multiple-Loop Negative Feedback Active Filters Using MATLAB and MicroCAP. Summer School, Advanced Aspects of Theoretical Electrical Engineering, Sozopol ’07, 22.09. – 25.09.2007, Sozopol, Bulgaria, Regular papers, Part II, pp. 58 – 63.

[6] Stoyanova, T., A. Borodzhieva. Analysis and Synthesis of Band-Pass Single-Amplifier Multiple-Loop Negative Feedback Active Filters Using MATLAB and MicroCAP. Summer School, Advanced Aspects of Theoretical Electrical Engineering, Sozopol ’07, 22.09. – 25.09.2007, Sozopol, Bulgaria, Regular papers, Part II, pp. 64 – 69.

[7] http://en.wikipedia.org/wiki/Sallen-key.

[8] http://www.mathworks.com.

[9] http://www.spectrum-soft.com/index.shtm

OPTICAL SYSTEMS WITH SATURABLE AMPLIFICATION, SATURABLE LOSSES AND FILTERING – SIMPLIFIED APPROACH FOR DESCRIPTION

Ivan M. Uzunov

Department of Applied Physics, Technical University – Sofia

Abstract: *Description of optical system with saturable amplification, saturable losses and filtering [7] (see also [8]) is studied. The aim of this work is to derive the system of ode's, that extends the earlier one proposed in [1-2], including additionally the temporal dependences of the saturated gain and losses. First, this extended system is applied to the case of fast changes in the amplification and losses [6]. Regarding the dissipative solitons, results of [6] have been confirmed. In addition to [6], nonlinear fixed points have been also studied and as result fronts were identified. Next, the extended system is applied to the case of temporal dependent amplification and losses [7]. Linear and nonlinear fixed points of this system have been calculated and their stability identified. Typical solutions discussed earlier in [7] have been found. Fronts have been also revealed. Phase space interpretation of obtained coherent structures is given.*

Keywords: (optical amplification, dissipative dynamical systems, nonlinear fiber optics)

1. INTRODUCTION

Search for the stable temporal dissipative solitons has attracted much interest lately [1-5]. Numerical analysis of basic equations performed in [7] revealed for the first time that stable temporal dissipative solitons (auto-solitons) can exist in such a single-mode fiber system. One-dimensional stationary localized "laser-autosolitons" in a wide aperture laser with a saturable absorber and hard lasing excitation have been studied earlier in [6]. The system of ode's, earlier proposed in [1-2] for the analysis of qubic-quintic Ginzburg-Landau equation, has been applied [6] and its fixed points have been obtained. The linear fixed points that are related to the existence of temporal dissipative solitons (pulses, or auto-solitons) have been studied.

The aim of this paper is to propose system of ode's, that extends the earlier one proposed in [1-2] for the analysis of qubic - quintic Ginzburg-Landau equation, including also the temporal dependences of the saturated gain and losses. This system of ode's will be applied to the physical model studied in [7]. Linear and nonlinear fixed points of this system will be calculated and their stability identified. By means of extended system of ode's we will first to reproduce typical solution discussed earlier in [7]. The appearance of new coherent structures like fronts will be studied. The phase space interpretation of obtained coherent structures will be presented.

2. SYSTEMS PROPOSED IN [7]

The field envelope u in single mode optical fiber system with saturable amplification, saturable losses and filtering (or finite with of the transmission function of amplifier or losses) is described by a following system of coupled equations [7]:

$$\begin{aligned}
&\frac{\partial u}{\partial z} + (-\varepsilon + \delta i)\frac{\partial^2 u}{\partial t^2} - (-1 + \alpha - \beta)u = 0 \\
&\tau_\alpha \frac{\partial \alpha}{\partial t} = \alpha_0 - \left(1 + |u|^2 \big/ I_\alpha\right)\alpha \\
&\tau_\beta \frac{\partial \beta}{\partial t} = \beta_0 - \left(1 + |u|^2 \big/ I_\beta\right)\beta
\end{aligned} \tag{1}$$

where distance z is normalized with respect to linear losses, t is a time in he moving with group velocity reference frame. δ represents dispersion, α and β are coefficients of amplification and losses, respectively, τ_α and τ_β describe the relaxation times of amplification and losses, I_α and I_β are the saturation intensities of amplification and losses. Term proportional to ε is responsible for the finite spectral width of amplification andor losses (or frequency filter).

2.1. Reduced system

I will consider solutions of system (1) given by the following ansatz:

$$u(z,t) = a(\xi)e^{i[\Phi(\xi) - \omega z + v\xi/2]}$$

$$\alpha = \alpha(\xi)$$

$$\beta = \beta(\xi)$$

where $\xi = z - vt$, ω and ν are arbitrary real constants. The reason for assuming that $\alpha = \alpha(\xi), \beta = \beta(\xi)$ is that they are determined by $a(\xi)^2$. We introduce variables [1-2]:

$$q(\xi) = \frac{d\phi}{d\xi};\ k(\xi) = \frac{1}{a}\frac{da}{d\xi}.$$

Inserting ansatz and new variables in (1) following reduced system of ode's is obtained:

$$\begin{aligned}
\frac{da}{d\xi} &= ak \\
\frac{dq}{d\xi} &= -\frac{-2(1 + \beta - \alpha - kv)\delta + 2k(2q + v)\delta^2 + \varepsilon(2q + v)(v + 2k\varepsilon) + 2\varepsilon\omega}{2(\delta^2 + \varepsilon^2)} \\
\frac{dk}{d\xi} &= \frac{4(1 + \beta - \alpha)\varepsilon - 4kv\varepsilon - 4k^2(\delta^2 + \varepsilon^2) + 4q^2(\delta^2 + \varepsilon^2) + 4qv(\delta + \delta^2 + \varepsilon^2) + v^2(\delta(2 + \delta) + \varepsilon^2) + 4\delta\omega}{4(\delta^2 + \varepsilon^2)} \\
\frac{d\alpha}{d\xi} &= \frac{\alpha(a^2 + I_\alpha) - \alpha_0 I_\alpha}{vI_\alpha\tau_\alpha} \\
\frac{d\beta}{d\xi} &= \frac{\beta(a^2 + I_\beta) - \beta_0 I_\beta}{vI_\beta\tau_\beta}
\end{aligned} \tag{2}$$

The ansatz $u(z,t)=a(\xi)e^{i[\Phi(\xi)-\omega z+v\xi/2]}$ has been first applied in [6]. The system of ode's (2) for the functions $a(\xi), q(\xi), k(\xi), \alpha(\xi), \beta(\xi)$ can be considered as extension of system proposed for analysis of cubic-quintic Ginzburg-Landau equation in [1-2] for the case of slow saturable amplification and saturable loss. Derivation of this system is the main result of this paper.

2.2. Fast relaxation [6]

Let us first consider the case of very small relaxation times of amplification and losses $\tau_\alpha = 0; \tau_\beta = 0$. If we assume further that $\varepsilon = 0$ and $\delta = -1$ we will obtain formally the same equation (1) that has been studied in [6]. The system (2), then obtain the following form:

$$\begin{aligned}
&\frac{da}{d\xi} = ak \\
&\frac{dq}{d\xi} = -1 - \beta + \alpha - 2kq \\
&\frac{dk}{d\xi} = -\omega - \frac{v^2}{4} + q^2 - k^2 \\
&\alpha = \frac{\alpha_0 I_\alpha}{\left(a^2 + I_\alpha\right)} \\
&\beta = \frac{\beta_0 I_\beta}{\left(a^2 + I_\beta\right)}
\end{aligned} \tag{2a}$$

This is a coupled system of ordinary differential equations and algebraic equations. It was mentioned that the quantity $s = \omega + v^2/4$ has a meaning of the eigenvalue [6]. In systems like (2a) two kinds of fixed points are expected: zero amplitude solutions or „linear solutions"- $a = 0$; and finite amplitude solutions or "nonlinear solutions"- $a \neq 0$ [1-2]. Linear and nonlinear solutions are denoted by $L_i, i = 1,2$ and N_j, $j = 1,2,..,8$, respectively.

General formulas are derived for the fixed points of system (2a). Because of the space needed to for the representation of general solutions for the fixed points, I will consider here only specific cases. As has been already discussed system 2(a) has two linear and four nonlinear fixed points [6]. The attention there was focused on dissipative temporal solitons (auto-solitons [6], or pulses [1-2]) , so the main interest were the linear fixed points. In what follows, applying the system 2(a), I will confirm results of [8] for pulses and also will obtain front solutions.

According to [6] s in this problem has a meaning of eigenvalue. Several values of eigenvalues of s has been found in [6] (see below). Here I will consider the case [6]: $\varepsilon = 0, I_\alpha = 10, I_\beta = 1, \alpha_0 = 2.102, \beta_0 = 2, s = 0.14175$. The corresponding solutions for the fixed points of system (2) are presented in the Table 1.

Table 1. Fixed point solutions of system 2(a) for $I_\alpha = 10, I_\beta = 1, \alpha_0 = 2.102, \beta_0 = 2, s = 0.14175$.

	a	q	k	α	β
N_1	2.583	-0.376	0	1,261	0.261
N_2	2.583	0.376	0	1,261	0.261
N_3	1.16	-0.376	0	1.853	0.853
N_4	1.16	0.376	0	1.853	0.853
L_1	0	-0.725	0.619	2.102	2
L_2	0	0.725	-0.619	2.102	2

In accordance with [1-2], dissipative solitons (auto-solitons, pulses) connect two linear fixed points, in our case L_1 and L_2. Note that the obtained values of the coefficients of amplification and losses are precisely in the region used in [6] (see Fig.1). In order to identify dissipative solitons, I solved numerically system 2(a) varying the values of s, suggested in [6]. Some of obtained dissipative solitons are shown in the Fig. 1(a-b):

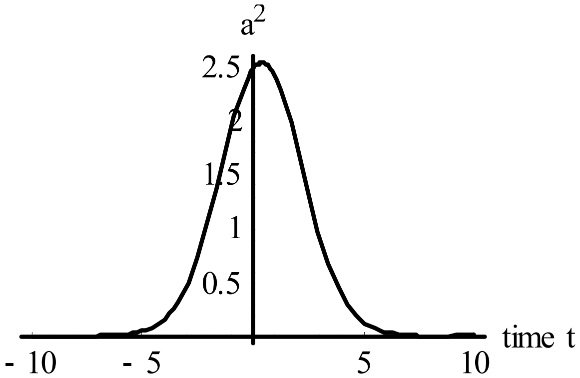

Fig. 1(a) Dissipative soliton with $s = 0.14175$

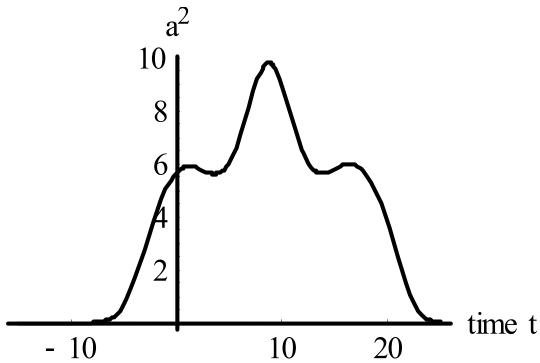

Fig. 1(b) Dissipative soliton with $s = 0.05934$

As can be seen, complete agreement with results of [6] (see Fig.2 there) can be established. Next in addition to [6], I studied possibility of existence of front solutions. According to [1-2], fronts connect nonlinear and linear fixed points. In order to demonstrate this statement, I consider system 2(a) with following parameters: $I_\alpha = 10, I_\beta = 1, \alpha_0 = 2.102, \beta_0 = 2, s = 2$. Calculated fixed points are presented in the Table 2.

I solved system 2(a), starting as initial condition close to the linear fixed point L_2. Front solution has been found, whose form is shown in the Fig. 2(a).

In the Fig. 2(b), the relation between the linear L_2 (starting) and nonlinear N_3 (final) fixed points is demonstrated by means of calculating of $k(q)$ dependence.

Table 2. Fixed point solutions of system 2(a) for $I_\alpha = 10, I_\beta = 1, \alpha_0 = 2.102, \beta_0 = 2, s = 2.$

	a	q	k	α	β
N_1	2.583	-1.414	0	1,261	0.261
N_2	2.583	1.414	0	1,261	0.261
N_3	1.16	-1.414	0	1.853	0.853
N_4	1.16	1.414	0	1.853	0.853
L_1	0	-1.448	0.310	2.102	2
L_2	0	1.448	-0.310	2.102	2

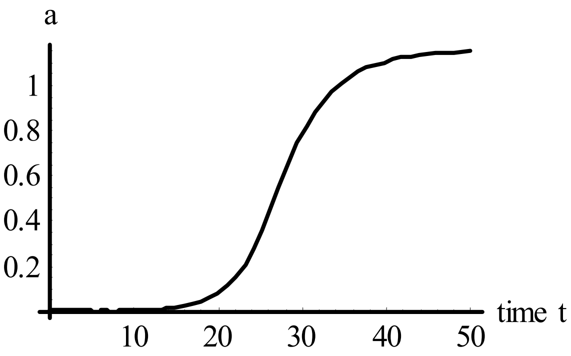

Fig. 2(a) Form of the front $L_2 - N_3$

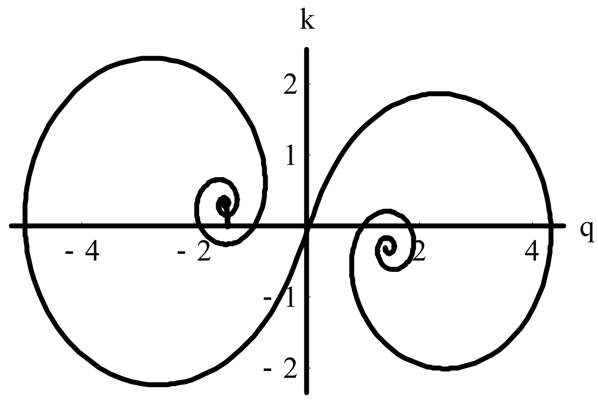

Fig. 2(b) $k(q)$ dependence and front $L_2 - N_3$

2.3. Slow relaxation [7]

Now we will consider the case of finite relaxation times of amplification and losses $\tau_\alpha \neq 0; \tau_\beta \neq 0$. Our aim here will be to apply the derived system (2) for description of the physical system analyzed in [7]. In [7], dissipative solitons have been observed b means of numerical solution of system (1) for the case of $\delta = 1$ and $\varepsilon = 0$. For this value of parameters, system (2) can be written in the form:

$$\begin{aligned}
\frac{da}{d\xi} &= ak \\
\frac{dq}{d\xi} &= 1 + \beta - \alpha - 2kq - 2kv \\
\frac{dk}{d\xi} &= \omega + \frac{3v^2}{4} + q^2 - k^2 + 2kq \\
\frac{d\alpha}{d\xi} &= \frac{\alpha\left(a^2 + I_\alpha\right) - \alpha_0 I_\alpha}{vI_\alpha \tau_\alpha} \\
\frac{d\beta}{d\xi} &= \frac{\beta\left(a^2 + I_\beta\right) - \beta_0 I_\beta}{vI_\beta \tau_\beta}
\end{aligned} \tag{2b}$$

This is a coupled system of five ordinary differential equations for the functions $a(\xi), q(\xi), k(\xi), \alpha(\xi), \beta(\xi)$. I solved it with parameters:
$\varepsilon = 0.1, I_\alpha = 10, I_\beta = 1, \alpha_0 = 2.102, \beta_0 = 2$ studied earlier in [7]. Calculated fixed points of reduced system are presented in Table 3.

Table 3. Fixed point solutions of system 2(a)
for $\varepsilon = 0.1, I_\alpha = 10, I_\beta = 1, \alpha_0 = 2.102, \beta_0 = 2$

	a	q	k	α	β
N_1	2.369	-1.16	0	1.32	0.302
N_2	1.295	-1.158	0	1.764	0.747
L_1	0	-2.19	-0.777	2.06	2
L_2	0	-0.755	0.63	2.06	2

As we see system has two linear and two nonlinear solutions. Stability of the obtained fixed points has been analyzed by solving the corresponding eigenvalue problems of linearized systems. Solving system (2b), with initial condition close to the linear fixed point L_1, pulse shown in Fig. 3 has been found.

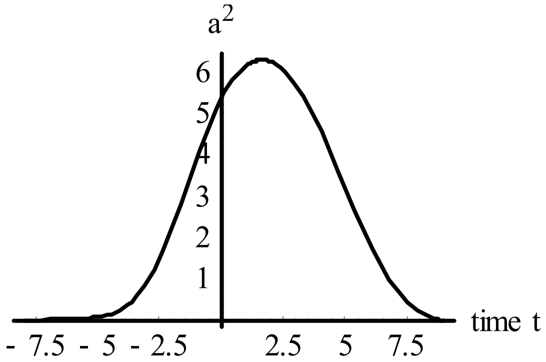

Fig. 3. Shape of the pulse $L_1 - L_2$

In this case both the linear fixed points L_1 and L_2 are related. Fig. 3 is similar to Fig. 1(b) of [7]. I apply the system (2b) for:
$\varepsilon = 0.1, I_\alpha = 10, I_\beta = 1, \alpha_0 = 2.102, \beta_0 = 2$ $(\alpha = 0.6, v = 3.5)$. Front shown in Fig. 4(a) has been found.

In Fig. 4(b) the relation between the linear L_2 and nonlinear N_2 fixed points is demonstrated by means of calculating of $k(q)$ dependence.

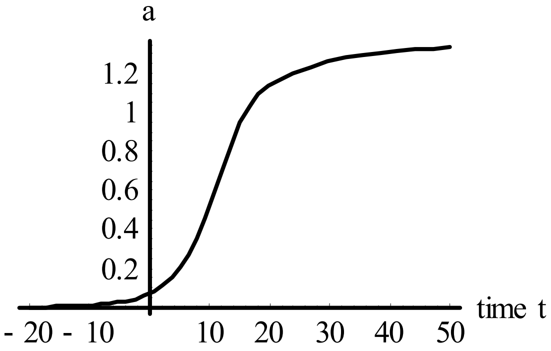

Fig. 4(a). Shape of the front $L_2 - N_2$

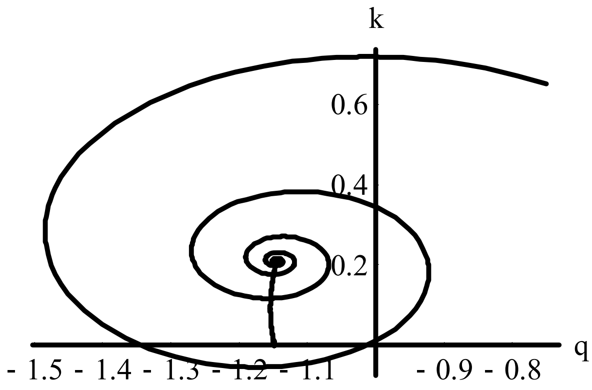

Fig. 4(b). $k(q)$ dependence and front $L_2 - N_2$

3. CONCLUSION

System of ode's that describes optical system with saturable amplification, saturable losses and filtering [7] has been proposed. It the case of fast changes in the amplification and losses [6], with this system dissipative solitons, found in [6] has been also obtained. In addition to [6], nonlinear fixed points have been studied and fronts identified.

In the case of temporal dependent amplification and losses [7], linear and nonlinear fixed points of this system have been calculated and their stability identified. Typical solutions discussed earlier in [7] have been obtained. Fronts have been also found.

REFERENCES

[1] M.C. Cross, and P.C. Hohenberg, "Pattern formation outside of equilibrium", Reviews of Modern Physics, 65, pp.854-1112 (1993).

[2] W. van Saarloos and P. C. Hohenberg, "Fronts, pulses and sources and sinks in the complex Ginzburg-Landau equations", Physica D, 56, pp. 303-367 (1992).

[3] N. N. Akhmediev, A.Ankiewicz, "Dissipative solitons in the complex Ginzburg-Landau and Swift-Hohenberg equations", in "Dissipative solitons", Lect. Notes Phys. 661, ed. N. Akhmediev and A.Ankievicz, Springer-Verlag (2005).

[4] N. N. Akhmediev, A.Ankiewicz, "Solitons. Nonlinear Pulses and Beams", Chapman and Hall, (1997).

[5] "Dissipative solitons", Lect. Notes Phys. 661, ed. N. Akhmediev and A.Ankievicz, Springer-Verlag (2005).

[6] A. G. Vladimirov, N.N. Rozanov, S. V. Fedorov, G.V. Khodova, "Bifurcation analysis of laser autosolitons", Quantum Electronics, 27(11), pp. 949-952, (1997).

[7] Н Н Розанов, С В Федоров, "Автосолитони в едномодовьх световодах с нелинейньм усилением и поглощением", Физическая и квантовая оптика, том 84, стр 849-852 (1998).

[8] Z. Bakony, D. Michaelis, U. Peschel, G. Onishchukov, and F. Lederer, Dissipative solitons and their critical slowing down near a supercritical bifurcations, JOSA B, 19, 487 (2002).

THEORETICAL ANALYSIS AND COMPARISON OF THE METHODS FOR NUMERICAL INVESTIGATION OF THE NONLINEAR SCHRÖDINGER EQUATION

Todor Arabadzhiev and Ivan Uzunov

Department of Applied Physics, Technical University-Sofia, blv. Kliment Ohridski, 8, Sofia, Bulgaria, phone: +359029653112, e-mail: tna@abv.bg

Abstract: *The aim of this paper is to investigate and compare the stability and accuracy of various numerical methods employed for the computation of the solitary waves propagation in optical fibers by using of the Nonlinear Schrödinger Equation (NSE), namely: i) the Crank-Nicholson implicit finite-difference method [1], ii) four variants of the split-step Fourier method (SSFM) [3-6].*

Keywords: Crank-Nicholson Method, SSFM, Nonlinear Schrödinger Equation

1. INTRODUCTION

By using of the NSE we can compute and theoretically predict physical phenomena as the modulation instability and propagation of optical solitons in waveguide fiber. The question for accuracy and stability of different numerical methods used for numerical investigation of the NSE (as the simple case of the most complicated equations) is studied for decades past but remain a live up to the present. Historically, after the development of a wide variety of finite-difference methods for the NSE [1] and the development of the algorithm of the fast Fourier transformation, Hardin and Tapert for the first time investigated the NSE by using of the SSFM [2]. This method was developed further in many versions [3-7], but the question for characteristics and applicability of each variant still remains important. The simplest way for investigating of the stability and accuracy of the mentioned numerical methods is using of the method of approach used in [1,4], where the classical case for the propagation of optical solitons and accuracy of the methods is considered. In our research however, we present the results by more accessible way by comparing of the numerical results with well known exact amplitude of optical solitons. As is well known, in a numerically stable algorithm, truncation error or errors in the input lessen in significance as the algorithm executes, having little effect on the final output [1,4]. In [7] was presented methods for selection of the propagation step size of the SSFM, which may be considered as next stage in improvement of the method.

In this paper, the NSE was investigated numerically by using of the implicit finite-difference method of Crank-Nicholson [1] (because of it universality and improved accuracy in comparison with other finite-difference methods) implemented by the algorithm of Thomas adapted for the NSE and some classical and extrapolation variants of the SSFM (because of it superior speed, stability and accuracy). Our aim is to compare methods and find the most stable method with constant propagation step for investigation of the solitary optical wave's propagation in waveguide fiber, described from the NSE, also to check a way for the stability's improving as the refining of the discretization or the propagation step.

2. THEORETICAL ANALYSIS OF THE NUMERICAL METHODS

2.1. The implicit finite-difference method of Crank-Nicholson for NLS

Let $\varphi_{n,i} = \varphi(t_n, x_i)$ is the pulse's amplitude determined over the rectangular lattice of points correspondingly in time t and in space x: $t_n = n\Delta t, x_i = ih$, where $n,i = 0,\pm1,\pm2,\ldots$ NSE can be approximated by the difference formula:

$$j\frac{\varphi_{n+1,i}-\varphi_{n,i}}{\Delta t} = -\frac{1}{2h^2}\left(\delta^2\frac{1}{2}[\varphi_{n+1}+\varphi_n]\right)_i - |\varphi|^2_{n,i}\varphi_{n,i}\text{, където: } \left(\delta^2\varphi_n\right)_i = \varphi_{n,i+1} - 2\varphi_{n,i} + \varphi_{n,i-1} \quad (2.1.1)$$

The implicit formula (2.1.1) which present the finite-difference method of Crank-Nicolson for NSE is preferred because of it stability, accuracy and possibility for using of bigger step Δt in comparison with the other implicit or explicit finite-difference formulas. As we can see (2.1.1) has an accuracy of order $O(h^2)$.

The implementation of the formula (2.1.1) we have done by presentation of Eq. (2.1.1) through a three-diagonal system $A\vec{\varphi} = b$ regarding to unknown values φ_i as [1]: $A_i^-\varphi_{n+1,i-1} + A_i^0\varphi_{n+1,i} + A_i^+\varphi_{n+1,i+1} = b_i$, where $A_i^\pm$ are the nonzero elements of the matrix A, b_i are known values. Equation from such type arise also when solve (2.1.1) regarding to φ_{i+1} as $\varphi_{0,N}$ are boundary conditions of Dirihlet. We accept that searched solution satisfy recurrence relations that connect φ_i and $\varphi_{i+1}: \varphi_{i+1} = \alpha_i\varphi_i + \beta_i$,

$$A_i^-\varphi_{n+1,i-1} + A_i^0\varphi_{n+1,i} + A_i^+\left(\alpha_i\varphi_i + \beta_i\right) = b_i\,, \beta_{i-1} = \gamma_i\left(A_i^+\beta_i - b_i\right), \alpha_{i-1} = \gamma_i A_i^-\,, \gamma_i = -1/A_i^0 + A_i^+\alpha_i\,,$$

$\alpha_{N-1} = 0$, $\beta_{N-1} = \varphi_N$. We achieve *ii)*: $\varphi_{n+1,i} = \gamma_i A_i^-\varphi_{n+1,i-1} + \gamma_i\left(A_i^+\beta_i - b_i\right)$, where: $B_i^\pm = -j\dfrac{\Delta t}{h^2}$, $B_i^0 = 1 + j\dfrac{\Delta t}{h^2}$, $A_i^\pm = j\dfrac{\Delta t}{h^2}$, $A_i^0 = 1 - j\dfrac{\Delta t}{h^2}$, $b_i = B_i^-\varphi_{n,i-1} + B_i^0\varphi_{n,i} + B_i^+\varphi_{n,i+1} - j\Delta t\left|\varphi_{n,i}\right|^2\varphi_{n,i}$

2.2. Split-Step Fourier Method

Because of its quickness, the SSFM is the most applied numerical method at the moment. This property is due to using of the fast Fourier transformation (FFT). To understand the principle of this method it is convenient to write NSE by the operators $\hat{D}$ and $\hat{N}$ for the effects of the group velocity dispersion and phase self-modulation (nonlinearity) [3]:

$$\frac{\partial\varphi}{\partial z} = \left(\hat{D} + \hat{N}\right)\varphi\text{, where } \hat{D} = -\frac{j}{2}\beta_2\frac{\partial^2}{\partial T^2} - \frac{\alpha}{2} \text{ and } \hat{\mathrm{N}} = \mathrm{j}\gamma|\varphi|^2\varphi \quad (2.2.1)$$

The dispersion and nonlinearity act simultaneously along the fiber, but SSFM is based on the approach that on small distances dispersive and nonlinear effects act independently. The advantage from approach is that the dispersive operator is carried out relative fast in the Fourier domain.

Four variants of the SSFM named: *Simple, Full, Agrawal and Blow-Wood* will be estimated.

In the *Simple* variant of the SSFM solution of Eq. (2.2.1) is given by:

$$\varphi(z+h,T)=\exp\left[\Delta z(\hat{D}+\hat{N})\right]\varphi(z,T) \tag{2.2.2}$$

To estimate the accuracy it is convenient to use the Baker–Hausdorff formula. For the (2.2.2) we can see that the dominant error term is found to result from the single commutator $\Delta z^2\left[\hat{D},\hat{N}\right]/2$. Thus the *Simple* SSFM is accurate to second order in the step size [3].

In the *Full* variant of SSFM, the accuracy can be improved by adopting a different procedure to propagate the optical pulse over the distance from *z* to *Δz + z*. In this procedure Eq. (2.2.2) is replaced by:

$$\varphi(z+\Delta z,T)\cong\exp\left[\frac{\Delta z}{2}\hat{D}\right]\exp\left[\Delta z\hat{N}\right]\exp\left[\frac{\Delta z}{2}\hat{D}\right]\varphi(z,T) \tag{2.2.3}$$

The main difference in this symmetrized form of the solution is that the effect of nonlinearity is included in the middle of *Δz* rather than at the boundary. The most important advantage here is that the leading error term is of third order in the step size.

In the *Agrawal* variant of SSFM, the accuracy can be improved further by the calculation of the nonlinearity in Eq. (2.2.3) as a function of *z* more accurately than approximating it by $\Delta z\hat{N}$. This can be done by using of the iteration procedure for the nonlinearity [3,4]:

$$\varphi(z+\Delta z,T)\cong\exp\left[\frac{\Delta z}{2}\hat{D}\right]\exp\left[\frac{\Delta z}{2}\left[\hat{N}(z)+\hat{N}(z+\Delta z)\right]\right]\exp\left[\frac{\Delta z}{2}\hat{D}\right]\varphi(z,T) \tag{2.2.4}$$

The leading error term in the *Agrawal* variant is of third order in the step size.

An attempt to elimination of the leading error term of third order in symmetrized variants (2.2.3) and (2.2.4) of the SSFM is the higher order extrapolation method suggested from *Blow* and *Wood* [6]:

$$\begin{gathered}\varphi(z+\Delta z,T)\cong\underbrace{\exp\left[\frac{\Delta z}{2}\hat{D}\right]\exp\left[\Delta z\hat{N}\right]\exp\left[\frac{\Delta z}{2}\hat{D}\right]}_{4 times}\exp\left[-\Delta z\hat{D}\right]\exp\left[-2\Delta z\hat{N}\right]\exp\left[-\Delta z\hat{D}\right]\\ \underbrace{\exp\left[\frac{\Delta z}{2}\hat{D}\right]\exp\left[\Delta z\hat{N}\right]\exp\left[\frac{\Delta z}{2}\hat{D}\right]}_{4 times}\varphi(z,T)\end{gathered} \tag{2.2.5}$$

The leading error term in the accumulated error is proportional to: $4\Delta z^3 + \left(-2\Delta z\right)^3 + 4\Delta z^3 \cong 0$, i.e., it cancels at this order, leaving the leading term proportional per step to Δz^5. We have realized the method by using of the procedures described for the symmetrized variants. Accordingly the received variants are named *Full-Blow-Wood* (2.2.5) and *Agrawal-Blow-Wood.*

2.3 Numerical stability of the methods

To compare the numerical methods, our approach for comparison is to (a) determine the soliton amplitude φ and correspondingly accuracy (L_∞) for computations beginning and ending. Then the stability condition is: $L_\infty = \max\left|\varphi_n - \tilde{\varphi}\right| < \varepsilon$, where φ_n is the numerical amplitude and $\tilde{\varphi}$ is the well known exact soliton's amplitude [3], ε is a small parameter. All results are presented graphically.

3. NUMERICAL TESTS AND COMPARISONS

3.1 The implicit finite-difference method of Crank-Nicholson for NSE

We have solved numerically NSE by using of the formula (2.1.1) in the time domain. To determine the correct size of the used lattice we have performed some tests for stability and correctness of our program realization. In this connection, the comparisons of the received numerical solutions with well known analytical soliton solutions of NSE are done. In the case of initial condition of kind *Sech*, the numerical result coincide with the analytical at lattice size 1000 x 1000 points along the axis *x* and *t* and step $\Delta t = 0.001$.

To ensure a stable solution for one soliton period in the case of multi-soliton solution of kind *2Sech*, the lattice size increase to 1000 x 6280 and step 0.00025. To ensure a slower increasing of the error suitable for long distance propagation (up to ~100 soliton periods) we increase the discretization along axis *x* to 10000 samples and propagation step to 0.000025. The result is presented on fig. 1. We can see a linear increasing of the error with slope 0.0006 for the soliton period. We have compared this result with the same solution computed by the SSFM (fig. 1).

To ensure a stable solution for long distance propagation (14 soliton periods) in the case of multi-soliton solution of kind *3Sech*, we had to fix discretization to 10000 points but to decrease propagation step to 0.00001. The result is presented on Fig. 1. We can see again a linear increasing of the error with slope 0.0019 for the soliton period. We have compared this result with the same case computed by the SSFM (Fig. 1).

The Crank-Nicholson method ensures a stable numerical solution of NSE with linear increasing of the error. This fact is observed for the first time. The slope of the solution line can be decreased further by using of the very fine discretization and propagation step but this way is limited because of the fast decreasing of the method's speed. The conclusion from performed comparison between the Crank-Nicholson method and SSFM is that at minimal possible lattice ensuring stable solution, the SSFM remains the more effective method (higher speed and accuracy).

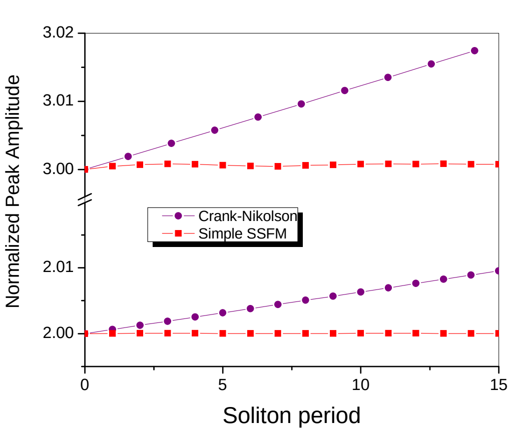

Fig.1

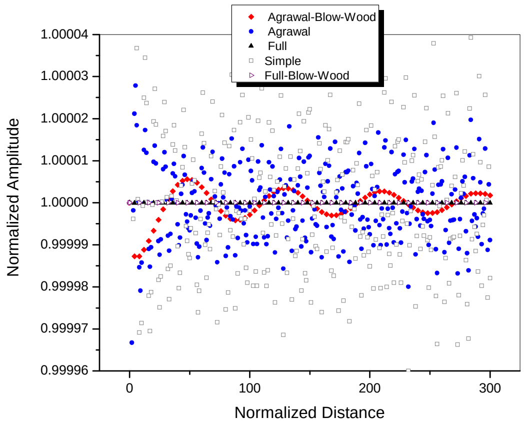

Fig.2

3.2. Split-Step Fourier Method

Our aim in this part is to compare variants of the SSFM, to check their stability and to find methods for optimization in conditions of complicated nonlinearities.

The general numerical parameters used for all computations are: discretization $k = 8192$ and propagation step $\Delta z = 0.001$.

3.2.1 Stability of the SSFM variants for one-soliton solution of the NSE

As we can see in Fig.2, all variants are stable for one-soliton solution of kind: $Sech(T)$ of the NSE, but the best accuracy shows the variant *Full-Blow-Wood*.

3.2.2 Stability of the SSFM variants for multi-soliton solutions of the NSE

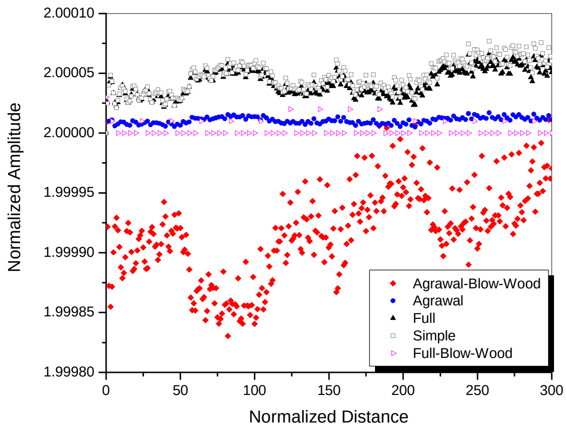

Fig. 3

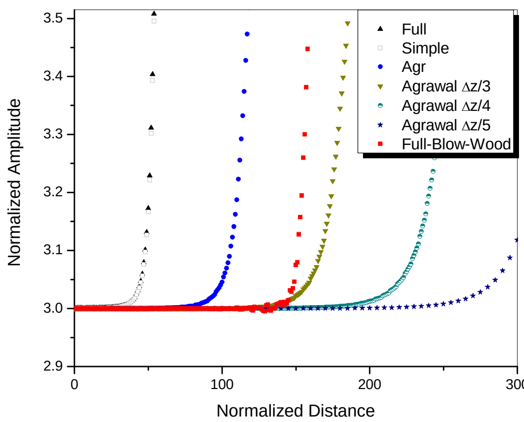

Fig. 4

In the figures 3, 4, 5, 6 it is shown the numerical solution of the NSE with different variants of the SSFM with multi-soliton initial conditions, accordingly: Fig.3: $2Sech(T)$, Fig.4: $3Sech(T)$, Fig.5: $4Sech(T)$ and $5Sech(T)$ and Fig.6: $6Sech(T)$. We ascertain the fact that the most effective variant of the SSFM is the *Full-Blow-Wood.* This variant demonstrates superior stability and accuracy for the multi-soliton solutions of the NSE.

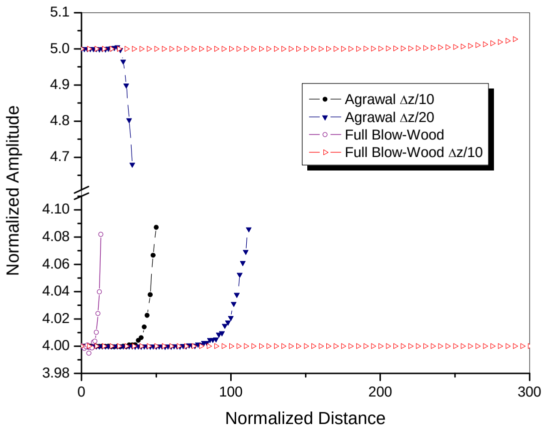

Fig. 5

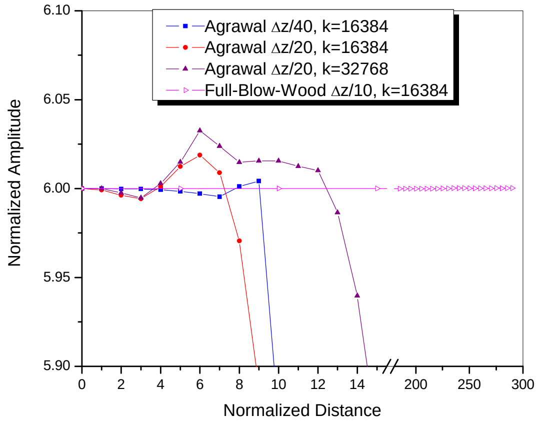

Fig. 6

As we can see in Fig. 4, 5, 6 the stability of the all methods increases at smaller propagation step. We also can increase stability by increasing of the spatial discretization k (Fig.6). We have tested variants with adaptive propagation step [7] but no one of them shows better stability than some of the variants with constant propagation step as the *Full-Blow-Wood*.

3.2.3 Speed of the SSFM Variants

The speed of the base SSFM variants is measured at fixed parameters: discretization 8192, propagation step 0.001 and distance 1 soliton period, on the computer with the AMD Athlon Dual Core Processor 4850e, 2.50 GHz. The speed is: *Simple*-10.6 s, *Full*-19.2 s, *Agrawal*-21 s, *Full-Blow-Wood*-29 s.

4. CONCLUSIONS

In this paper are investigated and compared four variants of the SSFM for propagation of optical solitons in waveguide fiber modeled by NSE. It is found that the variant Full-Blow-Wood has the best stability and accuracy for all considered cases and especially for the multi-soliton solutions of the NSE.

The implicit finite-difference method of Crank-Nicholson implemented by the algorithm of Thomas adapted for the NSE is presented in details. The comparison of this method with the SSFM proves the higher effectivity of the SSFM. The linear increasing of the error of the Crank-Nicholson method is found.

The stability of the methods can be improved by refining of the propagation step or discretization. This is important for the long-distance investigation of multi-soliton solutions of NSE.

REFERENCES

[1] T. Taha, M. Ablowitz, "Analytical and Numerical Aspects of Certain Nonlinear Evolution Equations. II. Numerical, Nonlinear Schrodinger Equation", J. Comput. Physics, 55, p. 203-230, 1984

[2] Hardin, Tapert, "Application of the split step Fourier method to the numerical solution of nonlinear and variable coefficient wave equation.", SIAM Rev. Cronicle, 15,423, 1973

[3] G. Agrawal, “Nonlinear Fiber Optics”, Acad. Press, 2001

[4] T. Hohage, F. Schmidt, “On the Numerical Solution of Nonlinear Schrodinger Type Equations in Fiber Optics”, Konrad-Zuze-Zentrum fur Informationstechnik Berlin, ZIB-Report 02-04, 2002

[5] M. Potasek, G. Agrawal S. Pinault, "Analytic and numerical study of pulse broadening in nonlinear dispersive fibers", JOSA B, 3 (2), p. 205-211, 1986

[6] K. Blow, D. Wood, "Theoretical Description of Transient Stimulated Raman Scattering in Optical Fibers", 25 (12), p. 2665-2673, 1989

[7] O. Sinkin, R. Holzlöhner, J. Zweck, C. Menyuk, “Optimization of the Split-step Fourier Method in Modeling Optical Fiber Communications Systems”, J. Lightwave Technologies, 21, 61-68, 2003

PARAMETER ESTIMATION FOR FAULT DIAGNOSTIC OF A SERVO SYSTEM

Alexandar Ichtev[1], Nasko Atanasov[2], Mihail Petrov[3]

[1] Faculty of Automatics, Technical University of Sofia, Blvd. Kliment Ohridski 8, 1000 Sofia, Bulgaria, phone: (+359 2) 965 2420, e-mail: ichtev@tu-sofia.bg

[2] Department of Automation, Technical University of Varna, 1st Studentska Str., 9010 Varna, Bulgaria, e-mail: nratanasov@yahoo.com

[3] Technical University of Sofia, Branch Plovdiv, Polvdiv 4000, Tsanko Dustabanov 25 str., Bulgaria, e-mail: mpetrov@tu-plovdiv.bg

Abstract: *In this paper fault diagnosis for a servo system is considered. The investigated approach uses parameter estimation. The estimates are obtained by recursive identification of the plant's model parameters. Then the deviation from the nominal values of these parameters is used for fault detection. The problem is stated in its general formulation as well as implementation to a servo system. Based on limit checking of the esteemed parameters, residuals for fault detection are obtained. Then they are used for fault isolation purposes. Both output (sensor) faults as well as input (actuator) faults are considered. Experiments with laboratory setup are carried out. The obtained results are discussed.*

Keywords: Fault Diagnostic, Parameter Estimation, Servo System, Laboratory Setup

1. INTRODUCTION

In the last decades, there is increasing demand on performance of systems working in different environments. In order to satisfy this demand, more and more sophisticated systems with a larger number of sensors, actuators and other components are being built. As a result, the probability of a fault is increasing. On the other hand there are increasing safety demands. In order to satisfy those demands for automated systems reliable fault detection and diagnostics is required.

In this paper the IFAC-Technical Committee definition of a fault is considered [1]: "A fault is an unpermitted deviation of at least one characteristic property (feature) of a system from the acceptable, usual, standard condition".

Two types from the most common faults are discussed, i.e. sensor and actuator faults. Especially hazardous for an automated control system is sensor fault due to the fact that even small deviation from the correct measurement forces the closed loop system in undesirable operational regime.

One can use the result form the fault detection for controller reconfiguration or for sub-systems reconfiguration, i.e. choosing a subset of redundant components [2, 3]. Thus, it is for great importance to avoid false alarms, i.e. the algorithm should not detect fault when the system is fault free. Also it is important to have no missed faults, i.e. the situation when there is a fault in the system, but the fault detection algorithm did not detect it. For reliable fault diagnosis components operation according to different physical principles are required.

2. REDUNDANCY

There are two types of redundant components. The first one is hardware redundancy and the second one is analytical redundancy [4].

According to the hardware redundancy special sensors are used for fault diagnostics purposes. The most common and most simple case involves multiple sensors, which are set to measure the same variable. If only two sensors are used fault detection is achievable by monitoring the difference between the two measurements. However, fault diagnosis is not possible, because the difference do not indicate in which sensor the fault occur. For the second part of the fault diagnosis procedure – fault isolation, additional sensor is required. This approach is straightforward one and is very simple from implementational point of view, but it requires multiple sensors, which is expensive, add additional weight and required additional space.

The other approach relies on analytical redundancy. It utilise knowledge of the system. This can be mathematical model in form of input output relations or can be relation between two measured signals [2, 5]. In this paper prior information regarding specific parameter is considered [2, 4].

3. PARAMETER ESTIMATION

For the automated control theory it is from great importance to know the precise model of the system. Thus, system identification is usually performed for most plants. This procedure can also be used for fault detection and diagnosis purposes, since some of the plants parameters are going to change as a result from the fault [2, 4]. In this case the fault detection procedure boils down to comparison of the estimated parameters with ones, obtained for the nominal (fault-free) operation of the plant. Any significant deviation is going to indicate a presence of a fault. An advantage of the parameter estimation method is that it allows even for single input single output system to estimate several parameters, which provide detail information of the plant. A particular fault can influence some of the parameters, but to have no effect on others, thus by analyzing the fault pattern fault isolation can be performed.

It is assumed that the plant can be described by the linear difference equation

$$y(k) + a_1 y(k-1) + \cdots + a_n y(k-n) = b_1 u(k-d-1) + \cdots + b_n u(k-d-n) \qquad (1)$$

Here

$$u(k) = U(k) - U_0\,; \quad y(k) = Y(k) - Y_0 \qquad (2)$$

are the deviation of the absolute input and output signals $U(k)$ and $Y(k)$ form the operating point U_0 and Y_0, k is the sampling time $k = t/T_0$ and $d = t_d/T_0$ is the discrete dead time of the plant. The corresponding transfer function is then

$$G(z) = \frac{B(z)}{A(z)} z^{-d} = \frac{b_1 z^{-1} + \cdots + b_n z^{-n}}{1 + a_1 z^{-1} + \cdots + a_n z^{-n}} z^{-d} \qquad (3)$$

The task is to estimate the unknown parameters a_i and b_i from measurements of the input and output signals.

Let the model parameters, obtained from data up to the sample $k-1$, are denoted with $\hat{a}_i$ and $\hat{b}_i$. In accordance with the least square method equation (1) can be written in the form

$$y(k)+\hat{a}_1 y(k-1)+\cdots+\hat{a}_n y(k-n)-\hat{b}_1 u(k-d-1)+\cdots+\hat{b}_n u(k-d-n)=e(k) \quad (4)$$

where the equation error $e(t)$ is introduced instead of zero. This error can also be presented in the form

$$\hat{A}(z^{-1})y(z)-\hat{B}(z^{-1})z^{-d}u(z)=e(z) \quad (5)$$

From equation (4) $\hat{y}(k\,|\,k-1)$ can be interpreted as one step ahead prediction, base on the measurements up to the moment $k-1$

$$\hat{y}(k\,|\,k-1)=\boldsymbol{\psi}^T(k)\hat{\boldsymbol{\theta}}(k-1) \quad (6)$$

where $\boldsymbol{\psi}^T(k)$ is vector, containing previous inputs and outputs

$$\boldsymbol{\psi}^T(k)=\begin{bmatrix}-y(k-1) & \cdots & -y(k-n) & u(k-d-1) & \cdots & u(k-d-n)\end{bmatrix} \quad (7)$$

and $\boldsymbol{\theta}(k-1)$ is the parameter vector

$$\hat{\boldsymbol{\theta}}(k-1)=\begin{bmatrix}\hat{a}_1 & \cdots & \hat{a}_n & \hat{b}_1 & \cdots & \hat{b}_n\end{bmatrix} \quad (8)$$

The parameter vector can be estimated recursively. This is needed for fault detection, since the change in parameter/parameters is used as an indication of a fault. The recursive parameter estimation is performed according to the formula

$$\hat{\boldsymbol{\theta}}(k)=\hat{\boldsymbol{\theta}}(k-1)+\mathbf{K}(k)\left[y(k)-\hat{y}(k\,|\,k-1)\right] \quad (9)$$

In this paper it is suggested to be used the forgetting factor adaptation algorithm. According to this algorithm the correcting vector is given by

$$\mathbf{K}(k)=\mathbf{P}(k)\boldsymbol{\psi}^T(k)=\frac{\mathbf{P}(k-1)\boldsymbol{\psi}^T(k)}{\lambda+\boldsymbol{\psi}^T(k)\mathbf{P}(k-1)\boldsymbol{\psi}(k)} \quad (10)$$

where λ is the forgetting factor and $\mathbf{P}$ is the covariance matrix.

$$\mathbf{P}(k)=\left[\mathbf{I}-\mathbf{K}(k-1)\boldsymbol{\psi}^T(k)\right]\mathbf{P}(k-1) \quad (11)$$

In case that the investigated parameter sufficiently deviates from its normal values a residual is triggered, i.e. changes its value form zero to one. This is done by checking limits and thus the residuals have binary characteristics.

5. SINGLE INPUT TWO OUTPUTS SYSTEM

The block-diagram of the investigated system is presented in Fig. 1. It has one input and two outputs. This system can be represented as two parallel subsystems with the same input, but with different outputs.

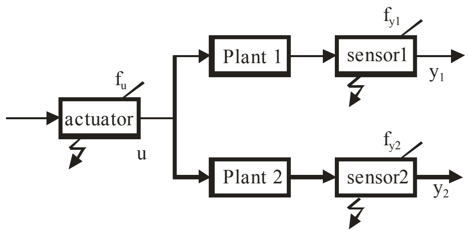

Fig. 1. Single input two output system

There will be only two residuals, i.e. one indicative parameter for each parallel plant is used. Each of them is obtained based on the recursive identification on the base of the common calculated input signal and only one from the outputs. In the investigated case input as well as output faults are considered. From Fig. 1 it can be seen that input fault is going to affect the system description in both parallel systems, however an output fault is going to affect only one of the outputs. This means that both residuals will be affected from input fault and only one residual will be affected from the output fault (corresponding parameter is going to deviate from its normal value). This is going to result to a fault isolation pattern shown on Table 1.

Table 1 Fault pattern for single input two output system

	no fault	f_u	f_{y1}	f_{y2}
r_1	0	1	1	0
r_2	0	1	0	1

6. SERVO SYSTEM

The experiments are carried out with a laboratory setup, manufactured by Inteco®. The setup is shown in the left part of Fig. 2. The control is applied to a DC motor, coupled with tachogenerator. The motor drives an inertia module, connected with backlash, magnetic break and gearbox. The rotation of the DC motor shaft is measured with incremental encoder. The DC motor is controlled with pulse width modulation (PWM). By varying the coefficient of the PWM the effective voltage is changed according to the formula $u(t) = v(t)/\mathrm{v}_{\max}$. The maximum voltage is $\mathrm{v}_{\max} = 12\ \mathrm{V}$ and the control is in the range $[-1 \quad 1]$ (the sign of the PWM coefficient determines the rotational direction).

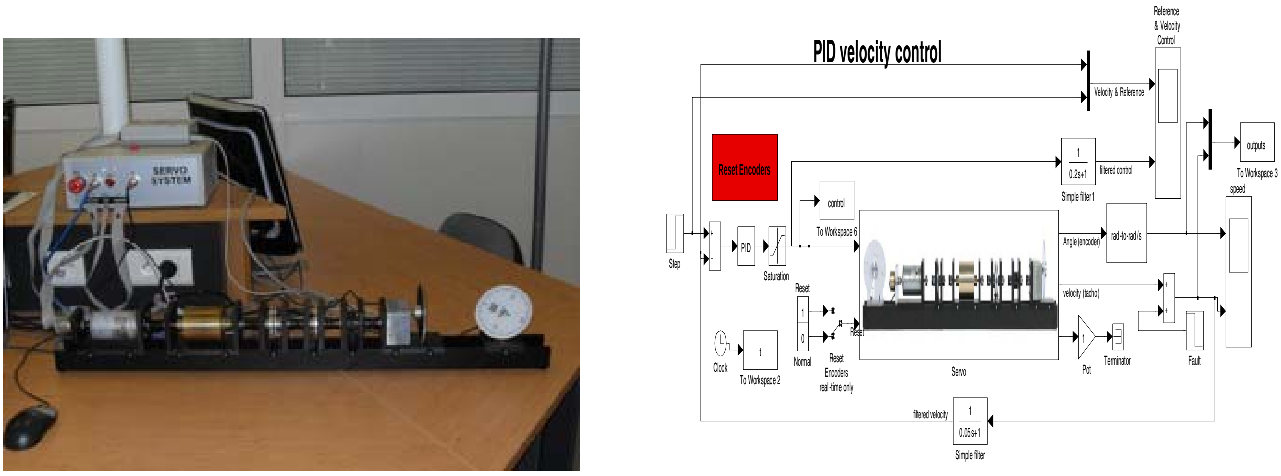

Fig. 2. Laboratory setup and Matlab/Simulink® Block-diagram

7. EXPERIMENTAL SETUP

The experiments are carried out in Matlab/Simulink® environment, with Real Time Workshop®. The block diagram of the system is presented in the right part of Fig. 2. In the middle of the figure is shown the driver for connection to the servo-mechanism. It is provided by the manufacturing company Inteco®. The controller is from PI type (general PID controller is used) with coefficients $K_P = 0.06$ and $K_I = 0.03$ (the D part coefficient is 0). This controller is used for demonstrational purposes only. Similar results are obtained with other controllers – LQR and fuzzy PI controller. They are not presented in this paper. On the right hand side of Fig. 2, the angle, measured from the encoder, is transformed to angular speed, thus the reading from the tachogenerator is reconstructed. The obtained data is evaluated recursively in order to obtain ARX model. One of the model parameters (b_1) is used as an indicator of the fault. The recursive estimation is performed independently for each output. The common input signal is also used in the estimation process.

During the first fifteen seconds of the experiment the system is in fault-free working regime. It operates in its nominal regime – following a reference of 30 rpm. At the fifteenth second an additive fault is introduced. It is sensor offset of with magnitude 5 rpm.

In the first experiment the fault is simulated in the second output. In the left part of Fig. 3 are presented the estimated values of the indicative parameter (b_1) for both subsystems. On the top is presented the estimated parameter, based on the reconstructed speed from the encoder and below it is presented the indicative parameter form the measured speed from the tachogenerator.

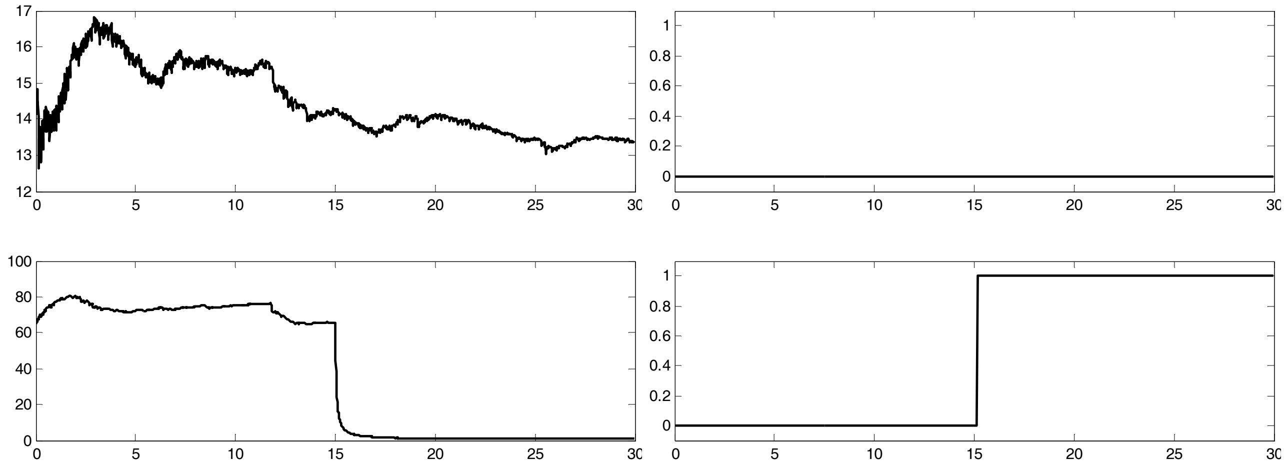

Fig. 3. Outputs from the system and binary residuals

The corresponding binary residuals are presented in the right part of Fig. 3. It can be seen that when the fault is introduced to the system the second residuals is triggered. Then form Table 1 it can be seen that this pattern corresponds to the fault in the second sensor. During the second experiment the fault is simulated in the first output (of the encoder). Obtained results are presented in Fig. 4. In the last figure (Fig. 5) are presented the same results, but the introduced fault is to the input of the plant (to the control signal) with magnitude 0.2. It can be seen that in all three experiments the fault diagnosis system correctly determines the fault situation. Faults in both sensors and the actuator can be successfully detected and isolated.

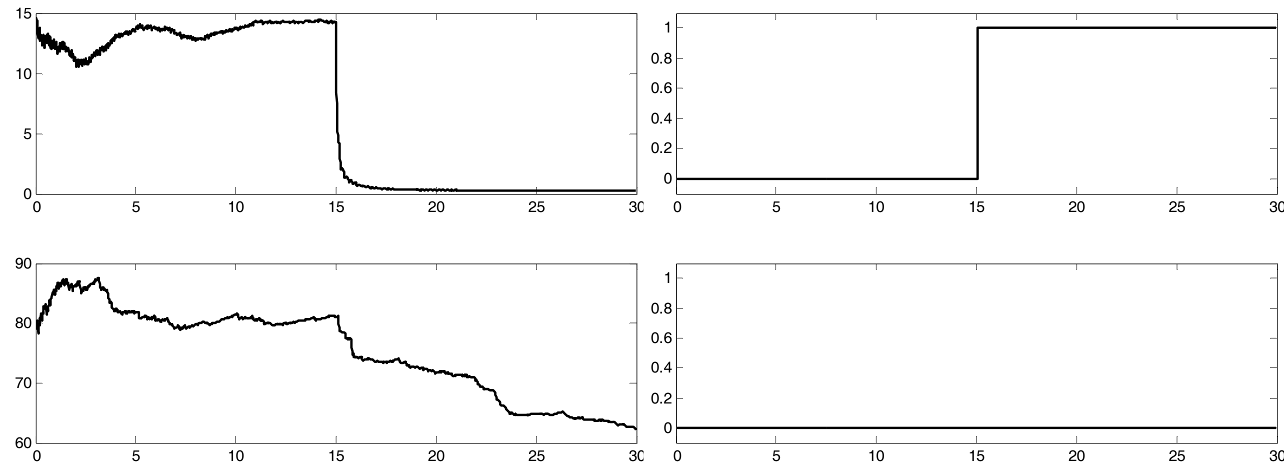

Fig. 4. Outputs from the system and binary residuals

8. CONCLUSION

In this paper fault diagnosis approach with recursive parameter estimation was presented. It is based on least square method with forgetting factor adaptation algorithm. An example with a servo system is investigated. Both sensors as well as actuator faults are detected and isolated form the diagnosis procedure.

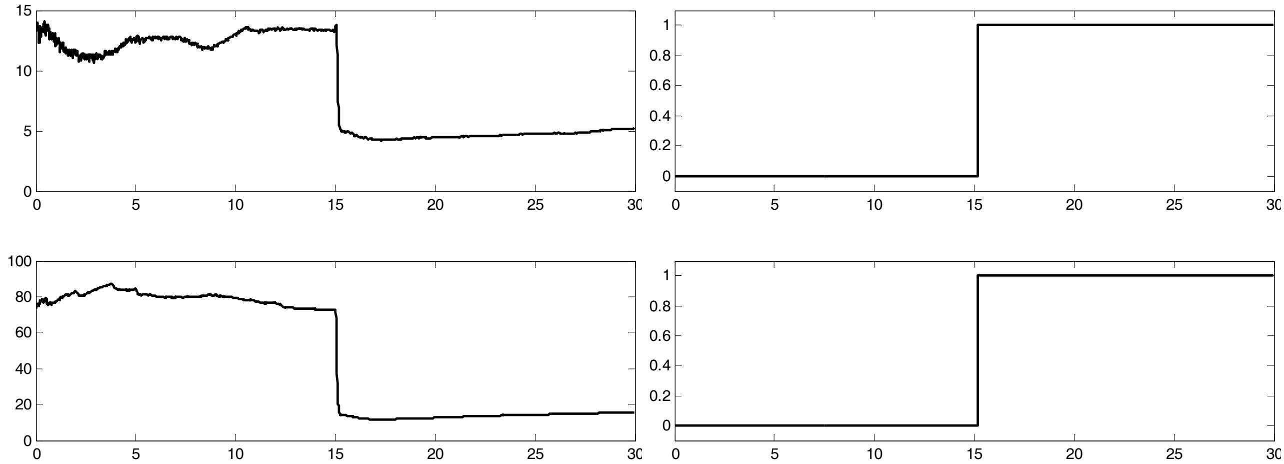

Fig. 5. Outputs from the system and binary residuals

9. ACKNOWLEDGEMENT

The research results presented in this paper are partially funded by Technical University – Sofia research project No. 091ни134-08.

BIBLIOGRAPHY

[1] R. Isermann, Balle P Trends in the application of model-based fault detection and diagnostics in technical processes. Control Engineering Practice, 5 (5), (1997),pp 638-652.

[2] R. Isermann Fault-Diagnosis Systems, Springer 2006.

[3] Patton, R. Fault-tolerant control: the 1997 situation. In Prepr. IFAC SAFEPROCESS, volume 2, 1997, pp 591-596

[4] Janos Gertler, Fault Detection and Diagnosis in engineering systems, Marcel Dekker, Inc., USA, 1998.

[5] Ron J. Patton, Paul M. Frank, and Robert N. Clark (Eds.), Issues of fault diagnosis for dynamic systems, Springer, London, UK, 2000.

„SMALL DNA PREDICTOR“ – A PROGRAM FOR DNA SEQUENCE PREDICTION

Alexandra Nikolova[1], Paul Cristea[2], Valeri Mladenov[3], Veselin Mladenov[3]

[1] Department of Computer Systems, Technical University of Sofia,
8 Kliment Ohridski St, 1000 Sofia, Bulgaria, email: sasha@gbg.bg

[2] Biomedical Engineering Center, "Politehnica" University of Bucharest,
Splaiul Independentei 313, 060042 Bucharest, Romania, email: pcristea@dsp.pub.ro

[3] Department of Theoretical Electrical Engineering, Technical University of Sofia,
8 St Kliment Ohridski Str., 1000 Sofia, Bulgaria, email: valerim@tu-sofia.bg

Abstract: *The “Small DNA Predictor” is a program for educational and non-commercial use. It is designed to read and process DNA data and to predict the nucleotides in the sequence in a way similar to time series prediction. The implementation is based on neural network theory, COM technology and an API for multi-platform shared-memory parallel programming in C/C++ called OpenMP [1]. COM technology and OpenMP allow the main library platform to be independent from the user interface. That means that the main library can work on various platforms (e.g. Windows, Linux, Macintosh) and only the user interface has to be created for the current platform.*

Data are processed in two modules – an n-dimensional Fast Fourier Transform block, and an Artificial Neural Network block. The FFT block reduces the number of dimensions from n input samples to m uncorrelated non-zero Fourier coefficients in the frequency domain, used as inputs of the ANN. This allows to simplify the training of the ANN, as a smaller number of parameters (weights and biases) has to be computed. A supervised learning approach and a feed-forward network are used. As output the program gives the predicted values g(t) which form a sequence approximating f(t). The prediction errors compare favorably with those corresponding to the 'naive' prediction approach.

KEYWORDS: software, DNA, predict, FFT, neural network, “Small DNA Predictor"

1. INTRODUCTION

Artificial neural networks are mathematical models inspired by the human brain and nervous system. The brain is a highly complex, nonlinear and parallel computer with the capability of organizing neurons so as to perform certain computations such as pattern recognition, perception, motor control and to be able to get and store knowledge [5]. All these activities are made parallel. Nowadays we have the opportunity to use multi core processors and parallel paradigms to solve problems. The challenge is not just to reach the right answer but to do that faster, more precise and as cheaper as possible. In this paper we will discuss problems which appear in the face of the software engineer who has to implement mathematical models from papers into computer programs. There is no universal recipe to do that. Each problem has to be analyzed in details then to choose the most appropriate technologies and algorithms for the current problem. The described software is based on the model of neural networks and is designed to read and process DNA data and to predict the nucleotides in the sequence in a way similar to time series prediction.

2. THE PROBLEM AND THE CHOICE OF TECHNOLOGIES

2.1. The Problem

The problem in front of the program is to read, process DNA data and to predict the nucleotides in the sequence in a way similar to time series prediction. The general scheme of the architecture of the system is shown in Fig. 1.

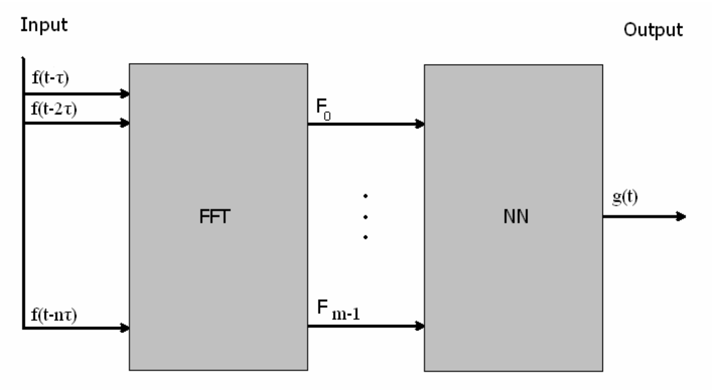

Fig. 1. Architecture of the "Small DNA Predictor"

The input data is a DNA sequence, which can be given as a series of letters representing the four nucleotide bases in a DNA strand: A – adenine, C – cytosine, G – guanine and T – thymine. Other possible letters are R, W, Y, S; B, D, H, V; N – which correspond to classes of two, three and four nucleotides, respectively, as defined by IUPAC [4]. These are fuzzy inputs, used when an instance is not crisply recognized as one of the four bases. As output the program gives the predicted values $g(t)$ which form a sequence approximating $f(t)$. The prediction errors compare favorably with those corresponding to the 'naive' prediction approach.

Concerning [2] and [3] the input data is processed in two modules – an n-dimensional Fast Fourier Transform block, and an Artificial Neural Network block. The FFT block reduces the number of dimensions from n input samples to m uncorrelated non-zero Fourier coefficients in the frequency domain, used as inputs of the ANN. This allows simplifying the training of the ANN, as a smaller number of parameters (weights and biases) has to be computed. A supervised learning approach and a feed-forward network are used.

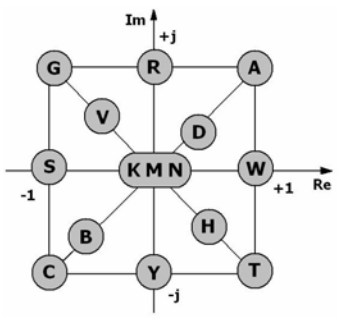

Fig. 2. Complex representation of nucleotide bases

When the problem is defined we have to decide how the different modules will communicate and what kind of data we need to keep during the execution. The input data in fact are letters which is inappropriate format for computations. By converting the sequences of nucleotides into digital genomic signals, this approach okiffers the possibility of using signal processing methods for the analysis of genomic [6]. The conversation method in our case is the complex representation shown in Fig.2. Details for FFT and ANN block are discussed later.

2.2. Choice of Technologies

DNA sequences are long tales of chars (several hundreds or thousands) where the size of char is 1 byte. Converted into complex representation each letter is coded with two signed integers – one for real part of complex number and one for the imaginary part. Depends on the machine where the data is stored the integer is 16, 32 or 64-bit (2, 4, or 8 bytes respectively) addressable word. So each nucleotide base is coded with 8 bytes for 32bit CPU and 18 bytes for 64bit CPU. For calculations in FFT and ANN block we need double precision (according to IEEE754 [8]). The data seems to be large enough so the first criterion for choice of technologies is performance and the choice is C++. The object oriented approach of C++ is important for the organization of ANN. The second criterion is the ability for parallel computations. The OpenMP [1] (Open Multi-Processing) is an application programming interface (API) that supports multi-platform shared memory multiprocessing programming in C++ and Fortran on many architectures, including Unix and Microsoft Windows platforms. It consists of a set of compiler directives, library routines, and environment variables that influence run-time behavior. When a code who includes OpenMP pragmas is compiled on non-parallel machine the directives are just ignored and there is no need to write the code twice – once for parallel computation and second for non-parallel. As third criterion we use the old Roman principle "DIVIDE ET IMPERA" which is the main principle in programming. Good organization of the program will facilitate the engineers work in many directions - fast implementation, make easier support of the product, gives a feasibility to improve and add new modules without need of rewriting the old parts. COM technology (Component Object Model) and OpenMP allow the main library to be independent from the platform and the user interface. That means that the main library can work on various platforms (e.g. Windows, Linux, Macintosh) and only the user interface has to be created for the current platform.

3. PROGRAM ARCHITECTURE

„Small DNA Predictor" consists of two parts – a dynamic link library (DLL) and a graphical user interface (UI). DLLs allow encapsulation of a piece of functionality in a standalone module with an explicit list of C functions that are available for external users. Internally, a DLL may be implemented in any language, but in order to be used from other languages and environments, a DLL interface should fall back to the lowest common denominator – the C language.

3.1. Main Library

As we mentioned above the main DLL is created under the terms of COM technology and object-oriented programming principles (OOP). The library consists of several modules with specified tasks which cooperate. Each module encapsulates data inside him and provides methods for management of the data. For realization of the modules are used OOP techniques and several design patterns. The organization of the library is shown on Fig. 3.

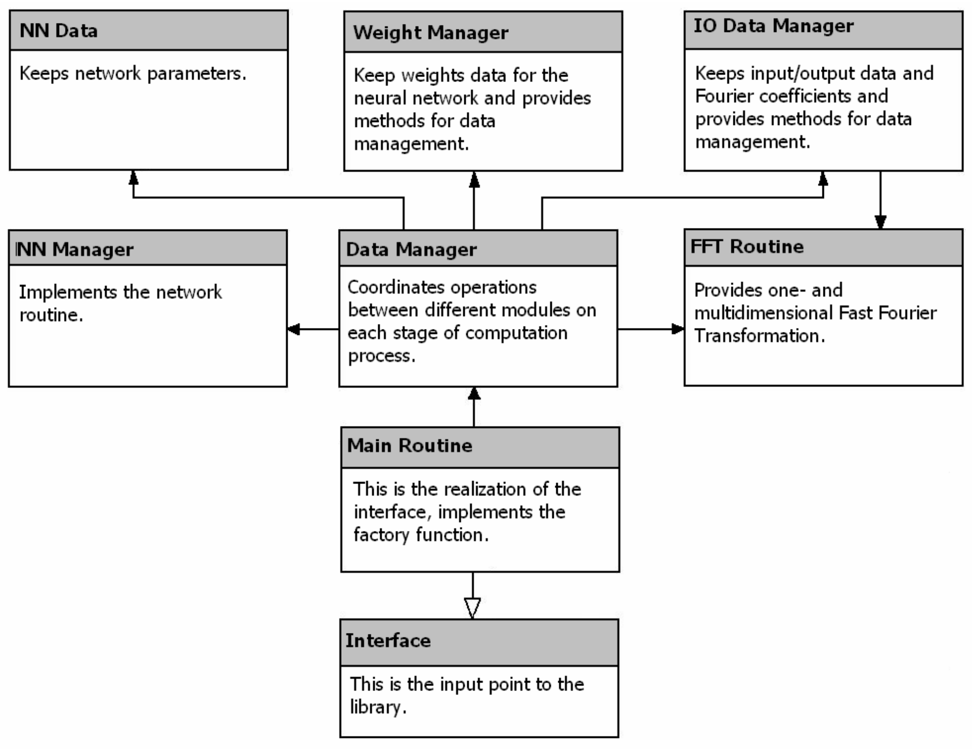

Fig. 3. DLLs' organization

The library exports functionality via Interface block. In context of programming *interface* is called an aggregate of definitions which declare how the object behaves. The implementation is separated from the definition. On that idea is founded Component Object Model. In context of program languages the interface is realized with an abstract class. The realization is in *Main Routine*. The other parts in the library are created by using of technique of aggregation. *Data Manager* aggregates a couple of blocks which solve specific problem. It is responsible for coordination between different modules and for reading/writing the configuration file. The latter is used to save network parameters and weight values.

ANN routine from Fig.1 consists of three blocks – *NN Data, NN Manager* and *Weight Manager*. *NN Data* keeps parameters of the network - number of layers, number of neurons in each layer, number of epochs used to train network, learning rate parameter value, momentum, activation function constants and the path to the configuration file. *NN Manager* implements the neural network model shown on Fig.4 and cooperates with *Weight Manager* during the prediction and train processes. The architecture of the program allows implementation of different training algorithms and their comparison. By default is used Back-Propagation Algorithm [5]. As activation function is used a sigmoidal nonlinearity in the form of a *hyperbolic tangent* defined by

$$\varphi(v) = a\tanh(bv) = a\frac{1-e^{-bv}}{1+e^{-bv}} \tag{3.1.1}$$

where a, b are constants. The initialization of the synaptic weights and threshold levels is done on neuron-by-neuron basis - values are distributed inside the range $\left(-\frac{2.4}{F_i};+\frac{2.4}{F_i};\right)$ where F_i is the fan-in (i.e. the total number of inputs of neuron i in the network. Adjustment of weights is done by using the generalized delta rule where the learning rate parameter η and momentum constant α are defined by user (by default they are initialized with random small values).

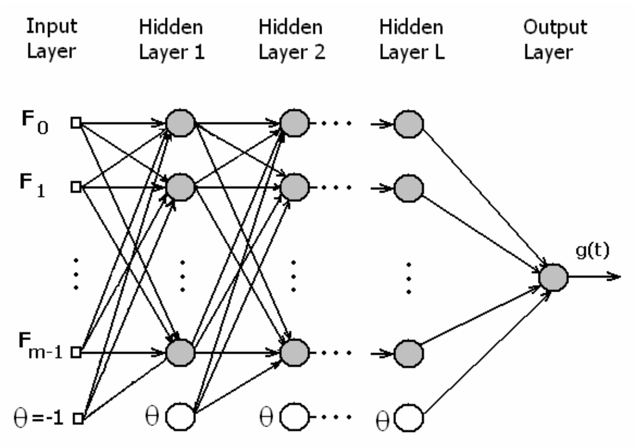

Fig. 4. Neural Network model

FFT Routine block is a routine and it does not contain private data. The algorithm is based on multidimensional Fast Fourier Transformation [7].

4. USER INTERFACE

The library has any specific requirements for the user interface. In our case the realization of the UI is with a MFC dialog based application [9].

5. RESULTS ANS CONCLUSIONS

The software development process can be generalized in three stages – choosing of architecture and algorithms, implementation and testing. This section gives an explanation of test results which were a surprise. Parameters like time and memory were measured in two modes – parallelized and non-parallelized code. Parallelized code is has been tested in two variants – parallelism on network level (threads of forjoin type cooperate to process all the data) and on layer level (each layer use threads to calculate the output values of its neurons). At this point it is important to notice that the idea of the program architecture is to save memory instead of wining time. Such dilemma occurs often in programming – can we use more resources in the way to be faster or we shall limit resource usage and complete computations in average or good time. In described software the data is stored as a single copy and all the routines access it. That means that there will be a lot of critical sections. *Table 1* and *Chart 1* show the results – the parallelized code is slower than the contiguous. The program uses more resources to organize multithreading than the code is executed in contiguous code.

The conclusion is that the performance depends more of the design of the software than of the computation power of the workstation. Software engineers should spend enough time to think about the architecture before start writing code.

Table 1. Test results

Representation in memory, doubles	256	512	1024	1024	2048	2048
Data Count / Code	100	223	446	500	669	892
OpenMP (Network level)	1554 ms (25.9 s)	10424 ms (173.7 s)	91872 ms (1531.2 s)	97056 ms (1617.6 s)	792600 ms (13210.0 s)	792600 ms (13210.0 s)
OpenMP (Layer level)	8544 ms (142.4 s)	17152 ms (285.9 s)	96256 ms (1604.3 s)	101864 ms (1604.3 s)	797032 ms (13283.9 s)	812592 ms (13543.2 s)
Contiguous code	1552 ms (25.9 s)	10232 ms (170.5 s)	91560 ms (1526.0 s)	95232 ms (1526.0 s)	797312 ms (13288.5 s)	852952 ms (14215.9 s)

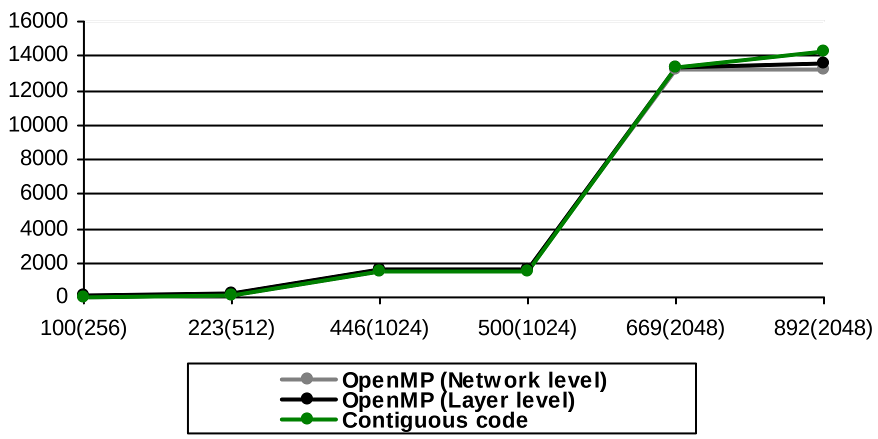

Chart 1. Test results time chart

ACKNOWLEDGEMENT

The work was supported by grant from the Ministry of Education and Science of Bulgaria, in the framework of the bilateral Scientific, Technological and Innovative Co-operation with Romania - project БРС-08.

REFERENCES

[1] *http://openmp.org/wp/*

[2] I. Năstac, P. D. Cristea, Neuro-Adaptive Forecasting for Nonstationary Sequences, *SOFA 2005 – IEEE International Workshop on Soft Computing Applications*, Szeged – Hungary & Arad - Romania, 27-30 August 2005, pp. 179-186.

[3] P. D. Cristea, Valeri Mladenov, Georgi Tsenov, Rodica Tuduce, Simona Petrakieva, Application of neural networks, PCA and feature extraction for prediction of nucleotide sequences by using genomic signals, *NEUREL-2008 – 9th Symposium on Neural Network Applications in Electrical Engineering,* Faculty of Electrical Engineering, University of Belgrade, Serbia, September 25-27, 2008

[4] http://www.bioinformatics.org/sms/iupac.html

[5] S. Haykin, "Neural Network. A Comprehensive Foundation", Macmillan College Publishing Company, New York, 1994, ISBN 0-02-362761-7

[6] P. D. Cristea, "*Large scale features in DNA genomic signals*", Bio-Medical Engineering Center, Politehnica, University of Bucharest, Romania, 2002

[7] W. H. Press, S. A. Teukolsky, W. T. Vetterling, B. P. Flannery, *"Numerical Recipes in C. The Art of Scientific Computing"*, Second edition, Cambridge University Press, 1992, ISBN 0-521-43108-5

[8] W. Kahan, *"Lecture Notes on the Status of IEEE Standard 754 for Binary Floating-Point Arithmetic"*, Elect. Eng. & Computer Science, University of California, Berkeley, 1997

[9] *http://msdn.microsoft.com/*

INFLUENCE OF DISPERSION ON SOME BASIC CHARACTERISTICS OF OPTICAL FIBERS

Snejana Terzieva, Georgi Toshev

Department of Theoretical Electrical Engineering, Technical University of Sofia,
8, Kliment Ohridski Str., Sofia 1000, Bulgaria, phone: +0359 965 23 94, e-mail: ster19@tu-sofia.bg

Abstract: *An attempt to give comparatively easy approaches for determination of quantitative characteristics and parameters in initial design of optical links is made. Some suitable examples illustrate determination of the dispersion and its influence on the basic parameters of the optical systems.*

Keywords: Optical fibers, Modal Dispersion, Chromatic Dispersion.

1. INTRODUCTION

Today transmission of sizable amounts of information with high speed and authenticity on long distances is exceptionally important. For this purpose high-speed optical systems are used [1]. Such systems, named point-to-point link, consist of three basic elements:

- Optical transmitter that transform the information into optical signal;
- Optical fiber – transmission medium;
- Optical receiver for reproducing the information.

The block diagram of a simple communication system with basic elements only is shown in Fig.1.

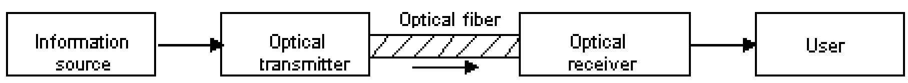

Fig. 1

There are additional components as modulators, amplifiers, couplers, and multiplexers (demultiplexers).

The signal attenuation, dispersion, optical losses and nonlinear effects are major limitations in the transmission medium. The attenuation is overcome with constantly regeneration from amplifiers like Erbium Doped Fiber Amplifiers (*EDFA*).

In this paper the dispersion influence on one of the most important characteristics of fibers – bandwidth (*BW*) is discussed. Suitable examples illustrate basic theoretical conclusions connected with data transmission on optical communication links.

2. THEORY

The optical fibers are divided in two large groups in accordance of modes that are transmitted. The first group is multimode fibers and the second one is single-mode fibers. Main reason for limitation of the BW is the pulse expansion in a time domain when it propagates on the fiber because of dispersion [2].

If on an optical fiber input (Fig. 2) a pulse with width t_{p1} is submitted, then at the fiber end this width will be t_{p2}. The dispersion of the fiber with enough accuracy can be written as

$$\Delta t = \sqrt{t_{p2}^2 - t_{p1}^2}\ . \tag{1}$$

Its unit of measure is *ns* (10^{-9} s) or *ps* (10^{-12} s).

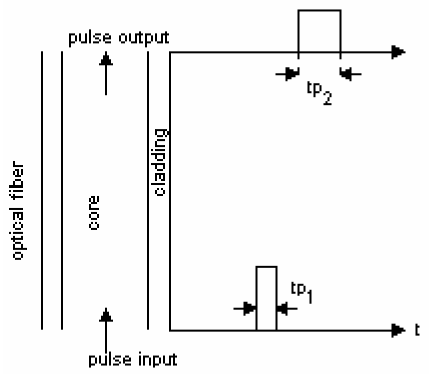

Fig. 2

The dispersion of the optical fiber depends on its length – L, therefore

$$\Delta t = L\text{x}(dispersion/km)\,. \tag{2}$$

A tolerable number of modes, which have different propagation constants and different group time delay, are propagated in multimode fibers. The delay is the reason for both the pulse expansion and the appearance of the modal dispersion [3]. The times for propagation of the fundamental mode (LP_{01}) and the critical one from input to output of the optical fiber with length L are

$$t_0 = \frac{L}{v} = \frac{Ln_1}{c}; \tag{3}$$

$$t_c = \frac{L/\sin\theta_c}{v} = \frac{Ln_1}{c\,\sin\theta_c}, \tag{4}$$

where $v = c/n_1$ is the phase velocity of light in the medium, c is the speed of light in a vacuum, n_1 is the refractive index of the fiber core, θ_c is the critical angle and there is a definition expression $\sin\theta_c = n_2/n_1$, n_2 is the refractive index of the fiber cladding. These two modes are shown in Fig. 3.

The difference between t_c and t_0 is the time for the pulse to reach the output. If the input pulse is extremely small in width then t_0 is the delay of the fundamental mode and t_c is the delay of the critical one. Therefore the dispersion can be given by

$$\Delta t = t_c - t_0 = \frac{Ln_1}{c}\frac{n_1 - n_2}{n_2} = \frac{Ln_1}{c}\Delta\,, \tag{5}$$

where Δ is normalized difference between refractive indexes. The expression $\Delta << 1$ is always valid.

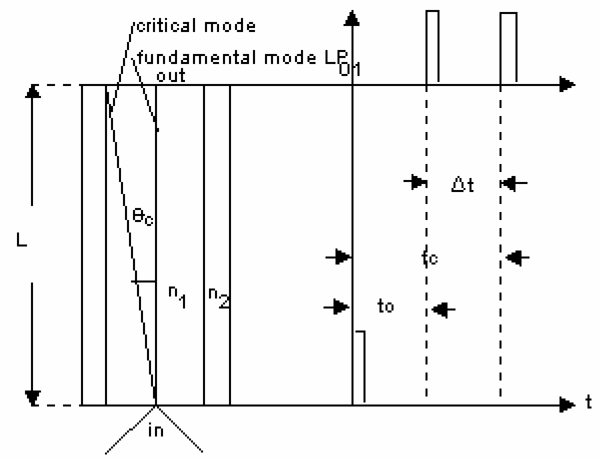

Fig. 3

It is known from geometrical optics [4] that

$$\Delta = \frac{n_1^2 - n_2^2}{2n_1^2} = \frac{NA^2}{2n_1^2}, \tag{6}$$

where $NA = \sin\theta = \sqrt{n_1^2 - n_2^2}$ is the numerical aperture. Then the dispersion for *1 km* can be written:

$$\frac{\Delta t}{L} = \frac{NA^2}{2n_1 c}. \tag{7}$$

It seems that modal dispersion directly depends on the numerical aperture of the fiber. When the angle of the acceptance light is bigger then the amount of received power in fiber is bigger too. But in this case the dispersion grows up, too. Discrepancy is obvious and the result is decreasing the bit rate (*BR*).

The other kind of dispersion that exists in all types of fibers with its two behaviours – material and waveguide, is the chromatic dispersion. It results from the fact that the light in the optical fiber is formed from the group of frequencies, i.e. it is connected with width $\Delta\lambda$ of spectrum light. Its unit of measure is $ps/(nm \text{ x } km)$. In short the reason for chromatic dispersion is the dependence of phase velocity of a light from its wavelength λ. Increase of $\Delta\lambda$ leads to increasing of this dispersion. For example for a wavelength of $\lambda = 820nm$ the speed of light is one, for a wavelength of $\lambda = 850nm$ it is another and this fact leads to a pulse expansion. For chromatic dispersion the following equation is valid

$$D = -\frac{1}{2\pi c}\left(2\lambda\frac{d\beta}{d\lambda} + \lambda^2\frac{d^2\beta}{d\lambda^2}\right), \tag{8}$$

where β is a propagation constant. This expression is known as a first order dispersion and it has a minimum at wavelength around $\lambda = 1300nm$. The effect of pulse expansion is not completely overcome because of presence of dispersion terms from second and higher order. Sometimes, for better estimation of the dispersion, Taylor's series of the group time delay in the spectrum area around this wavelength is used [4].

3. DISPERSION EFFECTS

As it is shown the dispersion causes expansion of the introduced light pulses on the optical fiber input when they travel on fiber core. The effect of this expansion is given in Fig.4.

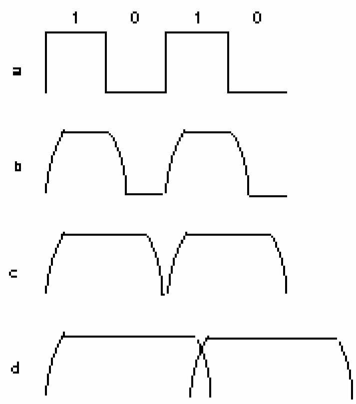

Фиг. 4

The signal on the input *1010* (Fig.4a) is idealized, i.e. the times for increment of the front and back pulse fronts are infinitely small. The output is given for three cases – *b*, *c* and *d*. In cases *c* and *d* pulses begin to re-cover. This effect is called intersymbol interference (ISI). In case *d* the receiver cannot identify received pulse – *0* or *1*.

An approximate formula for a *BW* of an optical communication link as a function of the dispersion that is used for a primary evaluation is

$$BW \approx \frac{1}{2\Delta t}. \tag{9}$$

The bandwidth of the optical fiber or system is a range of frequencies that can travel with minimal amplitude distortions. Another definition of the *BW* is a range of frequencies between two points where the output optical power decreases *50%* from the maximum (Fig.5), i.e. the decrease of *3dB*. As a rule there is no limitation of a lower limit.

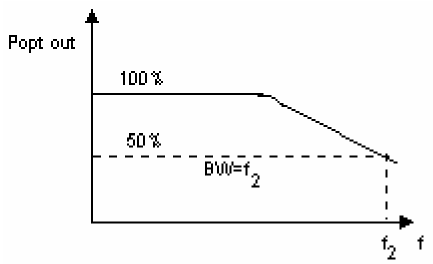

Fig. 5

An increase of *ISI* leads to increasing the *BER* (bit-error rate), which leads to limitation of the *BR*.

The dispersion depends on the type of the optical fiber and more exactly from its index profile. It is well known that optical fibers are realized with these profiles: step-index, grade index, triangular index and others with complex form. The modal dispersion is dominated in step-index fiber and in that case the *BW* depends on Δ, respectively on *NA*. As much as Δ(*NA*) is growing the *BW* becomes narrower.

In addition the *BW* depends on the optical link length. As much as the link is longer the *BW* decreases and that is why the characteristic *BW*x*L* is introduced. The product *BW*x*L* is necessary to be a constant for operative application of a given optical fiber. It is very important parameter that allows changing the *BW* in different practical cases depending on *L* (see Example 4.3).

4. EXAMPLES FOR PRACTICAL APPLICATIONS

4.1. Determination of modal dispersion

Let series of light pulses are transferred on optical fiber with $L = 400\,m, n_1 = 1.4$ and $n_2 = 1.36$ with two speeds $10\text{x}10^6\, pulse/s$ и $20\text{x}10^6\, pulse/s$. The modal dispersion for the above speeds and the dispersion for $1\,km$ should be determined.

From (6) the normalized difference between refractive indexes is

$$\Delta = 0.02816$$

After using (5) the final result for the modal dispersion is

$$\Delta t = \frac{400 \times 1.4 \times 0.02816}{3 \times 10^8} \approx 52.6 ns .$$

The results are shown in Fig. 6.

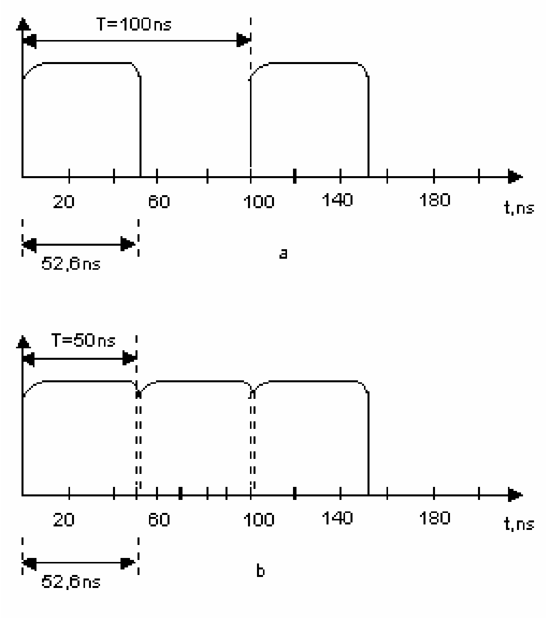

Fig. 6

It is seen (Fig.6) that at a transmission speed of $20\text{x}10^6\ pulse/s$ the output pulses are re-covered and they cannot be identified, i.e. for a link with $L = 400\,m$ one cannot use this transmission speed.

The dispersion for $1km$ is $131.4\,ns/km$.

4.2. Determination of total dispersion

An optical fiber with length $L = 5\,km$ and $\Delta\lambda = 40nm$ has modal dispersion $5\,ns/km$, chromatic dispersion $100\,ps/(nm\,\text{x}\,km)$. Determine the total dispersion at the end of the link.

The modal dispersion is $\Delta t = 25ns$.

The chromatic dispersion is $\Delta t_h = 20ns$.

The total dispersion is $\Delta t_{tot} = \sqrt{\Delta t^2 + \Delta t_h^2} \approx 32ns$.

4.3. BW dependence on the link's length.

An optical fiber with grade index profile and length $L = 8\,km$ has a dispersion $1.5\,ns/km$. Determine the BW at length $L_1 = 3\,km$.

The total dispersion of the fiber is $\Delta t_{tot} = 12ns$.

Following (9) the bandwidth is $BW = 42MHz$.

The characteristic $BW\text{x}L$ is: $BW\ \text{x}\ L = 336MHz\,\text{x}\,km$.

The condition

$$BW_1 \times L_1 = BW \times L \qquad (10)$$

has to be executed for realization of the link with $L_1 = 3\,km$.

Equation (10) gives $BW_1 = 112\,MHz$. It is evident that $BW_1 > BW$.

5. CONCLUSIONS

In a present work an attempt is made to show engineering approaches for determination of quantitative characteristics and parameters in the process of design of optical links. Some suitable examples illustrate comparatively simple ways for realization of preliminary approximate assessments for quantitative and qualitative indices of these links. The results received can be used in design of optical links with requiring parameters.

REFERENCES

[1] M. A. Khayer Azad, M. S. Islam, “Performanse Limitations of WDM Optical Transmission System Due to Cross-Phase Modulation in Presence of Chromatic Dispersion, Feb. 15-18, ICACT 2009.

[2] А. Снайдер, Дж. Лав, Теория оптических волноводов, Радио и связь, Москва,1987.

[3] Г. Тошев и др., Теоретична електротехника ч.4, Техника, София, 1993.

[4] P., Banerjee, T. Poon, Principles of Applied Optics, IRWIN&AAIP, USA, 1991.

[5] Д. Латева, Г. Тошев, С. Терзиева, “Възможности за разширяване на лентата на пропускане при разпространение на сигнали в оптични влакна”,”E+E”, кн.1-2, 1995.

SIMULATION INVESTIGATION OF CASCADED CONVOLUTIONAL ENCODERS USING MATLAB AND COMMUNICATION TOOLBOX

Adriana Naydenova Borodzhieva

Department of Communications and Communications Technologies,
Rousse University "Angel Kantchev", 8 Studentska Str.,
7017 Rousse, Bulgaria, phone: (00359 82) 888 734,
e-mail: aborodjieva@ecs.ru.acad.bg

Abstract: *In this paper cascaded convolutional codes are described. Two methods for modifying the generator matrix of the inner encoder in the cascade with the aim of improving the characteristics of digital communication systems are presented. A software system for simulation investigating cascaded convolutional codes when additive white Gaussian noise is available is presented in the paper. The results from investigating the cascaded convolutional codes using soft-decision Viterbi decoding are given in the paper. The results will be used in the educational process in the course "Channel Coding in Telecommunication Systems", included in the curriculum of the specialty "Communications and Communications Technologies" for the Bachelor educational degree.*

Keywords: Channel Coding, Cascaded Convolutional Codes, Simulation.

1. INTRODUCTION

Today digital communications systems (DCSs) are widely used, e.g., listening to music on a CD, making a call using a cellular phone, or sending an e-mail. Unfortunately, digital signals are affected by noise as well as analog signals. There exist disturbances in the transmission, respectively errors in the received signals. It can be due to scratches on the surface of the compact-disk or background noise for a satellite link. This motivates the use of error correcting codes in the modern DCSs where it is quite easy to add redundant data to the transmitted information that makes it possible to detect and correct some of the occurred errors. There will always be patterns of errors that cannot be corrected and the codes can be more or less effective in its work, which often result in more or less complex encoders and decoders. One way to construct good codes is to combine (concatenate) several simpler ones [1, 7].

In 1948, in the paper "A Mathematical Theory of Communication" [8] Shannon showed that without loss of optimality a communication system can be considered to be digital and that the transmission can be divided into two parts, source coding and channel coding. The first constructed codes were the Hamming codes, published in 1950. The convolutional codes were first introduced by Elias in 1955. The idea to concatenated codes was presented by Forney in his PhD thesis. Forney also invented the concept of the trellis in 1967 and began the structural analysis of convolutional codes in 1970. Concatenated convolutional codes are often suitable to be decoded by an iterative scheme. The concatenation of convolutional codes was first performed for Turbo codes in 1993 by Berrou, Glavieux, and Thitimajshima [1, 7].

In this paper a concatenation of convolutional codes is considered as the simulation results using MATLAB and Communication Toolbox [9] are presented and some conclusions are given.

2. PROBLEM STATEMENT – CASCADED CONVOLUTIONAL CODES

The structure of a convolutional encoder is illustrated in Fig. 1. Its operation is as follows: at every moment, k bits (an input frame) are led in the encoder and at the same time n bits (an output frame) are outputted from the encoder, as $n > k$. Therefore, each k-bit input frame produces n-bit output frame. The redundancy at the output is provided because $n > k$. As well, the encoder has a memory, since the output frame depends on the previous L input frames, where $L > 1$. The code rate is $R = k/n$, and it is 3/4 in the case of Fig. 1. The constraint length L is the number of the input frames stored in a kL-bit shift register. In the references several different definitions for constraint length are used [2, 5, 6]. Depending on the convolutional code that will be generated the data from kL bits (stages) of the register is added modulo 2 and is used to fix the bits in the output n-bit register [6].

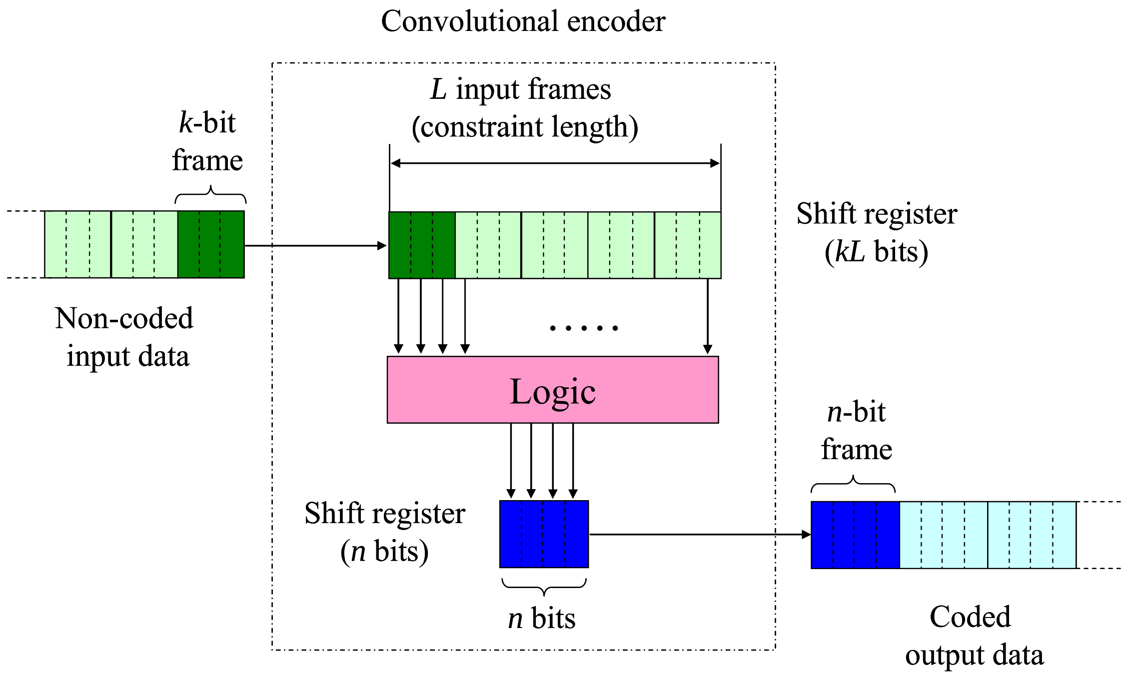

Fig. 1. Convolutional encoding ($k = 3$, $n = 4$, $L = 5$ and $R = 3/4$) [6]

Concatenation is a both powerful and practical method to obtain communication systems with low error probabilities. In the paper the simplest such construction is considered, namely a cascade of two convolutional encoders. However, to get a system with good error performance for low signal to noise ratios some sort of symbolwise permutations of the sequence between the encoders is required [7].

A cascaded convolutional encoder is a cascade of one outer encoder with code rate $R_o = k_o/n_o$ and constraint length L_o and one inner encoder with code rate $R_i = k_i/n_i$ and constraint length L_i (Fig. 2). Each binary k_o-tuple of the information sequence is encoded into a binary n_o-tuple. The encoded sequence is serialized and directly, without any permutations, fed as the information sequence for the inner encoder, where each binary k_i-tuple is encoded into a binary n_i-tuple.

Thus, the overall rate of the cascaded encoder is:

$$R_c = \frac{k_c}{n_c} = \frac{k_o}{\frac{n_o}{k_i} n_i} = \frac{k_o k_i}{n_o n_i} = R_o R_i . \tag{1}$$

It is said that the outer and inner encoders have matched rates if the outer code tuples serve directly as information tuples for the inner encoder, i.e., if $k_i = n_o$. Then the overall rate is $R_c = k_o/n_i$ [7].

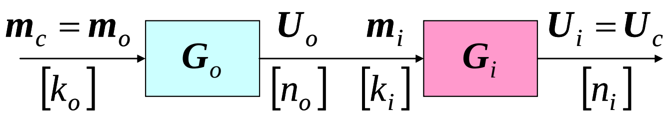

Fig. 2. A cascade of two convolutional encoders [7]

A cascaded convolutional code is a convolutional code encoded by a cascaded convolutional encoder. From

$$\boldsymbol{U}_c = \boldsymbol{U}_i = \boldsymbol{m}_i \boldsymbol{G}_i = \boldsymbol{U}_o \boldsymbol{G}_i = \boldsymbol{m}_o \boldsymbol{G}_o \boldsymbol{G}_i = \boldsymbol{m}_c \boldsymbol{G}_o \boldsymbol{G}_i \tag{2}$$

it is seen that the cascaded generator matrix $\boldsymbol{G}_c$ is given by:

$$\boldsymbol{G}_c = \boldsymbol{G}_o \boldsymbol{G}_i , \tag{3}$$

where $\boldsymbol{G}_o$ и $\boldsymbol{G}_i$ are the generator matrices of the outer and the inner encoders, respectively.

If the constituent encoders have matched rates, then equation (3) can be expressed equivalently as:

$$\boldsymbol{G}_c(D) = \boldsymbol{G}_o(D)\boldsymbol{G}_i(D), \tag{4}$$

where *D* is the delay operator, *D*-transform.

When the rates are not matched, i.e. $k_i \neq n_o$, the matrix multiplication in (4) is not defined, but (3) is still valid [7].

2.1. Cascaded Encoders Obtained from Equivalent Constituent Encoders

In this section two examples of cascaded convolutional codes are analyzed. Let the outer generator matrix $\boldsymbol{G}_o(D)$ be replaced with the equivalent generator matrix $\boldsymbol{G}'_o(D)=\boldsymbol{T}_o(D)\boldsymbol{G}_o(D)$ and the inner generator matrix $\boldsymbol{G}_i(D)$ be replaced with $\boldsymbol{G}'_i(D)=\boldsymbol{T}_i(D)\boldsymbol{G}_i(D)$, where $\boldsymbol{T}_o(D)$ and $\boldsymbol{T}_i(D)$ are non-singular. Then the generator matrix for the cascaded encoder is $\boldsymbol{G}'_c(D)=\boldsymbol{T}_o(D)\boldsymbol{G}_o(D)\boldsymbol{T}_i(D)\boldsymbol{G}_i(D)$. In general, $\boldsymbol{G}'_c(D)$ and $\boldsymbol{G}_c(D)$ are not equivalent. If only the outer generator matrix $\boldsymbol{G}_o(D)$ is replaced by an equivalent generator matrix, then the new cascaded generator matrix $\boldsymbol{G}'_c(D)$ and the cascaded generator matrix $\boldsymbol{G}_c(D)$ will be equivalent:

$$\boldsymbol{G}'_c(D)=\boldsymbol{G}'_o(D)\boldsymbol{G}_i(D)=\boldsymbol{T}(D)\boldsymbol{G}_o(D)\boldsymbol{G}_i(D)=\boldsymbol{T}(D)\boldsymbol{G}_c(D). \qquad (5)$$

The code sequences from the outer encoder serve as information sequences for the inner encoder. Therefore, the cascaded convolutional code is a proper subset of the inner convolutional code, $\boldsymbol{C}_c \subset \boldsymbol{C}_i$, assuming $R_o < 1$.

Replacing the inner encoder with an equivalent one changes the mapping from the inner information sequences to the inner code sequences and, consequently, also the subset of the inner convolutional code. In general, a different cascaded convolutional code will be obtained when the inner encoder is replaced by an equivalent one. This fact is illustrated by the following two examples [7].

Example 1. In this example the outer and the inner generator matrices are chosen to be as follows:

$$\boldsymbol{G}_o(D)=\begin{pmatrix}1+D & D\end{pmatrix},\ \boldsymbol{G}_i(D)=\begin{pmatrix}1 & 1 & D\\ 1+D & D & 1\end{pmatrix}. \qquad (6)$$

The structural models of the outer and the inner convolutional encoders are given in Fig. 3 and Fig. 4. The generators of both encoders are presented as polynomials and as binary and octal digits necessary for defining the encoder trellis in MATLAB.

The cascaded generator matrix is

$$\boldsymbol{G}_c(D)=\boldsymbol{G}_o(D)\boldsymbol{G}_i(D)=\begin{pmatrix}1+D^2 & 1+D+D^2 & D^2\end{pmatrix}, \qquad (7)$$

that generates a convolutional code with code rate $R=1/3$ and free distance $d_{\text{free}}=6$.

Let:

$$\boldsymbol{T}_j(D)=\begin{pmatrix}1 & 0\\ 0 & D^j\end{pmatrix} \qquad (8)$$

and let the inner generator matrix be replaced with the equivalent generator matrix $\boldsymbol{T}_j(D)\boldsymbol{G}_i(D)$. Then for $j=1$ the new cascaded generator matrix is:

$$\boldsymbol{G}_{1c}(D) = \boldsymbol{G}_o(D)\boldsymbol{T}_1(D)\boldsymbol{G}_i(D) = \begin{pmatrix}1+D+D^2+D^3 & 1+D+D^3 & D\end{pmatrix}, \qquad (9)$$

which gives $d_{\text{free}} = 8$. The free distance for $\boldsymbol{G}_{1c}(D)$ is superior to that of $\boldsymbol{G}_c(D)$.

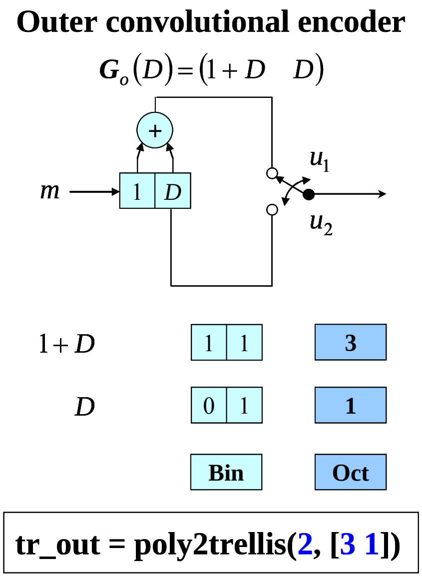

Fig. 3. Outer encoder

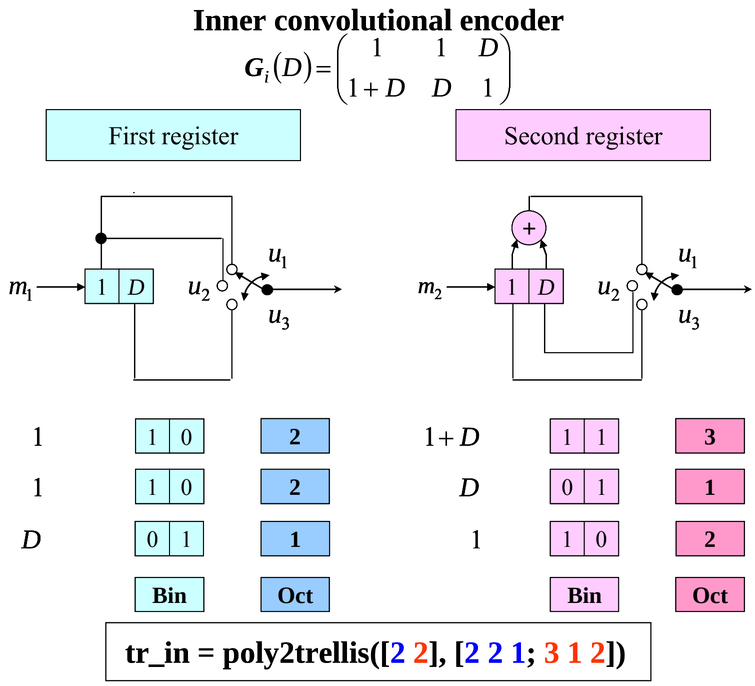

Fig. 4. Inner convolutional encoder

The structural models of the cascaded convolutional encoders are given in Fig. 5 and Fig. 6. The generators of both encoders are presented as polynomials and as binary and octal digits necessary for defining the encoder trellis in MATLAB [9].

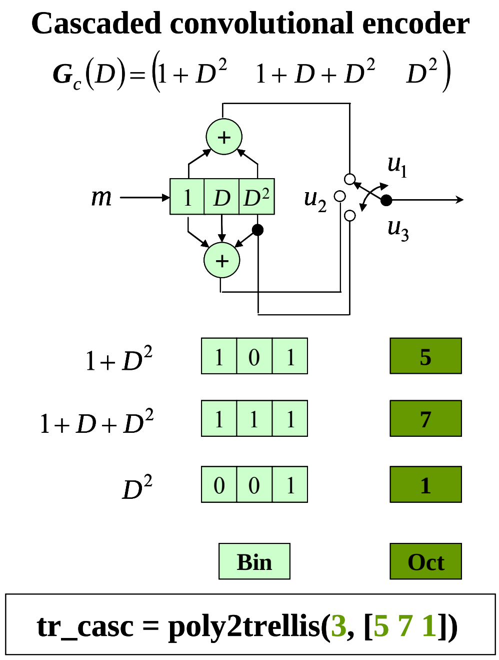

Fig. 5. Cascaded convolutional encoder

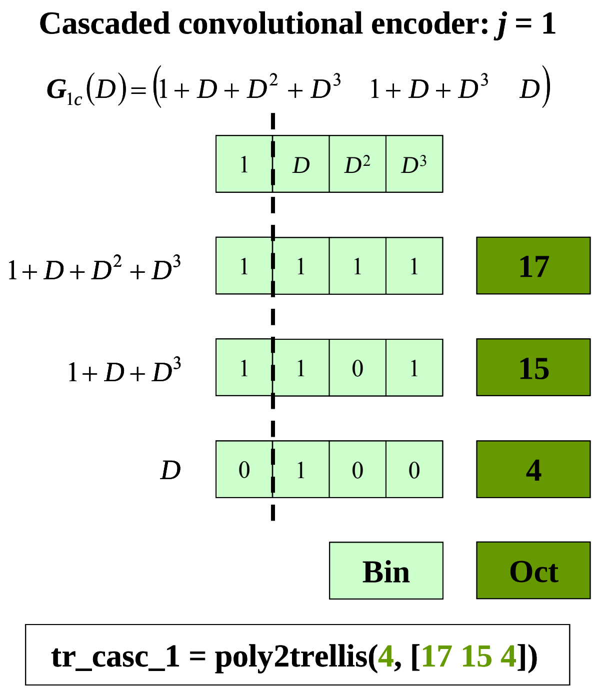

Fig. 6. Cascaded encoder, Case I, $j = 1$

Example 1 shows that the cascaded convolutional code is changed when the inner encoder is replaced by an equivalent inner encoder. Furthermore, for a given generator matrix $\boldsymbol{G}_i(D)$ there exists an infinite number of cascaded convolutional codes encoded by generator matrices $\boldsymbol{G}_{jc}(D)=\boldsymbol{G}_o(D)\boldsymbol{T}_j(D)\boldsymbol{G}_i(D),\ j=1,2,3,\ldots$.

The next example deals with catastrophic generator matrices. Since $\boldsymbol{C}_c \subset \boldsymbol{C}_i$ for $R_o<1$, catastrophicity of the inner generator matrix does not imply catastrophicity of the generator matrix for the cascade.

Example 2. In this example the outer and the inner generator matrices are chosen to be the same as in Example 1 and let:

$$\boldsymbol{T}_j(D)=\begin{pmatrix} 1+D^j & 0 \\ 0 & 1 \end{pmatrix}. \tag{10}$$

Then $\boldsymbol{G}_i'(D)=\boldsymbol{T}_j(D)\boldsymbol{G}_i(D)$ is catastrophic [7]. However, the cascaded generator matrix, $\boldsymbol{G}_{jc}(D)=\boldsymbol{G}_o(D)\boldsymbol{T}_j(D)\boldsymbol{G}_i(D)$ is non-catastrophic for $j\ge 1$. It can be seen that for $j=6$ a larger free distance than in Example 1 is obtained, namely $d_{\text{free}}=11$.

Mention may here be made that if decoding cascaded convolutional codes is performed in two steps (first the inner convolutional code and then the outer one), the catastrophicity of the inner generator matrix might still be damaging.

Table 1 represents the matrix for modifying the inner generator matrix, the modified inner generator matrix and the matrix of the cascaded convolutional encoder for both examples (Case I and Case II).

Table 1. Cascaded convolutional encoders

Case I	**Case II**
Matrix for modifying the inner generator matrix	
$\boldsymbol{T}_j(D)=\begin{pmatrix} 1 & 0 \\ 0 & D^j \end{pmatrix}$	$\boldsymbol{T}_j(D)=\begin{pmatrix} 1+D^j & 0 \\ 0 & 1 \end{pmatrix}$
Modified inner generator matrix $\boldsymbol{G}_i'(D)=\boldsymbol{T}_j(D).\boldsymbol{G}_i(D)$	
$\boldsymbol{G}_i'(D)=\begin{pmatrix} 1 & 1 & D \\ D^j+D^{j+1} & D^{j+1} & D^j \end{pmatrix}$	$\boldsymbol{G}_i'(D)=\begin{pmatrix} 1+D^j & 1+D^j & D+D^{j+1} \\ 1+D & D & 1 \end{pmatrix}$
Matrix of the cascaded convolutional encoder $\boldsymbol{G}_{jc}(D)=\boldsymbol{G}_o(D).\boldsymbol{T}_j(D).\boldsymbol{G}_i(D)$	
$\boldsymbol{G}_{jc}(D)=\begin{pmatrix} 1+D+D^{j+1}+D^{j+2} \\ 1+D+D^{j+2} \\ D+D^2+D^{j+1} \end{pmatrix}^T$	$\boldsymbol{G}_{jc}(D)=\begin{pmatrix} 1+D^2+D^j+D^{j+1} \\ 1+D+D^2+D^j+D^{j+1} \\ D^2+D^{j+1}+D^{j+2} \end{pmatrix}^T$

3. RESULTS

The generator matrices of the cascaded convolutional codes are given in Table 2 (for Case I) and in Table 3 (for Case II) for $j = 1 \div 10$.

MATLAB scripts are developed for calculating the number of erroneous bits and the bit error rate (BER) of the cascaded convolutional codes. The algorithms for investigating convolutional encoders and decoders in the presence of noise when hard-decision and soft-decision Viterbi decoding is used are presented in [2, 3, 4].

Table 2. Cascaded convolutional encoders – Case I

$j=1$	$\boldsymbol{G}_{1c}(D) = (1+D+D^2+D^3 \quad 1+D+D^3 \quad D)$
$j=2$	$\boldsymbol{G}_{2c}(D) = (1+D+D^3+D^4 \quad 1+D+D^4 \quad D+D^2+D^3)$
$j=3$	$\boldsymbol{G}_{3c}(D) = (1+D+D^4+D^5 \quad 1+D+D^5 \quad D+D^2+D^4)$
$j=4$	$\boldsymbol{G}_{4c}(D) = (1+D+D^5+D^6 \quad 1+D+D^6 \quad D+D^2+D^5)$
$j=5$	$\boldsymbol{G}_{5c}(D) = (1+D+D^6+D^7 \quad 1+D+D^7 \quad D+D^2+D^6)$
$j=6$	$\boldsymbol{G}_{6c}(D) = (1+D+D^7+D^8 \quad 1+D+D^8 \quad D+D^2+D^7)$
$j=7$	$\boldsymbol{G}_{7c}(D) = (1+D+D^8+D^9 \quad 1+D+D^9 \quad D+D^2+D^8)$
$j=8$	$\boldsymbol{G}_{8c}(D) = (1+D+D^9+D^{10} \quad 1+D+D^{10} \quad D+D^2+D^9)$
$j=9$	$\boldsymbol{G}_{9c}(D) = (1+D+D^{10}+D^{11} \quad 1+D+D^{11} \quad D+D^2+D^{10})$
$j=10$	$\boldsymbol{G}_{10c}(D) = (1+D+D^{11}+D^{12} \quad 1+D+D^{12} \quad D+D^2+D^{11})$

The simulation results (number of erroneous bits and BER) when soft-decision Viterbi decoding is used are given in Table 4.

Table 3. Cascaded convolutional encoders – Case II

$j=1$	$\boldsymbol{G}_{1c}(D) = (1+D \quad 1 \quad D^3)$
$j=2$	$\boldsymbol{G}_{2c}(D) = (1+D^3 \quad 1+D+D^3 \quad D^2+D^3+D^4)$
$j=3$	$\boldsymbol{G}_{3c}(D) = (1+D^2+D^3+D^4 \quad 1+D+D^2+D^3+D^4 \quad D^2+D^4+D^5)$
$j=4$	$\boldsymbol{G}_{4c}(D) = (1+D^2+D^4+D^5 \quad 1+D+D^2+D^4+D^5 \quad D^2+D^5+D^6)$
$j=5$	$\boldsymbol{G}_{5c}(D) = (1+D^2+D^5+D^6 \quad 1+D+D^2+D^5+D^6 \quad D^2+D^6+D^7)$
$j=6$	$\boldsymbol{G}_{6c}(D) = (1+D^2+D^6+D^7 \quad 1+D+D^2+D^6+D^7 \quad D^2+D^7+D^8)$
$j=7$	$\boldsymbol{G}_{7c}(D) = (1+D^2+D^7+D^8 \quad 1+D+D^2+D^7+D^8 \quad D^2+D^8+D^9)$
$j=8$	$\boldsymbol{G}_{8c}(D) = (1+D^2+D^8+D^9 \quad 1+D+D^2+D^8+D^9 \quad D^2+D^9+D^{10})$
$j=9$	$\boldsymbol{G}_{9c}(D) = (1+D^2+D^9+D^{10} \quad 1+D+D^2+D^9+D^{10} \quad D^2+D^{10}+D^{11})$
$j=10$	$\boldsymbol{G}_{10c}(D) = (1+D^2+D^{10}+D^{11} \quad 1+D+D^2+D^{10}+D^{11} \quad D^2+D^{11}+D^{12})$

Table 4. Simulation investigating of cascaded convolutional encoders using soft-decision Viterbi decoding (number & ratio) – Case I

Encoder	Number of input bits		
	10000	30000	1000000
tr_out (2,[3 1]) dfree = 3	138 0.0138	374 0.0125	13096 0.0131
tr_in ([2 2],[2 2 1; 3 1 2]) dfree = 3	4836 0.4851	14980 0.4998	500622 0.5006
tr_casc (3,[5 7 1]) dfree = 6	2 2.0048e-004	18 6.0048e-004	562 5.6201e-004
tr_casc_1 (4,[17 15 4]) dfree = 8	7 7.0211e-004	14 4.6713e-004	184 1.8401e-004
tr_casc_2 (5,[33 31 16]) dfree = 10	0 0	0 0	55 5.5002e-005
tr_casc_3 (6,[63 61 32]) dfree = 10	0 0	1 3.3380e-005	24 2.4001e-005
tr_casc_4 (7,[143 141 62]) dfree = 10	0 0	0 0	7 7.0003e-006
tr_casc_5 (8,[303 301 142]) dfree = 10	2 2.0109e-004	2 6.6787e-005	10 1.0001e-005
tr_casc_6 (9,[603 601 302]) dfree = 10	0 0	1 3.3400e-005	12 1.2001e-005
tr_casc_7 (10,[1403 1401 602]) dfree = 10	1 1.0066e-004	1 3.3407e-005	13 1.3001e-005
tr_casc_8 (11,[3003 3001 1402]) dfree = 10	0 0	0 0	15 1.5001e-005
tr_casc_9 (12,[6003 6001 3002]) dfree = 10	0 0	0 0	5 5.0004e-006
tr_casc_10 (13,[14003 14001 6002]) dfree = 10	0 0	0 0	8 8.0007e-006

In the 1st column of Table 4 the trellis representation in MATLAB of the convolutional encoders (according to Fig. 3 – Fig. 6), and the value of the free distance parameter of the encoder are given. Then the number of erroneous bits and BER are presented. The message consists of 10 000, 30 000 or 1 000 000 bits.

4. CONCLUSIONS

In this paper cascaded convolutional codes are described. Two methods for modifying the generator matrix of the inner encoder in the cascade with the aim of improving the characteristics of digital communication systems are presented. A software system for simulation investigating cascaded convolutional codes when additive white Gaussian noise is available is presented in the paper. The scripts developed in MATLAB allow cascaded convolutional codes to be investigated when hard-decision and soft-decision Viterbi decoding is used for both the cases of modifying the inner generator matrix presented in the paper. The results from investigating the cascaded convolutional codes using soft-decision Viterbi decoding are given. The results will be used in the educational process in the course “Channel Coding in Telecommunication Systems”, included in the curriculum of the specialty “Communications and Communications Technologies” for the Bachelor educational degree.

REFERENCES

[1] Бороджиева, А. Канално кодиране в цифровите комуникационни системи с използване на прости ефективни кодове. Научна сесия РУ – СУ'04; Русе; 29 – 30.10.2004г.; РУ „Ангел Кънчев”; Научни трудове, Том 41, серия 3.2, Комуникационна и компютърна техника и технологии; 90 – 94 стр.; ISSN 1311-3321.

[2] Borodzhieva, A., P. Manoilov. Simulating the Operation of Feed-forward Convolutional Encoders and Viterbi Decoders Applied in Additive White Gaussian Noise Communication Channels. International Conference CompSysTech’08, Gabrovo, 12 – 13 June 2008, pp. IIIB.13-1 – IIIB.13-6.

[3] Borodzhieva, A., P. Manoilov. Software Tool for Simulating Convolutional Encoding and Decoding Used in Communication Systems. Fourth International Bulgarian-Greek Conference – Computer Science’2008, 18 – 19 September 2008, Kavala, Greece, Proceedings, International Workshop BioComputing’2008, Part III, pp. 851 – 856.

[4] Бороджиева, А. Теория и приложения на конволюционното кодиране в комуникационните системи. Русе; Печатна база на Русенски университет „Ангел Кънчев”; 2008 г.; 160 страници; ISBN - 978-954-712-431-8.

[5] Скляр, Б. Цифровая связь. Теоретические основы и практическое применение. Москва, Вильямс, 2003.

[6] Couch, L. W. Digital and Analog Communication Systems. 6th edition, Prentice Hall International Editions, 2001.

[7] Höst, St. On Woven Convolutional Codes. PhD Thesis, Lund University, Sweden, 1999. http://www.it.lth.se/stefanh/Thesis/Thesis.pdf.

[8] Shannon, C. E. A Mathematical Theory of Communication. Bell System Technical Journal, vol. 27, July 1948, pp. 379 – 423, and October 1948, pp. 623 – 656.

[9] www.mathworks.com.

SOFTWARE SYSTEM FOR CONVOLUTIONAL ENCODERS INVESTIGATION USING MATLAB AND COMMUNICATION TOOLBOX

Adriana Naydenova Borodzhieva

Department of Communications and Communications Technologies,
Rousse University "Angel Kantchev",
8 Studentska Str., 7017 Rousse, Bulgaria, phone: (00359 82) 888 734,
e-mail: aborodjieva@ecs.ru.acad.bg

Abstract: *In this paper implemented and improved software system for investigating convolutional encoders widely used in digital communication systems when additive white Gaussian noise is available is described. The results regarding the time necessary for "searching" the "data bases" of the "candidates for the best encoders" when the constraint length and the number of the generator polynomials are known and finding out "the best encoder" for the practical example of the test using hard-decision and soft-decision Viterbi decoding are presented in the paper. The simulation time may be decreased after excluding the catastrophic convolutional encoders from the "data bases"; in fact, these encoders do not have a good chance of being "the best". In this way a new improved version of the software system for convolutional encoders' investigation is proposed in the paper. The results will be used in the educational process in the course "Channel Coding in Telecommunication Systems", included in the curriculum of the specialty "Communications and Communications Technologies" for the Bachelor educational degree.*

Keywords: Channel Coding, Convolutional Codes, Simulation.

1. INTRODUCTION

In telecommunications and information theory, error detection and correction has great practical importance in maintaining data integrity across noisy channels and less-than-reliable storage media [9]. Error detection is the ability to detect the presence of errors caused by noise or other impairments during transmission from the transmitter to the receiver in a digital communication system. Error correction is the additional ability to reconstruct the original, error-free data. There are two basic ways to design the channel code and protocol for an error correcting system: Automatic repeat-request (ARQ) and Forward error correction (FEC) [9].

In FEC systems, the transmitter encodes the data with an error-correcting code and sends the coded message. The receiver never sends any messages back to the transmitter. The receiver decodes what it receives into the "most likely" data [9]. The purpose of forward error correction is improving the capacity of a communication channel by adding redundant information to the data transmitted over the channel. The two main forms of channel coding are block coding and convolutional coding. Convolutional codes operate on serial data, while block codes operate on relatively large message blocks. Convolutional encoders accept a fixed number of message symbols and produce a fixed number of code symbols. Their computations depend on the current set of input symbols and on some previous input symbols [1, 3].

2. PROBLEM STATEMENT – CONVOLUTIONAL CODES

In telecommunications, a convolutional code is a type of error-correcting code in which each k-bit information symbol (each k-bit string) to be encoded is transformed into an n-bit symbol, where k/n is the code rate ($n \geq k$) and the transformation is a function of the last L information symbols, where L is the constraint length of the code [3, 7]. The structure of a convolutional encoder is illustrated in Fig. 1. The code rate is $R = k/n = 3/4$ (Fig. 1). The constraint length L is the number of the input frames stored in a kL-bit shift register.

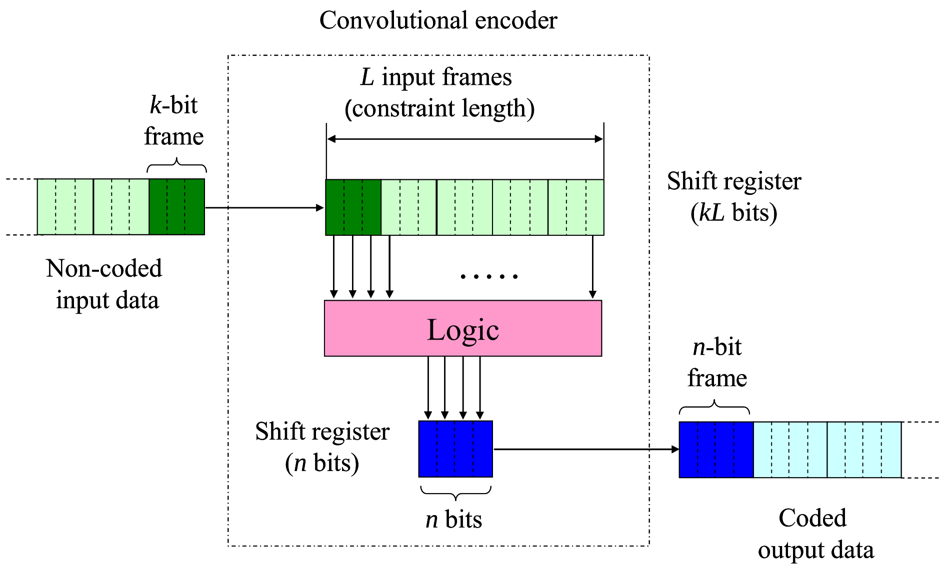

Fig. 1. Convolutional encoding ($k = 3$, $n = 4$, $L = 5$ and $R = 3/4$) [7]

Nowadays convolutional encoding with Viterbi decoding is widely used in modern communication systems. Convolutional codes [9] are often used to improve the performance of digital radio, mobile phones, satellite links, and Bluetooth implementations.

2.1. Software System for Convolutional Encoders Investigation

A software system for convolutional encoders' investigation is developed using the computational and graphical environment MATLAB and its extensions Communications Toolbox and Symbolic Math Toolbox [8]. It was presented in details in [1, 2, 6]. In this paper an improved version of the software system for convolutional encoders' investigation is proposed. It allows the simulation time to be decreased after excluding from the "data bases" the catastrophic convolutional encoders that do not have a good chance of being "the best encoders".

The software system is composed of four modules. Here, only Module 1 (“Divide and Search”) and Module 2 (“Convolutional encoding and decoding”) are considered.

2.1.1. Module 1

The first module (Fig. 2) consists of a multitude of created scripts DS_*L*_*GP*.m, implementing the procedure “Divide and Search”. It comprises the processes “dividing” the encoders’ generator polynomials combinations into two groups: valid and non-valid, and „searching” the valid combinations to find out the encoders with the maximum free distance parameter, a criterion for the correcting capabilities of the convolutional encoder. The scripts DS_*L*_*GP*.m allow to pass through all the possible combinations for generator polynomials of encoders with a code rate $R = 1/n$, with a given constraint length *L* and a given number of generator polynomials *GP*.

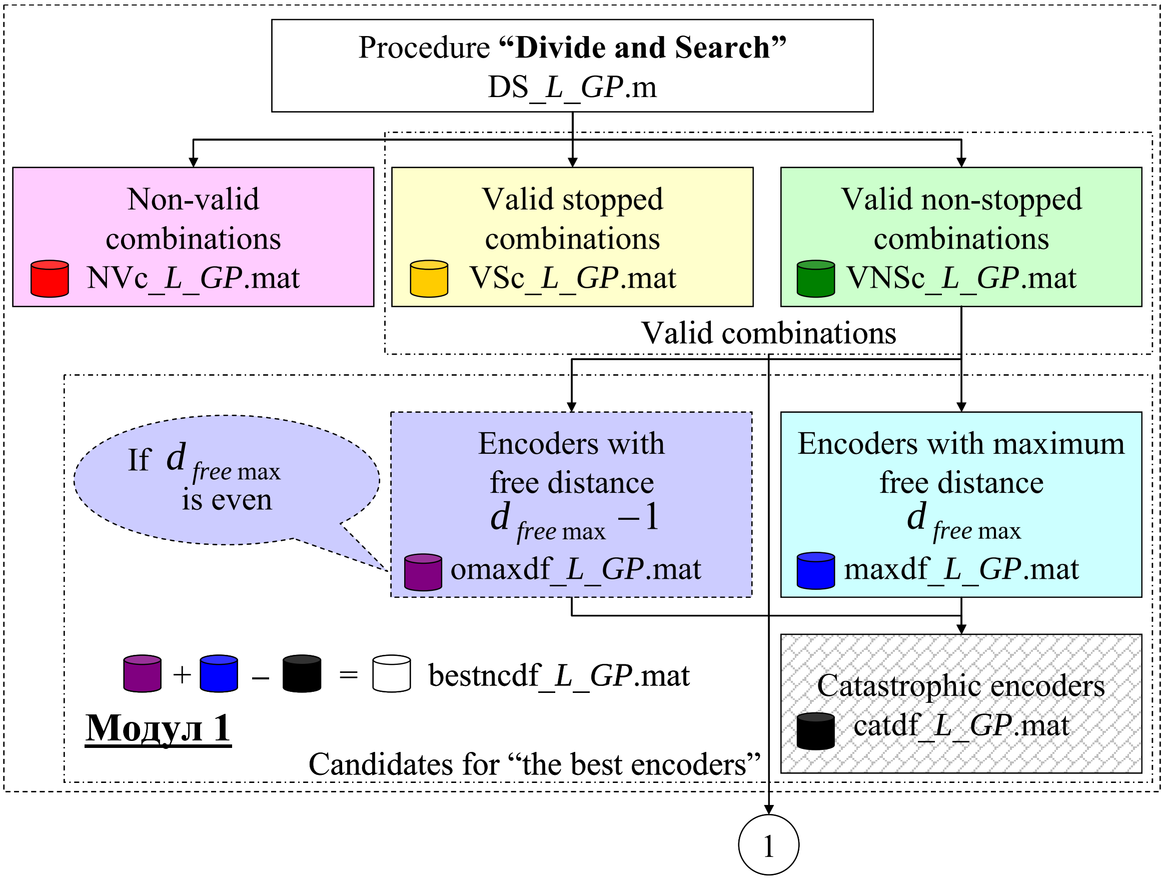

Fig. 2. The architecture of the software system – Module 1

After passing through all possible combinations for generator polynomials, they are divided into two groups: 1) non-valid combinations, stored in a “data-base” NVc_*L*_*GP*.mat and further not investigated – these are the combinations where the output code symbols do not depend on the current input bit of the message to be encoded and/or the most right flip-flop of the shift register, generating the convolutional code; it means that the condition for defining the code constraint length parameter is violated; 2) valid combinations, also divided into two sub-groups: valid “stopped” –

stored in a “data-base” VSc_*L*_*GP*.mat, where the simulation was stopped after expiring a fixed period of time while trying to determine their free distance parameter, and valid “non-stopped” combinations, stored in a “data-base” VNSc_*L*_*GP*.mat, where the simulation during the procedure “divide and search” is finished successfully as their free distance parameter is determined (calculated). Information about the corresponding value of the free distance parameter for all valid non-stopped combinations is stored in a separate “data base” VNSc_L_GP_df.mat. The combinations (from all valid “non-stopped” combinations) with maximum free distance parameter $d_{free\,\max}$ are stored in a separate “data-base” maxdf_*L*_*GP*.mat. If $d_{free\,\max}$ is an even number, then the “data base” omaxdf_*L*_*GP*.mat is generated where the encoders with free distance $d_{free\,\max}-1$ are stored. These two “data bases” form the “data base” best_*L*_*GP*.mat where all possible “candidates for the best encoders” are stored. The “data bases” maxdf_*L*_*GP*.mat, omaxdf_*L*_*GP*.mat and best_*L*_*GP*.mat also have duplicates (maxdf_*L*_*GP*_df.mat, omaxdf_*L*_*GP*_df.mat and best_*L*_*GP*_df.mat) where information about the corresponding value of the free distance parameter is stored in the last column.

At the present moment, the following cases are realized: 1) $L=3$ and $GP=2\div5$; 2) $L=4$ and $GP=2\div5$; 3) $L=5$ and $GP=2\div5$; 4) $L=6$ and $GP=2\div3$; 5) $L=7$ and $GP=2\div3$; 6) $L=8$ and $GP=2\div3$; 7) $L=9$ and $GP=2$; 8) $L=10$ and $GP=2$.

For these cases, the number of all possible combinations for generator polynomials of the convolutional encoders (N), the number of the non-valid (N_{NV}), valid “stopped” (N_{VS}) and valid “non-stopped” (N_{VNS}) combinations are given in Table 1. The number of the encoders with maximum free distance parameter $d_{free\,\max}$ (N_{maxdf}), the number of the encoders with free distance $d_{free\,\max}-1$ (N_{omaxdf}) and the number of all encoders-“candidates for the best encoders” (N_{best}) are also presented in Table 1.

In the last column of Table 1 the maximum free distance $d_{free\,\max}$ is given. It can be seen that the increase of the number *GP* of the generator polynomials and/or the constraint length *L* rises the maximum free distance of the encoder, respectively its correcting capabilities. Table 1 contains information about the number of the catastrophic convolutional encoders (N_{catdf}) that must be excluded from the “data bases” best_*L*_*GP*.mat, respectively best_*L*_*GP*_df.mat since these encoders do not have a good chance of being “the best”. This makes the simulation time to be decreased. For the case $L=3$ and $GP=2$ the number of the catastrophic encoders is determined from all valid combinations of the generator polynomials.

Table 1. Number of combinations in all "data bases" when *L* and *GP* are known

L*_*GP	***N***	N_{NV}	N_{VS}	N_{VNS}	N_{maxdf}	N_{omaxdf}	N_{best}	N_{catdf}	$N_{bestncdf}$	**max df**
3_2	**49**	17	4	28	2	0	**2**	8	**24**	**5**
3_3	**343**	53	8	282	3	15	**18**	6	**12**	**8**
3_4	**2401**	161	16	2224	34	112	**146**	0	**146**	**10**
3_5	**16807**	485	32	16290	10	0	**10**	0	**10**	**13**
4_2	**225**	89	14	122	16	32	**48**	6	**42**	**6**
4_3	**3375**	659	52	2664	12	54	**66**	0	**66**	**10**
4_4	**50625**	4721	170	45734	24	0	**24**	0	**24**	**13**
4_5	**759375**	33371	484	725520	830	3340	**4170**	0	**4170**	**16**
5_2	**961**	401	50	510	2	14	**16**	4	**12**	**8**
5_3	**29791**	6407	245	23139	6	72	**78**	0	**78**	**12**
5_4	**923521**	98849	1506	823166	54	528	**582**	6	**576**	**16**
5_5	**28629151**	1501943	7253	27119955	1086	2124	**3210**	0	**3210**	**20**
6_2	**3969**	1697	176	2096	202	334	**536**	94	**442**	**8**
6_3	**250047**	56207	1366	192474	168	0	**168**	0	**168**	**13**
7_2	**16129**	6977	584	8568	14	182	**196**	24	**172**	**10**
7_3	**2048383**	470303	7235	1570845	216	0	**216**	12	**204**	**15**
8_2	**65025**	28289	1914	34822	1706	3568	**5274**	1118	**4156**	**10**
8_3	**16581375**	3846719	40645	12694011	50246	152443	**202689**	0	**202689**	**16**
9_2	**261121**	113921	6076	141124	138	1104	**1242**	118	**1124**	**12**
10_2	**1046529**	457217	19264	570048	13492	31838	**45330**	0	**45330**	**12**

3. RESULTS

MATLAB scripts are developed for calculating the number of erroneous bits and the bit error rate (BER) of the convolutional codes. The algorithms for investigating convolutional encoders and decoders in the presence of noise when hard-decision and soft-decision Viterbi decoding is used are presented in [2, 3, 4].

The results regarding the time necessary for "searching" the "data bases" of the "candidates for the best encoders" when the constraint length *L* and the number of the generator polynomials *GP* are known and finding out "the best encoder" for the practical example of the test using hard-decision and soft-decision Viterbi decoding are presented in Table 2 (in seconds, minutes and hours). The number of the information bits is $k = 1\ 000\ 000$.

Table 3 shows that simulation time may be decreased after excluding the catastrophic convolutional encoders from the "data bases" since these encoders do not have a good chance of being "the best".

Table 2. Simulation results for all encoders in the "data bases" best_*L*_*GP*_df.mat

Number of information bits: $k = 10^6$							
Encoder *L*_*GP*	**Number of combinations for simulation (data bases)**	**Mode: Viterbi algorithm - hard-decision**			**Mode: Viterbi algorithm - soft-decision**		
		sec	**min**	**h**	**sec**	**min**	**h**
3_2	2 (best_3_2_df.mat)	101.859000	1.6977	-	15.062000	-	-
	4 (VSc_3_2.mat)	205.218000	3.4203	-	30.687000	-	-
	28 (VNSc_3_2_df.mat)	1442.093000	24.0349	-	219.829000	3.6638	-
3_3	18 (best_3_3_df.mat)	1374.859000	22.9143	-	56.016000	-	-
3_4	146 (best_3_4_df.mat)	14252.407000	237.5401	3.9590	1598.672000	26.6445	-
3_5	10 (best_3_5_df.mat)	1247.547000	20.7924	-	134.547000	2.2424	-
4_2	48 (best_4_2_df.mat)	2527.938000	42.1323	-	435.672000	7.2612	-
4_3	66 (best_4_3_df.mat)	4990.469000	83.1745	1.3862	702.141000	11.7024	-
4_4	24 (best_4_4_df.mat)	2399.266000	39.9878	-	302.000000	5.3333	-
4_5	4170 (best_4_5_df.mat)	577097.124000	9618.2854	160.3048	61382.876000	1023.0479	17.0508
5_2	16 (best_5_2_df.mat)	864.000000	14.4000	-	185.500000	3.0917	-
5_3	78 (best_5_3_df.mat)	7027.937000	117.1323	1.9522	1098.750000	18.3125	-
5_4	582 (best_5_4_df.mat)	60374.203000	1006.2367	16.7706	8467.640000	141.1273	2.3521
5_5	3210 (best_5_5_df.mat)	448601.452000	7476.6909	124.6115	54004.734000	900.0789	18.0016
6_2	536 (best_6_2_df.mat)	30916.532000	515.2755	8.5879	8028.359000	133.8060	2.2301
6_3	168 (best_6_3_df.mat)	13464.000000	224.4000	3.7400	2753.281000	45.8880	-
7_2	196 (best_7_2_df.mat)	12619.172000	210.3195	3.5053	4213.000000	70.2167	1.1703
7_3	216 (best_7_3_df.mat)	18911.281000	315.1880	5.2531	4973.125000	82.8854	1.3814
8_2	5274 (best_8_2_df.mat)	421863.910000	7031.0651	117.1844	178919.842000	2981.9974	49.7000
9_2	1242 (best_9_2_df.mat)	129143.394000	2152.3899	35.8732	72932.891000	1215.5482	20.2591

Table 3. Reducing the simulation time

Number of information bits: $k = 10^6$							
Encoder *L*_*GP*	**Number of combinations for simulation (data bases)**	**Mode: Viterbi algorithm - hard-decision**			**Mode: Viterbi algorithm - soft-decision**		
		sec	**min**	**h**	**sec**	**min**	**h**
6_2	536 (best_6_2_df.mat)	30916.532000	515.2755	8.5879	8028.359000	133.8060	2.2301
	442 (bestnc_6_2_df.mat)	25500.156000	425.0026	7.0834	6590.516000	109.8419	1.8307
	↓ 17.5 %	↓ 17.5 %			↓ 17.9 %		
8_2	5274 (best_8_2_df.mat)	421863.910000	7031.0651	117.1844	178919.842000	2981.9974	49.7000
	4156 (bestnc_8_2_df.mat)	318038.718000	5300.6453	88.3441	140743.031000	2345.7172	39.0953
	↓ 21.2 %	↓ 24.6 %			↓ 21.3 %		
9_2	1242 (best_9_2_df.mat)	129143.394000	2152.3899	35.8732	72932.891000	1215.5482	20.2591
	1124 (bestnc_9_2_df.mat)	113703.140000	1895.0523	31.5842	65961.766000	1099.3628	18.3227
	↓ 9.5 %	↓ 12.0 %			↓ 9.6 %		

It can be seen (Table 3) that:

- in case of $L = 6$ and $GP = 2$, the number of encoders to be tested is reduced by 17.5 %, the simulation time is reduced by 17.5 % when hard-decision Viterbi decoding is used and by 17.9 % when soft-decision Viterbi decoding is used.
- in case of $L = 8$ and $GP = 2$, the number of encoders to be tested is reduced by 21.2 %, the simulation time is reduced by 24.6 % when hard-decision Viterbi decoding is used and by 21.3 % when soft-decision Viterbi decoding is used.

- in case of $L = 9$ and $GP = 2$, the number of encoders to be tested is reduced by 9.5 %, the simulation time is reduced by 12.0 % when hard-decision Viterbi decoding is used and by 9.6 % when soft-decision Viterbi decoding is used.

4. CONCLUSIONS

In this paper implemented and improved software system for investigating convolutional encoders widely used in digital communication systems when additive white Gaussian noise is available is described. The results regarding the time necessary for "searching" the "data bases" of the "candidates for the best encoders" when the constraint length and the number of the generator polynomials are known and finding out "the best encoder" for the practical example of the test using hard-decision and soft-decision Viterbi decoding are presented in the paper. The simulation time may be decreased after excluding the catastrophic convolutional encoders from the "data bases" since these encoders do not have a good chance of being "the best". In this way a new improved version of the software system for convolutional encoders' investigation is proposed in the paper. The results will be used in the educational process in the course "Channel Coding in Telecommunication Systems", included in the curriculum of the specialty "Communications and Communications Technologies" for the Bachelor educational degree.

REFERENCES

[1] Бороджиева, А. Теория и приложения на конволюционното кодиране в комуникационните системи. Русе; Печатна база на Русенски университет „Ангел Кънчев"; 2008 г.; 160 страници; ISBN - 978-954-712-431-8.

[2] Бороджиева, А. Софтуерна система за симулационно изследване на конволюционни кодери и декодери. Научна конференция РУ – СУ'08; Русе; 31.10. – 01.11.2008г.; Научни трудове на РУ „Ангел Кънчев"; Том 47, серия 3.2, Комуникационна и компютърна техника и технологии; 73 – 79 стр.; ISSN 1311-3321.

[3] Скляр, Б. Цифровая связь. Теоретические основы и практическое применение. Москва, Вильямс, 2003.

[4] Borodzhieva, A., P. Manoilov. Simulating the Operation of Feed-forward Convolutional Encoders and Viterbi Decoders Applied in Additive White Gaussian Noise Communication Channels. International Conference CompSysTech'08, Gabrovo, 12 – 13 June 2008, pp. IIIB.13-1 – IIIB.13-6.

[5] Borodzhieva, A., P. Manoilov. Software Tool for Simulating Convolutional Encoding and Decoding Used in Communication Systems. Fourth International Bulgarian-Greek Conference – Computer Science'2008, 18 – 19 September 2008, Kavala, Greece, Proceedings, International Workshop BioComputing'2008, Part III, pp. 851 – 856.

[6] Borodzhieva, A. Software Instruments for Investigating Convolutional Encoding and Decoding Processes Applied in Communication Systems. International Symposium for Design and Technology of Electronic Packaging, 14th Edition, SIITME 2008, September 18 – 21, Predeal, Romania, Conference proceedings, pp. 135 – 139, ISSN 1843-5122.

[7] Couch, L. W. Digital and Analog Communication Systems. 6th edition, Prentice Hall International Editions, 2001.

[8] www.mathworks.com.

[9] http://en.wikipedia.org/wiki/Error_correction_and_detection.

INFLUENCE OF IONIZATION ON THE MATERIAL PARAMETERS IN THE PROPAGATION HIGH-INTENSITY FEMTOSECOND LASER PULSES

M. E. Todorova*, T. P. Todorov, M. D. Todorov***, I. G. Koprinkov******

* Integrated Technical College, Technical University of Sofia, 8 Kl. Ohridski Blvd, 1000 Sofia, Bulgaria, phone: +02 965 3072, e-mail: metodorova@tu-sofia.bg

** Department of Applied Physics, Technical University of Sofia, 8 Kl. Ohridski Blvd, 1000 Sofia, Bulgaria, phone: +02 965 3072, e-mail: totodorov@tu-sofia.bg

*** Faculty of Applied Mathematics and Informatics, Technical University of Sofia, 8 Kl. Ohridski Blvd, 1000 Sofia, Bulgaria, phone: +02 965 2358, e-mail: mtod@tu-sofia.bg

**** Department of Applied Physics, Technical University of Sofia, 8 Kl. Ochridski Blvd, 1000 Sofia, Bulgaria, phone: +02 965 3072, e-mail: igk@tu-sofia.bg

Резюме: *The influence of ionization on the material parameters in the propagation of high-intensity femtosecond laser pulse is studied. The spatio-temporal dynamics of the pulse and the evolution of the material parameters are described self-consistently within an advanced physical model, including (3+1)D nonlinear envelope equation as a propagation equation. The evolution of the material parameters and their influence on pulse propagation dynamics is found.*

Keywords: pulse propagation, nonlinear envelope equation, material parameters, ionization, pulse compression

1. INTRODUCTION

The high-intensity laser pulse propagation may cause strong modification of the material parameters by a number processes. Among these, the role of ionization is especially important because the generated free or quasi-free electrons have strong contribution to the refractive index, create substantial losses and, as has been recently shown, strongly modifies the group velocity dispersion [1]. The group velocity dispersion, and especially its sign, plays a crucial role in the pulse propagation. At positive group velocity dispersion, the optical pulse usually spreads and splits in time [2-4], while formation of an optical soliton may take place at negative group velocity dispersion [5]. Self-compression of femtosecond laser pulses and stable propagation of the compressed pulse has been discovered in a number of media at positive group velocity dispersion regime [6-8]. The modified material parameters may strongly affect the pulse propagation by a number of self-action processes. That is why knowledge of the role of ionization in a real propagation regime has great importance for the prediction of the pulse propagation dynamics. In this work have studied the influence of ionization on the material parameters in a dynamical propagation regime.

2. PHYSICAL MODEL

We consider an advanced physical model described in [9]. The field is presented in terms of the envelope-carrier concept [10]

$$E(t) = \tilde{E}_0(t)\exp(-i\omega_0 t + i\varphi) + c.c. \tag{1}$$

The propagation equation within the specified physical model is the (3+1)D non-linear envelope equation (NEE) (in standard notations [9])

$$\begin{aligned}\frac{\partial A}{\partial z} = {} & \frac{i}{2k_0}T^{-1}\nabla_\perp^2 A + iDA \\ & + i\frac{\omega_0}{c}n_2 T\left[(1-x)|A|^2 + x\int_{-\infty}^{t} h(t-t')|A(t')|^2 dt'\right]A - i\frac{\omega_0}{c}n_4 T|A|^4 A \\ & - i\frac{k_0}{2n_0^2\rho_c}T^{-1}\rho A - \frac{\sigma}{2}\rho A - \frac{\beta_{MPI}(A)}{2}A\end{aligned} \tag{2}$$

The physical processes involved in the model are: *linear processes*, diffraction and dispersion (the first and the second terms, respectively), *nonlinear processes in the neutrals*, cubic and quintic non-linearity (third and the forth terms, respectively), and *processes associated with the ionization*, the ionization modification of the refractive index, collisional ionization by inverse bremsstrahlung and multi-photon/tunneling ionization losses (fifth, sixth and the seventh terms, respectively). The cubic term includes both, the instantaneous and the non-instantaneous response of the medium.

The electron number density ρ is described by a kinetic equation (5), [9]

$$\frac{\partial\rho}{\partial t} = W(I)(\rho_n - \rho) + \frac{\sigma(\omega_0)}{I_P}|A|^2\rho - f(\rho) \tag{3}$$

The ionization rate $W(I)$ is described within the Perelomov-Popov-Terent'ev (PPT) theory [11], which appears to be the best general ionization theory.

$$\begin{aligned}W_{PPT}(t) = {} & \sqrt{\frac{6}{\pi}}\, I_P \left|C_{n^* l^*}\right|^2 \frac{(2l+1)(l+|m|)!}{2^{|m|}|m|!(l-|m|)!}\left(\frac{2(2I_P)^{3/2}}{E(t)}\right)^{2n^*-|m|-3/2}\left(1+\gamma^2\right)^{|m|/2+3/4} \\ & \times A_m(\omega,\gamma)\exp\left(-\frac{2(2I_P)^{3/2}}{3E(t)}g(\gamma)\right)\end{aligned} \tag{4}$$

In some cases, a direct fit of the experimental ionization data of given atom/molecule in terms of multiphoton ionization rate [9] may lead to better result.

$$W_{MPI} = \sigma_K \, I^K \tag{4'}$$

Both way of description of the ionization rate have been used in our studies.

We have further developed the physical model to account for the role of ionization on the group velocity dispersion (GVD). The ionization contribution to the GVD is given by (standard notations) [1]

$$\beta_{2i} = -\frac{e^2 \lambda^3 N_e}{2\pi^2 m_e c^4 \left(1 - \dfrac{e^2 \lambda^2 N_e}{\pi m_e c^2}\right)^{3/2}} \tag{5}$$

The high-intensity femtosecond pulse propagation is described solving self-consistently the equations (2)-(4), taking into account the ionization contribution (5) to the total GVD of the medium.

3. RESULTS AND DISCUSSION

We consider laser pulses of 2mJ energy propagating in pressurized argon of 5atm pressure. The initial pulse is a linearly polarized chirp-free Gaussian, $\widetilde{E}\,(r, z = 0, \tau) = E_0 \exp\left(-r^2/2r_0^2 - \tau^2/2\tau_0^2\right)$, in space and in time of 150 fs time duration (full width at half maximum (FWHM)).

The development of the ionization rate, the electron number density, and the ionization contribution to the group velocity dispersion are shown in Fig. 1 (a), (b), and (c), respectively. Due to the strong intensity dependence of the ionization rate, the substantial ionization of the medium is localized around the peak of the optical pulse only, Fig.1 (a). The electron number density shows an integral behavior because the electron recombination occurs in much longer time scale than the pulse duration, Fig.1 (b). The ionization contribution to the GVD is entirely negative, Fig.1 (c), and instantaneously follows the electron number density. The development of the beam radius, the peak intensity of the pulse and the time duration are shown in Fig. 2 (a), (b), and (c), respectively. The transversal width of the pulse, the beam radius, rapidly collapses down to about $45\mu m$ due to the self-focusing and then continues propagating keeping the beam size almost constant. In the same time, the peak intensity rapidly increases until the ionization rate becomes substantial. The further increase of the pulse intensity is limited due to the substantial ionization losses, Fig.2 (b). The growth of the peak intensity is accompanied by a self-compression of the pulse duration, Fig. 2 (c). The evolution of the total GVD during the pulse propagation is shown in Fig. 3. At low peak intensity, the total GVD remains unchanged. Once the pulse reaches high enough value to cause substantial ionization of the medium, the total GVD rapidly drops down, reaching even negative values. Such effect has been called *ionization induced inversion* (I^3) of the GVD [8]. At suitable conditions, one may expect substantial change in the pulse propagation dynamics due to the effect of the I^3. This is the first observation of inversion of the total GVD in a dynamical propagation regime. The evolution of the temporal profile of the pulse is show in Fig.4. The main stages of the pulse propagation, *i.e.*, the pulse compression, the stable propagation, and the pulse splitting, are well reproduced in the simulations.

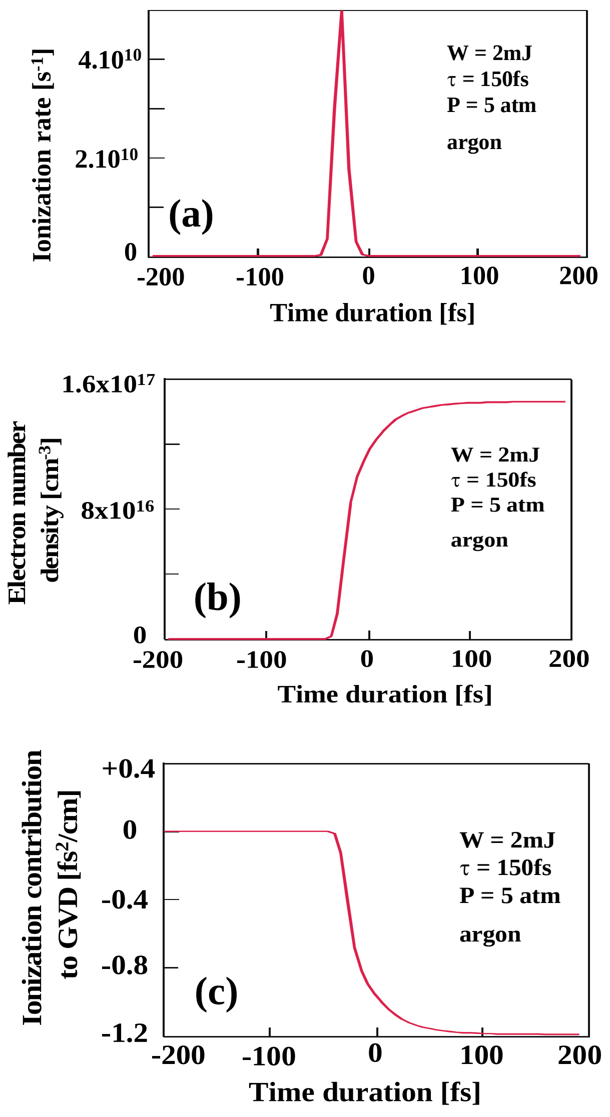

Fig.1. Evolution of ionization rate (a), electron number density (b) and plasma GVD (c) within the optical pulse.

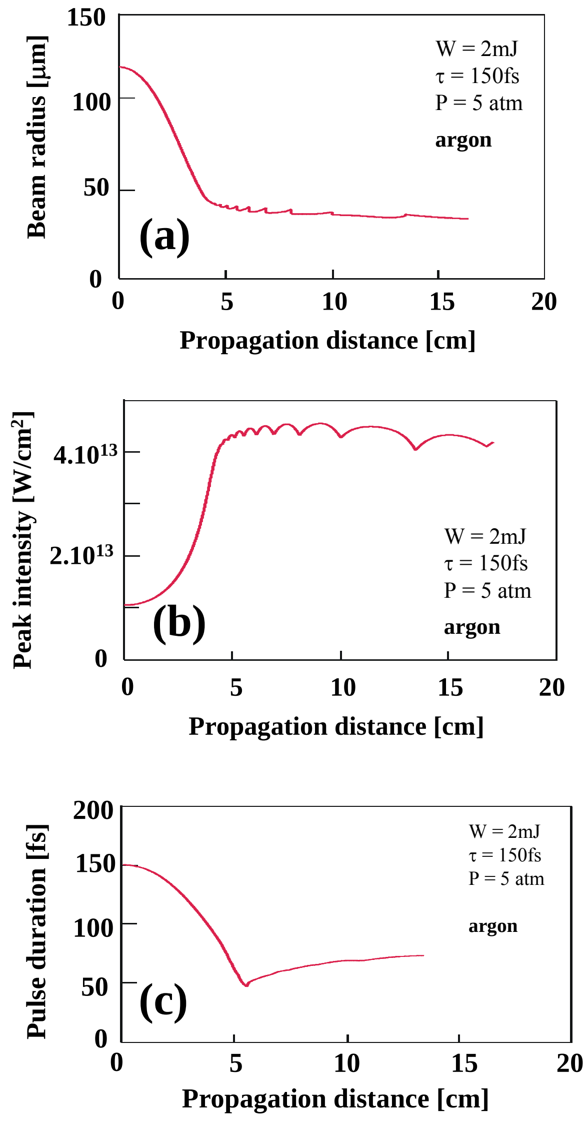

Fig. 2. Evolution of beam radius (a), peak intensity (b), and pulse duration (c) with the propagation.

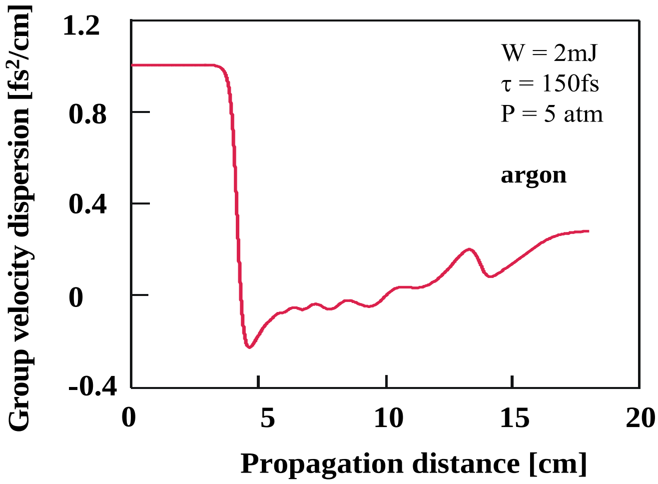

Fig. 3. Evolution of the total GVD of the medium with the pulse propagation

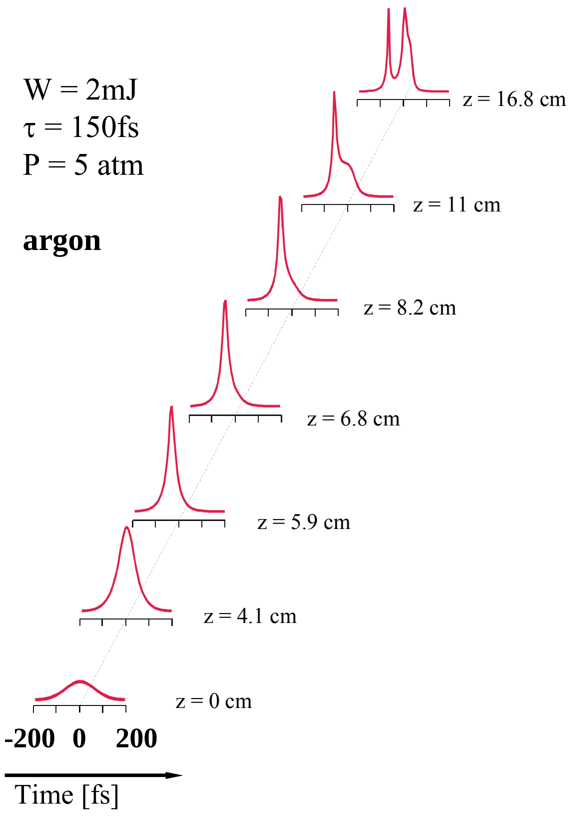

Fig. 4. Evolution of the temporal profile of the pulse

4. CONCLUSIONS

The influence of ionization on the material parameters has been studied in the propagation of high-intensity femtosecond laser pulses. Ionization induced inversion of the group velocity dispersion has been found for the first time in a dynamical propagation regime. The modified material parameters well reproduce qualitatively the main stages of the pulse propagation dynamics: pulse compression, stabilization of the pulse propagation along given distance and the pulse splitting.

Acknowledgment: This work was supported by a grant 091ни077-20/2009 of the Science and Research Department of the Technical University of Sofia.

REFERENCES

[1] I. G. Koprinkov, Applied Physics B - Lasers and Optics, **79**, 359 (2004).

[2] J. E. Rothenberg, Opt. Lett., **17**, 583 (1992)

[3] J. K. Ranka, R. W. Schirmer, and A. L. Gaeta, Phys. Rev. Lett., Vol. **77**, 3783 (1996)

[4] S. A. Diddans, H. K. Eaton, A. A. Zozulya, and T. S. Clement, IEEE, J. Selected Topics of Quant. Electron., Vol. **4**, 306-316 (1998)

[5] Y. Silberberg, Opt. Lett., **15**, 1282 (1990)

[6] I. G. Koprinkov, A. Suda, P. Wang, and K. Midorikawa, Jap. J. Appl. Phys., L 978 (1999).

[7] I. G. Koprinkov, A. Suda, P. Wang, and K. Midorikawa, Phys. Rev. Lett., **84**, 3847 (2000).

[8] I. G. Koprinkov, A. Suda, P. Wang, and K. Midorikawa, "Soliton-Driven Photonics", Kluwer Academic Publishers, Ed. A. D. Boardman and A. P. Sukhorukov, pp. 355-358, (2001).

[9] L. Berge, S. Skupin, R. Nuter, J. Casparian, and J-P Wolf, Rep. Prog. Phys.. **70**, 1633 (2007)

[10] T. Brabec and F. Krausz, Rev. Mod. Phys., 72, 545 (2000)

[11] A. M. Perelomov, V. S. Popov, M. V. Terent'ev, Sov. Phys. JETP, **23**, 924 (1966)

SYNTHESIS OF SELF-SUSTAINED SYSTEMS WITH TWO STABLE OSCILLATIONS

Irina Karagineva

Department of Theoretical Electrical Engineering, Technical University of Sofia,
8 Kliment Ohridski Str., Sofia 1000, Bulgaria
e-mail: ikaragineva@tu-sofia.bg

Abstract: *In this paper is presented the method for synthesis of generalized Van der Pol oscillator systems using Melnikov function. The oscillations in such systems are regarded as limit cycles in perturbed Hamiltonian systems under polynomial perturbations of arbitrary degree. The method of synthesis is based on appropriate computation of perturbation coefficients, so that the prescribed properties are fulfilled.*

Keywords: modified Van der Pol equation, limit cycles, Melnikov function

1. INTRODUCTION

The self-sustained oscillations appear in non-linear dynamical systems under the conditions that there is no external periodic signal. Form, amplitude and frequency of those oscillations stays constant win long period of time, they do not depend in range from the initial conditions and they are determined from the features of the system itself. It's possible that one or more areas of initial conditions exist, such that for every initial condition which belongs to a given area, the oscillator system has one and the same amplitude. This means that in self-sustained oscillator systems can exists few stationary process with different amplitudes, and every single process establish itself in the system depending of chosen area of initial conditions.

The presented paper proposes a method of synthesis of self-sustained systems, described by generalized Van de Pol equation, which have two stable oscillations with given in advance parameters.

2. BASIC PRINCIPLES OF SYNTHESIS SELF-SUSTAINED SYSTEMS, DESCRIBED BY GENERALIZED VAN DER POL EQUATIONS

Self-sustained systems, described by generalized Van der Pol equation generate sinusoidal oscillations with different amplitudes. These oscillations are depictured on the phase plane like limit cycles. For synthesis of such systems is very convenient to represent generalized Van der Pol equation like autonomous system which is close to the system of ideal harmonic oscillator, i.e.

$$\left| \begin{array}{l} \dot{x} = y + \varepsilon(a_1 x + a_3 x^3 + \cdots + a_{2n+1} x^{2n+1}) \\ \dot{y} = -x \end{array} \right. \quad (1)$$

When $\varepsilon = 0$ we have unperturbed system, which is Hamiltonian with Hamiltonian function

$$\mathrm{H}(x, y) = \frac{1}{2}x^2 + \frac{1}{2}y^2$$

Unperturbed system possesses a single equilibrium point - $(0,0)$, which is a “centre”. This equilibrium point is surrounded from a family of closed trajectories, for which we assume that they are parameterized with parameter h. In this case the equation of given closed trajectory is obtained in the following way:

$$\Gamma_0(h) : \mathrm{H}(x, y) = \frac{1}{2}x^2 + \frac{1}{2}y^2 = h, h \in \Omega \equiv (0, \infty) \tag{2}$$

In the phase plane the curve $\Gamma_0(h)$ is a circle with radius

$$r = \sqrt{2h} \tag{3}$$

Lets Σ is a Poankare section, which coincides with the positive part of y axes and let’s Σ is parameterized as well with parameter h. Then Melnikov function for system (1) build on Σ has the following form

$$\mathrm{M}(h) = 4\pi h.\mathcal{M}(h) \tag{4a}$$

where

$$\mathcal{M}(h) = \left[\left[\frac{a_1}{2^2}\right]\binom{2}{1} + \left[\frac{a_3}{2^3}\right]\binom{4}{2}h + \cdots + \left[\frac{a_{2n+1}}{2^{n+2}}\right]\binom{2n+2}{n+1}h^n \right] \tag{4b}$$

It is well known that positive roots of the equation

$$\mathrm{M}(h) = 0 \tag{5}$$

determine the limit cycles in system (1) [4], [5], [6]. Moreover if h_0 is positive root with multiplicity m, $m \geq 1$, for equation (5), then in $O(\varepsilon)$ neighbourhood of h_0 exist h_ε, such that system (1) has limit cycle $\Gamma_\varepsilon(h_\varepsilon)$ with multiplicity m, $m \geq 1$. The limit cycle $\Gamma_\varepsilon(h_\varepsilon)$ is localized in $O(\varepsilon)$ neighbourhood of $\Gamma_0(h_0)$ and it tends to $\Gamma_0(h_0)$, when $\varepsilon \to 0$.The stability of the limit cycle $\Gamma_\varepsilon(h_\varepsilon)$ is determined from the sign of $\varepsilon \mathrm{M}^{(m)}(h_0)$.

Practically in the time frame limit cycle is represented with the following functions

$$\left| \begin{array}{l} x(t) = \sqrt{2h_0}\sin t = A_m \sin t \\ y(t) = \sqrt{2h_0}\cos t = A_m \cos t \end{array} \right. \tag{6}$$

It is easy to see, that positive roots (along with their multiplicity) of equation (5) are determined from the equation

$$\mathcal{M}(h)=\left[\frac{a_1}{2^2}\binom{2}{1}+\left[\frac{a_3}{2^3}\right]\binom{4}{2}h+\cdots+\left[\frac{a_{2n+1}}{2^{n+2}}\right]\binom{2n+2}{n+1}h^n\right] \tag{7}$$

From equations

$$\mathrm{M}'(h)=4\pi h\mathcal{M}'(h)+4\pi h\mathcal{M}(h),$$
$$\mathrm{M}''(h)=4\pi h\mathcal{M}''(h)+8\pi h\mathcal{M}'(h),$$
$$\mathrm{M}'''(h)=4\pi h\mathcal{M}'''(h)+12\pi h\mathcal{M}''(h)\text{, and so on}$$

It follows that if h_0 is a positive root with multiplicity m of equation (5), than $\mathrm{M}^{(m)}(h_0)$ and $\mathcal{M}^{(m)}(h_0)$ have one and the same sign. Therefore with limit cycle analysis from now on, instead of roots of equation (5) we will seek the roots of equation (7) and instead of sign of derivative $\mathrm{M}^{(m)}(h)$ we will determine sign of $\mathcal{M}^{(m)}(h)$.

Equation (7) is homogeneous with respect to constants $a_1,a_3,\ldots,a_{2n+1}$, therefore we will assume, that $a_1=1$ and this will not decrease the generalization of our discussion.

Equation (7) is polynomial equation from power n with respect to h and it is possible to have no more than n positive roots. These roots (when we have given in advance coefficients $a_1,a_3,\ldots,a_{2n+1}$) determine according to equation (6) amplitudes of arisen in system (1) limit cycles, or oscillations. From here, if we think backwards we will obtain the main idea of synthesis of self-sustained systems, described by system (1). For example, if we want to derive system having oscillations with given amplitudes, then to these amplitudes according to equation (6) correspond values of parameter h. In fact these values are zeroes of Melnikov function $\mathrm{M}(h)$ (respectively zeroes of $\mathcal{M}(h)$ function). But it is well known that if we have given in advance zeroes of a polynomial, then his coefficients can be determined definitively. One way to do this is by using Viet formulas. In this way, if the amplitudes of desired oscillations are given in advance we can determine the coefficients of perturbation $a_1,a_3,\ldots,a_{2n+1}$ in polynomial $\mathcal{M}(h)$, and from here in the system (1), so in this way it will possess the desired oscillations.

3. SYNTHESIS OF SELF-SUSTAINED SYSTEMS WITH TWO STABLE OSCILLATORS

From the common theory of limit cycles we have that systems with two stable oscillations should poses three limit cycles (two stable limit cycles and one unstable), or two limit cycles (one stable limit cycle and one semi-stable limit cycles, which has multiplicity 2). If we have in mind that for every limit cycle corresponds root of the equation (7), this lead us to the conclusion, that in the first case equation (7) should has three different positive roots, and in the second case two different positive roots, and one of this roots should has multiplicity 2. In both cases $\mathcal{M}(h)$ function has to be cubic polynomial. In this case from equation (7) we obtain:

$$\mathcal{M}(h) = \frac{35}{16} a_7 h^3 + \frac{5}{4} a_5 h^2 + \frac{3}{4} a_3 h + \frac{1}{2} = 0 \tag{8}$$

Therefore in this case Melnikov function and perturbation in the system (1) as well contains the coefficients $a_1 = 1, a_3, a_5$ and a_7. Then system (1) has the following form:

$$\left| \begin{aligned} &\dot{x} = y + \varepsilon(x + a_3 x^3 + a_5 x^5 + a_7 x^7) \\ &\dot{y} = -x \end{aligned} \right. \tag{9}$$

Further we will determine the coefficients $a_1 = 1, a_3, a_5$ and a_7, such as the system (9) to posses oscillations with amplitudes given in advance.

Lets have given amplitudes $A_{m,i}$, $i = 1,2,3$, of sinusoidal oscillations, that we want system (9) to posses. These amplitudes are equal to radiuses of corresponding to the oscillations limit cycles, i.e. $r_i = A_{m,i}$. Then from equation (3) we obtain

$$h_{0,i} = \frac{1}{2} r_i^2 = \frac{1}{2} A_{m,i}^2, \, i = 1, 2, 3 \tag{10}$$

The values $h_{0,i}, i = 1, 2, 3$, are roots of cubic equation (8). Thus according to Viet formulas we obtain:

$$\left| \begin{aligned} &h_{0,1} + h_{0,2} + h_{0,3} = -\frac{(5/4) a_5}{(35/16) a_7} = -\frac{4 a_5}{7 a_7} \\ &h_{0,1} h_{0,2} + h_{0,2} h_{0,3} + h_{0,3} h_{0,1} = \frac{(3/4) a_3}{(35/16) a_7} = \frac{12 a_3}{35 a_7} \\ &h_{0,1} h_{0,2} h_{0,3} = -\frac{(1/2)}{(35/16) a_7} = -\frac{8}{35 a_7} \end{aligned} \right. \tag{11}$$

System (11) allows, if the roots $h_{0,i}, i = 1, 2, 3$ are known, to determine coefficients a_3, a_5 and a_7, such as system (9) to posses desired oscillations. To determine stability of limit cycles (as well stability of oscillations) we use the following derivates:

$$\mathcal{M}'(h) = \frac{105}{16} a_7 h^2 + \frac{5}{2} a_5 h + \frac{3}{4} a_3, \tag{12a}$$

$$\mathcal{M}''(h) = \frac{105}{8} a_7 h + \frac{5}{2} a_5, \tag{12b}$$

Now finally we can define the problem and the procedure for synthesis of self-sustained systems with two stable oscillations.

Defining the problem of synthesis:

Problem 1: Determine the coefficients a_3, a_5 and a_7, such as the system (9) to posses two stable oscillations with corresponding amplitudes $A_{m,1}$ and $A_{m,3}$ and one unstable oscillation with amplitude $A_{m,2}$, where $A_{m,1} > A_{m,2} > A_{m,2}$. Note that to these oscillations correspond three simple limit cycles.

Problem 2: Determine coefficients a_3, a_5 and a_7, such as the system (9) to posses one stable oscillation with amplitude $A_{m,1}$ and one unstable oscillation with amplitude $A_{m,2}$, where $A_{m,1} > A_{m,2}$. Note that in this case to the oscillation with amplitude $A_{m,1}$ corresponds simple limit cycle with multiplicity 2 and root of polynomial (8) with multiplicity 2.

Synthesis procedure:

1) Determine values $h_{0,i}, i = 1, 2, 3$, using formula (10)
2) Solve system (11) and determine a_3, a_5 and a_7.
3) Determine derivates $\mathcal{M}'(h_{0,i})$ and $\mathcal{M}''(h_{0,i}), i = 1, 2, 3$ and choosing ε, such as the corresponding oscillations to have a given stability

4. EXAMPLES OF SYNTHESIS OF SELF-SUSTAINED SYSTEMS WITH TWO STABLE OSCILLATIONS

Example 1: Synthesize self-sustained system with two stable oscillations with amplitudes $A_{m,1} = 3$ and $A_{m,3} = 1$ and one unstable oscillation with amplitude $A_{m,2} = 2$.

Solution:

1) We determine values $h_{0,i}, i = 1, 2, 3$ using formula (10)

$$\left| \begin{aligned} h_{0,1} &= \frac{1}{2} A_{m,1}^2 = \frac{1}{2} 3^2 = \frac{9}{2} \\ h_{0,2} &= \frac{1}{2} A_{m,2}^2 = \frac{1}{2} 2^2 = 2 \\ h_{0,3} &= \frac{1}{2} A_{m,3}^2 = \frac{1}{2} 1^2 = \frac{1}{2} \end{aligned} \right. \tag{13}$$

2) System (11) takes the following form

$$\left|\begin{aligned} &-\frac{4a_5}{7a_7}=7 \\ &\frac{12a_3}{35a_7}=\frac{49}{4} \\ &-\frac{8}{35a_7}=\frac{9}{2} \end{aligned}\right. \tag{14}$$

from here we obtain

$$a_3=-\frac{49}{27},\ a_5=\frac{28}{45},\ a_5=-\frac{16}{315} \tag{15}$$

From here we get the final form of system (9):

$$\left|\begin{aligned} &\dot{x}=y+\varepsilon(x-\frac{49}{27}x^3+\frac{28}{45}x^5-\frac{16}{315}x^7) \\ &\dot{y}=-x \end{aligned}\right. \tag{16}$$

3) From (12a) we obtain

$$\mathcal{M}'(h)=-\frac{1}{3}h^2+\frac{14}{9}h+\frac{49}{36}$$

$$\mathcal{M}'(h_{0,1})=\mathcal{M}'\left(\frac{9}{2}\right)=-\frac{1}{3}\left(\frac{9}{2}\right)^2+\frac{14}{9}\frac{9}{2}h+\frac{49}{36}=-\frac{10}{9}<0$$

$$\mathcal{M}'(h_{0,2})=\mathcal{M}'(2)=-\frac{1}{3}2^2+\frac{14}{9}2h+\frac{49}{36}=\frac{5}{12}>0$$

$$\mathcal{M}'(h_{0,3})=\mathcal{M}'\left(\frac{1}{2}\right)=-\frac{1}{3}\left(\frac{1}{2}\right)^2+\frac{14}{9}\frac{1}{2}h+\frac{49}{36}=-\frac{2}{3}<0$$

We choose $\varepsilon>0$, because inequalities $\varepsilon\mathcal{M}'(h_{0,1})<0$, $\varepsilon\mathcal{M}'(h_{0,2})>0$, $\varepsilon\mathcal{M}'(h_{0,3})<0$, mean that, oscillations with amplitudes $A_{m,1}$ and $A_{m,3}$ are stable, but oscillation with amplitude $A_{m,2}$ is unstable. On fig. 1 is depicted the phase portrait of system (16).

<u>Example 2:</u> Synthesize self-sustained system with one semi-stable oscillation with amplitude $A_{m,1}=2$ and one stable oscillation with amplitude $A_{m,3}=1$.

Solution:

1) Determining of values $h_{0,i}$, $i=1,2,3$ with formula (7):

$$\begin{cases} h_{0,1} = h_{0,2} = \dfrac{1}{2} A_{m,1}^2 = \dfrac{1}{2} 2^2 = 2 \\ h_{0,3} = \dfrac{1}{2} A_{m,3}^2 = \dfrac{1}{2} 1^2 = \dfrac{1}{2} \end{cases} \tag{17}$$

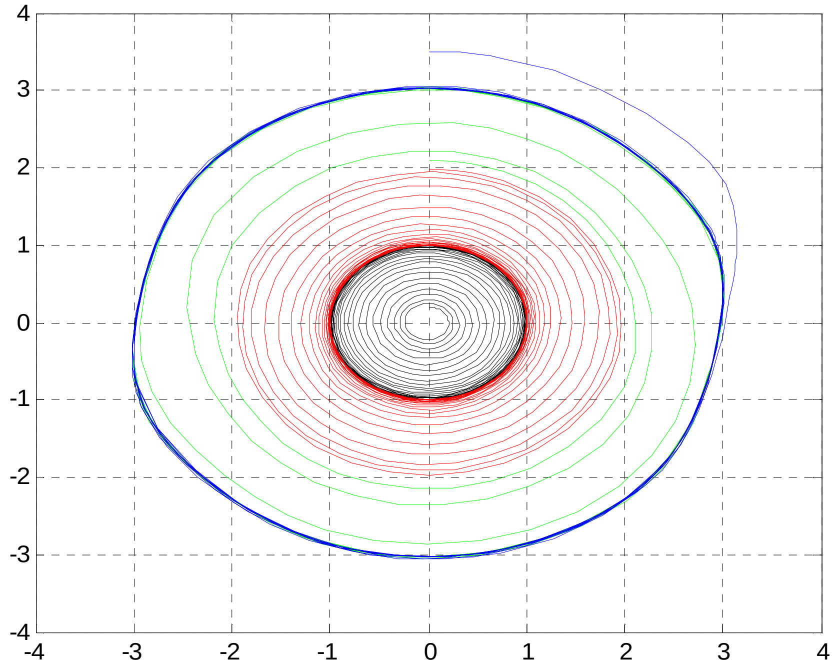

Fig. 1. Phase plane of system (17), with $\varepsilon = 0.07$

2) Formula (8) has the following expression:

$$\begin{cases} -\dfrac{4a_5}{7a_7} = \dfrac{9}{2} \\ \dfrac{12a_3}{35a_7} = 6 \\ -\dfrac{8}{35a_7} = 2 \end{cases} \tag{18}$$

From where we obtain

$$a_3 = -2,\ a_5 = \frac{9}{10}, a_5 = -\frac{4}{35} \tag{19}$$

Thus we obtain the final expression of system (10):

$$\begin{cases} \dot{x} = y + \varepsilon(x - 3x^3 + \dfrac{12}{5}x^5 - \dfrac{16}{35}x^7) \\ \dot{y} = -x \end{cases} \tag{20}$$

3) From eq.(5) and (9) we obtain

$$\mathcal{M}(h) = -h^3 + 3h^2 + \frac{9}{4}h + \frac{1}{2} = -(h-2)(h-\frac{1}{2})^2$$

$$\mathcal{M}'(h) = -3h^2 + 6h - \frac{9}{4}$$

$$\mathcal{M}''(h) = -6h + 6$$

$$\mathcal{M}'(h_{0,1}) = \mathcal{M}'(2) = -3.2^2 + 6.2 - \frac{9}{4} = -\frac{9}{4} < 0$$

$$\mathcal{M}'(h_{0,1}) = \mathcal{M}'\left(\frac{1}{2}\right) = -3.\frac{1}{4} + 6.\frac{1}{2} - \frac{9}{4} = 0$$

$$\mathcal{M}''(h_{0,2}) = \mathcal{M}''\left(\frac{1}{2}\right) = -6.\frac{1}{2} + 6 = 3 > 0$$

We choose $\varepsilon > 0$, because inequalities $\varepsilon\mathcal{M}'(h_{0,1}) < 0$, $\varepsilon\mathcal{M}'(h_{0,2}) > 0$, mean that, oscillation with amplitudes $A_{m,1}$ is stable, and oscillation with amplitude $A_{m,2}$ is stable inside and unstable outside.

On fig. 2 is depicted the phase portrait of system (17)

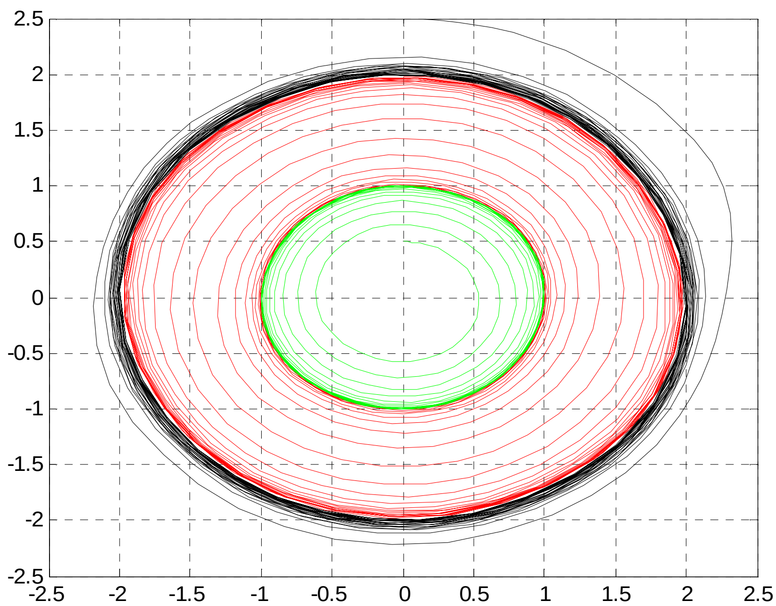

Fig. 2. Phase plane of system (17), with $\varepsilon = 0.15$

5. CONCLUSION

I choose $\varepsilon > 0$, because inequalities $\varepsilon\mathcal{M}'(h_{0,1}) < 0$, $\varepsilon\mathcal{M}'(h_{0,2}) > 0$, mean that, oscillation with amplitudes $A_{m,1}$ is stable, and oscillation with amplitude $A_{m,2}$ is stable inside and unstable outside.

REFERENCES

[1] A. Andronov, E. Leontovich, I. Gordon, A. Maier. “Theory of Bifurcations of Dynamical Systems on the Plane”, Wiley: New York, 1973.

[2] N. Bautin, E. Leontovitch, “Methods and Tools for Qualitative Analysis of Dynamical Systems on the Plane” Nauka: Moscow, 1976 (in Russian).

[3] J Guckenheimer, P. Holmes, “Nonlinear Oscillations, Dynamical Systems and Bifurcations of Vector Fields”, Springer: New York, 1983.

[4] L. Perko, “Differential Equation and Dynamical Systems” (3^{rd} edn). Springer: New York, 2001.

[5] T. Blows, L. Perko, “Bifurcation of Limit Cycles from Center and Separatrix Cycles of Planar Analytic Systems”, SIAM Review 1994; 36(3):341-376.

[6] M. Sanjuan, Lienard,“Systems, Limit Cycles, and Melnikov Theory”, Physical Review E 1998; E57(1):340-344.

[7] M, Itoh, “Synthesis of electronic circuits for simulating nonlinear dynamics”, International Journal of Bifurcation and Chaos 2001, 11(3):605-653.

LONG-DISTANCE ON-CHIP SFQ PULSE TRANSMISSION VIA PASSIVE TRANSMISSION LINES

Valery Todorov[1], Anton Andonov[1], Valeri Mladenov[2]

[1]University of Chemical Technology and Metallurgy, Department of Electrical Engineering and Electronics,
8 Kl. Ohridski St., BG-1756 Sofia, Bulgaria
[2]Technical University of Sofia, Department of Theoretical Electrical Engineering,
8 Kl. Ohridski St., BG-1000 Sofia, Bulgaria

Abstract: *The Passive Transmission Lines (PTLs) are promising technique for long-distance on-chip SFQ pulse transmission. Their main drawback, however, is the bad matching with the Rapid Single Flux Quantum (RSFQ) circuits, causing signal reflections and even misfunctionality of the latter. A novel methodology for design of PTL drivers and receivers matching any RSFQ circuit to a PTL with certain characteristic impedance has been recently proposed in the literature. Two layouts for experimental verification of the functionality of this methodology have been fabricated and successfully tested. Here we present the experimental verification results of both fabricated layouts.*

Keywords: Single Flux Quantum (SFQ) pulse transmission, Passive Transmission Lines.

1. INTRODUCTION

With the increasing speed and complexity of low-temperature superconductive Rapid Single Flux Quantum (RSFQ) digital circuit [1, 2], the efficiency of long-distance on-chip SFQ pulse transmission becomes more and more important in respect of the total circuit performance. Currently, the modern RSFQ designs use two techniques for such a signal exchange – via Josephson transmission lines (JTLs) and via passive transmission lines (PTLs). The JTLs are very robust, have large parameter margins, provide a perfect matching to the RSFQ circuits, and perform an excellent regeneration and shaping of the transmitted SFQ pulses. The main drawbacks of the JTLs – the low SFQ pulse propagation speed and large dc bias current consumption – restricting the application of the JTLs as long-distance SFQ pulse transmitters within ultra-high-speed RSFQ digital devices. The characteristics of the PTLs are just opposite. Their SFQ pulse propagation speed is 5-10 times higher than the JTLs and they do not consume dc bias current. Nevertheless, their main drawback is the bad matching with the RSFQ circuits, causing signal reflections and even misfunctionality of the latter.

The aim of our previous studies [3-5] had been the improving of the drawbacks of the both techniques for SFQ pulse transmission. Many design efforts have been dedicated to the invention of PTL Drivers and Receivers ensuring an acceptable matching between the real and frequency independent impedance of the PTLs and strongly nonlinear RSFQ digital circuits [6-9].

A novel methodology for design of PTL drivers and receivers matching any RSFQ circuit to a PTL with certain characteristic impedance has been recently proposed in [10]. Two layouts for experimental verification of the functionality of this methodology have been fabricated and successfully tested [11]. Here we present the experimental verification results of both fabricated layouts.

2. SFQ PULSE TRANSMISSION VIA PASSIVE TRANSMISSION LINES

The RSFQ circuits are extremely nonlinear and practically cannot be described in frequency domain, while the impedance of the superconductive PTLs can be considered as real and frequency independent. Therefore, a full matching between a PTL and an RSFQ circuits is impossible. The problem can be partly solved by introducing a Driver and a Receiver between the PTL and the communicated RSFQ circuits, as shown below on Fig. 1.

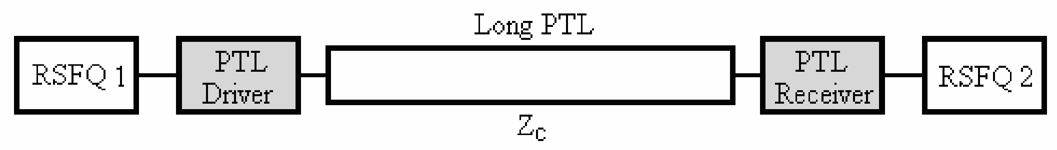

Fig. 1. Matching of the PTL to the RSFQ digital circuits via PTL Driver and Receiver

The design methodology of the PTL Driver and Receiver showed in this work is mainly based on [9], but 2-stage schemes of JTLs are used for both gates. As we have already demonstrated in [12], both the SFQ pulse propagation impedance and the weak-signal impedance of a JTL with at least 2 stages are invariant from the JTL termination, i.e. with 2-stage Driver and Receiver the matching requirements can be fulfilled for any RSFQ termination of these gates.

The SFQ pulse propagation impedances both of the PTL Driver and PTL Receiver can be approximated as a resistor and a capacitor in parallel [6]. The topology of the PTL Driver and Receiver, shown on Fig. 2, allows matching only of real part of the gates' SFQ pulse propagation impedances to the impedance of the PTL.

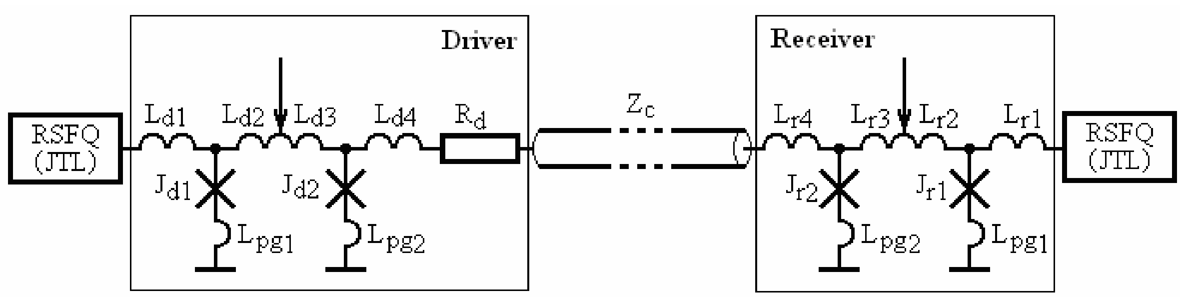

Fig. 2. Topologies of the PTL Driver and Receiver performing the matching between RSFQ gates and PTLs with the characteristic impedance of the PTL – Z_c.

A small resistor R_d is put at the output of the PTL Driver to break the large superconductive loop formed by the Driver's output junction, PTL and the Receiver's input junction. Thus, undesired trapping of SFQ pulses within this loop is avoided. The element values and the gates' layouts designed according to the rules of the 4μm 1kA/cm^2 Nb/Al_2O_3-Al/Nb fabrication technology of PTB-Braunschweig [13] can be found in [10]. An optimal matching is reached for a characteristic impedance of the PTL $Z_c = 2.4\Omega$.

3. LAYOUTS AND TESTING OF THE PTL DRIVER AND RECEIVER

Two circuits for the experimental verification of the functionality of the PTL Driver and Receiver have been designed, fabricated and successfully tested. Their layouts are schematically shown below:

1) The circuit for experimental verification of the functionality of the PTL Driver and Receiver – Fig. 3.

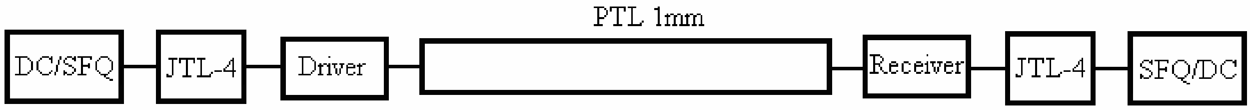

a)

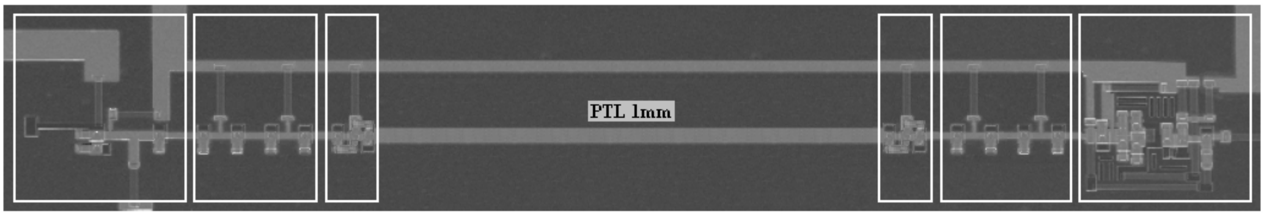

b)

Fig. 3: a) block-scheme and b) photo of the DC/DC convertor for testing the PTL Drivers and Receiver

The circuit performs a DC/DC conversion – include the DC/SFQ convertor, two 4-stage JTLs, PTL Driver, 1 mm long PTL, PTL Receiver and the SFQ/DC convertor.

The result of experimental verification is monitored at the oscilloscope and it is shown on Fig. 4.

The period of the input chain has been 1 ms, and a high-speed test of this circuit has not been performed. The result of experimental verification present correct work of the PTL and the Drivers and the Receiver.

2) Ring-shaped SFQ oscillators for direct experimental verification of the matching between an RSFQ circuits and a PTL and with Driver and Receiver – Fig. 5.

Ring-shaped SFQ oscillators for direct experimental verification of the matching between an RSFQ circuits and a PTL and with Driver and Receiver consists four equal sections with two 2-stage JTLs, PTL Driver, 1 mm long PTL and PTL Receiver.

If a single SFQ pulse is generated by the DC/SFQ converter, it goes through the merger into the ringshaped oscillator, and starts to circulate in it.

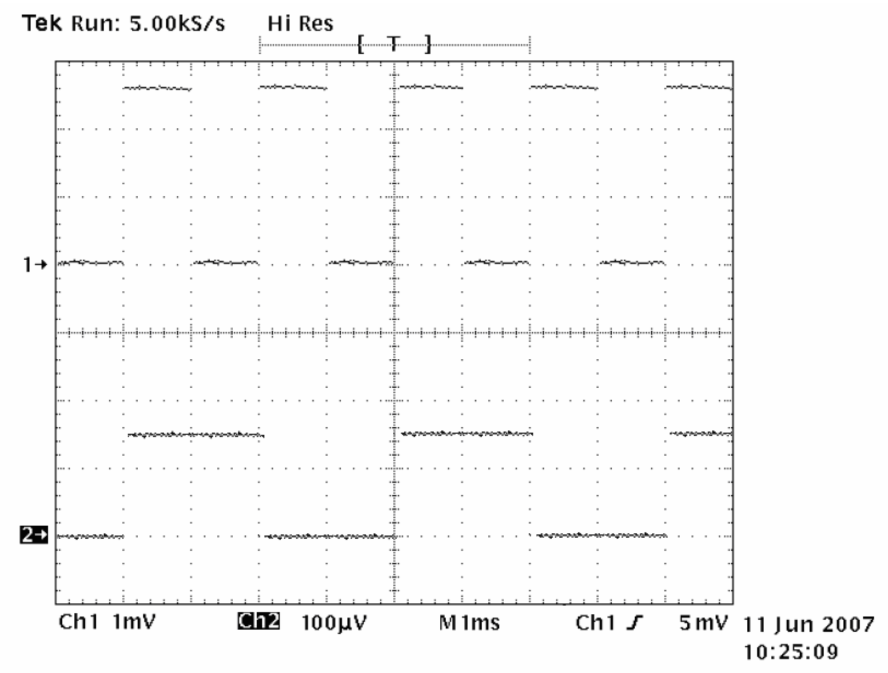

Fig. 4. Signal flow in the case of DC/Dc conversion.
1 - excitation signal of the DC/SFQ convertor, 2 - output signal of the SFQ/DC convertor.

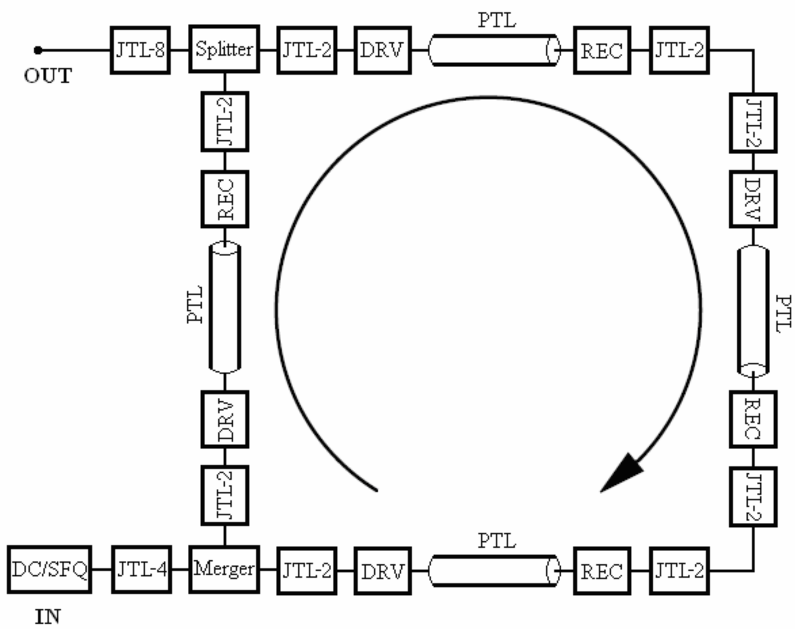

Fig. 5. Block-scheme of the test circuit for the experimental verification of
the matching between an RSFQ circuits and a PTL and with Driver and Receiver.

If τ_{ring} is the total delay of the oscillator, a chain of SFQ pulses with period τ_{ring} appears at node OUT and the mean voltage measured at OUT is

$$\overline{U} = \frac{\Phi_0}{\tau_{ring}}. \tag{1}$$

In this way, τ_{ring} is obtained experimentally as

$$\tau_{ring} = \frac{\Phi_0}{\overline{U}}, \tag{2}$$

and the time-delay of the PTL acquired

$$\tau_{PTL} = \frac{(\tau_{ring} - \tau_{add})}{4} - \tau_{DRV-REC}, \tag{3}$$

where:

– τ_{add} is time-delay of the additional components – Merger, 2-stage JTLs and Splitter, determinated experimentally;

– τ_{DRV} and τ_{REC} are time-delay of the Driver and Receiver, determinated by simulation.

Layouts of the ring-shaped oscillators for the experimental verification of the matching between an RSFQ circuits and a PTL and with Driver and Receiver shown on Fig. 6 and Fig. 7 (ring-shaped oscillator of the additional components).

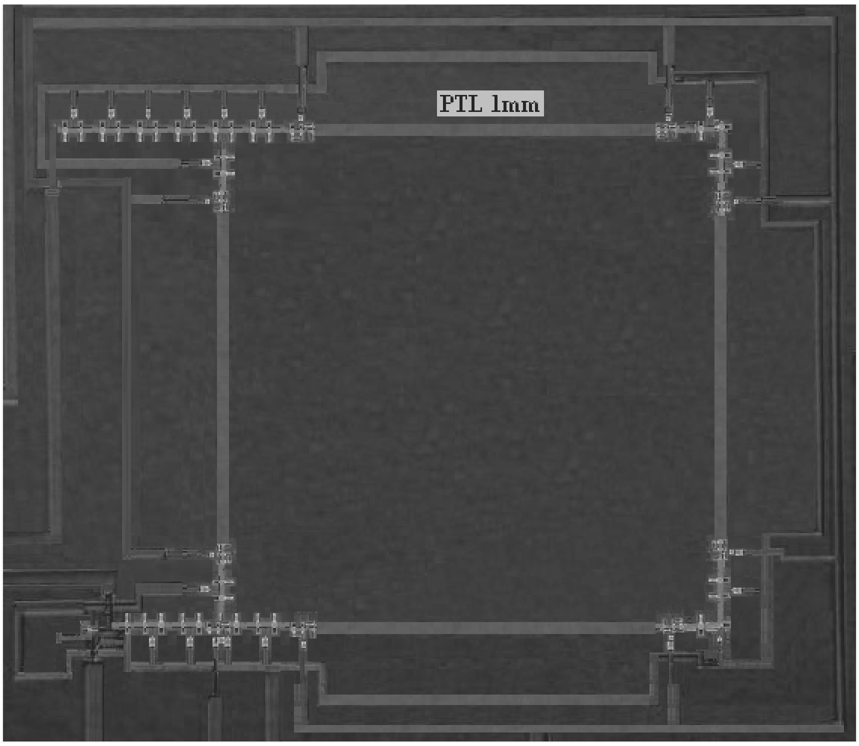

Fig. 6. Ring-shaped SFQ oscillators for the experimental verification of the matching between an RSFQ circuits and a PTL and with Driver and Receiver

Of the results of the experimental verification for the time-delay of the long 1 mm PTL obtain $\tau_{PTL} = 8.4 ps/mm$.

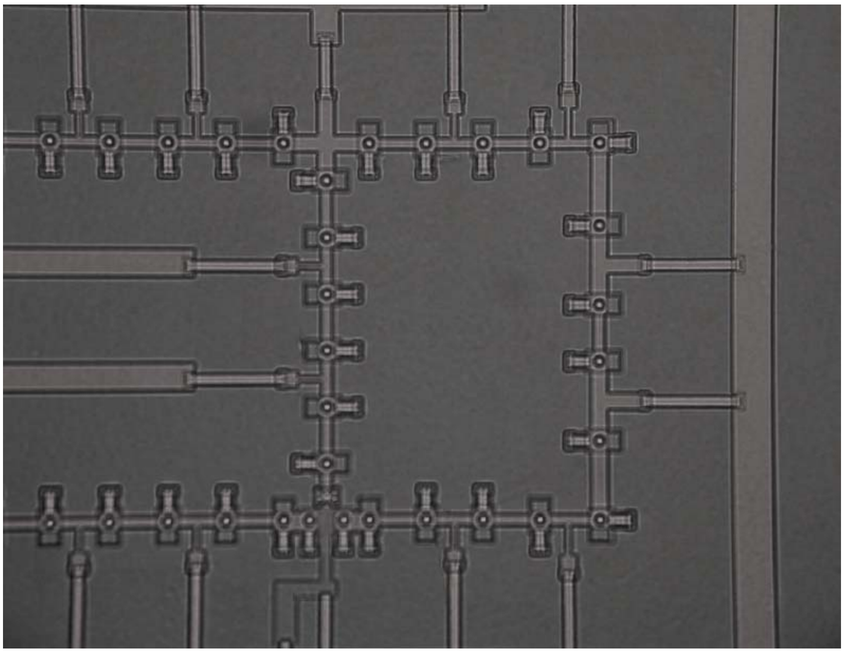

Fig. 7. Ring-shaped SFQ oscillators of the additional components

5. CONCLUSION

The bad matching of the PTLs to the RSFQ circuits, which currently restrict their application as long-distance SFQ pulse transmission, san be improved if PTL Drivers and Receivers are used.

The existing techniques for matching of the PTLs to the RSFQ circuits have been also improved. Here, 2-stage RSFQ PTL drivers and receivers have been designed as separate gates. Their structure is chosen to make their weak-signal and SFQ pulse propagation impedances independent on the RSFQ terminations. Thus, a matching between any RSFQ circuit and a long PTL with certain characteristic impedance is ensured.

6. ACKNOWLEDGEMENT

The author wants to thank to the RSFQ design group at the Technical University of Ilmenau for the valuable suggestions and discussions.

REFERENCES

[1] K. K. Likharev and V. K. Semenov, “RSFQ Logic/Memory Family: A new Josephson-Junction Technology for Sub-Terahertz-Clock-Frequency Digital Systems”, *IEEE Trans. Appl. Supercond.*, vol. 1, pp. 3-28, 1991.

[2] P. Bunyk, M. Leung, J. Spargo, M. Dorojevets, “FLUX-1 RSFQ Microprocessor: Physical Design and Test Results”, *IEEE Trans. Appl. Supercond* vol.13, pp.433-436, 2003.

[3] B. D. Dimov, V. D. Todorov, V. M. Mladenov, F. H. Uhlmann, “Optimal signal propagation speed of a Josephson Transmission Line”, *Superconducting Science and Technology*, 17, pp. 819-822, 2004.

[4] B. Dimov, V. Todorov, V. Mladenov, F. H. Uhlmann, “Improved Techniques for Long-Distance Signal Propagation within the Rapid Single-Flux Quantum Digital Circuits”, *Proceedings of 7th International Symposium on Signals, Circuits and Systems ISSCS 2005,* vol. 2, pp. 733-736, 2005.

[5] B. Dimov, V. Todorov, V. Mladenov, M. Khabipov, D. Balashov, D. Hagedorn, F.-Im. Buchholz, J. Niemeyer, F. H. Uhlmann, “An Improved Technique for the Design of Josephson Transmission Lines”, *Supercond. Sci. Technol.*, vol. 19, pp.213-216, 2006.

[6] S. V. Polonsky, V. K. Semenov, D. F. Schneider, “Transmission of Single Flux Quantum Pulses Along Superconducting Microstrip Lines”, *Trans. Appl. Supercond.*, vol. 3, pp. 2598-2600, 1993.

[7] N. A. Joukov, D. E. Kirichenko, A. Yu. Kidiyarova-Shevchenko, M. Yu Kupriyanov, “Matching of Rapid Single Flux Quantum Digital Circuits and Superconductive Microstrip Lines”, *Inst. Phys. Conf.*, Ser. No 167, pp. 745-748, 2000.

[8] H. Suzuki, Sh. Nagasawa, K. Miyahara, Yu. Enomoto, “Characteristics of Driver and Receiver Circuits with a Passive Transmission Line in RSFQ Circuits”, *Trans. Appl. Supercond.*, vol. 10, pp.1637-1641, 2000.

[9] N. Joukov, Yo. Hashimoto, V. Semenov, “Matching Josephson Junctions with Microstrip Lines for SFQ Pulses and Weak Signals”, *IEICE Trans. Electron.*, vol. E85-C, pp. 636-640, 2002.

[10] B. Dimov, “General Restriction and Their Possible Solutions for the Development of Ultra High-Speed Integration RSFQ Digital Circuits”, PhD Thesis at the Faculty of Electrical Engineering of Technical University-Ilmenau, Germany, 2005.

[11] V. Todorov, “Ultra Low-Power Circuits based of the RSFQ Technology”, PhD Thesis at the Department of Theoretical Electrical Engineering of Technical University-Sofia, Bulgaria, 2009.

[12] B. Dimov, V. Todorov, V. Mladenov, F. H. Uhlmann, “The Josephson Transmission Line as an Impedance Matching Circuits”, *WSEAS Trans. Circuits and Systems*, vol. 3, No 5, pp.1341-1347, 2004.

[13] R. Dolata, M. I. Khabipov, F.-Im. Buchholz, W. Kessel, J. Niemeyer, ”Nb/Al_2O_3-Al/Nb Process Development for the Fabrication of Fast-Switching Circuits in RSFQ Logic”, *Appl. Supercond.,* vol.2, pp.1705-1708, 1995

INTELIGENT FEEDBACK CORRECTION OF TOTAL HARMONICS DISTORTION

Plamen Angelov Angelov[1], George Ilinchev Popov[2]

[1]Plamen A. Angelov, Faculty of Computer Science and Engineering,
Burgras Free University, 62 San Stefano Str., Burgas-8001, Bulgaria,
phone:+359 56 900404 E-mail: pangelov@bfu.bg
[2]George I. Popov, Faculty of Faculty of Computer Science and Engineering,
Technical University of Sofia, 8 Kl. Ohridski Str., Sofia 1000, Bulgaria,
phone +359 2 965 2224, e-mail: popovg@tu-sofia.bg

Abstract. *The subject of the present article is the study of a new feedback method of analysis by the harmonics correction of the signal. The present article offers some possible solutions of achieving this feedback correction while using a PC Scope. The emphasis is laid on a practical solution in the study of the harmonic component of the signal.*

Keywords: total harmonic distortion (THD), intelligent spectral correction, measuring and rejection of the f_{in}.

INTRODUCTION

This article is the our next step in the development of intelligent system for correction of nonlinear distortions. The present article examines a new method of analysis and correction of the total harmonic distortions by correction the input spectrum. The article offers a model for structural feedback correction in it, using tracking harmonious composition of the source signal. The measured output signals after Fourier decomposition can be represented by their harmonics. This information serves as a baseline assessment of distortions [3], [5]. Selective inhibition of entry and correction spectrum gives us the possibility of correction. The article proposes a structural model for intelligent feedback correction the input spectrum. This will lead to reducing the number of harmonics in the nature of the output signal and a significant reduction of nonlinear distortions.

1. Know methods for THD measurement and development the model of the system

In the theory of the measurement of the THD it is indicated that the periodical signal is not always sinusoidal [1]. When this signal passes through electrical and electronic devices, they modify it. When in the input of a non-linear system can be submitted a harmonic signal in the output, we have additional spectrum components [5]. Most reasons often are: non-linearity characteristics of the semiconductors [6] in the linear amplification [4], non-linearity characteristics of the reference generator in Class D audio, non-linearity caused by the attached modulation limiting the input signals; complex output load; method for designing the printed circuit boards. Distortions of this type are called total harmonic distortion (THD) [1].

Analysis of these signals can be presented as a sum of sinusoidal (harmonic) values with different frequency and initial phase (Fourier transformation). For example, a periodic voltage without a DC component can be determined by this equation:

$$u(t) = U_{1\max}\sin(\omega.t + \varphi_1) + U_{2\max}\sin(\omega.t + \varphi_2) + U_{3\max}\sin(\omega.t + \varphi_3) + U_{n\max}\sin(\omega.t + \varphi_n) \quad (1)$$

Where: $U_{1\max}, U_{2\max}, \ldots, U_{n\max}$, is amplitude value of the harmonic components and φ1, φ2, ..., φn is the starting phase of the voltage harmonics.

The efficiency value of voltage $u(t)$ can be determined by the effective values U_1, U_2, …,U_n of the harmonic components:

$$U = \sqrt{U_1^{\ 2} + U_2^{\ 2} + U_3^{\ 2} + U_4^{\ 2} + \ldots + U_n^{\ 2}} \quad (2)$$

If the voltage u (t) is not distorted, only sinusoidal one, in expression (2), it will be only the cost of the basic (first) harmonics, or $U = U_1$. In all other cases $U > U_1$.

The degree of nonlinear distortion is also called total harmonics distortion (THD). It is an effective relation of the total value of all harmonics, without the effective value of the first harmonics. This method of presentation may be presented by the equation:

$$K_{THD_1} = \frac{\sqrt{U_2^{\ 2} + U_3^{\ 2} + U_4^{\ 2} + \ldots + U_n^{\ 2}}}{U_1}.100\% \quad (3)$$

A different equation may be given when the value, instead of performing the first voltage harmonics U_1, measures the effective value of the whole voltage U. Coefficient of nonlinear distortions in this case is defined by the equation:

$$K_{THD_2} = \frac{\sqrt{U_2^{\ 2} + U_3^{\ 2} + U_4^{\ 2} + \ldots + U_n^{\ 2}}}{U}.100\% \quad (4)$$

At low rates of THD ($K_{THD} < 0.1\%$) the coefficient $K_{THD_1} = K_{THD_2}$. Both coefficients are interrelated by the equation:

$$K_{THD_1} = \frac{K_{THD_2}}{\sqrt{1 - K_{THD_2}^{\ 2}}}; \qquad K_{THD_2} = \frac{K_{THD_1}}{\sqrt{1 - K_{THD_1}^{\ 2}}}; \quad (5)$$

From expressions (3) and (4) it is noted that the coefficient of nonlinear distortions can be determined by pre-measured values U_1, U_2, U_3,…,U_n of all harmonics. This is done by spectrum analyzers. Coefficients K_{THD_1} and K_{THD_2} may be determined by a method where the estimated accuracy of measurement is 0.5%. This is achieved by direct measurement of complex variables of the voltage representing numerator and denominator. Expressions (4) and (5) show the relationship

$$K_{THD_3} = \sqrt{\frac{U_2^{\ 2} + U_3^{\ 2} + U_4^{\ 2} + \ldots + U_n^{\ 2}}{U_1^{\ 2} + U_2^{\ 2} + U_3^{\ 2} + U_4^{\ 2} + \ldots + U_n^{\ 2}}}.100\% \tag{6}$$

The known methods evaluate the distortion from the value of the individual harmonics [5], but the spectrum of the input signal should be taken into consideration. This spectrum can be corrected, thus reducing the output distortion.

The idea of adjusting the input spectrum came up during a research of digital audio amplifiers [6]. We must comply with the minimum distortion in the output signal. Often times when measuring the THD different distortions are observed and they are caused by: signal modulation being used, poor filtration in the output signal in digital audio amplifiers, the lack of stability in the supply voltage. This causes a significant change in the output spectrum and the introduction of nonlinear distortions. Decomposition and evaluation of this spectrum is not sufficient from where comes the idea of correcting it. A similar analysis can be applied and under the correction in the low frequency range for example - audio equalizer, reference generators, audio power stages, systems for control of the output parameters, and a continuous filtration at different switching power supply.

1.1. Development of the model

General block scheme implementing this type of feedback spectral modification is shown in Fig.1. A reference signal from the generator shall be made at the entrance of the study device. In the output of the survey device we connected a PC Scope which compares the amplitudes of both signals. This comparison serves to determine the boundaries of the input amplitude at which the output signal is not limited.

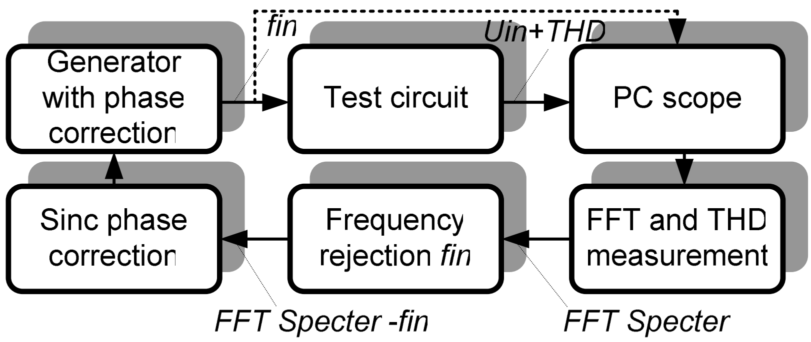

Fig.1. The base structure

The output signals measured are partitioned by Fast Fourier Transformation (FFT) [1] from where the THD are calculated (equation.3. equation.4.). Thus, the result obtained by the FFT transformation is passed to a system for rejection of the useful frequency (input) signal - so the spectrum is given only to non-linear distortion. Using this spectrum to the input of the reference generator, we will be able to adjust the signal before its submission to the studied device. After phase correction, the resulting modified spectrum moves to the input of the device being researched and thereby removed from the incoming signal [3]. Thus, resulting output signal will represent the amount of input (reference) frequency and the nature of nonlinear distortion, which is defined by the equation:

$$U_{out2} = [U_{in_{\max}}.\sin(2.\pi.f \pm \varphi)] + THD \tag{7}$$

The definition of amplitude stability will allow us to determine the boundaries of the input amplitude with minimum distortion. The research is conducted in the following sequence:

- Connecting the etalon frequency $f_{in} = 1kHz$
- Determining the minimal input voltage $U_{in_{\min}}$ of the test system ($f_{in} = 1kHz$) at which is observed an output signal corresponding to the requirements of the inspect system
- Determining the maximal input voltage $U_{in\max}$ of the test system ($f_{in} = 1kHz$) at which is observed an output signal corresponding to the requirements of the inspect system
- FFT analysis
- Calculating of the THD in case of minimal and maximal input level $U_{in} = U_{in_{\min}} \div U_{in_{\max}}$ (when $f_{in} = 1kHz$), where the input level necessary should be adjusted to minimum THD.

After the optimal voltage range is determined we measure bandwidth. The research is conducted in the following sequence:

- Connecting the etalon frequency $f_{in} = 1kHz$ and input voltage $U_{in} = U_{in_{\min}}$ (minimal THD)
- Measuring the amplitude characteristic of the device. This research is held by stabilization of the input amplitude and correction of frequency
- Determining the nonlinearity of the amplitude characteristic and the distortions arising from it. This research is done when loading the test system with etalon load.
- Reporting the measuring values at which there are minimal distortions.

After determining the values of the input level, where there are minimum distortions, the system is adjusted in this way:

- Setting the etalon frequency $f_{in} = 1kHz$ and input voltage $U_{in} = U_{in_{\min}}$ (minimal THD)
- FFT analysis and THD measurement;
- Rejection of the input frequency from the resulting spectre;

- Phase correction in the resultant signal;
- The resulting spectrum is subtracted from the reference signal generator.
- Measuring the THD. This will report significantly lower distortions.

Advantage of the system is that it can adjust the spectrum or the non-linear distortions of various types of electronic systems. What will be enough is the possibility of external intervention and correction of the signal parameters.

CONCLUSIONS

Derived from the system for the measurement and correction of nonlinear distortions, the following major conclusions can be made:

- inclusion of a feedback control system contributes to linearization of the test signal and improving the nature of bias signal;
- phase alignment of the signal is essential to achieve the maximum effect of reducing the output distortion

REFERENCES

[1] Койчев, К., Садинов, С. Сигнали и Ситеми, Габрово, изд. Алма Матер Интернационал 2002.

[2] Angelov, Pl. "One possibility to indicate the harmonic composition of current". Conference of Electronics 2004 - The Technical Writer's collection. page: 395–400. Bulgaria, Burgas Free University, Burgas 8001 2004.

[3] Angelov, Pl. "Measurement and control of total harmonic distortion in frequency range 0,02 – 10 kHz" Conference of Electronics 2004 - The Technical Writer's collection. page: 150–154. Bulgaria, Burgas Free University, Burgas 8001 2005.

[4] Bortoni, R., Filho, S., Seara, R. (2002). On the Design and Efficiency of Class A, B, AB, G, and H Audio Power Amplifier Output Stages. Journall of Audio engineering society, Paper 0547. Volume 50 Number 7 pp. 547-563.

[5] Farina, A., (2000). Simultaneous measurement of impulse response and distortion with a swept-sine technique, Convention of Audio engineering society, 108th, Paris, Convention Paper 5093.

[6] Gaalaas, Eric. (2006) Class D Audio Amplifiers: What, Why, and How. Journal of Analog Dialogue Vol.40, Analog Devices.

A CAR SECURITY SYSTEM MODEL BASED ON TIMED PETRI NETS

George Ilinchev Popov[1], Plamen Angelov Angelov[2]

[1]George I. Popov, Faculty of Faculty of Computer Science and Engineering, Technical University of Sofia, 8 Kl. Ohridski Str., Sofia 1000, Bulgaria, phone +359 2 965 2224, e-mail: popovg@tu-sofia.bg

[2] Plamen A. Angelov, Faculty of Computer Science and Engineering, Burgras Free University, 62 San Stefano Str., Burgas-8001, Bulgaria, phone:+359 56 900404 E-mail: pangelov@bfu.bg

Abstract. *This report presents a Time(-d) Petri Net based model of a hypothetical car security system with RF remote control unit. Our suggestion possess most important features found on such type of systems realized with set of buttons - arm, disarm and silent. The Petri Net-oriented techniques with interval timing are used for our design purposes to reach a control recoverability modeling time-outs. The proposed solution can be charged to modify or add features as required. The code can also be moved to a various type of functionality microcontrollers for different I/O or code space.*

Keywords: Petri Nets, Time-out Nets, Security System, Alarm, Interval Specifying

1. INTRODUCTION

The time ordering to the design process and its decomposition allow to detect the existing errors, which value is in an exponential dependence of phase model levels.

The aim of this paper is to propose an appropriate security system design tool with own formal syntax, simulation rules and transformations, conserving initial semantics. Petri Nets based techniques [1,2] are advantageous for these purposes. The formalisms with interval specifying are suitable to describe their real-time behavior including a set of parallel processes, protocols, time-outs, conditions etc. The general classes of Petri Nets type extended with temporal restrictions allow modeling various timed parameters and correct net and system implementation respectively.

2. A CAR SECURITY SYSTEM MODEL

In the present work, we suggest an automobile security system block diagram with RF remote control unit shown in fig. 1. Our solution implements the following basic functions: code hopping alarm system; Arm/Disarming; Silent mode; Trunk release; locking/unlocking of doors; door and sensor trigger inputs.

A system model using Interval Timed Petri Nets - oriented techniques [4] is presented in fig. 2. The structural elements (places and transitions) of our suggestion are specified at table 1 (transitions) and table 2 (places).

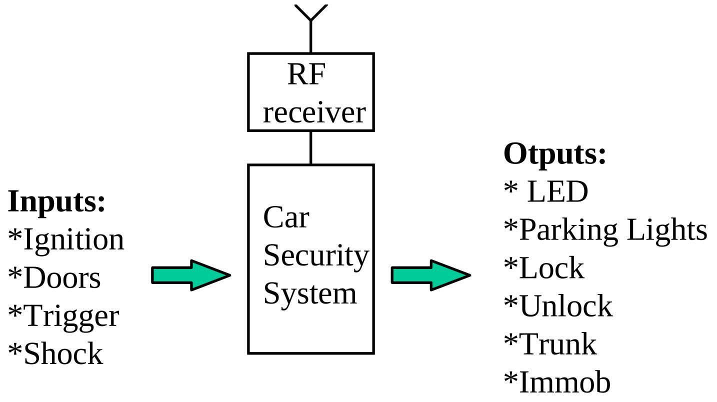

Fig. 1. Car security system functions

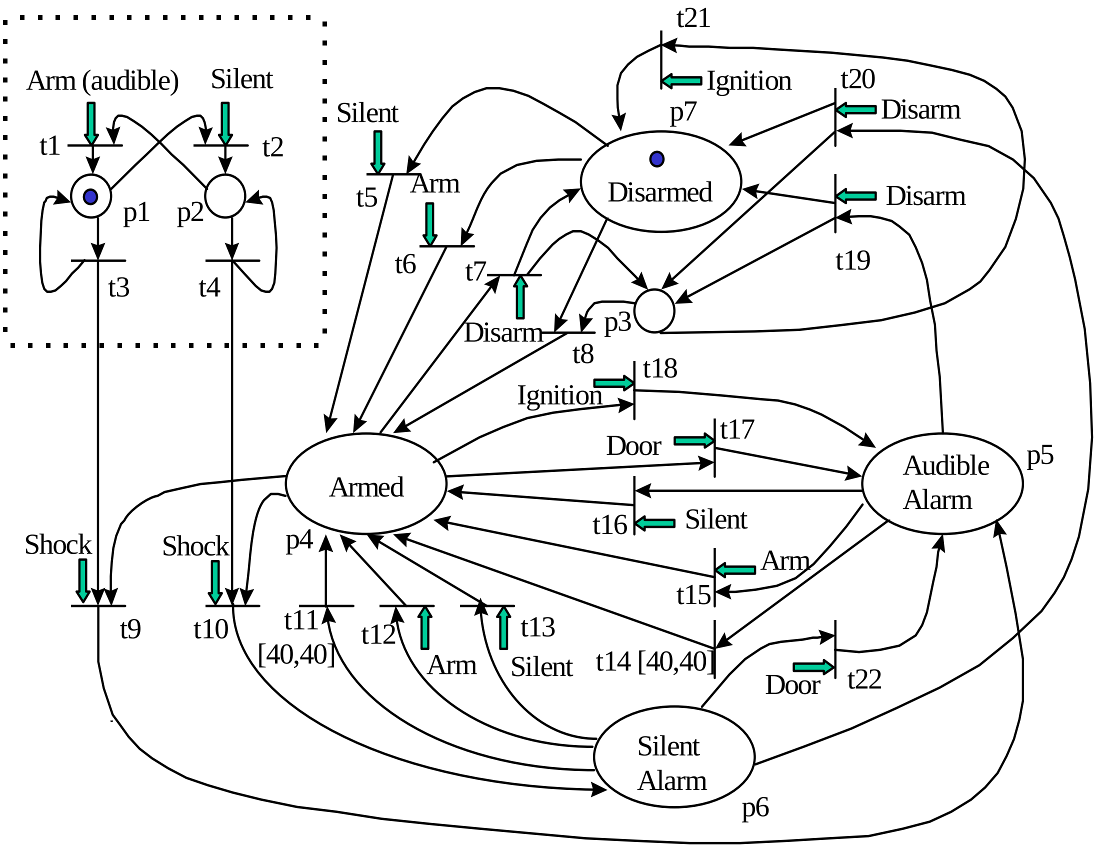

Fig. 2. A TPN model of car security system

Table 1 - Transitions

t1,t2,t3,t4: Trigger Type Events;	t14: Re-Arm Time-Out 2 (40s);
t5: Silent Arm;	t15: Cancel Alarm With Audible Arm Button;
t6: Audible Arm;	t16: Cancel Alarm With Silent Arm Button;
t7: Disarm;	t17: Alarm After Opened Door;
t8: Autoarming Time-Out 1 (20s);	t18: Alarm After Turn Ignition;
t9: Audible Alarm After Shock Activation;	t19: Disarm After Audible Alarm;
t10: Silent Alarm After Shock Activation;	t20: Disarm After Silent Alarm;
t11: Re-Arm Time-Out 2 (40s);	t21: Auto Arm Off (Ignition On);
t12: Cancel Alarm With Audible Arm Button	t22: Audible Alarm (Opened Door).
t13: Cancel Alarm With Silent Arm Button	

Table 2 - Places

I. BASIC STATES:
p4-"Armed": State with action upon entry:
*the parking lights flash one time (50ms);
*the siren chirp one time for 50rns (if the system is audible armed);
*lock door for 500ms;
*disable engine;
*led flash;
p5-"Audible Alarm": State with action upon entry:
* the parking lights flash;
* the siren on;
* pager send;
* LED flash;
p6-"Silent Alarm": State with action upon entry:
* the parking lights flash;
* pager send;
* LED flash;
p7-"Disarmed": State with action upon entry:
* the parking lights flash two times for 40ms;
* the siren chirp two times for 40rns(if the system is audible armed);
* the siren chirp two times (if an alarm has been occurred);
* unlock door for 500rns;
* enable engine;
* led off;

II. SUBSIDIARY STATES:
p1 - A System Audible Mode;
p2 - A System Silent Mode;
p3 - An Internal Auto arm Flag.

The system can be armed in two modes: silent (p2 is marked) or audible (p1 is marked). In the silent mode, the shock sensors cause a silent alarm - the bell is off, only the pager and parking lights are active. The arming in this mode is required for noisy places - towns, streets etc.

The opening the door (t22, t17) in the arm mode, always cause the audible alarm. The alarm duration is 40s (t11,t14). If no remote control signal generated, the system will rearm automatically.

After remote control disarm command, the system establishes to the disarmed state for 20s and rearms. During this time-out, the user must turn on the engine key to disable rearming (t21).

3. CONCLUSIONS

The presented solution is optimized using our program product "PetSym". The following model properties are proved: safeness, boundness, liveness etc. On the base of these results would be realized a prototype of a system.

Functional example of Car alarm system (fig. 3) is taken from [3], where the system is represented by graph model. The main advantage of the model by graph lies in its readability, because graph notation is more popular than the timed Petri nets.

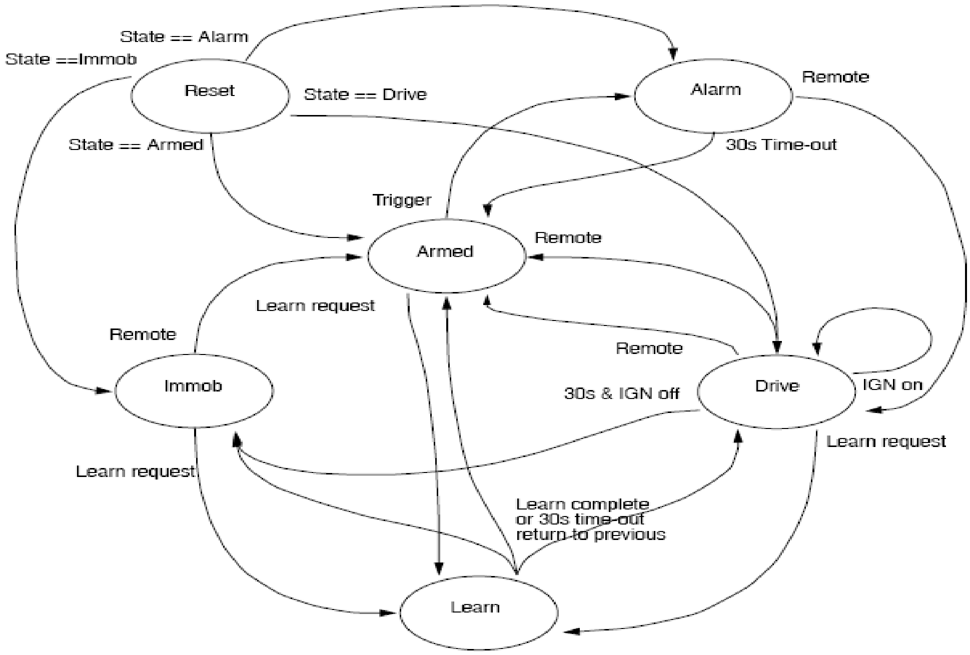

Fig. 3. Graph model of car system

This model has the following disadvantages:

- During a 30s time-out (state Alarm), if the button is pressed ARM, the system goes into state Armed. Also on condition Drive, if the button is pressed ARM (box of Remote), must be completed in two states and Immob Armed;
- Due to limited capacity of the columns compared to timed Petri nets do not fully describe the conflict situations in time;
- Model is not suitable for simulation.

The suggested system kernel with proven correct behavior during the verification procedure can be developed and extended adding new feature: and functions - code learning, antirobe, only immobilize, alarm memory etc. Proposed model based on Time(-d) Petri Nets is an advantageous as compare as other similar solution [5] specified with FSA state diagrams and change tables. The introduced temporal restrictions allow reaching a structural recoverability and demonstrating a real-time behavior of the complex security systems.

REFERENCES

[1] Petrova P., Popov G., A Model of Car Security System using TPNets, 12-th International Conference: Systems for Automation of Engineering and Research" and DECUS NUG Seminar'98, St. Konstantin Resort, Sept.,20-21th,1998.

[2] Petrova P., Popov G., A Model of a Code Interface Control Panel for Security Systems with Time-out Nets, SAER'97, St. Konstantin resort, Sept. 20-21, 1997, pp. 64-67.

[3] Microchip "Secure Data Products Handbook", 1997/1998.

HALF DUPLEX PROTOCOL FOR WIRELESS SENSOR SYSTEMS

George Ilinchev Popov[1], Tasho Angelov Tashev[2]

[1]George I. Popov, Faculty of Faculty of Computer Science and Engineering, Technical University of Sofia, 8 Kl. Ohridski Str., Sofia 1000, Bulgaria, phone +359 2 965 2224, e-mail: popovg@tu-sofia.bg

[2] Tasho A. Angelov, Faculty of Automation, Technical University of Sofia, 8 Kl. Ohridski Str., Sofia 1000, Bulgaria, phone +359 2 965 2324, e-mail: ttashev@tu-sofia.bg

Abstract: *This paper concerns the problems about modeling radio protocols in wireless security systems. The parameters of the link are: length of packages; number of repetitions of packages, number of transmitters, repeater and receivers, parameters of channel. A Timed Petri Net model of wireless half duplex protocol is presented.*

Keywords: wireless alarm system, radio transmitter, security system, alarm, security radio network, Timed Petri Nets

1. INTRODUCTION

This investigation is oriented to connection between wireless unit (as detector, siren) and control panel. Specifically for wireless security unit (WSU) is the fact, that they are battery powered and protocols have to save the energy. The WSU sends specific signals, correspond to the change of status of his status.

One control panel serves up to **N** wireless units (N ordinary is between 16 to 128). If happens a common ccause, several WSU transmits the signals at the same moment. The receiver (SMC) will receive only one signal at the highest level, another signal will be loss (as an message). This may have dangerous result, if any signal is alarm or personal attack.

Another problem is an ether noise might be casual or made by a tamper.

We are searching for methods to suspend of loses of the signal.

There are two possibilities:

– One possibility method is the duplex link, but it makes the equipment too complex and dear.

– Another approach is the repetition of the signals. Every signal will be transmitted several (n-) times in to ether, for a casual interval of time.

Wireless protocols are comparatively complex. It is needed to use of a formal method for specification and verification these protocols. The idea is the errors themselves to be found in the process of the designing.

Timed Petri Nets (PN) are most appropriate techniques as compared with the approaches existing so far. This fact is conditional by the presence of a set of asynchronous parallel processes, the usage of exchange protocols, the solving of coordinate tasks and the realization of alternate transitions.

2. HALF DUPLEX PROTOCOL MODEL

In this case wireless unit (detector) sends the signals until receiver talks him to stop, because information is received [1]. The intervals between packages are approx. 5s. After every transmission, detector turns on listen (receive) mode. In this mode detector tries to get acknowledge form receiver. If this acknowledge is not received, detector sends encore one time the signal. In other case communication will be cancelled.

Marker in t1 (SEND) correspond to the change of detector status. This means that detector will send a signal. The signals are:

- alarm / restore of alarm;
- low battery / restore battery;
- tamper / restore of tamper;
- system test - emits every 12 hours.

Position P1 is generation place. If a marker persists in this position, a generation will make. P2 is subsidiary place. Marker in this place means, that after 10s a new generation will be made. Position P3 and transaction t4 and t5 model ether. If transaction t5 is fired, the message is lost. In this case after approx. 10s t2 will fire and new generation will be made.

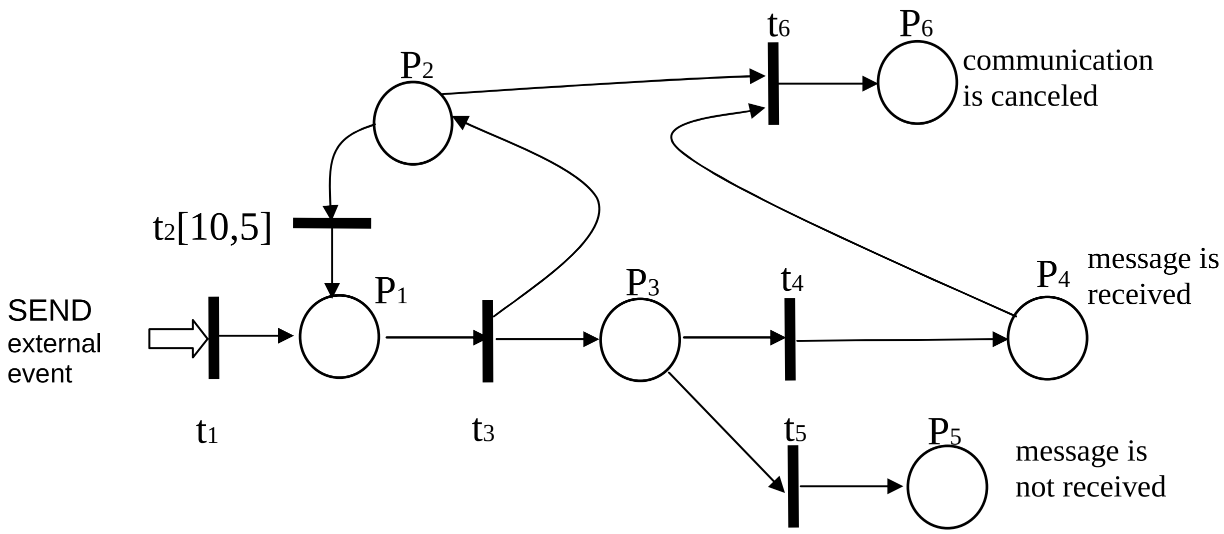

Fig. 1. A TPN model of half duplex protocol

Otherwise, if t4 is fired, the message will receive successfully. Then receiver sends the signal “OK”. Transaction t7 is fired and communication is canceled (the marker inhibits from position P2. A marker in Position P6 means that communication has been made successfully.

Table 1 - Places

P1	Main state – generation place
P2	Subsidiary place – new generation after approx. 10s.
P3	The message passes though ether. It might be received or lost
P4	The message is received
P5	The message is not received
P6	Communication is canceled successfully.

Table 2 - Transitions

T1	An event is occurred
T2	Generation will make after 5-15s
T3	Signal is sent trough ether
T4	The message is received
T5	The message is received
T6	Inhibition of generation marker.

3. EXPERIMENTAL RESULTS

Two models have been created. First model is simplex communication and it includes five repetitions of the signal [2, 3]. Every time the message is received, but there are occasions of particularly signal loss.

Second model is similar to described above. It is seen that he is too complex as first, but he is too economical with battery energy. If it is placed possibility to t3 and t4 it will be possible to model noise in ether. At fig.2 is shown dependability between signal repetition and noise.

If it is associated 100mW energy with every transmition (generation), battery life will be saved with 30% by using half duplex protocol.

The presented solutions are analyzed, simulated and tested using created in TU-Sofia program product “Petsym”. During verification procedure are investigated and demonstrated the following properties: safeness, boundless, liveness etc.

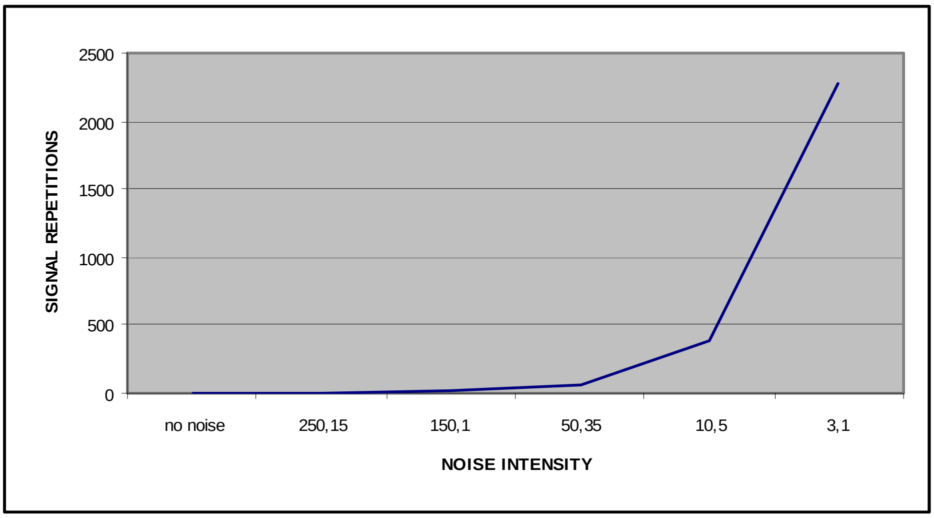

Fig. 2. Dependability between noise and signal repetitions in half duplex protocol

4. CONCLUSIONS

A comparative analysis between two security wireless protocols has been made. Second protocol saves battery life, but it makes electronic too complex. An additional receiver must be incorporated in detector, and one additional transmitter in receiver (control unit).

Half duplex link has additional advantages, as possibility to program each detector by control unit. Otherwise, installer must set every detector with DIP switch and potentiometer. Another advantage is possibility to upgrade protocol with polling by control unit.

The presented model with Time-out Petri Nets solves the problems in protocol designing. The suggested formalism gives opportunity for automatization. This formalism would be used to simplify the designer's work in the new system creation.

REFERENCES

[1] Hristov H., Popov G., Adequacy of Identification of Controlled Phenomena in the Security Systems, International Scientific Conference Communication, Electronic and Computer Systems 2000, Sofia, May 2000, Vol. 1, p 188-193.

[2] Popov G., *Optimization of Communications Signals of Public Address Systems*, international Scientific Conference "Electronics' 2004", pp.150-155, Sozopol, 22-24 Sept. 2004.

[3] Popov G., *Investigation of Protocol with Signal Repetition for Wireless Security Systems*, *16TH* national scientific symposium with international participation «Metrology and Metrology Assurance 2006", September 12-16, 2006, Sozopol, Bulgaria

[4] Technical documentation from Paradox Magellan wireless system- www.paradox.ca

THE SHORT PERIOD 160-MIN. RADIAL PULSATIONS OF SUN

Ivan T. Ivanov[(1)], Valentina T. Taneva[(2)], Boris Komitov[(3)] and Radostina Tasheva[(4)]

(1) Department of Physics and Biophysics, Medical Institute, Thracian University, 6000 Stara Zagora;
(2) Department of Applied Physics, Technical University of Sofia, uraa@dir.bg
(3) Institute of Astronomy, Bulgarian Academy of Sciences, 6000, Stara Zagora, P.O. Box 179
(4) Department of Applied Physics, Technical University of Sofia

Abstract: *The visible diameter of Sun oscillates with a period of 160 min. The same type of periodicity is also found in a huge number of solar radiation parameters. To elucidate the origin of these longitudinal radial pulsations we have used the equation for the equilibrium of inner layers which, after linearization, turned into the harmonic oscillator equation. The latter equation allows radial pulsations whose period and wave length were calculated using regresion expressions for the gas presure and density in various layers. The radial pulsations originate at the surface of active zone and propagate til the litosphere, where they undergo full inner reflection producing undersurface stationary waves with a period of 150 min.*

Key words: Sun; 160 min radial pulsations; mechanical waves; balance equation

INTRODUCTION

Ever since the discovery of the 160-min radial pulsations of the Sun ample data have been collected suggesting their impact on the sollar physics [1,2]. 160-min oscillations are observed in the intensity of light, radio and infrared radiation emitted from the resting regions of Sun [3]. The pulsations observed in the radiobrightness lag behind the cyclic radial movements by about 12 min [3]. A 0.02% variation in the intensity of the 1.65 mm infrared sollar radiation is detected with a 160-min period [4]. Oscillations with the same period are established in the cyrcular polarized radio emition of Sun at 13.5 mm, which lag behind the oscillations of the radiant velocity by 34 minutes [5].

These observations could not be explained as pure atmospheric effects [6]. The radiant pulsations of Sun have been unsuccefully related to the particularities of the radiant energy transfer [7], to the possible interferense between the Sun gravity modes [8,12] or even to the possible existence of a particular object orbiting the Sun center at appr. 20 000 km under the surface of the Sun [9]. Thus at present there is no commonly accepted theory that could explain the radiant pulsations of the Sun. [13] recently suggested swing wave–wave interaction. Therefore the amplified waves have periods of several hours. They can propagate upwards through the convection zone to the solar atmosphere and cause the observed long-period oscillations in the solar wind.

In this paper we offer a model based on the linearization of the Sun status equations. This model represents the radiant oscillations as staying waves generated on the surface of the active zone and propagating to the surface of the Sun where they have a period of about 160 minutes.

DESCRIPTION OF THE MODEL

The equilibrium status of the star core is usually found as a solution of the system of basic equations describing the star physics. For the Sun, several solutions are obtained which give the equlibrium values of pressure P, temperature T etc as functions of the distance r from solar centre. These functions are averaged in the summarised model [10] which will be used futher.

The status of the Sun intestine is a stable equilibrium. If a thin concentric layer inside the Sun is displaced from its equilibrium distance r_o from the center of gravity, it will commence to oscilate. What will be the frequency of these oscillations? The equation that describes the movement of the layer is

$$\rho\left(\frac{\partial^2 r}{\partial t^2}\right)+\frac{\partial P}{\partial r}=-\rho\frac{Gm}{r^2} \tag{1}$$

where m is the mass of the gas placed under the layer. Let this layer be shifted from a place with distance r_o to a place with a distance $r_o + \Delta r$. Since $\Delta r \ll r_o$, the pressure gradient will change as given by

$$\frac{\partial P}{\partial r}=\left(\frac{\partial P}{\partial r}\right)_{r=r0}.\Delta r+0.\left(\Delta r^2\right) \tag{2}$$

The gravity force attracting the layer to the center of Sun will also change according to the variations in the distance r

$$\frac{1}{r^2}=\frac{1}{r_0^2}.\left(1-2\frac{\Delta r}{r_0}\right)+0.\left[\frac{\Delta r}{r_0}\right]^2 \tag{3}$$

Let us combine the equations (2) and (3) with the equation (1). Inserting a new variable $x=\frac{\Delta r}{r_0}$, a new equation will be obtained

$$\frac{\partial^2 x}{\partial t^2}+\left(\frac{1}{\rho_0}.\frac{\partial^2 P}{\partial r^2}-\frac{2Gm}{r_0^3}\right).x=\frac{1}{\rho_0 r_0}\left(\frac{\partial P}{\partial r}\right)-\frac{Gm}{r_0^3} \tag{4}$$

The right side of the latter equation is equal to zero since a hydrostatic equilibrium holds at $r = r_o$. Equalizing the left side of the equation to zero a new equation will be obtained which resembles the harmonic oscillator relation. Thus, the respective frequency f of the adiabatic radiant oscillations will be given by the formula

$$\omega^2 = \frac{1}{\rho}\left(\frac{\partial^2 P}{\partial r^2}\right) - \frac{2Gm}{r^3} \qquad (5)$$

The period of oscillation of the layer will be T = 2 π /ω. Once generated these oscillations will apparently subside down provided there is no source of energy for their rejuvanation.

The above linearizations appear fairly correct since the visible diameter of the Sun is found to oscillate with an amplitude of only a few km and a radiant velocity of about several m/s. Similar pulsations are found for the variable stars however the corresponding parameters of pulsations are three orders of magnitude greater in respect to these of Sun. Nevertheless, similar linearization theory has been also applied for the variable stars giving constant amplitude, frequency and phase at different distances from the star centre [11]. In contrast to the oscillations of variable stars, the oscilations that could occur within the Sun are very small and should be consequently allowed to have different amplitude, frequency and phase at different distances from the center of Sun as given by the formula (5).

RESULTS

According to formula (5), the period T of oscilation of different layers could be calculated using proper expressions for the dependence of P, ρ and m on the relative distance $x = r/R_{\odot}$.from the Sun center. Using the model [10] and 16 cited values for each parameter, these expressions were obtained as regression formulae and are shown in Table I. For each parameter the correlation coefficient K_r, reliability factor F and probability weight factor P_w between the cited data and the calculated values demonstrate that the obtained expressions are fairly satisfactory.

Table I. Regression formulae for the density p and gas presure P within the Sun as functions of the relative distance y = r/R from its centre. m is the mass of solar gas beneath a concentric layer with a radius r. R and M are the Sun radius and mass correspondingly.

Regression formula	**Kr**	**F**	**Pw**
m = M.(2.84 y - 1.70 y - 0.06)	0.991	52.1	4.10
P = exp (38.94 - 24.68 y)	0.92	6.08	0.0008
ρ = exp (3.85 -17.36 y)	0.942	8.28	0.00015

Allowing x to vary with a step of Δx = 0.01, a set of discrete values of T were calculated which are shown on plot (Fig.1). Generally, the intestine of Sun is sharply divided into three zones; active core, intermidiant zone and convective zone, according to the nature of the physical processes in them. Each of these zones is clearly distinguished on the given plot.

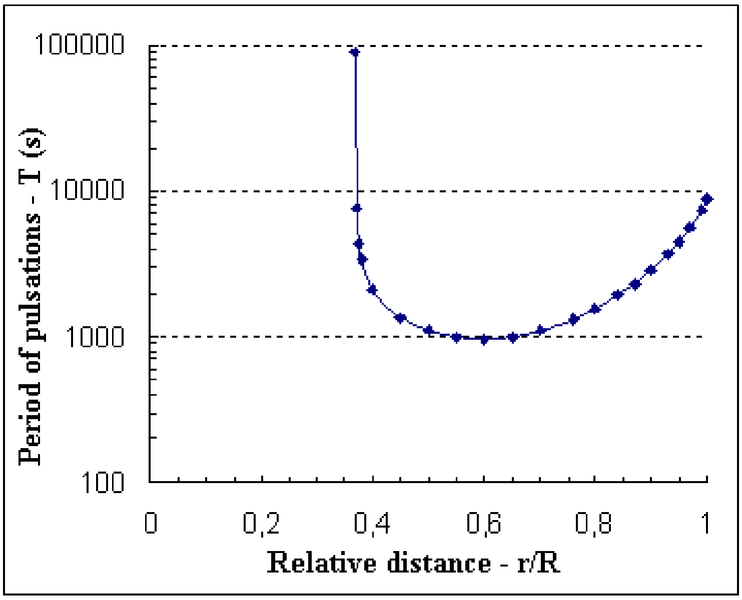

Fig. 1. Period of radial pulsations within the Sun as a function of the distance from its centre.

Oscillations should be apparently impossible throughout the active zone (0 <x< 0.38) as $\omega^2 < 0$. It could be assumed that the period of oscillations there will be close to infinity. In the vast convective zone of radiative energy transfer, oscillations might occur with a nearly constant period of about 1000 s. However, at the boundary between this zone and the active zone the period of pulsations sharply increased inclining to infinity (Fig.1) in accordance with the result that oscilations are not allowed in the active core. This result indicates that any slow mechanical disturbance that might occur on the surface of the active zone could be transfered into the interior of the middle zone as periodic pulsations. Hence, the radial oscillations that might occur within the Sun could originate from this boundary. Such a conclusion is apprehensible since the surface of the active zone must be mechanically unstable.

According to Fig.1, the period of pulsations slowly increases near the outside boundary of the convective zone reaching the value of 8900 s (148 min) just on the Sun surface. This value differs by about 8 % from the experimentally obtained value of 160 min. The striking coincidence between the calculated and measured values of solar pulsations supports the proposed model.

DISCUSSIONS

According to the proposed model, the pulsations of the Sun radius are brought about by a slight disturbance of the dynamic equilibrium of forces balancing the inner layers and could be described by the mechanism of the charmonic oscilator. The energy source generating the oscillations and maintaining their amplitude constant is possibly found at the boundary between the active and the middle zones. Once generated, the oscillations should further propagate towards the Sun surface with the velocity "C" of the sound. This velocity could be calculated using the formula $C = (P/\rho)^{1/2}$ and the expressions for the P, and p as given in Table I. We have calculated the velocity C and the wave length $\lambda = T.c$ of these mechanical pulsations as a function of the distance x form the centre of Sun. Surprisingly λ was nearly constant for both the middle and convective zones (data not shown).

When the radial oscillations reach the Solar atmosphere (the chromosphere), they should sustain a complete backward reflection without change in phase as suggested by the strong fulfilment of the respective mandatory condition $\lambda > 4\pi H$. Here H is the depth of the solar atmosphere. As the wave length is practically constant within a broad segment under the visible surface of Sun, the formation of standing mechanical wave shoud be allowed deep under the chromosphere. These oscillations have the capacity to impact a huge number of physical phenomena close to the surface of Sun introducing a variable component with the same 160 min periodicity in the observed parameters of Sun.

REFERENCES

[1] Severny A. B., V. A. Kotov, T. T. Tsap. Nature (1976) Observations of solar pulsations. № 5539, v. 259, pp. 87-89

[2] Scherrer P. H., J. M. Wilson (1983) Structure of the solar oscillations with period near 160 -minutes. Solar Phys., v.82, pp. 37-42

[3] Kotov V. A., A. B. Severny, T. T. Tsap, I. G. Moiseev, V. A. Efanov, H. S. Nesterov. (1983) Manifestation of the 160-min solar oscillations in velocity and brightness (optical and radio observations). Solar Physics, v. 82 pp. 9-19

[4] Kotov V.A., S. Kouchmy, G. Kouchmy (1983) Observation of global 160 -min infrared (differential) intensity variation of the Sun. Solar Physics, v. 82, pp. 21-35

[5] Efanov V. A., V. A. Kotov, I. G. Moiseev, N. S. Nesterov, A. B. Severny (1983) Reports of Krim astrophysical observatory, v. 67, pp. 111-118

[6] Hill H. A., T. J. Boss, T. P. Candel (1983) On the origin of oscilations in a solar diameter observed through the Barth`s atmosphere: a terrestrial atmospheric or a solar phemomenon. Solar Phisics, v. 82, pp. 129 - 138

[7] Christensen - Dalsgaard J., S. Frandsen (1983) Radiative transfer and oscilations of the Sun. Solar Physics, v. 82, pp. 165-204

[8] Dsiombovsky W. (1983) Resonant coupling between solar gravity modes. Solar Physics, v. 82, pp. 253-266

[9] Blinnikov S. I., M. Yu. Khlopov (1983) Excitation of the solar oscilations by objects consisting of y-matter. Solar Physics, v. 82, pp. 383-385

[10] Allen C. W. (1973) Astrophysical Quantities. University of London. The Athlon Press.

[11] Cox J. P. In: Theory of stellar pulsations. Princeton, New Jersy, Princeton University Press, 1980

[12] S. V. Kotov Jr., V. A. Kotov The most resonant pulsation frequency of δScuti stars Astronomische Nachrichten: A Journal on all Fields of Astronomy Volume 318, Issue 2, Date: 1997, Pages: 121-128

[13] T. V. Zaqarashvili, G. Belvedere The origin of long-period Alfvén waves in the solar wind, Monthly Notices of the Royal Astronomical Society: Letters Volume 362, Issue 1, Date: September 2005, Pages: L35-L39

NOVEL METHODS OF ANALYSIS OF SMART ANTENNAS, BASED ON UNIFORM ARRAYS

Sava Savov, Vyara Vasileva, Miroslava Doneva

Department of Electrical Engineering, Technical University of Varna, 1 Studentska str., 9010 Varna, phone: +35952383408, e-mail: savovsv@yahoo.com

Abstract: *In this paper, the adaptive beamforming (ABF) and direction of arrival (DOA) estimation methods of uniform rectangular array (URA) are introduced. An URA is composed of a number of uniformly distributed identical omnidirectional antenna elements or half-wavelength dipoles. LMS algorithm is applied to antenna beamforming in URA. ESPRIT technique is utilized for DOA estimation. Simulation results and numerical examples are presented to illustrate the adaptive beamforming (ABF) and direction of arrival (DOA) methods.*

Keywords: smart antenna, uniform rectangular array, adaptive beamforming, direction of arrival

1. INTRODUCTION

Smart antennas become popular during the recent years. The central idea of these adaptive arrays is spatial processing. The investigation of smart antennas suitable for wireless communication systems has involved primary uniform linear arrays (ULA) and uniform rectangular arrays (URA). The URA is more attractive for mobile communications.

Different methods have been proposed for adaptive beamforming (ABF) estimation. One of the most popular methods among them is the classical least mean squares (LMS) algorithm [1], [2]. DOA estimation algorithms are introduced for the significant improvement in smart antenna resolution. This paper presents the 2-D unitary ESPRIT for direction of arrival estimation analysis.

2. UNIFORM RECTANGULAR ARRAY STRUCTURE

The URA consisting N x M equally distributed identical omnidirectional antenna elements or half-wavelength dipoles (M, N – even), as illustrated in Fig. 1 is located symmetrical in *x*-*y* plane.

An incoming narrowband signal (plane wave with wavelength λ) arrives at the array from elevation angle θ and azimuth angle ϕ. The origin of coordinate system is located at the center of the array.

As demonstrated in Fig. 1, the array factor *(AF)* of URA with its maximum along θ_0, ϕ_0 is given by [4]

$$[\mathrm{AF}(\theta,\phi)]_{\mathrm{MxN}} = 4\sum_{m=1}^{M/2}\sum_{n=1}^{N/2}\mathrm{A}_{mn}\cos[(2m-1)u]\cos[(2n-1)v] \tag{1}$$

where $u = \frac{\pi d_x}{\lambda}(\sin\theta\cos\phi - \sin\theta_0\cos\phi_0)$ and $v = \frac{\pi d_y}{\lambda}(\sin\theta\sin\phi - \sin\theta_0\sin\phi_0)$
and A_{mn} is the amplitude excitation of the individual element, and d_x, d_y are the interelement spacing along the x-axis and the y-axis, respectively.

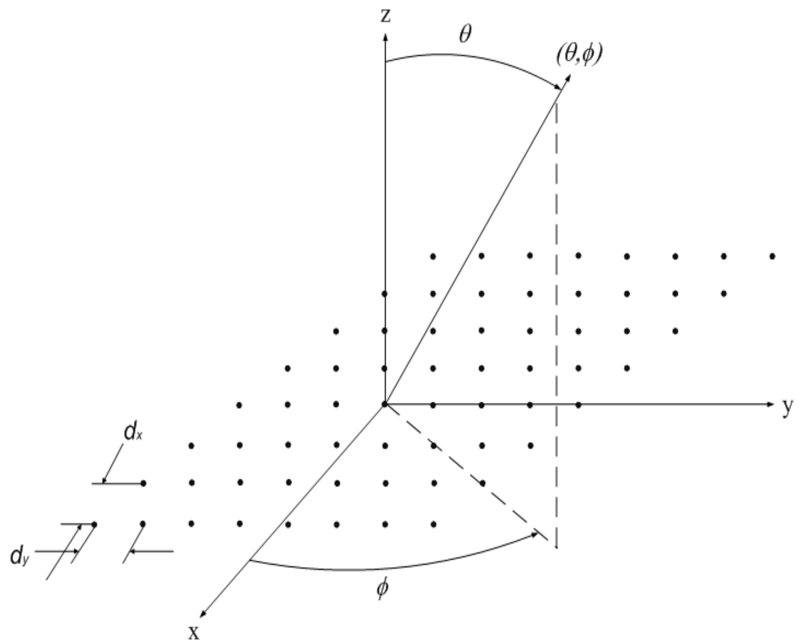

Fig. 1. Geometry of URA, along with an incoming plane wave

3. ADAPTIVE BEAMFORMING ESTIMATION

The LMS algorithm is one of the simplest methods applicable to estimate optimal weights of an antenna array.

The expression of optimal weights is given by [3, 5, 6]

$$\mathbf{w}(n+1) = \mathbf{w}(n) - \mu\mathbf{g}(\mathbf{w}(n)) \tag{2}$$

where $\mathbf{w}(n+1)$ denotes a new computed weights vector at the (n+1)th iteration, μ is the gradient step size, and the array output is given by

$$y(\mathbf{w}(n)) = \mathbf{w}^H(n)\mathbf{x}(n+1) \tag{3}$$

where $\mathbf{x}(n+1)$ is array signal vector computed at the (n+1)th iteration, and $y(\mathrm{w}(n))$ is output signal.

In its standard form it uses an estimate of the gradient by replacing array correlation matrix **R** and correlation between array signals and reference signal **r** by their noisy estimates at the (n+1)th iteration [4]

$$\mathrm{g}(\mathrm{w}(n)) = 2\mathrm{x}(n+1)\mathrm{x}^{H}(n+1)\mathrm{w}(n) - 2\mathrm{x}(n+1)r^{*}(n+1) \tag{4}$$

where **g** is the gradient vector.

The error between array output and the reference signal is given by [4]

$$\varepsilon(\mathbf{w}(n)) = r(n+1) - \mathbf{w}^{H}(n)\mathbf{x}(n+1) \tag{5}$$

and

$$\mathbf{g}(\mathbf{w}(n)) = -2\mathbf{x}(n+1)\varepsilon^{*}(\mathbf{w}(n)) \tag{6}$$

The estimated gradient is a product of the error between the reference signal and the output of the array and the signals after the *n*th iteration.

4. 2-D UNITARY ESPRIT ALGORITHM FOR DOA ESTIMATION

Applying the 2-D unitary ESPRIT algorithm the conditions of a URA structure (fig. 1), the array manifold has the matrix form [7]

$$\mathrm{A}(\mu, \nu) = \mathrm{a}_{N}(\mu)\mathrm{a}_{M}^{T}(\nu) \tag{7}$$

where the array manifold is

$$\mathbf{a}_{N}(\mu) = \left[e^{-j\left(\frac{N-1}{2}\right)\mu}, \ldots, e^{-j\mu}, 1, e^{j\mu}, \ldots, e^{j\left(\frac{N-1}{2}\right)\mu} \right]^{T} \tag{8}$$

$$\mu = \frac{2\pi}{\lambda} d_{x} p \tag{9}$$

λ is the wavelength, *p* is the direction cosine variable relative to the *x*-axis and

$$\mathbf{a}_{M}(\nu) = \left[e^{-j\left(\frac{M-1}{2}\right)\nu}, \ldots, e^{-j\nu}, 1, e^{j\nu}, \ldots, e^{j\left(\frac{M-1}{2}\right)\nu} \right]^{T} \tag{10}$$

is defined from $\mathbf{a}_{N}(\mu)$ with *N*, μ replaced by *M*, ν respectively

$$\nu = \frac{2\pi}{\lambda} d_{y} q \tag{11}$$

is the spatial frequency variable, *q* is the direction cosine variable relative to the *y*-axis.

The 2-D unitary ESPRIT provides closed form 2-D angle estimation in real time. This method gives several advantages in comparison with classical ESPRIT, such as: a) reduced computational complexity; b) lower SNR (signal-to-noise ratio) resolution thresholds; c) very accurate finds simultaneously both the elevation and azimuth angles of arrival for impinging signals at the antenna array.

5. NUMERICAL EXAMPLES AND SIMULATION RESULTS

Simulation results, utilizing the LMS algorithm gave precise results when adapt the beamforming pattern. To illustrate the ABF algorithm applicability for URA, we considered the two cases where LMS algorithm is used: a) the URA with omnidirectional elements (N=M=6) and interelement spacing $d_x = d_y = 0.5\lambda$; b) the URA with half-wavelength dipoles (N=M=6) and interelement spacing $d_x = d_y = 0.5\lambda$. The results from simulations are depicted in figures. The URA is examined about following scenario: the signal of interest (SOI) impinges from ($\theta = 20^\circ, \phi = 170^\circ$) in the presence of the signal not of interest (SNOI) from direction ($\theta = 25^\circ, \phi = 165^\circ$), and Additive White Gaussian Noise (AWGN) with the zero mean, and variance 0.1. These simulation results are based on 100 times Monte Carlo simulations. A stepsize $\mu = 0.001$ and a signal is with uncoded BPSK modulation are used in the numerical examples to simplify the simulations. Figures 2 and 3 illustrate the resulting beamforming pattern with respect to $\theta_0 = 90^\circ$. The results demonstrate its great performance, and accurate estimation ability.

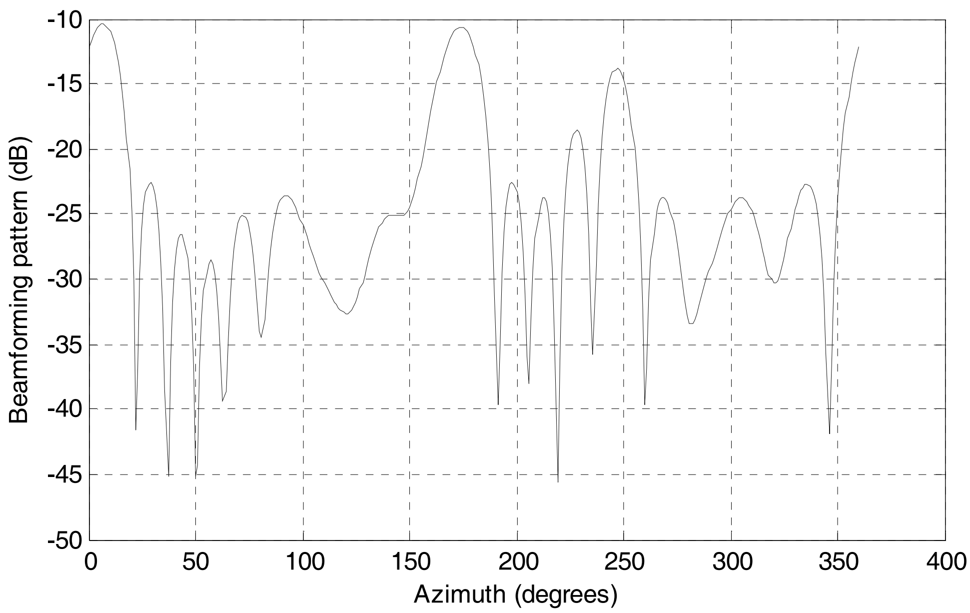

Fig. 2. The beamforming pattern of the URA with omnidirectional elements

We investigate the DOA estimation under the conditions of a URA structure. The 2-D unitary ESPRIT method is used to perform the estimation [7, 8]. The signal of interest (SOI) impinges from ($\theta = 20^0, \phi = 170^0$), while the two signals not of interest (SNOI) are directed from ($\theta = 25^0, \phi = 165^0$) and ($\theta = 22^0, \phi = 172^0$). Simulations were conducted employing: a) a *N*=*M*=6 elements uniform rectangular omnidirectional array with $d_x = d_y = 0.5\lambda$; b) a *N*=*M*=6 elements uniform rectangular array with half-wavelength dipoles and $d_x = d_y = 0.5\lambda$. The URA is examined in the presence of the Additive White Gaussian Noise (AWGN) with the zero mean, and variance 0.1. The results demonstrate its great performance, accurate estimation ability, and robustness.

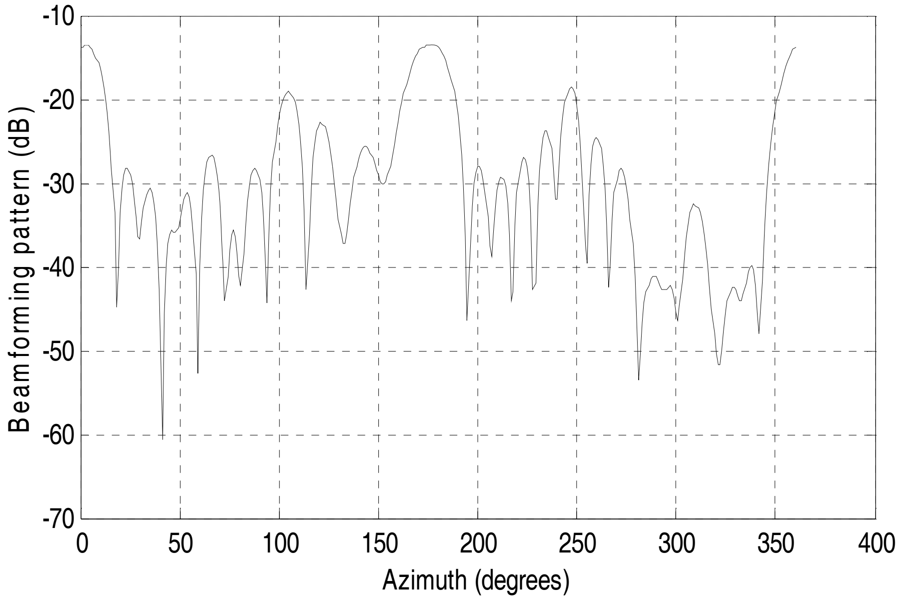

Fig. 3. The beamforming pattern of the URA with half-wavelength dipoles.

Table 1. The DOA estimations obtained utilizing 2-D Unitary ESPRIT

	Case 1	Case 3
Number of elements	M=6 ,N=6 omnidirectional elements	M=6, N=6 half-wavelength dipoles
Interelement spacing	0.5λ	0.5λ
Number of incoming signals	1	1
Number of data samples	2000	2000
Actual		
SOI	$\theta_1=20^0$, $\varphi_1=170^0$	$\theta_1=20^0$, $\varphi_1=170^0$
SNOI 1	$\theta_2=25^0$, $\varphi_2=165^0$	$\theta_2=25^0$, $\varphi_2=165^0$
SNOI 2	$\theta_3=18^0$, $\varphi_3=172^0$	$\theta_3=18^0$, $\varphi_3=172^0$
DOA Estimations		
SOI	$\theta_1=19.999^0$, $\varphi_1=170.097^0$	$\theta_1=20.009^0$, $\varphi_1=169.935^0$
SNOI 1	$\theta_2=24.992^0$, $\varphi_2=165.051^0$	$\theta_2=25.010^0$, $\varphi_2=164.962^0$
SNOI 2	$\theta_3=18.031^0$, $\varphi_3=171.897^0$	$\theta_3=18.026^0$, $\varphi_3=171.955^0$

6. CONCLUSION

This paper investigated uniform rectangular smart antennas with omnidirectional elements and half-wavelength dipoles. A brief theory of two methods for different antenna arrays is considered. Estimation of direction of arrival (DOA) and adaptive beamforming (ABF) were examined. Matlab programs are used for simulations. Concerning beamforming the URA has shown to be accurate and stable enough regarding both: desired signal (maximum) and interfering signals (deep nulls). The figures have shown that the adaptive array puts the maximum of the beamforming pattern to the SOI and at the same time – deep nulls towards the SNOIs.

The 2-D unitary ESPRIT is a method that provides closed-form automatically-paired source azimuth and elevation estimates. These results are proved to be accurate enough (see the Table).

ACKNOWLEDGEMENT

Научноизследователски проект № НП6 "Превръщане на катедра “ТИЕ” в съвременен образователен център по фундаментална електротехника".

Project no. 21 "Improvement of the research potential in the area of engineering and information technology" in the frame of Program "Development of human resources" and Ministry of Education of Bulgaria.

REFERENCES

[1] S. Bellofiore et al., “Smart-antenna system analysis, integration and performance for mobile ad-hoc networks (MANETs)”, IEEE Antennas and Propag., vol. 50, pp. 571-581, 2002.

[2] S. Bellofiore et al., “Smart-antenna systems for mobile communication networks, part 2: beamforming and network throughput”, IEEE Antennas and Propag. Magazine, vol. 44, pp. 106-114, 2002.

[3] P.Ioannides, C. Balanis, “Uniform circular and rectangular arrays for adaptive beamforming applications”, IEEE Antennas and Wireless Propag. Letters, vol. 4, pp. 351-354, 2005.

[4] L. C. Godara, “Smart Antennas”, CRC Press LLC, Florida, 2004.

[5] C. Sun et al., “Fast Beamforming of Electronically Steerable parasitic Array Radiator Antennas: Theory & Experiment”, vol. 52, no. 7, pp. 1819 – 1832, 2004.

[6] J. Foutz et al, “Adaptive eigen-projection beamforming algorithms for 1-D and 2-D antenna arrays”, IEEE Antennas and Wireless Propag. Letters, vol. 2, pp. 62-65, 2005.

[7] M. Zoltowski et al., “Closed-Form 2-D Angle Estimation with Rectangular Arrays in Element Space or Beamspace via Unitary ESPRIT”, IEEE Transactions on Signal Processing, vol. 44, no. 2, pp. 316-328, 1996.

[8] P. Strobach, “Two-dimensional equirotatioal stack subspace fitting with an application to uniform rectangular arrays and ESPRIT”, IEEE Transactions on Signal Processing, vol. 48, no. 7, pp. 1902-1914, 2000.

EXAMINATION OF DISTRIBUTION OF AC CONTACT SYSTEM ELECTRIC FIELD

Galina Petkova Cherneva

Department of Electrical Engineering, Higher School of Transport "Todor Kableshkov"
Geo Milev Str.158, 1574 Sofia, Bulgaria, phone: +359 888 498 478,
e-mail: cherneva@vtu.bg

Abstract: *The paper presents the mathematical model of electric field and the distribution of electric intensity by single-phase AC contact system. The obtained analytical expressions and graphic dependencies of assessment give a possibility to determine the distribution of the electric field as an essential component of electromagnetic compatibility.*

Keywords: Electric Field, AC Contact System, Electric Field Intensity, Potential

1. INTRODUCTION

The contact system is one of the main equipment of the electrical railway transport that implements the electrical connection between the traction substations and the rolling stock. But it is also one of the main sources of interferences due to the presence of its strong electromagnetic field.

From the viewpoint of electromagnetic compatibility [3] and the safety of the serving staff [4], it is of certain interest to determine the potential and strength of a random point of the AC contact network electric field.

This paper presents the distribution of electric intensity by single-phase AC contact system.

2. A MATHEMATICAL MODEL OF ELECTRIC FIELD BY CONTACT SYSTEM

The electric field intensity can be determined using the mirror images [1].

Let examine the case of the electric field caused by contact conductor *k* of potential φ_k, radius r_k and charge q_k per a unit of length. The field effects neighboring conductor *m* of potential φ_m, radius r_m and charge q_m per a unit of length (Fig.1).

The heights of conductors towards the ground are relatively h_k and h_m, and the distance between their horizontal projections is *d*.

On the base of the mirror images it can be written:

$$\varphi = \alpha \mathbf{q}\,, \tag{1}$$

where:

$\varphi = [\varphi_i]$ is the matrix of the conductor system potentials, *i*=1-*n*;

$\alpha = [\alpha_i]$ is the matrix of the conductor system potential coefficients;
$\boldsymbol{q} = [q_i]$ is the matrix of the linear densities of charges.

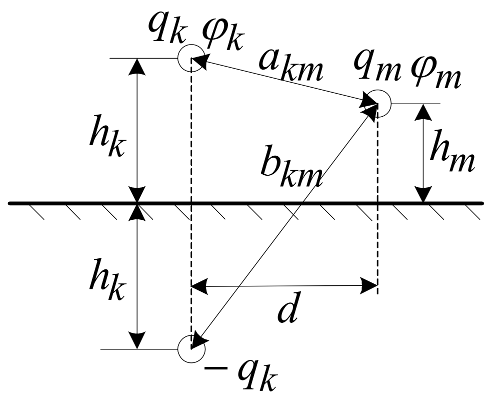

Fig.1

In this case according to equation (1) it can be written:

$$\begin{aligned} \varphi_k &= \alpha_{kk} q_k + \alpha_{km} q_m \\ \varphi_m &= \alpha_{mk} q_k + \alpha_{mm} q_m \end{aligned}, \tag{2}$$

where :

$$\alpha_{kk} = \frac{1}{2\pi\varepsilon} ln \frac{2h_k}{r_k}, \tag{3}$$

$$\alpha_{mm} = \frac{1}{2\pi\varepsilon} ln \frac{2h_m}{r_m} \tag{4}$$

are the natural potential coefficients,

$$\alpha_{km} = \alpha_{mk} = \frac{1}{2\pi\varepsilon} ln \frac{b_{km}}{a_{km}} \tag{5}$$

are the mutual potential coefficients,

ε is the dielectric permittivity.

Since a conductor of connection or an isolated and unsupplied conductor have been examined in the part of a neighboring conductor, it can be assumed that its charge is $q_m = 0$.

From (2), (3), (4) and (5) it is obtained that:

$$\varphi_m = \varphi_k \frac{ln \frac{b_{km}}{a_{km}}}{ln \frac{2h_k}{r_k}}, \tag{6}$$

where:

$$b_{km} = \sqrt{(h_k + h_m)^2 + d^2} \tag{7}$$

is the distance between the second conductor and the mirror image of the contact conductor,

$$a_{km} = \sqrt{(h_k - h_m)^2 + d^2} \tag{8}$$

is the distance between the two conductors.

Since

$$\varphi_k = U_k ,$$

where U_k=25 kV is the voltage by contact system, it follows that:

$$\varphi_m = \frac{U_k}{ln\frac{2h_k}{r_k}} ln \frac{\sqrt{(h_k + h_m)^2 + d^2}}{\sqrt{(h_k - h_m)^2 + d^2}} . \tag{9}$$

Hence for random point M of the electric field with coordinates x**,** y the potential in the common case is:

$$\varphi_M = \frac{U_k}{ln\frac{2h_k}{r_k}} ln \frac{\sqrt{(h_k + y)^2 + x^2}}{\sqrt{(h_k - y)^2 + x^2}} . \tag{10}$$

Then for the vertical component of the electric field strength at that point it can be written that:

$$E_y = \frac{d\varphi_M}{dy} = \frac{U_k}{ln\frac{2h_k}{r_k}} \left[\frac{h_k + y}{(h_k + y)^2 + x^2} + \frac{h_k - y}{(h_k - y)^2 + x^2} \right] . \tag{11}$$

3. CALCULATION RESULTS AND GRAPHIC DEPENDENCIES

The numerical results in Table 1 have been found on the base of analytical dependency (11) for two typical values of y (y_1=1,8m – curve 1 and y_2=6m – curve 2) and the graphic dependencies of E_y=$f(x)$ have been built in Fig. 2.

The contact conductor is МФ 100 (r_k = 0.056 m) [2].

Table 1

E_y, *kV/m* / *y, m*	Distance *x, m*								
	0	1	2	2,5	3	4	5	6	8
1,8	1,7	1,6	1,5	1,4	1,3	1,1	1	0,8	0,6
6	7,2	3,1	1,3	1	0,8	0,6	0,5	0,4	0,3

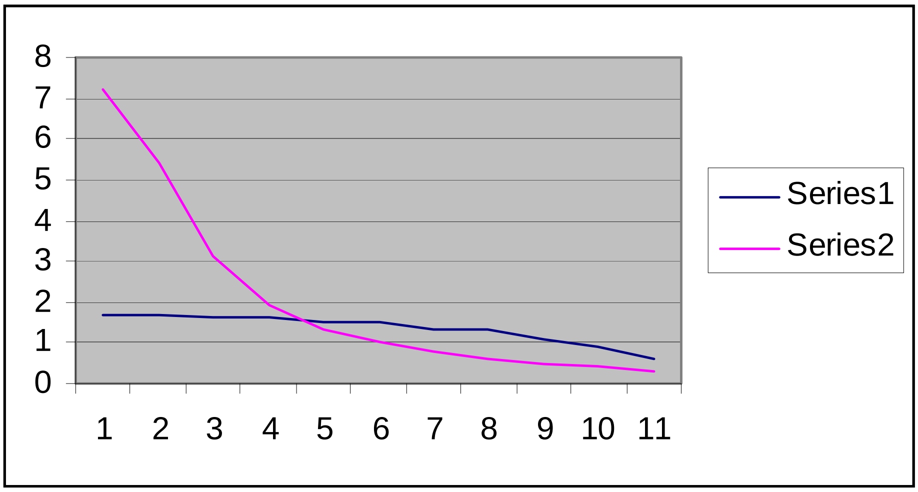

Fig. 2

4. CONCLUSIONS

The analytical dependencies worked out for contact network electric field potential and strength as well as the numerical results obtained give a possibility to look for providing the admissible effect of these interferences. This effect should be in compliance with the existing standards in this field. The problems of increasing the stability of radio and electronic equipment used in railway transport against the effect of electric and magnetic fields are part of the general theory of providing electromagnetic compatibility. In certain important aspects, which determine the operation of radio equipment under the conditions of railway transport, the distribution of contact network electric field strength has a specific character. In that sense, the obtained graphic dependencies and analytical expressions of assessment give a possibility to determine the distribution of the electric field as an essential component of electromagnetic compatibility. This distribution determines the quality and reliability of radio electronic equipment.

REFERENCES

[1] Jr.W.H. Hayt and J.A. Buck, Engineering Electromagnetics (7th edition), McGraw-Hill, 2006.

[2] Minkov P., N. Ibrishimova. Electrical transport, t.1. Sofia. 1972.

[3] Kenneth L. Electromagnetic Compatibility Handbook. N.Y. 2008.

[4] Weston D. Electromagnetic Compatibility. Principles and applications. N.Y. 2001.

НЯКОИ ОСОБЕНОСТИ ПРИ ИЗПОЛЗВАНЕ НА МЕТОДА С ЕЛЕКТРИЧЕСКИ ВЕКТОР-ПОТЕНЦИАЛ И ВЗАИМНА ЕЛЕКТРИЧЕСКА ПРОВОДИМОСТ ЗА ОПРЕДЕЛЯНЕ НА СИЛОВИТЕ ВЗАИМОДЕЙСТВИЯ В ИНДУКЦИОННИ МЕХАНИЗМИ

Петко З. Костадинов, Стефчо Г. Гунински,
Живко А. Даскалов, Калинка М. Тодорова

Катедра „Обща електротехника", Технически Университет – София

Абстракт: *В представения доклад е проведен анализ на предложения от проф. М. П. Златев (и впоследствие прилаган и от други автори) метод за решаване на някои електродинамични задачи , и по-специално за изчисляване на индуктираните вихрови токове и силовите взаимодействия в индукционни механизми (електромери за измерване на количества електрическа енергия, индукционни спирачки и др. подобни) с помощта на електрически вектор-потенциал и взаимна електрическа проводимост.*

Като се оценява преимуществото му за непосредствено записване на решението на задачата се обръща внимание на някои особености при използването му, и по-конкретно при прецизиране на теоретичните модели в случаите на наличие или отсъствие на движение и използване на линейни магнитни възбудители с последващо интегриране за отчитане на формата и размерите на реалните възбудители.

Keywords: 3-5 keywords (Times New Roman, 14pt, right sided, single spaced)

1. ВЪВЕДЕНИЕ

Настоящата работа е пряко продължение на [1], отнасящ се до използване на вектор-потенциали при аналитичното решаване на някои гранични задачи на приложната електродинамика, и в частност – на разработения от проф. М. П. Златев метод с използване на електрически вектор-потенциал за определяне на вихрови токове, индуктирани от магнитни възбудителни контури.

В [2] е показан метод с електрически вектор – потенциал $\vec{A}$:

$$\vec{A} = \frac{e}{4\pi} \oint_{\Gamma} \left(\frac{\partial \vec{l}}{r} \right) \tag{1}$$

и взаимна електрическа проводимост G:

$$G = \frac{\sigma}{4\pi} \oint_{\Gamma} \oint_{\Gamma'} \frac{d\vec{l} \cdot d\vec{l}'}{r} \tag{2}$$

за определяне на токовете на Фуко, които се индуктират от затворен неразклонен магнитен възбудителен контур Г и преминават през произволно сечение, ограничено от затворен приемен контур $\Gamma^{/}$ (фиг. 1). В случая с *e* е означено индуктираното е.д.н. ; *dl* е линеен елемент от контура Г ; $dl^{/}$ е линеен елемент от контура $\Gamma^{/}$; *r* е разстоянието между двата линейни елемента и σ е специфичната електрическа проводимост на средата, ограничена от контура $\Gamma^{/}$.

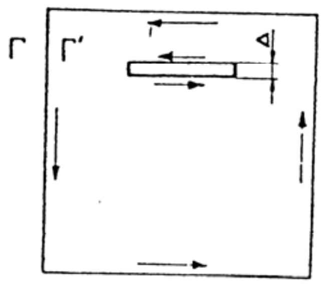

Фиг. 1

Посоченият метод се използва в [3, 4 - … - 9] за определяне на вихрови токове и електромагнитни силови моменти в ограничено проводящо тяло (диск с дебелина Δ) като се допуска, че повърхността му е тангентна към линиите на електрическото поле $\vec{E}$ и че напречните геометрични размери на магнитните възбудители са достатъчно малки спрямо радиуса R на диска.

Трябва да се отбележи, че понятието „взаимна електрическа проводимост” е въведено от проф. М. П. Златев само на основание еднаквостта на формула (2) с известната формула на Нойман за взаимната индуктивност М на два токови контура. Както е показано в [12], където е проведено компютърно изчисление на картината полето (силови и еквипотенциални линии), всъщност G е електрическата проводимост на силова тръба с основа сечението на контура $\Gamma^{/}$.

При използването на така предложения метод за определяне на вихрови токове и силови взаимодействия в реални конструкции на индукционни системи (електромери с диск, дискови индукционни спирачки, електрически двигатели с проводящ неферомагнитен цилиндричен ротор и др.) винаги възникват проблеми при определянето на реалните размери на линейния възбудителен контур поради неопределеността на средната силова линия.

Целта на настоящия доклад е да се прецизира теоретичния модел с оглед развитие на метод за по-точно отразяване на реалните физически постановки.

2. СЪЩНОСТ НА МЕТОДА

2.1. Принципна постановка

Задачата за определяне на вихровите токове, индуктирани в проводящ неферомагнитен диск, е типична електродинамична задача при квазистационарно електромагнитно поле, за която са в сила уравненията:

$$rot\,\vec{E} = -\frac{\partial \vec{B}}{\partial t} + rot\,\vec{v} \times \vec{B} \tag{3}$$

$$div\,\vec{E} = 0 \tag{4}$$

$$\vec{J} = \sigma\,\vec{E} \tag{5}$$

Ако се въведе електрически вектор-потенциал съгласно израза:

$$\vec{E} = rot\,\vec{A} \tag{6}$$

и при нормировката на Кулон:

$$div\,\vec{A} = 0 \tag{7}$$

се достига до уравнението:

$$\nabla^2 \vec{A} = \frac{\partial \vec{B}}{\partial t} - rot\,\vec{v} \times \vec{B} \tag{8}$$

От друга страна от (5) като се има предвид (6) и се приложи теоремата на Стокс за индуктирания вихров ток i се получава:

$$i = \sigma \iint_{(s)} \vec{E}\,d\vec{s}^{/} = \sigma \oint_{\Gamma^{/}} \vec{A}\,d\vec{l}^{/}\,, \tag{9}$$

където повърхността $s^{/}$ представлява сечение от диска, ограничено от контура $\Gamma^{/}$.

Вихровите токове в диска могат да се определят сравнително лесно от (9), ако може да се реши (8) по отношение на $\vec{A}$. Общото решение на уравнението на Поасон (8) е известно [10]:

$$\vec{A} = \frac{1}{4\pi} \iiint_{(V)} \left(\frac{\partial \vec{B}}{\partial t} - rot\,\vec{v} \times \vec{B} \right) \frac{d\vec{V}}{r} \tag{10}$$

В случая r е разстоянието от елементарния обем dV до точката на наблюдението, а интегрирането се разпростира по целия обем V, зает от магнитните възбудители.

Интегрирането на (10) при нехомогенна среда и сложни форми на контурите и на напречните сечения на възбудителите (фиг. 2) е тежка математическа задача, която може да бъде решена само при редица опростяващи предположения и за най-прости случаи.

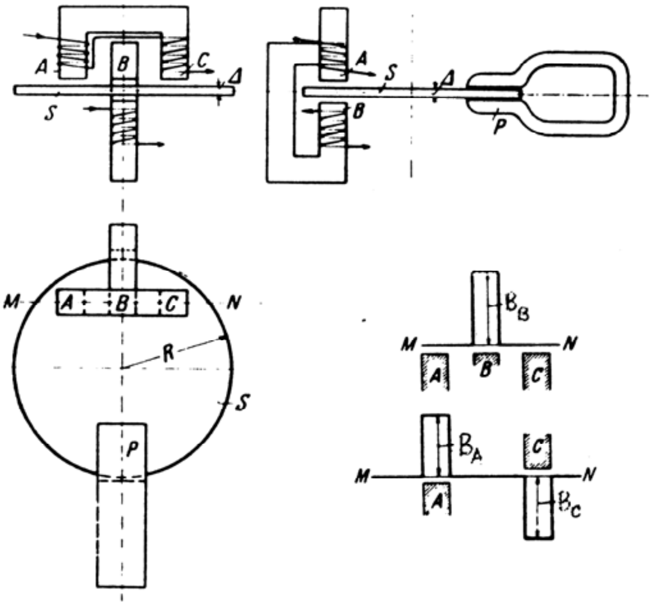

Фиг. 2

В доклада тази задача се решава при следните условия:

– приема се, че електрическият вектор-потенциал $\vec{A}$ не зависи от координатата z, т.е. че областите V_i представляват безкрайно дълги прави цилиндри, чиято околна повърхност пресича равнината на диска по някакви контури L_i ;

– приема се, че магнитните полета $\vec{B}_i$ са съставени от определен брой **безкрайно дълги линейни магнитни възбудители** (фиг. 3) и се прилага принципа на наслагването;

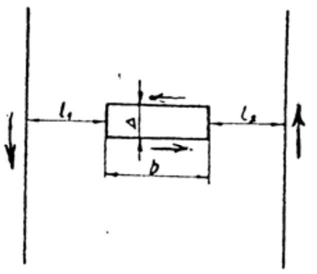

Фиг. 3

– пренебрегват се разсейването на магнитните силови линии във въздушната междина и обратното действие на вихровите токове в диска;

– вместо уравнение (8) се решават поотделно двете уравнения:

$$\nabla^2 \vec{A}_t = \frac{\partial \vec{B}}{\partial t} \tag{11}$$

$$\nabla^2 \vec{A}_r = -rot\, \vec{v} \times \vec{B} \tag{12}$$

По този начин могат да се определят поотделно токовете, индуктирани от промяната на магнитното поле във времето и тези, предизвикани от въртенето на диска.

2.2. Идентификация на магнитния възбудител с отчитане на нееднородността на средата

А. При неподвижен диск

В съответствие с казаното по-горе новият теоретичен модел за изчисляване на въртящия момент на еднофазен индукционен електромер се състои от:

1) неподвижен неферомагнитен диск с радиус R, дебелина Δ и специфична електрическа проводимост σ ;
2) безкраен праволинеен магнитен възбудител Γ_1 с индукция $\vec{B}(t)$, който е успореден на оста *z* и пресича диска в т. P (фиг. 4).

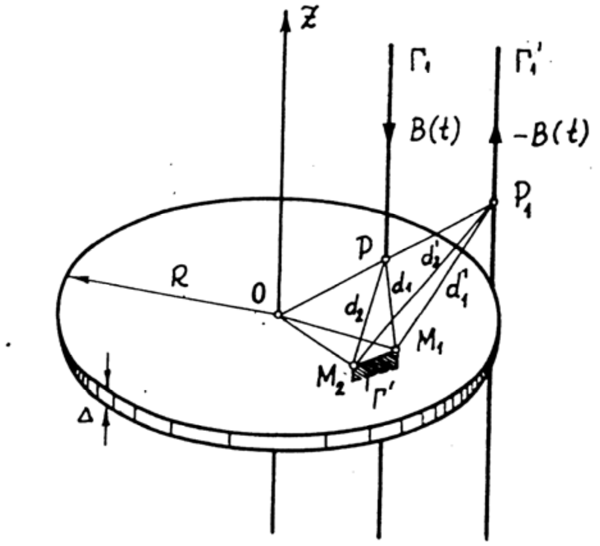

Фиг. 4

Влиянието на електрическата нееднородност, и в частност на въздушната среда извън цилиндричната гранична повърхност на диска, се отразява посредством огледален образ $\Gamma_1^{/}$ [11], който канализира индукция $-\vec{B}(t)$ и е разположен на разстояние $\overline{OP_1} = \dfrac{R^2}{\overline{OP}}$.

За тази постановка електрическият вектор-потенциал в произволна точка M се определя от израза:

$$A = \frac{e(t)}{2\pi} \ln \frac{d_1^{/}}{d_1} \tag{13}$$

където $e(t) = -s\dfrac{\partial \vec{B}}{\partial t}$ е индуктираното е.д.н., d_1 е разстоянието от магнитния възбудител Γ_1 до точката M(r, φ) , а $d_1^{/}$ – разстоянието от огледалния образ $\Gamma_1^{/}$ до същата точка.

Понеже A е постоянен по протежение на дебелината на диска Δ (9) се записва във вида:

$$i = \frac{\sigma \Delta}{e(t)} \left(A_1 - A_2 \right), \tag{14}$$

където A_1 и A_2 са стойностите на електрическия вектор-потенциал A съответно в граничните точки M_1 и M_2 на сечението $s^{/}$.

Като се вземе предвид, че взаимната електропроводимост е равна на $\dfrac{i}{e(t)}$ от (13) и (14) след преобразуване се получава:

$$G = \frac{\sigma \Delta}{2\pi} \left(\ln \frac{d_2}{d_1} - \ln \frac{d_2^{/}}{d_1^{/}} \right), \tag{15}$$

където първият член е за случая на безкрайна проводяща пластина с дебелина Δ, а вторият отразява влиянието на граничната повърхност.

B. При въртене на диска

За решаването на (12) може отново да се използва намереният израз (в случая на неподвижен диск) за електрическия вектор-потенциал на безкраен линеен контур и неговия огледален образ като се има предвид, че вместо възбудителя $-\dfrac{\partial \vec{B}}{\partial t}$ ще участва $rot\ \vec{v} \times \vec{B} = \Omega \dfrac{\partial B}{\partial \alpha}$ и следователно е.д.н. *e(t)* трябва да се замести с е.д.н, което се определя от израза:

$$e_v = \Omega B \int_{\rho_1}^{\rho_2} \rho \, d\rho = \frac{1}{2} \Omega B \left(\rho_2^2 - \rho_1^2 \right) \tag{16}$$

Тъй като ρ_2 и ρ_1 са функции на ъгъла θ се въвежда средна стойност $\overline{e_v}$ на е.д.н. e_v съгласно формулата:

$$\overline{e_v} = \frac{\Omega B}{2\left(\theta_2 - \theta_1 \right)} \int_{\theta_1}^{\theta_2} \left(\rho_2^2 - \rho_1^2 \right) d\theta \tag{17}$$

При произволна форма на контура на следата на полюса вектор-потенциалът A_{vL} е равен на:

$$A_{vL} = \frac{\overline{e_v}}{2\pi l} \oint \ln \frac{d_1^{/}}{d_1} \, dl \tag{18}$$

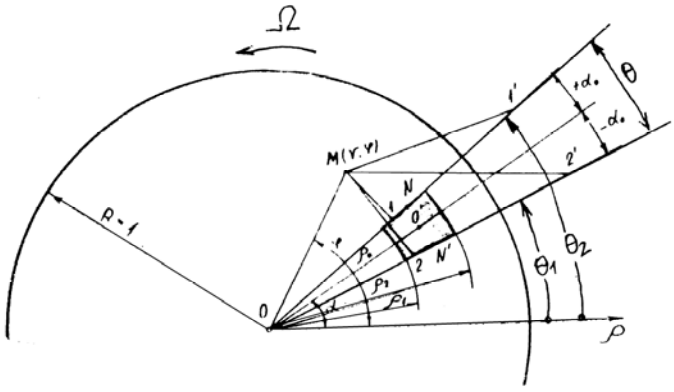

Фиг. 5

При условие, че контурът L има вида, показан на фиг. 5 формула (18) се трансформира в:

$$A_{vL} = \frac{\overline{e}_v}{2\pi l}\left(\int\limits_{\overline{CB}} \ln\frac{d_1^{/}}{d_1} dl - \int\limits_{\overline{DA}} \ln\frac{d_1^{/}}{d_1} dl \right) \tag{19}$$

3. ЗАКЛЮЧЕНИЕ

Представеният доклад позволява да бъдат направени следните изводи:

1. Показани са уточнения при изграждане на теоретичния модел за решаване на задачата, в резултат на които се избягват двусмислията и по същество представляват по-нататъшно развитие на метода с електрически вектор-потенциал.
2. Посоченият подход разширява използването на метода за определяне на вихровия ток и силовите взаимодействия при разнообразни инженерни задачи.

БИБЛИОГРАФИЯ

[1] Даскалов, Ж. А., С. Г. Гунински и П. З. Костадинов. Използване на вектор-потенциали при аналитичното решаване на някои гранични задачи на приложната електродинамика. Advanced Aspects of Theoretical Engineering, Sozopol’2007.

[2] Златев, М. П. Определяне на вихрови токове посредством електрически вектор-потенциал. Годишник на ВМЕИ, том VI, кн. 1, 1959.

[3] Златев, М. П. Метод определения момента вращения некоторых индукционных аппаратов. Известия АН СССР, ОТН „Энергетика и автоматика”, 1960, № 6.

[4] Златев, М. П., И. М. Панамски и С. Л. Фархи. Определяне на момента на индукционен двигател с диск и екранираща намотка. Годишник на ВМЕИ, том XI, кн. 1, 1961.

[5] Zlatev, M. P. et D. N. Tzwetkov. Determination du moment de force resistant de systems a induction a disque et a aimant. Buletinul Institutului Politehnic DIN Jasi Tomul X (XIV) Fasc 1-2, 1965.

[6] Zlatev, M. P. et P. Z. Kostadinov. L'amortissment par aimant des systemes a disques. Influence des parametres geometriques des aimants bipolaires. Mesures, controle et automatisme, 1967.

[7] Savastano, G., C. Savy. Determinazione delle coppie prodotte da un equipaggio motore ad induzione. L'elettrotechnica, vol. LIII, № 8, agosto 1966.

[8] Златев, М. П. и П. З. Костадинов. Токове Фуко в неферомагнитен диск на действена индукционна система. Доклади на научната конференция на ВМЕИ "Ленин". София, 1974.

[9] Златев, М. П. и П. З. Костадинов. Токове Фуко в неферомагнитен диск на противодействени електромагнитни индукционни системн. Доклади на научната конференция на ВМЕИ "Ленин". София, 1974.

[10] Костадинов, П. З. Върху някои въпроси от теорията, изследването и проектирането на индукционни системи за електромери. Автореферат на дисертация за присъждане на научна степен „доктор". Технически Университет – София, 1975 г.

[11] Бинс, К. и П. Лауренсон. Анализ и расчет электрических и магнитных полей. Энергия, Москва, 1970.

[12] Златев, М. П., Б. И Матраков, С. П. Папазов. Определяне на електрическата проводимост на силови тръби в индуктирано поле. Годишник на ВМЕИ, том XIX, кн. 4, 1966.

[13] Златев, М. П. Идентификация на променлива и постоянна електромагнитна индукция и използване. „Техническа мисъл", бр. 6, 1972.

[14] Златев, М. П. и В. С. Димова. Взаимная электрическая проводимость двух некоаксиальных прямоугольных контуров. Известия АН СССР , Энергетика и транспорт, № 5, 1965.

[15] Златев, М. П. и В. С. Димова. Определение взаимной электрической проводимости двух прямоугольных контуров лежащих в непаралельных плоскостях. Известия АН СССР , Энергетика и транспорт, № 6, 1965.

[16] Златев, М. П. и Б. Е. Ташева. Електромагнитни индукционни системи с неферомагнитен цилиндричен ротор. Известия на Института по техническа кибернетика, том XII, 1971.

ВИСОКОТЕМПЕРАТУРНИ СВРЪХПРОВОДНИЦИ. ХАРАКТЕРИСТИКИ, ПАРАМЕТРИ И МЕТОДИ ЗА КОНТРОЛ

Калинка М. Тодорова

Кат. Обща електротехника, Технически университет – София,
бул. "Кл. Охридски" №8, 1000 София, тел.(+359 2) 965 36 65
e-mail: ktodorova@tu-sofia.bg

Резюме: *Свръхпроводимостта е явление, което се оценява от учените като невероятен феномен. В доклада се проследява в хронологичен ред откритието на това явление, неговия физичен смисъл, откриването на материали, при които възниква това явление. Описано е поведението на различните свръхпроводящи в магнитно поле. Проследява се откриването на високотемпературните свръхпроводници. Разглеждат се важните характеристики и параметри на свръхпроводниците, чрез които те се изследват и се оценява тяхното поведение. Прави се анализ на методите, чрез които е подходящо да се извършва изследване на основните характеристики и параметри на свръхпроводници и високотемпературни свръхпроводници. Показано е, че вихровотоковите безразрушителни методи са едни от най-подходящите за измерване на различните параметри и характеристики на свръхпроводящи обекти.*

Ключови думи: свръхпроводимост, високотемпературни свръхпроводници, характеристики и параметри на свръхпроводниците.

1. ВЪВЕДЕНИЕ

През 1911 г. холандският физик Хайке Онес прави своето най-поразително откритие. Той установява, че под 4º K електрическото съпротивлението на живака рязко пада до нула и остава такова до постижимите тогава ниски температури (~ 0.1ºK) [1]. Получените резултати са напълно неочаквани. Онес сполучливо назовава това явление *свръхпроводимост* (вместо идеална проводимост например) , а температурата, при която става скокът на съпротивлението, нарича *критична температура* ($\boldsymbol{T_c}$). Явно той веднага разбира, че става дума за нещо много по-различно от *идеална* проводимост - явление, което следва да се появи в метал с идеално подредена кристална решетка при T = 0.

2. ИЗЛОЖЕНИЕ

В различните видове материали (метали, съединения, сплави), намиращи се в свръхпроводящо състояние, се наблюдават явления от общ характер. Това показва, че причините за възникване на свръхпроводимостта, имат еднаква физична природа. Поради този факт към всички свръхпроводници трябва да се прилага единен подход за обяснение на неговия механизъм. Физичната природа на свръхпроводимостта е разгадана през 1957 г. въз основа на Общата теорията на фазовите преходи от втори род, предложена от Ландау през 1937 г. [2]. Теорията на свръхпроводимостта (БКШ) е създадена от американските физици Дж. Бардин, Л. Купър и Дж. Шрифър (например [3]) и доразвита от Н. Боголюбов.

Оказва се, че освен формалната прилика между явленията свръхфлуидност и свръхпроводимост (както свръхфлуидната течност протича без триене, т.е. без съпротивление, по капилярни тръбички, така и електричният ток протича безпрепятствено в свръхпроводника) между тези две явления съществува аналогия с дълбок физичен смисъл. Явлението свръхпроводимост може качествено да се обясни по следния начин. Освен силите на кулоновото отблъскване, намалени значително вследствие екранирането от положителните йони на решетката, между електроните в метала действат и слаби сили на привличане, възникващи в резултат на електрон – фононното взаимодействие. При определени условия тези сили могат да надвишават силите на отблъскване. В резултат на взаимното привличане между електроните на проводимост се образува своеобразно свързано състояние на два електрона, наречено *куперова двойка*. “Размерите” на такава двойка са много по-големи от междуатомните разстояния, т.е.между електроните, свързани в такава двойка , се намират много други “обикновени” (свободни) електрони. За да се разруши една такава куперова двойка, т.е. да се откъсне от нея един електрон, е необходимо да се изразходи някаква енергия за преодоляване на силите на привличане между електроните ѝ. По принцип такава енергия може да се получи за сметка на взаимодействието с фононите. Но двойките се противопоставят на всеки опит да бъдат разрушени, тъй като образуват система от взаимодействащи си частици. Електроните, образуващи куперовата двойка, имат противоположно ориентирани спинове и спинът на двойката е равен на нула, т.е. тя представлява бозон. Както е известно, принципът на Паули е неприложим към бозоните, т.е. броят им в дадено енергетично състояние не е ограничен. Затова при свръхниски температури бозоните заемат предимно основното състояние, от което трудно биха могли да преминат във възбудено състояние. Под действието на електрично поле такава система от устойчиви куперови двойки може свободно да се движи в проводника, без да изпитва каквото и да е съпротивление. Това всъщност е електрическият ток при свръхпроводимостта.

Свръхпроводимостта има още едно характерно свойство – *идеалният диамагнетизъм* (ефект на Майснер и Оксенфелд [4], по-често споменаван като *“ефект на Майснер”*). Идеалният диамагнетизъм е термин, означаващ, че магнитната индукция $\mathbf{B} = (\mathbf{H} + 4\pi\mathbf{M})$ във всяка точка $\mathbf{r}$ в обема на тялото $\mathbf{V}$ е равна на нула, $\mathbf{B}(\mathbf{r}) = \mathbf{0}$, т.е. че външното магнитно поле $\mathbf{H}$ и намагнитването $\mathbf{M}$ удовлетворяват равенството $\mathbf{H}(\mathbf{r}) = -4\pi\mathbf{M}(\mathbf{r})$. Трябва да се отбележи, че съгласно електродинамиката от идеалната проводимост следва свойството идеален парамагнетизъм ($\mathbf{B} = \mathbf{H}$, т.е.$\mathbf{M} = \mathbf{0}$), а не идеален диамагнетизъм, както е в свръхпроводимостта.

Детайлното изследване на поведението на различните свръхпроводници в магнитно поле показва, че по характера на разрушаването на свръхпроводимостта от магнитното поле, свръхпроводниците се подразделят на свръхпроводници от I род и свръхпроводници от II род [6].

При **ρ = 0** свръхпроводниците от I род изтласкват и не пропускат магнитното поле. Това свойство може да се запише така: вътре в свръхпроводника от I род магнитната индукция **B** винаги е равна на нула **B(r) = 0**. Това свойство принципно различава свръхпроводника от нормалния метал с нулево електрическо съпротивление. В свръхпроводниците от I род магнитното поле не прониква до стойност на полето, разрушаваща свръхпроводимостта, така нареченото *критично магнитно поле* $\mathbf{H_c}$.

Характерна особеност на свръхпроводниците от II род е, че магнитното поле може да прониква в тях без да разрушава свръхпроводимостта. При някакво поле $\mathbf{H_{к1}}$ (*първо критично поле*) външното магнитно поле започва да прониква в образеца и неговото проникване се увеличава с увеличаване на **H** до някаква стойност на полето $\mathbf{H_{к2}}$, наречено *второ критично поле*. В поле от нулева стойност до $\mathbf{H_{к1}}$ свръхпроводникът от II род се държи като свръхпроводник от I род. В него се наблюдава идеален диамагнитизъм, неговото електрическо съпротивление е равно на нула. В областта $\mathbf{H_{к1} < H < H_{к2}}$ проникването на потока е частично, при това магнитното поле прониква в образеца във вид на отделни вихри (така наречените *вихри на Абрикосов* [8]), всеки от които съдържа поток $\mathbf{\Phi_0}$. Състоянието на образеца се нарича *смесено състояние.* В този случай свръхпроводимостта на образеца се запазва до тогава, докато отделните вихри не се слеят, което става в магнитно поле $\mathbf{H_{к2}}$. В магнитно поле $\mathbf{H > H_{к2}}$ свръхпроводимостта вътре в образеца се разрушава, но се запазва в тънък повърхностен слой. Повърхностната свръхпроводимост се запазва в диапазон $\mathbf{H_{к2} < H < H_{к3}}$, като $\mathbf{H_{к3} \approx 1.69\ H_{к2}}$. В поле $\mathbf{H > H_{к3}}$ образецът напълно преминава в нормално състояние. Най-важната особеност на свръхпроводници от II род се явява способността им да се намират в смесено състояние.

Външното магнитно поле в дълбочина на свръхпроводника екранира повърхностните токове в слой, който се нарича *дълбочина на проникване* $\lambda(T)$. Характерът на поведение на свръхпроводниците в магнитно поле се определя от величината κ (безразмерна "веществена" константа, наречена *параметър на Гинзбруг – Ландау*) [5], $\kappa = \dfrac{\lambda(T)}{\xi(T)}$ (където $\xi(T)$ е дължина на кохерентност, размера на *куперова двойка*). Ако $\kappa < \dfrac{1}{\sqrt{2}}$, свръхпроводникът е от I $^{\text{- ви}}$ род. Ако $\kappa > \dfrac{1}{\sqrt{2}}$, свръхпроводникът е от II род [6]. Голяма част от свръхпроводящите елементи са свръхпроводници от I род , а сплавите и съединенията обикновено притежават свойствата на свръхпроводници от II род. На практика потенциално всички нови свръхпроводящи съединения, открити от началото на 60$^{\text{-те}}$ години до днес са свръхпроводници от II род.

Изучаването на свръхпроводниците е съпроводено с преодоляването на някои трудности, най-важната от които е температурната бариера. Температурната бариера е свързана с необходимостта за охлаждане на свръхпроводника да се използват скъпо струващи и капризни охладители – напр. течен хелий (доколкото съществуващите до 1987 г. свръхпроводници са с много ниска критична температура $\mathbf{T_c}$). Пример е съединението $\mathbf{Nb_3Ge}$, чиято критична температура $\mathbf{T_c = 23.2^oK}$ (80-те години тази критична температура се е считала за висока). Тази стойност е близка до температурата на кипене на течния водород и течния неон и те успешно биха могли да се използват за охлаждане на свръхпроводници от $\mathbf{Nb_3Ge}$. Охлаждането на свръхпроводници с по-ниска критична температура $\mathbf{T_c}$ е свързано с още по-големи трудности. Заветната граница за критична температура $\mathbf{T_c}$ е температурата на кипене на течния азот (77°K), който представлява евтин и достъпен охладител, произвеждащ се в промишлеността в големи количества. Решението на този проблем е преодоляването на азотната бариера, т.е. създаването на свръхпроводящи материали с висока критична температура. Това се случва през 1986 – 1987 г., когато са открити нови *високотемпературни свръхпроводници* [7]. Високотемпературните свръхпроводници са свръхпроводници от II род.

През 1986 г. немският физик Георг Беднорц и швейцарският физик Александър Мюлер провеждат експеримент, в който наблюдават свръхпроводимост в керамиката *барий – лантан – меден окис* при критична температура $\mathbf{T_c = 35^o}$ **K**, което е значително повече от последната най-висока температура на свръхпроводимост – 23° K, постигната през 1973 г. В края на 1986 г. Пол Чу от Хюстънския университет потвърждава резултатите им. Следват съобщения за новооткритите свръхпроводящи керамики – $\mathbf{La_{2-x}Sr_xCuO_4}$ с критична температура $\mathbf{T_c = 36^o}$ **K** и $\mathbf{YBa_2Cu_3O_{9-y}}$ с температура на свръхпроводящия преход $\mathbf{T_c \approx 92^o}$ **K**. Така е преодоляна азотната бариера по отношение на критична температура $\mathbf{T_c}$ на свръхпроводящите преходи. Това е сензация и всички започват да говорят за “свръхпроводящия бум”.

Основната причина за големия успех през 1986г. – 1987г. е свързана с преодоляване на “хипнозата” на чистите метали и с прехода към различните двойни, тройни, четворни съединения от различен тип и тестването им за свръхпроводимост. Именно по такъв начин са открити в началото “екзотичните свръхпроводници” – органични, магнитни [9], а след това и новите високотемпературни свръхпроводници. В тази връзка трябва да се отбележи, че големите успехи в повишаването на критичната температура $\mathbf{T_c}$ са постигнати с металооксидните свръхпроводници, силно отличаващи се от простите метали. За сега обаче, температура $\mathbf{T_c}$ по-висока от 40°K може да се получи само при медно-окисни свръхпроводници. Докладваната най-висока стойност на $\mathbf{T_c}$ на свръхпроводимост на ***не*** *медно-окисни материали* е 39° K за $\mathbf{MgB_2}$ [10]. Температурата от 40 ° K е близка до или над теоретичната стойност, прогнозирана от теорията БКШ [11]. Поради това е много важно да се намери ***не*** *медно-окисен* свръхпроводник с критична температура $\mathbf{T_c}$ по-висока от 40° K, за да може да се разбере механизма на свръхпроводимостта при висока $\mathbf{T_c}$.

За откриването на обемна свръхпроводимост в окиси на самариево-арсенови съединения $\mathbf{SmFeAs\ O_{1-x}F_x}$ със структура от вида **ZrCuAiAs** е докладвано в [12]. Измерването на специфичното обемно съпротивление и на намагнитеността дават силни доказателства за температура на прехода от порядъка на 43° К. Съединението **SmFeAs** $\mathbf{O_{1-x}F_x}$ е първият ***не*** *медно-окисен* свръхпроводник с критична температура $\mathbf{T_c}$ по-висока от 40° К. Това е силен аргумент съединението **SmFeAs** $\mathbf{O_{1-x}F_x}$ да се счита за един нетрадиционен свръхпроводник.

Филмовите рядко-метало-земни окиси **LaOMPn** (M=Fe,Co,Ni, Ru и Pn=P и As) привлякоха голямо внимание към себе си поради откриването при тях на свръхпроводимост при $\mathbf{T_c = 26^oK}$ в желязната база $\mathbf{LaO_{1-x}F_xFeAs}$ (x=0.05 – 0.12) [13].

Паралелно с търсенето и откриването на нови високотемпературни свръхпроводници се поставя и задачата за изследване и изучаване на техните физични свойства. За практическото използване на свръхпроводниците най-голям интерес представляват следните параметри: критичната температура $\mathbf{T_c}$, второто критично поле $\mathbf{H_{к2}}$, критичния ток $\mathbf{I_c}$, специфичното обемно съпротивление. Измерването на различните параметри на свръхпроводниците може да се извърши като се използват различни методи. Най-общо те могат да се разделят на контактни и безконтактни. Към контактните се отнасят различните конвенционални мостови методи. За реализирането им е необходимо да се осигурят контакти към свръхпроводящите образци. В [14] се разглежда метод за нанасяне на нискоомен контакт /чрез разпрашване/. Използват се също така сребърни пасти и евтектики на базата на индий и галий. В [15] се описва един СВ4 – метод /отново контактен/. Общ недостатък на тези методи е скъпата и капризна технология за нанасяне на контакти с малко преходно съпротивление и опасността от възникване на бариери на повърхността на свръхпроводящия образец. Това води до допълнителни затруднения при реализиране на необходимите измервания. Ето защо контактните методи са трудни за използване при изследване и измерване на характеристиките на свръхпроводящи образци.

Посочените по-горе недостатъци на контактните методи не съществуват при безконтактните методи. Те спадат към групата на косвените методи. При тях се оценяват (или измерват) различни физични величини на изследвания обект, посредством които се съди за свойствата на обекта. Следователно за получаване на достоверна информация (тъй като тя е косвена) е необходимо добре да се познават корелационните връзки между физичните величини и контролираните свойства на обекта.

През 1988 г. в [16] се публикува съобщение, че група изследователи от националната лаборатория в Лос Аламос са разработили апарат за безкантактно измерване на характеристиките на свръхпроводници с висока $\mathbf{T_c}$, основан на метода с вихровите токове. От своя страна вихровотоковите методи имат своите предимства – безконтактност, слаба зависимост от условията на околната среда, висока информативност, висока температурна стабилност.

3. ЗАКЛЮЧЕНИЕ

От изложеното по-горе можем да обобщим, че за изследването на свръхпроводящи образци и за измерването на различните им характеристики и параметри е подходящо да бъдат използвани безконтакти методи. Следователно може да се очаква приложението на вихровотоковите безразрушителни методи за измерване на различните параметри на свръхпроводящи обекти да бъде все по-голямо и да даде очакваните добри резултати.

ЛИТЕРАТУРА

[1] Onnes H. Kamerlingh, leiden Comm. Suppl. 34 (1913);

[2] Landau L. D., Phys. Z. der Sowjet Union, 11, 26 (1937); ibid. 11, 129 (1937);

[3] Лифшиц Е. М., Л. П. Питаевский, Статистическая физика, 4.2 (Наука, М., 1978);

[4] Meissner W., R. Ochsenfeld, Naturwiss. 21 (1933) 787;

[5] Ginzburg V. L. and L. D. Landau, Zh. Eksp. Teor. Fiz 20, 1064 (1950);

[6] Abrikosov A. A., Doklady Akademii Nauk SSSR, 489 (1952);

[7] Bednorz J. G. and K. A. Mueller, Zs. Phyzik, B 64, 189 (1986);

[8] Abrikosov A. A., Sovet physics JETP 5, 1174 (1957);

[9] Буздин А. И., Мощалков В. В., Экзотические сверхпроводники, М., Знание, 1986г.;

[10] Nagamatsu J. et al., Superconductivity at 39 K in magnesium diboride, nature 410, 63-64 (2001);

[11] McMillan W. L., Transition temperature of Strong-coupled superconductors, Phys. Rev. 167, 331-344 (1968);

[12] Chen X. H., T. Wu, G. Wu, R. H. Liu and D. P. Fang, Superconductivity at 43K in Samarium-arsenide Oxides $SmFeAsO_{1-x}F_x$ Hefei National laboratory for Physical Science at Microscale and Department of Phisics, University of Scinence and Tehnology of China, 2008;

[13] Kamihara Y. et al., Iron-based layered superconductor $LaO_{1-x}F_xFeAs$ (x=0.05-0.12) with T_c=26 K, J.Am.Chem.Sco.130, 3296 (2008);

[14] Superconductivity News, Vol. 1, №5, p.4, 1987;

[15] Superconductivity News, Vol. 1, №7, p.5, 1987;

[16] Superconductivity News, Vol. 1, №2, p.9, 1988;

ВЪРХУ ТОЧНОСТТА НА ЧИСЛЕНОТО ИНТЕГРИРАНЕ НА ИЗРАЗА ЗА ИЗХОДНИЯ СИГНАЛ НА ТРАНСФОРМАТОРЕН ВИХРОВОТОКОВ ПРЕОБРАЗУВАТЕЛ, РАЗПОЛОЖЕН НАД ДВИЖЕЩИ СЕ ПЛОСКИ ПРОВОДЯЩИ ФЕРОМАГНИТНИ ОБЕКТИ

Стефчо Гунински, Валери Иванов

Технически университет София, кат. "Обща електротехника",
e-mail: sgg@tu-sofia.bg ЮЗУ "Н. Рилски", email: val_iv@abv.bg

Резюме: *В доклада е анализиран въпроса за избор на стъпката и границите на интегриране при численото интегриране на израза за изходния сигнал на трансформаторен електромагнитен преобразувател, разположен над движещи се плоски обекти. Като изходен сигнал се разглежда комплексната ефективна стойност на внесеното напрежение, индуктирано в измервателната намотка. Полученият израз представлява двоен несобствен интеграл от комплексна подинтегрална функция. Показано е, че при наличие на движение и в двете компоненти (реална и имагинерна) на подинтегралната функция се получават изменения, които налагат специален подбор на стъпката и границите на интегриране. Ако не се държи сметка за тези изменения в някои случай (например при големи стойностит на обобщения параметър) се получават завишени грешки в резултата от интегрирането, които може да доведат до непрецизни зависимости и изводи.*

Ключови думи: аналитичен метод, електромагнитен преобразувател

1. ВЪВЕДЕНИЕ

В предишна научна работа [1] авторите са извели по метода с интегралните трансформации аналитичен израз за изходния сигнала на допиращ трансформаторен вихровотоков преобразувател (ВТП) с правоъгълни намотки, разположени над еднослоен плосък проводящ феромагнитен обект. Възбудителната и измервателната намотки са с успоредни страни и лежат в равнини, успоредни на повърхността на измервания (контролирания) обект. Отчита се транслационно относително движение между ВТП и обекта със скорост $\vec{v} = v_x\vec{e}_x + v_y\vec{e}_y$. Възбудителният ток е синусоидален с ъглова честота $\omega = 2\pi f$ и средите се считат линейни и хомогенни (γ = const и μ_r = const), поради което се работи с комплексните ефективни стойности на променливите величини.

Като изходен сигнал се разглежда комплексната ефективна стойност на внесеното напрежение $\dot{U}_И$ [2], индуктирано в измервателната намотка. Полученият израз представлява двоен несобствен интеграл от комплексна подинтегрална функция, в който са използвани възможностите за преминаване към относителни (безразмерни) величини и параметри. Тъй като интеграла не може да се реши аналитично, се налага численото му решаване. Показано е, че при наличие на движение и в двете компоненти (реална и имагинерна) на подинтегралната функция се получава несиметрия по отношение на интеграционните променливи и области на бързи изменения, които добавени към относително малкия дял на кинематичната съставка от пълния изходен сигнал, изискват специален подбор на стъпките и границите на двете интегрирания. Ако не се държи сметка за това в редица случаи (например при големи стойности на обобщения параметър) се получават значителни грешки в резултата от интегрирането, които може да доведат до непрецизни зависимости и изводи.

2. АНАЛИТИЧЕН ОПРЕДЕЛЯНЕ НА ИЗХОДНИЯ СИГНАЛ НА ВТП ПРИ НАЛИЧИЕ НА ДВИЖЕНИЕ

2.1 Аналитичен израз за внесенето напрежение в измервателната намотка на трансформаторен ВТП

В [1] по метода с интегралните трансформации е получен следният израз за изходния сигнал:

$$\dot{U}_И = -j\tilde{g}\int_{-\infty}^{\infty}\int_{\infty}^{\infty} p\lambda^{-2}\nu^{-2} f_m Q \sin\nu b_1 \sin\lambda a_2 \sin\nu b_2 \, d\lambda d\nu , \qquad (1)$$

където:

$$\tilde{g} = 2\pi^{-2}\mu_0\omega\dot{I}N_1N_2 , \quad f_m = f_1/f_2 , \quad Q = \sin\lambda a_1 e^{-p(h_1+h_2)} e^{j[\lambda(c_2-c_1)+\nu(d_2-d_1)]} \qquad (2)$$

$$p = \sqrt{\lambda^2+\nu^2} , \quad q_v = \sqrt{p^2+k^2+j\mu\gamma(\lambda v_x + \nu v_y)} , \qquad (3)$$

$$f_1 = \mu_r p - q_v \quad , \quad f_2 = \mu_r p + q_v , \; k_1^2 = 0 , \; k_2^2 = k^2 = j\omega\mu_0\mu_r\gamma . \qquad (4)$$

a_1, a_2, ... c_1, ...h_1, h_2 са геометричните размери. “1” показва принадлежност на величината към възбудителната намотка (ВН), а “2” – към измервателната намотка (ИН).

Двойният несобствен интеграл се получава в резултат на прилагането на двойната безкрайна Фурие-трансформация [3] с параметри λ и ν. Удобно е да се премине към безразмерни (относителни) величини [2]. В частност интегрирането се извършва по отношение на безразмерните променливи $x = a_1\lambda$ и $y = a_1\nu$ (това не са декартовите координати!).

$$\dot{U}_И = -j\tilde{g}Int , \quad Int = \int_{-l_X}^{l_X} F(x)dx, \quad F(x) = x^{-2}\sin x \sin(a_2^* x) e^{jx(c_2^*-c_1^*)} \int_{-l_Y}^{l_Y} f(x,y)dy , \qquad (5)$$

$$f(x,y) = p^* y^{-2} f_m \sin b_1^* y . \sin b_2^* y . e^{-p^*(h_1^*+h_2^*)} . e^{jy(d_2^*-d_1^*)} . \qquad (6)$$

2.2. Анализ на особеностите на израза за изходния сигнал на ВТП

От формула (1) се вижда, че подинтегралната функция по принцип е симетрична по отношение на интеграционните променливи x и y. Несиметрия има само в членовете, в които участва скоростта – q_v от формула (3), а след нормирането:

$$q_v^* = \sqrt{p^{*2} + j\mu_r\beta^2\left(1+\tau_X x+\tau_Y y\right)}\,, \quad \tau_m = \frac{v_m}{\omega a_1}, \quad m = x, y\ . \tag{7}$$

Тъй като двойният интеграл от (1) не може да се реши с помощта на известните функции, налага се неговото числено решение. Това е свързано с избора на две важни величини – стъпката на интегриране $\Delta x = \Delta y$ и границите на интегриране $\pm l_x = \pm l_y = \pm l$.

Прието е, че първо се интегрира по y , а след това по x.

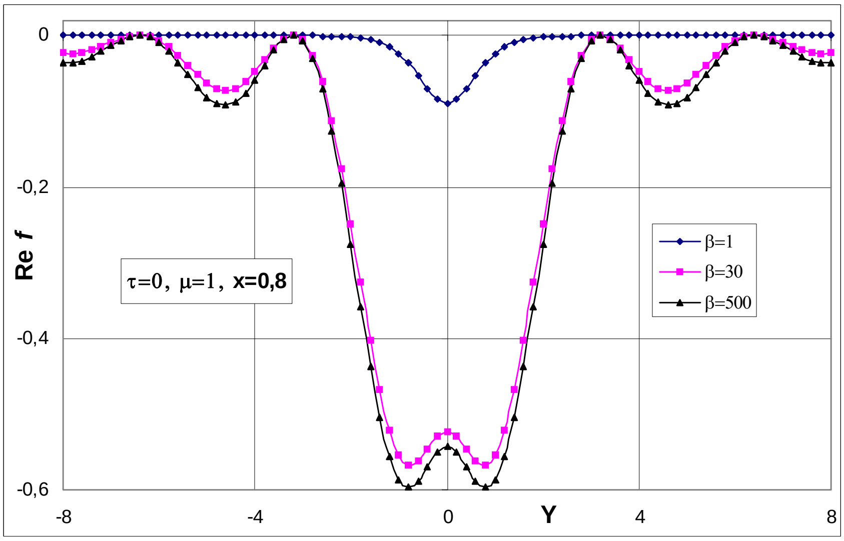

Фиг. 1

При липса на движение стъпката се определя от по по-голямата от двете величини $(a_1 + a_2)$ или $(b_1 + b_2)$. Грешката не надвишава 1%, ако се избере стъпка:

$$\Delta x = \Delta y \le 0{,}1\ \pi / A_{12}\ , \tag{8}$$

където A_{12} е по-голямата стойност от $(a_1 + a_2)$ или $(b_1 + b_2)$.

Границата l много силно зависи от стойността на обобщения параметър

$$\beta^2 = a_1^{\,2}\gamma\mu_0\omega \tag{9}$$

При липса на движение същата точност се получава при

$$l \ge 0{,}2\beta + 65. \tag{10}$$

Типичният вид на комплексната подинтегрална функция $f(x,y)$ за първото интегриране при липса на движение е показана на фиг. 1 (при различни стойности на β) и фиг. 3 (при различни стойности на x) за реалната част и на фиг. 2

(параметър β) и фиг. 4 (параметър *x*) – за имагинерната. На фиг. 5 и фиг. 6 са показани компонентите на комплексната функция *F(x)* при второто интегриране при различни стойности на β.

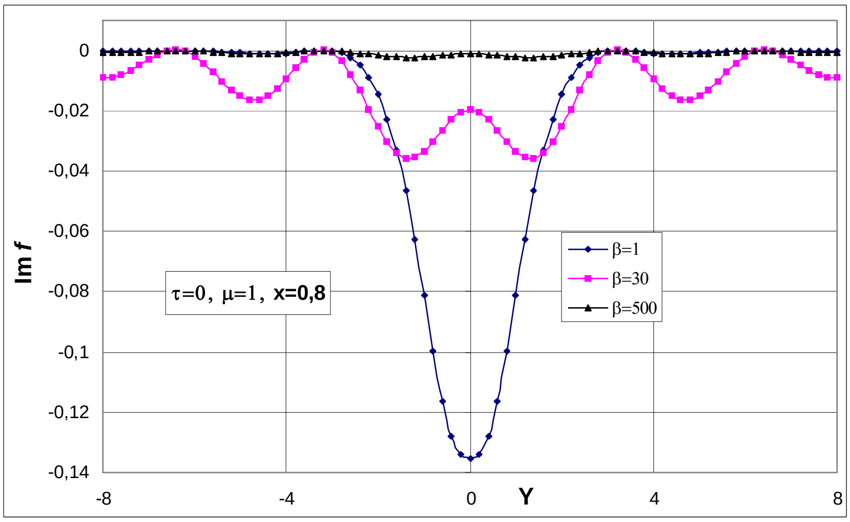

Фиг. 2

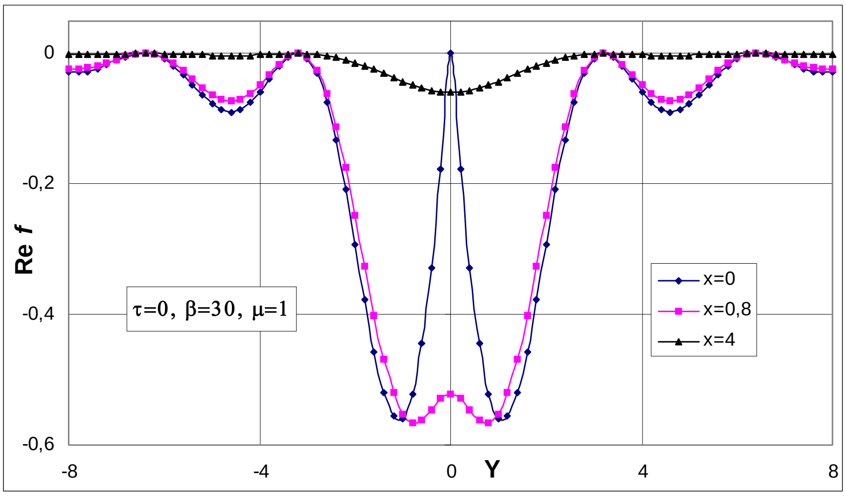

Фиг. 3

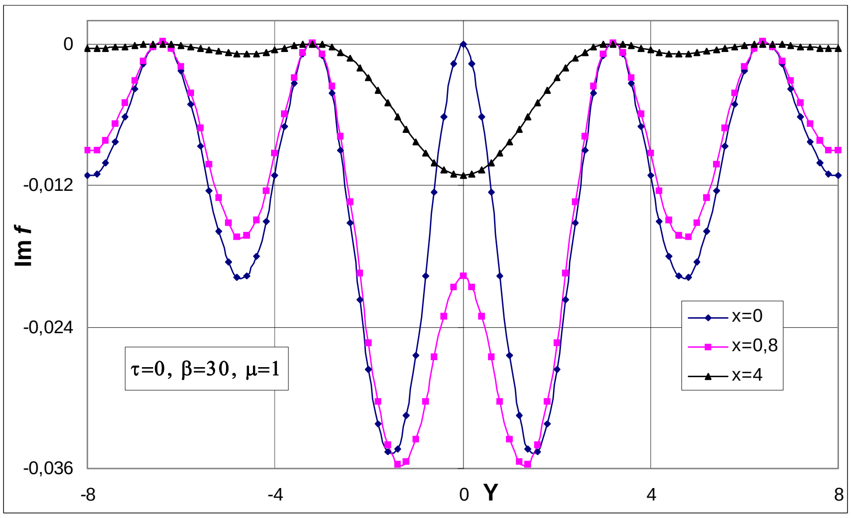

Фиг. 4

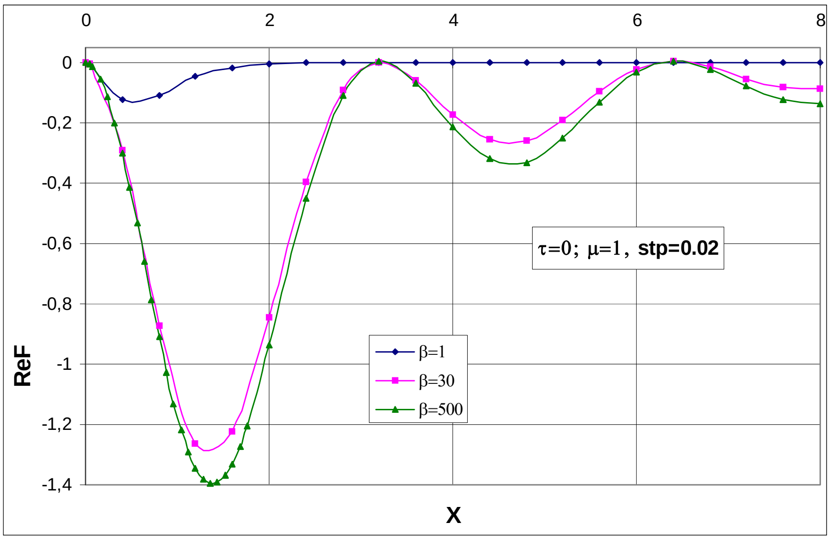

Фиг. 5

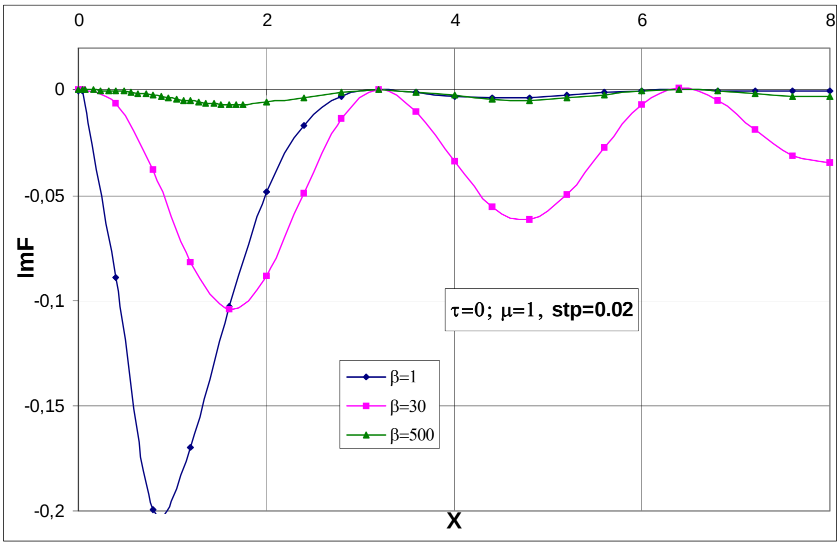

Фиг. 6

2.3. Проблеми с точността на интегриране при наличие на движение

При наличие на относително движение възникват проблеми при численото интегриране при големи стойности на обобщения параметър β, които се дължат на силна деформация на вида подинтегралните функции както при първото интегриране, така и при второто.

От формула (7) се вижда, че изразът в скобите за q_v^* може да стане нула. Например при $\tau_Y = 0$ това става за $x_\tau = 1/\tau_X$ (респективно при $y_\tau = 1/\tau_Y$, ако $\tau_X = 0$). От (7) следва, че $q_v^* = p^*$, а от (2), че

$$f_m = \frac{\mu_r - 1}{\mu_r + 1}\ , \tag{11}$$

което при неферомагнитни обекти ($\mu_r = 1$) означава, че $f_m = 0$. От (5) и (6) веднага следва, че и реалната, и имагинерната част на комплексните функции *f(y),* и *F(x)* стават нули.

Видът на компонентите на подинтегралната функция *f(y)* при първото интегриране при τ_Y = 083(3) за три стойности на обобщения параметър е показан на фиг. 7 за реалната част, а на фиг. 8 – за имагинерната. При $y_\tau = 1/\tau_Y$ = -1,2 и двете компоненти стават нула като при по-големи β при реалната част това е свързано с екстремум, които е много "остър", а при имагинерната част – със много "стръмна" промяна на знака между два екстремума в близост до y_τ. Очевидно е, че интегрирането по y около y_τ изисква силно намаляване на стъпката на интегриране при $\beta > 20$.

Аналогичните зависимости на компонентите на подинтегралната функция *F(x)* за второто интегриране са показани на фиг.9 (за реалната част) и на фиг.10 (за имагинерната част) за β = 30 и три стойности на τ_X = 0; 1,25 и 2 при τ_Y = 0. И тук при $x_{\tau=1,25}$ = 0,8 и $x_{\tau=2}$ = 0,5 и двете компоненти на *F(x)* стават нула. При реалната част (фиг. 9) това става с остър максимум, а при имагинерната – с много стръмен участък между два близки и остри разнопосочни екстремума. За сравнение са показани и гладките линии в този участък на компонентите подинтегралната функция при τ_X = 0.

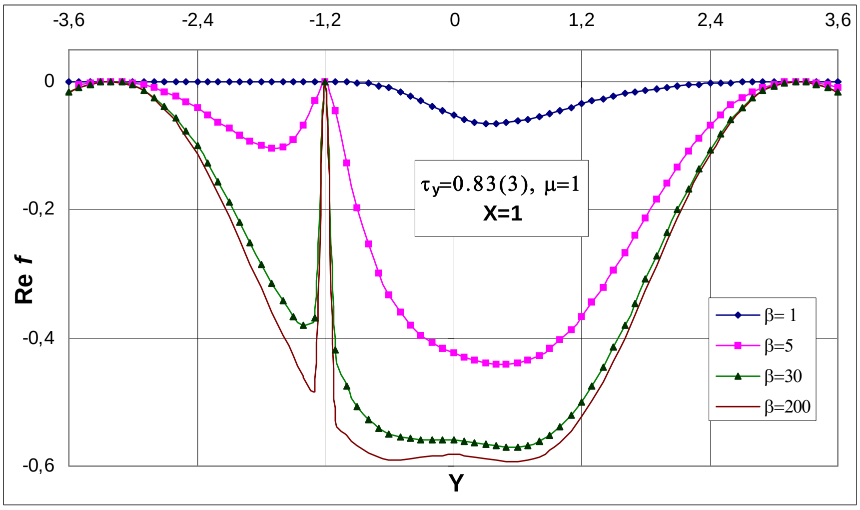

Фиг. 7

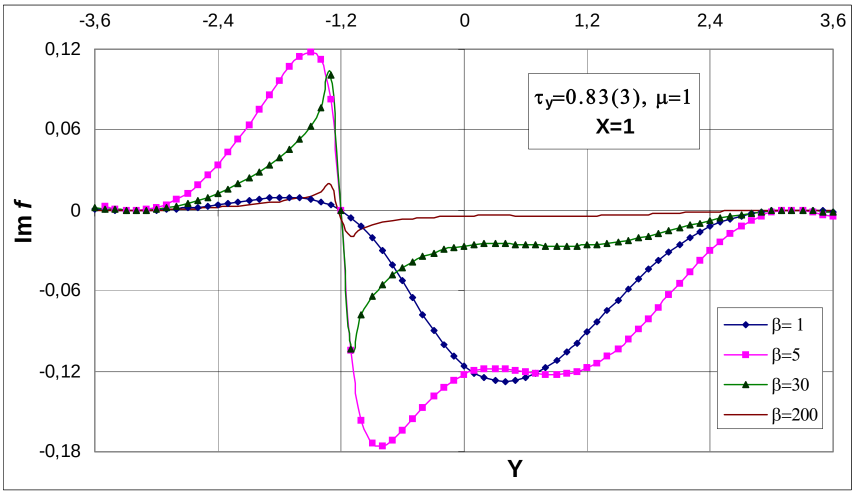

Фиг. 8

3. ЗАКЛЮЧЕНИЕ

От направените изследвания на вида на подинтегралните функции израза за изходния сигнал на трансформаторен електромагнитен преобразувател с квадратни успоредни намотки от (5) може да се направят следните изводи:

- И двете компоненти на комплексните функции f и F са затихващи, като с увеличаването на стойността на обобщения параметър β затихването е по-бавно, но във всички интересни за практиката случаи след $|x| > 100$ и $|y| > 100$ стойностите им са пренебрежими. Изразът (10) осигурява грешка от интегрирането под 1% и приналичие, и при отсъствие на движение.
- Формула (8) осигурява добра точност при липса на движение или при β < 3 при наличие на относително движение. При движение и β < 3 стъпката трябва да е под 0,02.
- При наличие на движение и по-големи стойности на β не е ефективно интегрирането с неизменна стъпка. Много ефективни ще са алгоритми, при които само в интервалите около x_τ и y_τ стъпката силно е намалена, а извън тях се интегрира със стъпка, определена от (8).

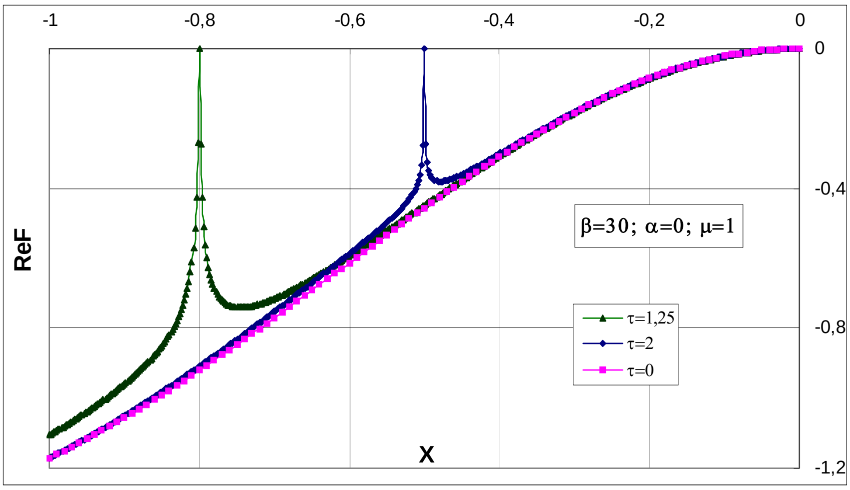

Фиг. 9

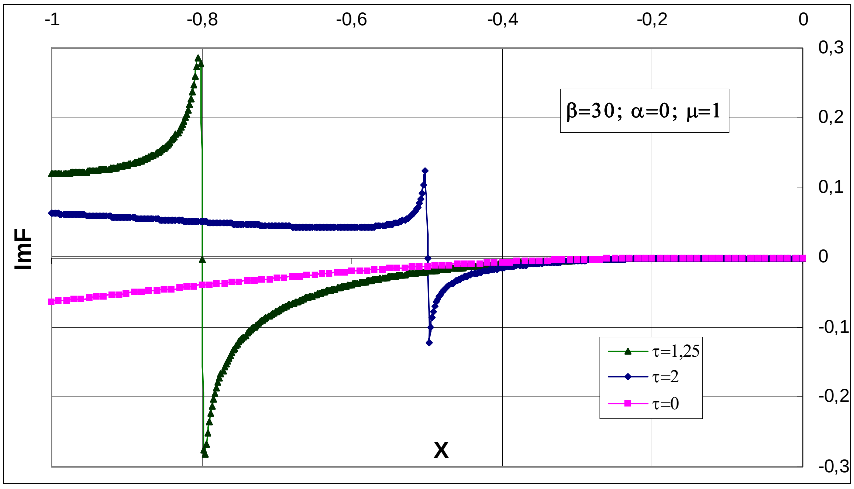

Фиг. 10

ЛИТЕРАТУРА

[1] С. Гунински, “Изходен сигнал на електромагнитен преобразувател с перпендикулярни намотки при наличие на относително движение”, Годишник на Техническия университет – София, том 53, 2004 г., с. 191 – 199.

[2] Д. Цветков, “Електромагнитна дефектометрия” , София, Техника, 1981, 280 с.

[3] В. Диткин и А. Прудников, “Интегральние преобразования и операционное исчисление” , М., Наука, 1974, 450 с.